Mathematical models of the roles of IL-2 and IL-7 in T cell homeostasis

Joseph Benjamin Reynolds

School of Mathematics

University of Leeds

Submitted in accordance with the requirements for the degree of

Doctor of Philosophy

March, 2014

The candidate confirms that the work submitted is his own, except where work which has formed part of a jointly-authored publication has been included. The contribution of the candidate and the other authors to this work has been explicitly indicated below. The candidate confirms that appropriate credit has been given within the thesis where reference had been made to the work of others.

Joint Publications

Work from the following jointly-authored publications is included in this thesis:

- Reynolds, J., Coles, M., Lythe, G. & Molina-París, C. *Mathematical model of naive T cell division and survival IL-7 thresholds.* Frontiers in Immunology, 4, 2013.
- Reynolds, J., Amado, I.F., Freitas, A.A., Lythe, G. & Molina-París, C. *A mathematical perspective on $CD4^+$ T cell quorum-sensing.* Journal of Theoretical Biology. 2013.

Sections 5.1 and 5.2 follow the first of the above publications. The latter half of Section 5.2 diverges from the paper, since the model in Chapter 5 is formulated with different assumptions. For these sections, credit is given to Carmen Molina-París for editing the writing style.

Chapter 6 is a lightly modified version of the second paper listed above. Inês Amado and Antonio Freitas are recognised for contributing their biological insight in establishing the equations for the model, and for providing feedback on the interpretation of the mathematical analysis.

Carmen Molina-París and Grant Lythe are due credit for helping to establish the model. Additionally, a large amount of credit is due to Carmen for editing the writing style of the paper.

The remaining work in this paper, which includes the analysis of the model, the interpretation of the results and the writing, was contributed by Joseph Reynolds.

Acknowledgements

This research was funded by a White Rose Scholarship, provided jointly by the Universities of Leeds, Sheffield and York.

First and foremost, I thank my supervisors Carmen Molina-París and Grant Lythe for their unrelenting support during my time spent as a post-graduate at the University of Leeds. Quite simply, this work would not have not been possible without your constant enthusiasm for mathematics and immunology. Thank you!

I also thank Mark Coles for his input on all things biological. Our discussions around immunology have helped immensely in retaining some semblance of reality in the mathematical models developed in this thesis.

I thank Ben Seddon and Thea Hogan for sharing the experimental data used in Chapter 5.

Additionally, I thank all the researchers in the field of mathematical modelling of immunological processes with whom I have discussed my work, particularly Robin Callard.

To my family, most notably my parents, I give my thanks for your support, both during my post-graduate studies, and throughout my life prior to this undertaking.

Lastly, I thank the most important person in my life, Saph, for being with me these past four years. In contrast to this mathematical study, what I gain from your companionship is incalculable.

Abstract

We study the homeostasis of a peripheral naive T cell population through the use of deterministic mathematical models. A two compartment approach is used, where, naive T cells are assumed to be either in a resting state, or undergoing the cell cycle. We begin by assuming all rates are linear, then discuss the limitations in doing so. We next explore examples of published methods which improve this simple description. Finally, we introduce a model in which resting T cell survival and entry into the cell cycle is assumed to be dependent on the amount of available IL-7.

To aid our description of T cell homeostasis, a stochastic model of IL-7 signalling is developed. In this model we consider the number of IL-7 receptors, either membrane bound or internalised, the extra-cellular concentration of IL-7, and the amount of IL-7 induced signalling. The model is used to derive a relationship between the amount of IL-7 induced signalling to the extra-cellular concentration of IL-7. The survival and proliferative ability of the T cell population is then assumed to be dependent on the amount of IL-7 induced signalling with respect to IL-7 signalling thresholds for survival and division.

This signalling relation is then used with the model of T cell homeostasis. The model is fitted to experimental data measuring the expansion of transgenic naive T cells in lymphopenic mice. We show this approach can capture the homeostatic equilibrium, and notably, time scales required to reach equilibrium. The model is then explored in the context of the human periphery.

In a separate piece of work we develop a stochastic Markov model of the peripheral $CD4^+$ T cell pool, in which we consider sub-populations of naive, IL-2 producing, IL-2 non-producing and regulatory T cells. The balance between the IL-2 producing and regulatory sub-populations is assumed to be determined by a recently proposed quorum-sensing hypothesis. This model is explored in scenarios where no antigen is

presented to the $CD4^+$ population, before and after a challenge, and when antigen is presented at a constant level. We show, amongst other results, that the number of regulatory T cells in equilibrium is greater when antigen is presented, whilst the number of IL-2 producing T cells remains the same. We finally use the stochastic aspect of this model to explore probabilities of and times to extinction of the sub-populations.

Contents

List of Figures

Chapter 1

Biological introduction

1.1 The immune system

With the evolution of the first multicellular organisms arose a need for regulation of the individual cells and inter-cellular environments within organisms. A group of cells belonging to the same organism must work together to promote survival of the organism as a whole. However, the processes at work within each cell are, whilst highly controlled, not perfect. Intra-cellular processes may begin to function in a detrimental manner to the organism. There is therefore, an evolutionary advantage for mechanisms by which the collective group of cells of an organism can recognise individual, misbehaving cells, and remove them for the collective good.

The intra and inter cellular space within an organism is a highly regulated environment specifically tailored to support the biological processes involved in life. This environment in complex organisms has, for aeons past, been exploited by other organisms. Such relationships between cells differing in the genetic identification encoded in the DNA can be beneficial for both organisms. In humans for example, digestion is aided by the micro flora in the intestinal tract (Sears, 2005). Alternatively, the presence of one organism may be detrimental to the survival of the other, as in the case of a bacterial infection. For complex organisms there has therefore been an evolutionary pressure for the development of immune mechanisms, through which harmful foreign bodies can be recognised and removed.

The mechanisms by which unwanted cells or foreign organisms are removed from the host, along with the cells responsible for mediating these actions, are collectively referred to as an organism's immune system. The immune system has evolved to protect an organism from detrimental cellular behaviour, both from misbehaving

cells within the organism itself and from pathogens. Pathogens take many forms, including bacteria, viruses, fungi and unicellular/multicellular eukaryotes, collectively termed parasites (Janeway *et al.*, 2001).
An example of misbehaving cells in humans are cancer cells. Cancer cells undergo rapid proliferation, the possible causes of which are numerous. Various cell types of the human immune system are responsible for recognising and destroying cancer cells. Cancer cells which are not recognised by the immune system are called malignant and can grow into tumours, which are often harmful. In the most severe cases, tumour growth can cause an early death. Humans are susceptible to infection by a plethora of pathogens, many of which would rapidly kill if not for the immune response.

1.1.1 Innate and adaptive immunity

Cells of the immune system recognise pathogens and mutant host cells using receptors on the cell's surface. Such receptors recognise the molecular pattern of invading pathogens and signal to the immune cells to initiate effector functions of an immune response. If successful, effector functions eradicate the pathogen from the host. A distinction is made between immune cells which possess receptors capable of recognising a wide array of pathogens, and immune cells which possess receptors capable of recognising a limited repertoire of pathogens. Immune components which recognise a wide array of pathogens typically display the same group of receptors on all cells of the same type. Such receptors are called non-specific. These immune components form the innate immune system. Conversely, cells which possess receptors capable of recognising a limited diversity of pathogens are called specific. To maintain immune coverage, there exist many clones of cells possessing specific receptors. Each clone differs only in the receptor expressed; thus clones differ in the pathogens they respond to. Such cell types form the adaptive branch of the immune system. Upon detecting a pathogen, a handful of clones will respond, whilst the rest of the population remains quiescent. The adaptive immune system generates a large number of clones potentially allowing response to any possible pathogen.
The innate immune system is the first line of defence against pathogens following physical and chemical boundaries such as the skin mucous membranes, not typically considered immune components. The cells of the innate immune response are always active and respond to pathogens within hours of recognition (Janeway *et al.*, 2001). The type of protection conferred by the innate immune system is non-specific; whilst

fast acting, innate responses are metabolically costly and can confer damage on healthy host tissue. Conversely, the adaptive immune response takes days before effector functions are mediated against pathogens. Whilst slower than the innate immune response, during an adaptive immune response, a population of immune cells specifically tailored to combat the recognised pathogen is generated, resulting in a specific and highly efficient response. These two components of the immune response work in tandem to confer immune protection, indeed, the adaptive immune response is initiated by cells of the innate system and promotes the activity of additional innate cells as one of several response strategies.

1.1.2 Cell types of the immune system

All cell types of the immune system (leukocytes) are generated from hematopoietic stem cells (HSCs), found in the bone marrow. HSCs give rise to two distinct lineages: the myeloid lineage and the lymphoid lineage. Progenitors of the myeloid lineage generate cells of the innate immune system such as granulocytes and dendritic cells. Progenitors of the lymphoid lineage develop into cells of the adaptive immune system, which are T and B cells and natural killer (NK) cells. The lineage tree of the various cells of the immune system is presented in Figure 1.1.

1.2 T cells

This study is focused on the homeostasis of T cells, we therefore present over the next sections, a brief introduction to T cells.

1.2.1 Antigen presentation to T cells

T cells recognise antigen bound to the surface of antigen-presenting cells (APCs). During an infection, pathogens are engulfed by phagocytic cells such as macrophages and dendritic cells. Inside these cells the proteins of the pathogens are broken down into peptide fragments. The peptide fragments are bound to host-cell glycoproteins known as MHC molecules. These proteins are encoded by a gene cluster known as the major histocompatibility complex (MHC) (Janeway *et al.*, 2001). Peptides bound to MHC molecules (peptide:MHC) are displayed on the surface of APCs. These membrane expressed complexes can be recognised by T cells.
T cell recognition of peptide bound to the surface of APCs is mediated through the T cell receptor (TCR). If the T cell receptor is specific for the peptide fragment

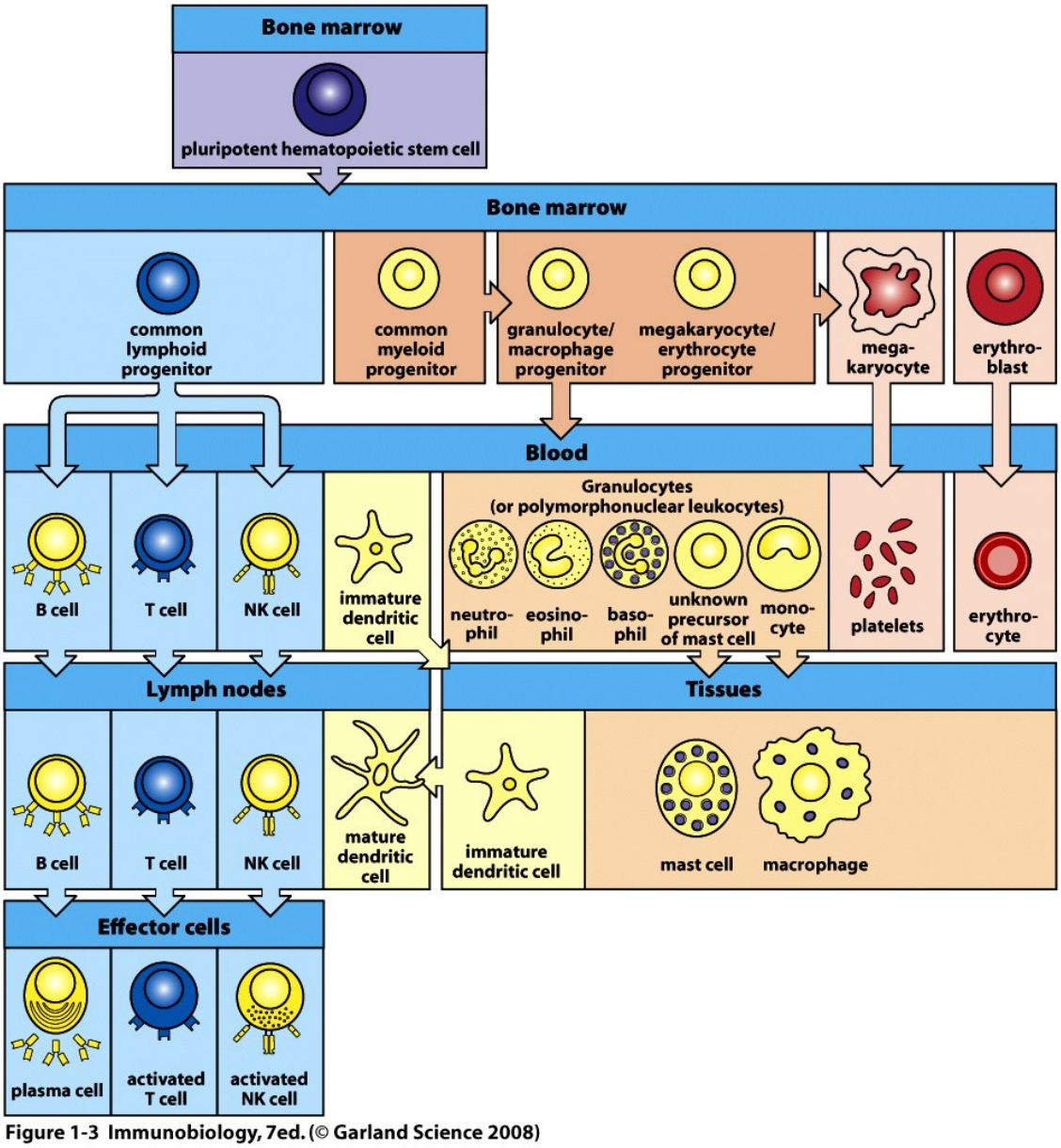

Figure 1.1: Cell types of the immune system.

displayed on the surface of the APC, a stable bond is formed. Following this preliminary bond formation, T cells recruit the co-receptors CD4 and CD8 to further stabilise the bond formed resulting in an activation signal being transduced to the T cell (Janeway *et al.*, 2001). This signal then induces the T cell to exhibit effector functions. Such events are referred to as T cell activation.

There are two classes of MHC molecules defined as class I and class II. The classes differ in their molecular structure and expression pattern within the tissues of the body (Janeway *et al.*, 2001). MHC class I is displayed on virtually all nucleated cells. MHC class I binds to protein fragments of viruses; it enables nucleated cells to display virus peptides on their surface, indicating that they have been infected. Only T cells possessing the CD8 co-receptor recognise MHC class I, these cells are referred to as cytotoxic T cells. Cytotoxic T cells, upon recognition of virus peptide displayed on the surface of host cells, signal to the host cells to die, thus preventing replication of the virus in these cell (Janeway *et al.*, 2001).

On the other hand, MHC class II molecules are expressed by professional cells such as macrophages, dendritic cells and B cells. These cells phagocytose bacterial pathogens, displaying peptide fragments bound to MHC class II on their surface. T cells possessing the co-receptor CD4 recognise the bacterial derived peptide expressed by these APCs. Upon activation, effector CD4 T cells perform antibacterial functions. These functions include stimulating B cells to produce antibodies and activating macrophages to further phagocytose bacteria at the sight of infection (Janeway *et al.*, 2001).

1.2.2 T cell development in the thymus

Progenitor T cells are derived from HSCs in the bone marrow. Progenitors migrate from the bone marrow to the thymus, an organ located above the heart. The thymus is composed of an outer cortical region named the thymic cortex and an inner region named the medulla. Progenitor T cells enter the outer cortex in which they begin a maturation programme. As T cell development continues, cells migrate towards the medulla. Mature T cells leave the medulla and enter the peripheral lymphoid tissues (Janeway *et al.*, 2001).

Mature T cells are defined by expression of surface markers, namely the CD3:T-cell receptor complex, and the co-receptors CD4 and CD8. Progenitor T cells entering the thymus do not yet express any of these markers. Two distinct lineages of T cells develop in the thymus, the α:β lineage and the γ:δ lineage. The lineage pathway

is displayed in Figure 1.2. The two lineages of T cells differ in the type of T cell receptor expressed, as well as the co-receptors CD4 and CD8. Whilst all mature T cells express CD3, γ:δ T cell express only CD3 whereas α:β T cells express CD3 and either CD4 or CD8 (Janeway *et al.*, 2001). α:β T cells comprise approximately 95% of the mature T cell population, and are the focus of this study.

Development of the α:β lineage

Progenitor cells entering the thymus are said to be double negative (DN); these cells do not express either of the CD4 or CD8 co-receptors. The DN stage is split into four distinct stages of T cell development, termed DN1-DN4. The stages of development are distinguished by expression of the molecules CD44 and CD25. During these stages the T cell receptor (TCR) is generated.

The TCR allows mature T cells to recognise antigen displayed by antigen-presenting cells (APCs) and subsequently initiate an immune response. The TCR is generated by somatic recombination of gene segments encoding the α and β chains of the receptor. This process allows in theory up to 10^{18} distinct T cell receptors to be generated (Janeway *et al.*, 2001).

Rearrangement of the β chain locus begins in the DN2 stage and continues into the DN3 stage. Cells which fail to rearrange the β chain remain in the DN3 stage and eventually die. During the DN4 stage, thymocytes undergo proliferation before expressing both CD4 and CD8. At this point thymocytes are referred to as being double positive (DP). During the transition from the late DN3/DN4 to the DP stage, thymocytes undergo several rounds of division, greatly increasing the size of the population (Germain, 2002). Following this burst of division, thymocytes reduce in size, after which rearrangement of the α chain locus of the TCR occurs. DP cells may make several attempts to rearrange the α chain locus and therefore most DP cells will generate a TCR.

A fully formed TCR is then tested against self-peptide:MHC complexes (sp:MHC) displayed on the surface of APCs. Two selection events must be passed before the T cell completes its maturation programme. First, the TCR must recognise sp:MHC (positive selection). This ensures the generated TCR is functional and will potentially recognise a not yet encountered foreign antigen. If the TCR does not recognise sp:MHC, the thymocyte dies by neglect since no signal is transduced via the TCR. Secondly, the TCR must not recognise sp:MHC too strongly (negative selection). If a TCR induced signal through recognition of sp:MHC is too strong,

the thymocyte will die by apoptosis. This ensures that the thymus does not generate T cells which respond to self-tissue and elicit effector functions. Self-reactivity is a major factor in the onset of many autoimmune disorders.

T cells which pass positive and negative selection cease to express one of either the CD4 or CD8 co-receptors, becoming single positive (SP) cells. Mature T cells expressing either CD4 or CD8, then leave the thymus and enter the peripheral lymphoid tissues. The entire process takes about 3 weeks (McCaughtry *et al.*, 2007).

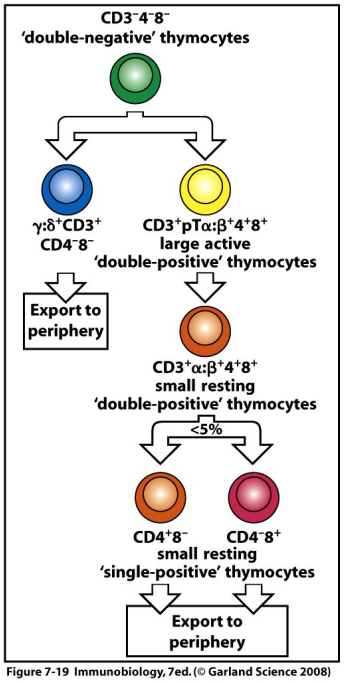

Figure 1.2: T cell development lineages in the thymus.

1.2.3 Naive T cells

T cells which have matured and left the thymus enter the peripheral lymphoid organs. The peripheral lymphoid organs are the lymph nodes, spleen and the mucosa-associated lymphoid tissues, such as the Peyer's patches in the gut (Janeway *et al.*, 2001). T cells sequentially visit the peripheral lymphoid organs, circulating between them via the bloodstream. The process of circulation allows T cells to regularly scan APCs for peptide:MHC complexes which will trigger the T cell to respond. T cells which have matured and left the thymus, but have not yet encountered antigen specific for their TCR, are classified as naive T cells.

The survival of naive T cells in circulation is dependent on signals from cytokines

and signals resulting from TCR recognition of self ligands (Sprent & Surh, 2011; Takada & Jameson, 2009). In particular, interleukin-7 (IL-7) has been identified as the foremost required cytokine for naive T cell survival (Fry & Mackall, 2005; Schluns *et al.*, 2000; Tan *et al.*, 2001). Signals from both the TCR and the IL-7 receptor are sufficient to maintain survival of naive T cells independently of each other, but, these signals may also combine to promote survival (Seddon & Zamoyska, 2002).

Signals received from IL-7 and sp:MHC binding promote cell survival by preventing the accumulation of pro-apoptotic proteins such as the Bim family (Li *et al.*, 2004). Cells that do not receive sufficient stimulus from IL-7 or TCR signalling will die by apoptosis (Kieper *et al.*, 2004; Tan *et al.*, 2001). The same signals may also induce naive T cell division, when lymphocyte numbers are low, presumably because the availability of these signals is in excess (Seddon & Zamoyska, 2002). The availability of survival signals, in combination with the influx of new naive T cells from the thymus determines the number of naive T cells in circulation. This is termed the homeostasis of naive T cells.

Self-peptide:TCR interactions not only regulate the total number of naive T cells, but also the abundance of clonotypes within the population. For the T cell population to respond to an invading pathogen, there must exist at least one T cell clonotype possessing a TCR capable of recognising antigen from the pathogen. Since no prior knowledge of the pathogen is known, the antigen that needs to be recognised is essentially random. Effective response therefore requires a large enough number of distinct TCRs to be present within the population such that any possible antigen can be recognised. However, maintaining a large pool of cells is also metabolically costly, and so the repertoire of T cell clonotypes is ideally optimised such that structurally similar TCRs (that recognise the same antigen), are not needlessly maintained. It is likely that IL-7 also plays a role in maintaining clonotype diversity within the naive T cell pool (Palmer *et al.*, 2011; Troy & Shen, 2003).

1.2.4 Activation of naive T cells

Recognition of specific antigen by the TCR alone is insufficient to activate a naive T cell. Two further co-stimulatory signals are required before the T cell undergoes a programme of proliferation and differentiation into effector T cells (Curtsinger *et al.*, 1999; Linsley & Ledbetter, 1993). Naive T cells continually circulate through the peripheral lymphoid organs, transiently coming into contact with APCs. When a

naive T cell encounters an APC, adhesion molecules on the surface of the T cell and APC bind, thereby allowing the naive T cell to remain in contact with the APC for a limited length of time. The area of contact between the two cell types is called the immunological synapse (Grakoui *et al.*, 1999). During the contact period, TCRs in the synapse come into contact with many peptide:MHC complexes (Janeway *et al.*, 2001). If there is no recognition of peptides specific for the TCR in this period, the immunological synapse breaks and the T cell continues circulation.

If the TCR recognises a p:MHC molecule, a bond is formed between peptide:MHC and the TCR. This bond is further stabilised by binding of either of the co-receptors CD4 or CD8 to the peptide:MHC molecule. Two further signals are then required for the naive T cell to become an effector T cell. The first of these is signalling through the CD28 co-receptor, mediated by the B7 family of proteins found on dendritic cells. Signalling through the CD28 co-receptor induces the T cell to produce interleukin-2 (IL-2) and up-regulate the α chain of the IL-2 receptor (IL-2R) (Janeway *et al.*, 2001). This then allows the T cell to proliferate in response to IL-2, produced locally by the T cells responding to antigen.

The form of the third signal varies with the type of infection antigen is derived from. Naive CD4 T cells differentiate into one of several functionally different effector types. This signal determines the type of effector cell the naive T cell will become. The different CD4 effector T cells, as well as the nature of the signal which induces them, are presented in Figure 1.3.

Naive CD8 T cells, when activated, become cytotoxic CD8 cells. This activation process, likely, requires the dendritic cell to be stimulated by CD4 T cells to express higher levels of B7, since the basal amount of signalling through the CD28 co-receptor is insufficient for naive CD8 T cells (Janeway *et al.*, 2001).

1.2.5 Effector T cells

CD8 cytotoxic T cells

Cytotoxic T cells are induced from CD8 naive T cells. The TCR of CD8 expressing T cells recognises MHC class I, expressed by all nucleated cells. Viruses cannot replicate by themselves, instead, replication of a virus can only occur by the virus exploiting the intra-cellular machinery of host cells. When a cell is infected by a virus, peptides specific to the virus are expressed on the surface of the cell in peptide:MHC class I complexes. This allows cytotoxic T cells to recognise that the cell is infected.

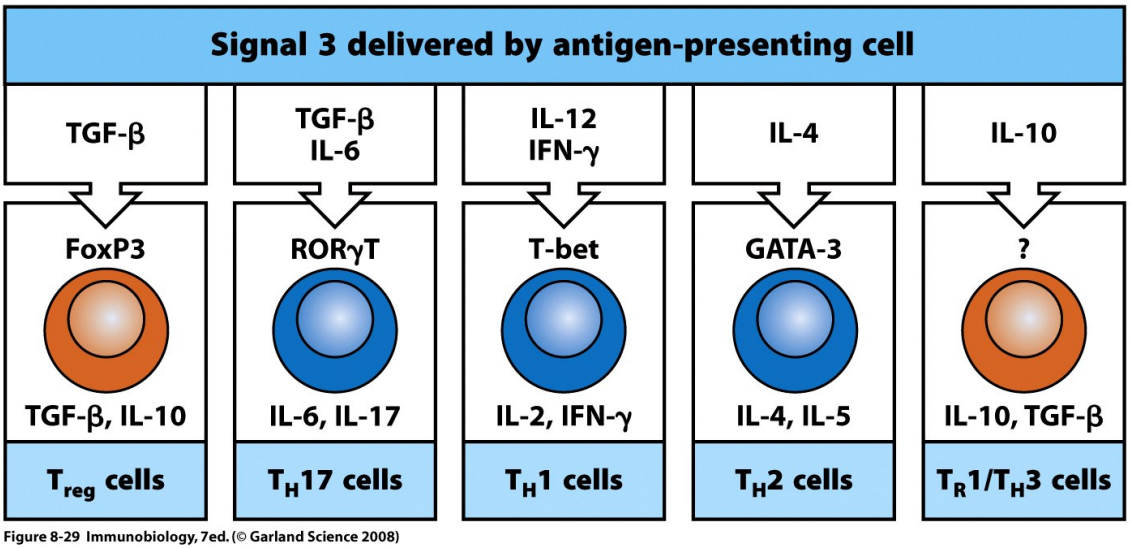

Figure 1.3: The different types of CD4 effector T cells.

Upon recognition of foreign peptide, a cytotoxic T cell forms an immunological synapse with the infected cell. The cytotoxic T cell signals to the infected cell to die by secreting pro-apoptotic molecules through the immunological synapse. Apoptosis is primarily induced through the release of cytotoxic granules through the immunological synapse (Janeway *et al.*, 2001). Cytotoxic granules are modified lysosomes that contain three families of proteins used to induce apoptosis. These protein families include perforin which enables the contents of the granules to be delivered to the target cell membrane. The other two families are called granzymes and granulysin, the latter of which has anti-microbial properties (Janeway *et al.*, 2001).
Cytotoxic CD8 T cells may also induce apoptosis in other cell types by interaction of Fas and Fas ligand, members of the TNF family of proteins (Janeway *et al.*, 2001). Typically, all activated lymphocytes express Fas and Fas ligand and these interactions between activated cells serve as a regulatory mechanism which limits the numbers of these cells.

CD4 T_H1 T cells

Macrophages remove pathogens by phagocytosis, ingesting pathogens and breaking them down in lysosomes. Some micro-organisms, such as mycobacteria, inhibit the anti-bacterial mechanisms of macrophages and are able to survive and grow inside the macrophage (Janeway *et al.*, 2001). The principal effector function of CD4 T_H1 T cells is to enhance the antibacterial function of macrophages, called macrophage

activation (Janeway *et al.*, 2001). The activation of macrophages is required for protection against some intracellular pathogens, such as mycobacteria.
T_H1 T cells secrete interferon-γ (IFN-γ), one of two signals required for activation of macrophages. The second signal is interaction through the ligand CD40, expressed by both T_H1 T cells and macrophages (Janeway *et al.*, 2001). The antibacterial actions of macrophages are detrimental to host tissue, as well as foreign pathogens. Furthermore, activated macrophages require a large amount of energy (Janeway *et al.*, 2001). It is therefore beneficial if macrophages are activated only in response to a foreign pathogen, rather than being maintained in a constantly activated state. T_H1 T cells coordinate the activity of macrophages, such that host tissue damage and energy consumption is minimised, whilst still providing protection against the pathogen (Janeway *et al.*, 2001).

CD4 T_H2 T cells

Antibodies, similar to the TCR, are antigen specific, but are produced by B cells (Janeway *et al.*, 2001). Unlike the TCR, which is membrane bound to T cells, antibodies can be either membrane bound to B cells or secreted. Membrane bound antibodies are required for activation of B cells whereas the soluble form is secreted to mediate effector functions. Antibodies bind to pathogens and the products produced by pathogens. T_H2 CD4 T cells enhance immune responses by stimulating naive B cells into production of antibodies. This enhancement is mediated through the release of various cytokines required by B cells to proliferate and differentiate into activated cells. In particular, T_H2 T cells induce activated B cells to isotype switch into cells which produce the IgE class of antibodies, the main function of which, is to fight parasites (Janeway *et al.*, 2001).
IL-10 is one the various cytokines produced by T_H2 T cells. This particular cytokine can inhibit the development of T_H1 T cells. On the other hand, IFN-γ, produced by T_H1 T cells, can prevent the development of T_H2 T cells (Janeway *et al.*, 2001). Each of these two types of effector cells has a distinct role within response to infection, and the pathology of many responses favours one of these cell types. However, they have also been observed to act in a complementary manner (Janeway *et al.*, 2001).

CD4 T_H17 T cells

CD4 T_H17 T cells are induced in the early phase of an immune response. Following activation they migrate to the site of infection at which they secrete a number of cytokines, the predominant being members of the IL-17 family (Janeway *et al.*, 2001). IL-17 induces tissue cells to secrete cytokines which aid immune function. Furthermore, stimulation by IL-17 induces tissue cells to secrete chemokines which attract neutrophils to the site of infection.

1.2.6 Regulatory T cells

Regulatory T cells suppress the effector activity of other lymphocytes. They express CD4 and are derived from progenitor T cells in the thymus, but also can be induced from naive CD4 T cells (Chen *et al.*, 2003). Regulatory T cells which develop in the thymus are called natural regulatory T cells, on the other hand, regulatory T cells induced from naive CD4 T cells are called adaptive (or induced) regulatory T cells (Bluestone & Abbas, 2003). Natural regulatory T cells typically make up around 10-15% of the total CD4 T cell population in circulation in humans (Janeway *et al.*, 2001). They are identified by expression of the α chain of the IL-2 receptor (CD25), as well as the transcription factor Foxp3 (Janeway *et al.*, 2001). In contrast to non-activated lymphocytes, peripheral maintenance of the regulatory T cell population requires IL-2 (Shen *et al.*, 2013). It has been established that CD25 is expressed constitutively by resting regulatory T cells, whereas other lymphocytes express CD25 following recognition of antigen through the TCR (Malek *et al.*, 2002). Regulatory T cells have evolved to suppress the effector activity of other lymphocytes. They are critical to the control of many autoimmune diseases, indeed, it has been shown that removal of the regulatory T cell population induces severe autoimmunity in mouse models (Janeway *et al.*, 2001; Sakaguchi, 2004). In contrast, it has been demonstrated that they suppress other, beneficial immune responses, such as the removal of tumours (Antony *et al.*, 2005; Belkaid & Rouse, 2005).
The mechanisms by which regulatory T cells inhibit the effector activity of activated lymphocytes are unclear. It is largely accepted that suppression is contact dependent (interaction between the regulatory T cell and the activated lymphocyte), furthermore this contact may require the interaction to be mediated at binding sites on antigen presenting cells (León *et al.*, 2000). However, regulatory T cells may also secrete IL-10 and TGF-β, which inhibit the activation and proliferation of activated lymphocytes (Janeway *et al.*, 2001).

1.2.7 Memory T cells

Following an immune response and the elimination of a pathogen, most effector T cells are lost through apoptosis. This loss ensures effector responses, which may have detrimental effects on the tissue near an infection site, are not mediated unnecessarily. Whilst the frequency of surviving effector T cells is unclear, and likely pathogen specific, it has been estimated that more than 95% of the effector population is lost following the response (Janeway *et al.*, 2001). The remaining T cells are called memory T cells.

Memory T cells retain some of the characteristic markers of effector T cells such as CD44, whilst down-regulating others such as CD69 (Janeway *et al.*, 2001). Furthermore, they are characterised by two subclasses, termed central memory and effector memory. Central memory T cells are phenotypically similar to naive T cells in that they are found in the peripheral lymphoid tissues and are relatively slower than effector memory to respond to antigen derived signalling. Effector memory T cells are phenotypically similar to effector T cells in that they are quick to respond to infection. The distinction between central and effector memory is likely a simplification of a heterogeneous population of cells.

An antigen specific memory T cell population is typically 100-1000 fold bigger than the naive population from which it was generated (Janeway *et al.*, 2001). Survival of memory T cells largely requires IL-7 for CD4 memory. On the other hand, IL-15 is critical for CD8 memory. Recognition of sp:MHC via the TCR is apparently less important for memory T cells than it is for the naive population (Janeway *et al.*, 2001).

Primary infection by a pathogen canonically results in the generation of a memory T cell population specific for the pathogen. Upon secondary infection, which can occur years later, the memory population will respond to the invading pathogen. This response is typically faster than the response of a naive population, which results in the pathogen being removed or suppressed more efficiently. In conjunction, the severity of disease resulting from the pathogen is often reduced. The aim of vaccinations (offered for example, by the National Health Service in the UK) is to generate a memory T cell population for specific diseases.

1.3 Objectives of this thesis

In this study our aims are to develop mathematical models of T cell homeostasis. Such models are developed to offer further insight into the balance between thymic output, peripheral survival and peripheral division in maintaining a peripheral T cell population. We begin, in Chapter 2, by recapping the mathematical theory behind the modelling approaches we take in later chapters. In Chapter 3 we introduce deterministic mathematical approaches to modelling a population of naive T cells in the periphery. The first model in this chapter is a simple description of the dynamics of the naive T cell population, the limitations of this model are discussed. We next present examples of approaches which have been taken in the literature to improve the simple description. We finish this chapter by introducing a model describing naive T cell homeostasis in which we encode, in a mechanistic manner, naive T cell requirement for IL-7.

In Chapter 4 we consider a single naive T cell suspended in a medium of soluble IL-7. We present a stochastic model describing IL-7 receptor dynamics during binding of IL-7 to the IL-7 receptor. We introduce a variable to quantify the amount of IL-7 induced signal. This variable is used to determine whether a cell survives or divides for a given amount of IL-7. We conclude the chapter with the derivation of a relationship between the concentration of IL-7 in the extra-cellular medium to the amount of IL-7 induced signal inside the cell. This signalling relation is then used to refine the resource model presented in Section 3.3.

In Chapter 5 we introduce and analyse the refined model. The model is fitted to experimental data obtained from studies of lymphopenia induced proliferation in mice (Hogan *et al.*, 2013). In doing so we estimate the parameters of the model, from which the numerical model behaviour is analysed and discussed. The model is also presented in the context of the human periphery. Taking into account involution of the human thymus (Aspinall & Andrew, 2000), we analyse the human model and compare it with clinical observations.

Somewhat separate from the preceding chapters, in Chapter 6 we introduce a stochastic model of the peripheral $CD4^+$ T cell population in which is included sub-populations of naive, IL-2 producing, IL-2 non-producing and regulatory T cells. In this chapter we focus on the population dynamics between the effector and regulatory T cell populations, which behave similarly to a predator-prey system. The model presented in this chapter is a stochastic reformulation of an earlier model pub-

lished to describe a quorum-sensing mechanism for $CD4^+$ T cells (Almeida *et al.*, 2012). This chapter was published in reference (Reynolds *et al.*, 2013a).
Finally, in Chapter 7 we present some concluding remarks to the study.

Chapter 2

Mathematical summary

In Chapters 3 and 5, we introduce mathematical models formulated as systems of ordinary differential equations (ODEs). The reader is assumed to be familiar with the concept of an ODE, however in Section 2.1, we review the requirements for asymptotic stability of stationary solutions of systems of ODEs. In Chapters 4 and 6, we formulate models as continuous time Markov processes; in particular, we shall work with birth and death processes defined on multidimensional lattices. In Section 2.2 we review basic concepts in probability, define a stochastic process and introduce the birth and death process.

2.1 Stability of steady-state solutions of ODEs

In Section 2.1.1 we present the requirements for asymptotic stability of steady-state solutions of systems of ODEs. In Section 2.1.2, we introduce a convenient method for evaluating the conditions for stability.

2.1.1 Linear stability approximation

Let $\boldsymbol{x}(t)$ be a vector of deterministic trajectories defined on $\mathbb{R}^n$. Consider the system of ordinary differential equations

$$\frac{\mathrm{d}\boldsymbol{x}(t)}{\mathrm{d}t} = f(\boldsymbol{x}(t); t), \quad \boldsymbol{x}(0) = \boldsymbol{x}_0. \tag{2.1}$$

In this thesis, we shall interchangeably refer to solutions $\boldsymbol{x}_s$ which satisfy $f(\boldsymbol{x}_s) = 0$, as either *stationary solutions*, *steady-state solutions*, *equilibrium solutions* or *fixed-point solutions*. We derive the requirements for asymptotic stability of stationary

solutions $\boldsymbol{x}_s$. First, we linearise the system about the stationary solution $\boldsymbol{x}_s$. Define a change of variables

$$\boldsymbol{y}(t) = \boldsymbol{x}(t) - \boldsymbol{x}_s, \tag{2.2}$$

where $\boldsymbol{y}(t)$ is defined on $\mathbb{R}^n$. A Taylor expansion of the function f about the steady-state solution $\boldsymbol{x}_s$, retaining only linear terms gives

$$\begin{aligned} f(\boldsymbol{x}(t)) &\approx f(\boldsymbol{x}_s) + \left.\frac{\mathrm{d}f(\boldsymbol{x})}{\mathrm{d}\boldsymbol{x}}\right|_{\boldsymbol{x}=\boldsymbol{x}_s} (\boldsymbol{x}(t) - \boldsymbol{x}_s), \\ &= A\boldsymbol{y}(t), \end{aligned} \tag{2.3}$$

where A is the Jacobian of the function f evaluated at the vector of stationary solutions $\boldsymbol{x}_s$. By construction, the derivatives of $\boldsymbol{x}$ and $\boldsymbol{y}$, are equal,

$$\frac{\mathrm{d}\boldsymbol{x}(t)}{\mathrm{d}t} = \frac{\mathrm{d}\boldsymbol{y}(t)}{\mathrm{d}t}. \tag{2.4}$$

Therefore, the linearised set of equations is

$$\frac{\mathrm{d}\boldsymbol{y}(t)}{\mathrm{d}t} = A\boldsymbol{y}(t). \tag{2.5}$$

This system of linear, homogeneous, ODEs has solution (Perko, 1991)

$$\boldsymbol{y}(t) = \boldsymbol{y}_0 \mathrm{e}^{At}, \tag{2.6}$$

for initial condition $\boldsymbol{y}(0) = \boldsymbol{y}_0$. The system exhibits stationary solutions, if and only if, all eigenvalues of A are negative, $\lambda_1, \lambda_2, \ldots, \lambda_n < 0$ (Coddington & Levinson, 1955). In the case that any of the eigenvalues λ_i are complex, we require the real part of λ_i to be negative. If such a condition is met, then the solution $\boldsymbol{x}(t)$ converges to the steady-state solution $\boldsymbol{x}_s$ in some neighbourhood about $\boldsymbol{x}_s$.

If f is linear in $\boldsymbol{x}$, then the Taylor expansion of f in equation (2.3) is exact. For a linear system, if a steady-state solution is stable, it is also globally stable. Global stability implies that deterministic trajectories will converge to the steady-state solution from any given initial condition. In general this is not true, deterministic trajectories will converge to a stable steady-state solution in some neighbourhood about the solution.

2.1.2 Routh-Hurwitz criterion

Let A be the Jacobian of the function f in equation (2.1), evaluated at the steady-state solution $\boldsymbol{x}_s$. Let the characteristic polynomial of the matrix A be

$$\lambda^k + a_1\lambda^{k-1} + \ldots + a_k = 0. \tag{2.7}$$

We define the following matrices, usually referred to as Hurwitz matrices (Gantmakher, 2005)

$$\begin{aligned} H_1 &= (a_1); & H_2 &= \begin{pmatrix} a_1 & 1 \\ a_3 & a_2 \end{pmatrix}; \\ H_3 &= \begin{pmatrix} a_1 & 1 & 0 \\ a_3 & a_2 & a_1 \\ a_5 & a_4 & a_3 \end{pmatrix}; & H_k &= \begin{pmatrix} a_1 & 1 & 0 & \ldots & 0 \\ a_3 & a_2 & a_1 & \ldots & 0 \\ \vdots & \vdots & \vdots & \vdots & \vdots \\ 0 & 0 & 0 & \ldots & a_k \end{pmatrix}. \end{aligned} \tag{2.8}$$

For the characteristic polynomial above, all solutions λ satisfy $Re(\lambda) < 0$, if and only if, $det(H_j) \geq 0$ for all $j = 1, 2, \ldots, k$ (Hurwitz, 1964). In practice, for polynomials of order 2, $\lambda^2 + a_1\lambda + a_2$, these conditions are met if both a_1 and a_2 are positive. For third order polynomials, $\lambda^3 + a_1\lambda^2 + a_2\lambda + a_3$, stability is ensured if $a_n > 0$, $n = 1, 2, 3$, and $a_1 a_2 > a_3$.

2.2 Probability review

In this section, we review basic concepts in the theory of probability. The introductory material primarily follows that published in reference (DeGroot & Schervish, 2002).

2.2.1 State space and outcomes

The collection of all possible outcomes of an experiment is called the *state space* or *sample space*. Let the number of distinct outcomes of an experiment be N. We note that N may be infinite. Mathematically, the state space, $\mathcal{S}$, is the set of all possible disjoint outcomes, s, of an experiment. We express $\mathcal{S}$ as the union of all possible

outcomes s,

$$\mathcal{S} = \bigcup_{i}^{N} s_i. \tag{2.9}$$

2.2.2 Events of an experiment

An event, $\mathcal{A}$, of an experiment, is a collection of outcomes, s_i, $i = 1, 2, \ldots$, of the state space $\mathcal{S}$. An event $\mathcal{A}$ is defined to be a subset of $\mathcal{S}$, $\mathcal{A} \subset \mathcal{S}$. Each event $\mathcal{A}$ is a union of one or more outcomes $s_i \in \mathcal{S}$, $i = 1, 2, \ldots$. The probability of an event $\mathcal{A}$ is a positive number, $\Pr(\mathcal{A})$, which quantitatively describes the chance that the event $\mathcal{A}$ will occur.

2.2.3 The axioms of probability

The probabilities of events, $\Pr(\mathcal{A})$, satisfy the following three axioms of probability (DeGroot & Schervish, 2002):

1. The first axiom states that the probability of any event $\mathcal{A}$, is positive,

$$\Pr(\mathcal{A}) \geq 0, \quad \text{for all } \mathcal{A} \subset \mathcal{S}. \tag{2.10}$$

2. The second axiom states that the probability of events guaranteed to occur is one. Since $\mathcal{S}$ is the collection of all outcomes, we may formally write,

$$\Pr(\mathcal{S}) = 1. \tag{2.11}$$

3. Let $\mathcal{A}_i$, $i = 1, 2, \ldots$, be a finite or countably infinite set of disjoint events. Disjoint implies that for any two events $\mathcal{A}_i$, $\mathcal{A}_j$, the intersection between events is equal to the empty set, $\mathcal{A}_i \cap \mathcal{A}_j = \phi$, $i \neq j$. The third axiom states that the probability of a union of disjoint events is equal to the sum of the probabilities of each individual event,

$$\Pr\left(\bigcup_{i=1}^{\infty} \mathcal{A}_i\right) = \sum_{i=1}^{\infty} \Pr(\mathcal{A}_i). \tag{2.12}$$

In this thesis we also use the notation $\text{Prob}\{\bullet\}$ to denote the probability of the event inside the parentheses occurring. That is,

$$\Pr(\mathcal{A}) = \text{Prob}\{\text{Event } \mathcal{A} \text{ has occurred}\}. \tag{2.13}$$

2.2.4 Law of total probability

Let $\mathcal{S}$ be the sample space of an experiment and let $\{s_i : i = 1, 2, \ldots\}$ be a finite or countably infinite partition of the sample space, as expressed by equation (2.9). The law of total probability proposes that

$$\Pr(\mathcal{A}) = \sum_i \Pr(\mathcal{A} \text{ and } \mathcal{B}_i), \tag{2.14}$$

where $\Pr(\mathcal{A}$ and $\mathcal{B}_i)$ is the probability that events $\mathcal{A}$ and $\mathcal{B}_i$, $i = 1, 2, \ldots$, both occur.

2.2.5 Conditional probability

Suppose two events may occur in which the outcome of the first event affects the chances of the second event occurring. We say that the two events are dependent. Let the first event be $\mathcal{A}$ and the second event be $\mathcal{B}$, the probability that event $\mathcal{A}$ occurs, given that event $\mathcal{B}$ has occurred is called a *conditional probability of* $\mathcal{A}$ *given* $\mathcal{B}$, and is defined (DeGroot & Schervish, 2002)

$$\Pr(\mathcal{A} \mid \mathcal{B}) = \frac{\Pr(\mathcal{A} \text{ and } \mathcal{B})}{\Pr(\mathcal{B})}. \tag{2.15}$$

If two events $\mathcal{A}$ and $\mathcal{B}$ are *independent*, that is, the occurrence of one event does not change the probability of the second event occurring, then $\Pr(\mathcal{A}$ and $\mathcal{B}) = \Pr(\mathcal{A})\Pr(\mathcal{B})$. In this case, $\Pr(\mathcal{A} \mid \mathcal{B}) = \Pr(\mathcal{A})$.

2.2.6 Probability space

A *probability space* $(\Omega, \mathcal{F}, \mathcal{P})$ is a mathematical triplet built with the intention of quantifying random phenomena. A probability space is constructed of three components.

- The sample space is denoted by Ω and is the collection of all possible outcomes.
- $\mathcal{F}$ is the set of all possible events (collection of outcomes), consisting of zero or more elements of Ω.
- $\mathcal{P}$ is a function which assigns a probability to each event, $\mathcal{A} \in \mathcal{F}$.

2.2.7 Random variables

A *random variable* is a function $\mathbb{X} : \Omega \to \mathbb{R}$ such that for all $a \in \mathbb{R}$, the event $\{\mathbb{X} \leq a\} = \{\omega; \mathbb{X}(\omega) \leq a\}$ for $\omega \in \Omega$. It can be assigned a probability, that is (Bremaud, 1999),

$$\{\mathbb{X} \leq a\} \in \mathcal{F}. \tag{2.16}$$

In this definition, Ω is the sample space of the probability space, ω is an outcome in the sample space, and $\mathcal{F}$ is the collection of all possible events. Suppose now we define $\mathbb{X} : \Omega \to \mathcal{D}$ where $\mathcal{D}$ is a denumerable set. Then $\mathbb{X}$ is said to be a *discrete random variable* where for all $x \in \mathcal{D}$

$$\{\mathbb{X} = x\} \in \mathcal{F}. \tag{2.17}$$

Random variables for which the output is a real value are usually referred to as being *continuous*. The set $\mathbb{R}$ (in the discrete case, $\mathcal{D}$) is called the *state space* of the random variable (DeGroot & Schervish, 2002).

Example Consider an experiment in which two 6-sided dice are thrown, after which, the sum of both upturned faces is recorded. The sample space is the set of all pairs $\{i, j\}$ where $i, j \in \{1, 2, \ldots, 6\}$. All possible events in $\mathcal{F}$, with the respective assigned probabilities, are shown in the table below.

$A \in \mathcal{F}$	2	3	4	5	6	7	8	9	10	11	12
$\mathcal{P}(A \in \mathcal{F})$	1/36	1/18	1/12	1/9	5/36	1/6	5/36	1/9	1/12	1/18	1/36

In this example our discrete random variable takes the outcome $\{i, j\}$, $i, j \in \{1, 2, \ldots, 6\}$ and returns the event $i + j$.

2.2.8 Cumulative distribution function

Given a probability distribution defined over all possible outcomes of an experiment, we assign a probability for each value a random variable may take. Let A be some interval on the real line, and let ω be one of possibly many distinct outcomes in the sample space, such that, for a random variable $\mathbb{X}$, we have $\mathbb{X}(\omega) \in A$. Then

$$\Pr(\mathbb{X} \in A) = \sum_{\omega} \Pr(\omega : \mathbb{X}(\omega) \in A). \tag{2.18}$$

In the case that the random variable has a discrete state space, let A be some value in state space of the random variable. Let ω be one of, possibly many, distinct outcomes in the sample space, such that, $\mathbb{X}(\omega) = A$. We define

$$\Pr(\mathbb{X} = A) = \sum_{\omega} \Pr(\omega : \mathbb{X}(\omega) = A). \tag{2.19}$$

Let x denote the upper boundary of the semi-closed interval $(-\infty, x]$ on the real line. The *cumulative distribution function* of a random variable $\mathbb{X}$, with continuous state space, is the function

$$F_{\mathbb{X}}(x) = \Pr(\mathbb{X} \leq x). \tag{2.20}$$

In the discrete case, let x_i, $i = 1, \ldots, n$, be n (n may be countably infinite) ordered elements of the state space of a random variable $\mathbb{X}$, with $x = \sup\{x_1, x_2, \ldots\}$. The discrete cumulative density function (CDF), is given by

$$F_{\mathbb{X}}(x) = \sum_{i=1}^{n} \Pr(\mathbb{X} = x_i). \tag{2.21}$$

Example Consider again the experiment in which two dice are thrown and the sum of the upturned face values is recorded. Let A be the event that the value observed is 4. The three outcomes ω which give this value are $\{1, 3\}$, $\{2, 2\}$ and $\{3, 1\}$, each occurring with probability 1/36. The probability of observing 4 is 1/12 from equation (2.19). In Figure 2.1 we plot the CDF for this example as defined by (2.21).

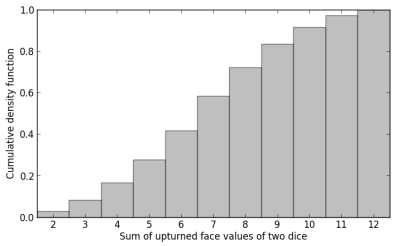

Figure 2.1: Cumulative density function for the sum of upturned face values of two dice.

2.2.9 Probability distribution functions

The *probability density function* (PDF) of the continuous random variable $\mathbb{X}$, is the integrable function $f_{\mathbb{X}} : \mathbb{R} \to [0, 1]$, such that

$$F_{\mathbb{X}}(x) = \int_{-\infty}^{x} f_{\mathbb{X}}(y)\, \mathrm{d}y, \tag{2.22}$$

where $F_{\mathbb{X}}(x)$ is the cumulative density function of $\mathbb{X}$. The PDF, $f_{\mathbb{X}}(x)$, for any continuous random variable, satisfies

$$\int_{-\infty}^{\infty} f_{\mathbb{X}}(y)\, \mathrm{d}y = 1. \tag{2.23}$$

That is to say, the probability that the random variable takes some value is certain, i.e., the experiment is guaranteed to occur. The PDF of a random variable allows the computation (or specification) of probabilities of any event. Let $A = [a_1, a_2]$ be an event on the real line, then for a random variable $\mathbb{X} : \Omega \to \mathbb{R}$ with PDF $f_{\mathbb{X}}(x)$, the probability that $\mathbb{X} \in A$, is given by

$$\Pr(\mathbb{X} \in A) = \int_{a_1}^{a_2} f_{\mathbb{X}}(y)\, \mathrm{d}y. \tag{2.24}$$

The *probability mass function* (PMF) of a discrete random variable, $\mathbb{X}$, is the function

$$f_{\mathbb{X}}(x) = \Pr(\mathbb{X} = x). \tag{2.25}$$

Let $\mathcal{S}$ be the set of distinct values $\mathbb{X}$ may take, then the PMF satisfies

$$\sum_{x \in \mathcal{S}} f_{\mathbb{X}}(x) = 1. \tag{2.26}$$

Example For the example in which two dice are thrown, the PMF for the sum of upturned faces is given in Figure 2.2.

2.2.10 Expectation

The *expectation* of a continuous random variable corresponds, in an intuitive sense, to the average value one would expect to observe if an experiment is repeated a large number of times. The expectation of a random variable $\mathbb{X}$, with PDF $f_{\mathbb{X}}(x)$,

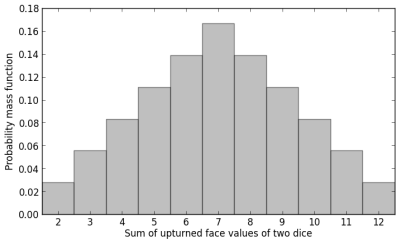

Figure 2.2: Probability mass function for the sum of upturned face value of two thrown dice.

is defined (DeGroot & Schervish, 2002)

$$\mathbb{E}[\mathbb{X}] = \int_{-\infty}^{\infty} y f_{\mathbb{X}}(y)\ \mathrm{d}y. \tag{2.27}$$

More generally, the expected value of a measurable function of a random variable, $g(\mathbb{X})$, is defined as,

$$\mathbb{E}[g(\mathbb{X})] = \int_{-\infty}^{\infty} g(y) f_{\mathbb{X}}(y)\ \mathrm{d}y. \tag{2.28}$$

For a discrete random variable $\mathbb{X}$, taking values in $\mathcal{S}$, the expected value of a measurable function of the random variable, $g(\mathbb{X})$, is defined as

$$\mathbb{E}[g(\mathbb{X})] = \sum_{x \in \mathcal{S}} g(x) f_{\mathbb{X}}(x). \tag{2.29}$$

2.2.11 Moments

The *moment* of a random variable $\mathbb{X}$, is a quantitative measure of some "feature" of the random variable's probability distribution. For example, the first moment of a random variable is the *mean*, which corresponds to the "centre" of the probability distribution. The second moment of a random variable is the *variance*, which characterises the "width" of the random variable's probability distribution. Higher moments characterise further descriptions of the shape of a random variable's probability distribution, such as for example how symmetric the distribution is, more commonly known as *skewness* (Ziegel, 2002).
The kth moment about c of a random variable $\mathbb{X}$, with PDF $f_{\mathbb{X}}(x)$, is defined as

$$m^{(k)} = \mathbb{E}[(\mathbb{X} - c)^k] = \int_{-\infty}^{\infty} (y - c)^k f_{\mathbb{X}}(y)\ \mathrm{d}y. \tag{2.30}$$

For a discrete random variable $\mathbb{X}$ taking values in $\mathcal{S}$, with PMF $f_{\mathbb{X}}(x)$, the kth

moment about c is defined as

$$m^{(k)} = \mathbb{E}[(\mathbb{X} - c)^k] = \sum_{x \in \mathcal{S}} (x - c)^k f_{\mathbb{X}}(x). \tag{2.31}$$

In the case that $c = 0$, the moment is referred to as the *uncentred* or *raw* moment of the random variable. In the case that $c = \mu = \mathbb{E}[\mathbb{X}]$, the moment is referred to as the *central moment* or the *moment of* $\mathbb{X}$ *about the mean*. For example, the variance, σ^2, of a random variable $\mathbb{X}$ is the second central moment,

$$\sigma^2 = \mathbb{V}[\mathbb{X}] = \mathbb{E}[(\mathbb{X} - \mu)^2] \tag{2.32}$$

A useful relation derived directly from (2.32), in both the continuous and discrete case, is

$$\sigma^2 = \mathbb{E}[\mathbb{X}^2] - (\mathbb{E}[\mathbb{X}])^2. \tag{2.33}$$

Example Let us return to our example in which two dice are thrown and the sum of upturned face values is recorded. The mean is 7 and the variance is 35/6.

2.2.12 Generating functions

Generating functions provide an alternative representation of a random variable's probability distribution. They provide convenient methods for investigating various properties of random variables, such as the probability of a random variable taking a particular value or deriving the moments of a random variable.

Probability generating functions

The *probability generating function* (PGF) of a random variable $\mathbb{X}$ is defined

$$G(z) = \mathbb{E}[z^{\mathbb{X}}] = \begin{cases} \displaystyle\int_{-\infty}^{\infty} z^y f_{\mathbb{X}}(y)\, \mathrm{d}y, & \text{if } \mathbb{X} \text{ is continuous,} \\ \displaystyle\sum_{x \in \mathcal{S}} z^x f_{\mathbb{X}}(x), & \text{if } \mathbb{X} \text{ is discrete.} \end{cases} \tag{2.34}$$

If the PGF of a random variable $\mathbb{X}$ is known, one can recover the probability distribution of the random variable. Taking repeated derivatives of G with respect to z,

we find

$$\frac{\mathrm{d}^k G(z)}{\mathrm{d}z^k} \stackrel{\text{def}}{=} G^{(k)}(z) = \begin{cases} \displaystyle\int_{-\infty}^{\infty} \frac{y!}{(y-k)!} z^{y-k} f_{\mathbb{X}}(y)\, \mathrm{d}y, & \text{if } \mathbb{X} \text{ is continuous,} \\ \displaystyle\sum_{x \in \mathcal{S}} \frac{y!}{(y-k)!} z^{y-k} f_{\mathbb{X}}(x), & \text{if } \mathbb{X} \text{ is discrete.} \end{cases} \tag{2.35}$$

Evaluating the derivatives of G at $z = 0$ and dividing the resulting expressions by $k!$, we find

$$\frac{G^{(k)}(0)}{k!} = \begin{cases} \displaystyle\frac{1}{k!} \int_{-\infty}^{\infty} \frac{y!}{(y-k)!} f_{\mathbb{X}}(y) \delta(y-k)\, \mathrm{d}y = f_{\mathbb{X}}(k), & \text{if } \mathbb{X} \text{ is continuous,} \\ \displaystyle\frac{k!}{(k-k)!} f_{\mathbb{X}}(k) = f_{\mathbb{X}}(k) & \text{if, } \mathbb{X} \text{ is discrete,} \end{cases} \tag{2.36}$$

where $\delta(y-k)$ is the Dirac delta function (Dirac, 1947).

Moment generating functions

The *moment generating function* (MGF) of a random variable $\mathbb{X}$ is defined

$$M(t) = \mathbb{E}[\mathrm{e}^{t\mathbb{X}}] = \begin{cases} \displaystyle\int_{-\infty}^{\infty} \mathrm{e}^{ty} f_{\mathbb{X}}(y)\, \mathrm{d}y, & \text{if } \mathbb{X} \text{ is continuous,} \\ \displaystyle\sum_{x \in \mathcal{S}} \mathrm{e}^{tx} f_{\mathbb{X}}(x), & \text{if } \mathbb{X} \text{ is discrete.} \end{cases} \tag{2.37}$$

The MGF allows immediate computation of the moments of a random variable. Taking the derivatives of M we have

$$\frac{\mathrm{d}^k M(t)}{\mathrm{d}t^k} \stackrel{\text{def}}{=} M^{(k)}(t) = \begin{cases} \displaystyle\int_{-\infty}^{\infty} y^k \mathrm{e}^{ty} f_{\mathbb{X}}(y)\, \mathrm{d}y, & \text{if } \mathbb{X} \text{ is continuous,} \\ \displaystyle\sum_{x \in \mathcal{S}} x^k \mathrm{e}^{tx} f_{\mathbb{X}}(x), & \text{if } \mathbb{X} \text{ is discrete.} \end{cases} \tag{2.38}$$

Evaluating the derivatives of the moment generating function at $t = 0$, we derive

$$M^{(k)}(0) = \begin{cases} \displaystyle\int_{-\infty}^{\infty} y^k f_{\mathbb{X}}(y)\, \mathrm{d}y = m^{(k)}, & \text{if } \mathbb{X} \text{ is continuous,} \\ \displaystyle\sum_{x \in \mathcal{S}} x^k f_{\mathbb{X}}(x) = m^{(k)}, & \text{if } \mathbb{X} \text{ is discrete,} \end{cases} \tag{2.39}$$

where $m^{(k)}$ are the kth raw moments of the random variable $\mathbb{X}$.

2.2.13 Common probability distributions

Exponential distribution

The probability density function of an *exponentially distributed* random variable $\mathbb{X}$ is

$$f_{\mathbb{X}}(x;\lambda) = \begin{cases} \lambda \mathrm{e}^{-\lambda x} & \text{if } x \geq 0, \\ 0 & \text{if } x < 0. \end{cases} \tag{2.40}$$

A random variable with an exponential PDF has mean λ^{-1} and variance λ^{-2}.

Normal distribution

A *normally distributed* random variable $\mathbb{X}$ has probability density function

$$f_{\mathbb{X}}(x;\mu,\sigma^2) = \frac{1}{\sqrt{2\pi\sigma^2}} \mathrm{e}^{-\frac{(x-\mu)^2}{2\sigma^2}}. \tag{2.41}$$

The parameters μ and σ^2 are respectively the mean and variance of the normally distributed random variable $\mathbb{X}$.

Log-normal distribution

The probability density function of a *log-normally distributed* random variable is

$$f_{\mathbb{X}}(x;\mu,\sigma^2) = \begin{cases} \dfrac{1}{x\sqrt{2\pi\sigma^2}} \mathrm{e}^{-\frac{(\log x-\mu)^2}{2\sigma^2}} & \text{if } x > 0, \\ 0 & \text{if } x \leq 0. \end{cases} \tag{2.42}$$

The mean and variance of a random variable with log-normal PDF are respectively,

$$\mathbb{E}[\mathbb{X}] = \mathrm{e}^{\mu+\frac{1}{2}\sigma^2}, \tag{2.43}$$

$$\mathbb{V}[\mathbb{X}] = (\mathrm{e}^{\sigma^2}-1)\mathrm{e}^{2\mu+\sigma^2}. \tag{2.44}$$

2.3 Stochastic processes

2.3.1 Stochastic process

A *stochastic process* is a family of random variables $\{\mathbb{X}(t)\colon t \in \mathcal{T}\}$, taking values in a common sample space, $\mathcal{S}$ (Allen, 2003). Stochastic processes are the probabilistic counterpart to deterministic processes, such as the time evolution of the solutions of ordinary differential equations. In the stochastic models introduced in this thesis, the index set $\mathcal{T}$, represents time. We only deal with stochastic processes with discrete sample spaces. Typically, random variables in this thesis represent some discrete measurable quantity, such as the number of cells in a population, or the number of receptors on the surface of a cell. Such stochastic processes are said to be *continuous in time* and *discrete in space*.

2.3.2 Markov chains

The following definition is taken directly from reference (Allen, 2003). The stochastic process $\{\mathbb{X}(t)\}$, $t \in [0, \infty)$, is called a *continuous time Markov chain*, if it satisfies the following condition: for any sequence of real numbers satisfying $0 \leq t_0 \leq t_1 \leq \ldots \leq t_n \leq t_{n+1}$,

$$\begin{aligned} &\text{Prob}\{\mathbb{X}(t_{n+1}) = i_{n+1} \mid \mathbb{X}(t_0) = i_0, \mathbb{X}(t_1) = i_1, \ldots, \mathbb{X}(t_n) = i_n\} \\ =&\text{Prob}\{\mathbb{X}(t_{n+1}) = i_{n+1} \mid \mathbb{X}(t_n) = i_n\}. \end{aligned} \tag{2.45}$$

Loosely speaking: this definition guarantees that the state of a stochastic process, in the immediate future, depends only on the state of the process in the present. All past information about the process is forgotten. This condition is called the *Markov property*. Stochastic processes with this property are often referred to as being *memoryless*. All the stochastic processes introduced in this thesis are memoryless.

State probabilities

Each random variable of a stochastic process $\{\mathbb{X}(t)\}$, $t \in [0, \infty)$, which takes values on the set of natural numbers (including zero), $\mathcal{S} = \mathbb{N}_0$, has an associated probability distribution $\{p_n(t)\}_{n=0}^{\infty}$, where

$$p_n(t) = \text{Prob}\{\mathbb{X}(t) = n\}. \tag{2.46}$$

Each *state probability*, $p_n(t)$, gives the probability that the process is in the state n at time t.

Transition probabilities

Let $t_1 < t_2$ be two different times in $\mathcal{T}$. The *transition probabilities* relate the random variables $\mathbb{X}(t_1)$ and $\mathbb{X}(t_2)$. Define

$$p_{j,i}(t_1, t_2) = \text{Prob}\{\mathbb{X}(t_2) = j \mid \mathbb{X}(t_1) = i\}, \tag{2.47}$$

for all $i, j \in \mathcal{S}$. In this thesis, all transition probabilities depend only on the difference between t_1 and t_2. Such stochastic processes are said to be *stationary* or *homogeneous*. Let $t_2 - t_1 = \tau$ be some time interval, then

$$p_{j,i}(\tau) = \text{Prob}\{\mathbb{X}(t_2) = j \mid \mathbb{X}(t_1) = i\} = \text{Prob}\{\mathbb{X}(\tau) = j \mid \mathbb{X}(0) = i\}. \tag{2.48}$$

The *transition rates* for a stochastic process are defined (Allen, 2003)

$$q_{j,i} = \begin{cases} \lim_{\Delta t \to 0^+} \dfrac{p_{j,i}(\Delta t)}{\Delta t}, & \text{if } i \neq j, \\ \lim_{\Delta t \to 0^+} \dfrac{p_{j,i}(\Delta t) - 1}{\Delta t}, & \text{if } i = j. \end{cases} \tag{2.49}$$

2.3.3 Chapman-Kolmogorov equations

The *Chapman-Kolmogorov* equations for a continuous time stochastic process are (Allen, 2003; Bremaud, 1999)

$$p_{j,i}(t + \Delta t) = \sum_{k=0}^{\infty} p_{j,k}(\Delta t) p_{k,i}(t). \tag{2.50}$$

Intuitively, these equations can be thought of as expressing the probability of a stochastic process visiting state j, from state i, in time $t + \Delta t$, as equal to the sum of the probabilities for each possible path from i from j (via intermediate states k) in time Δt.

2.3.4 Birth and death processes

A specific type of continuous time Markov process, which we make use of in this thesis, is the *birth and death process*. In a birth and death process, the state space is a well ordered set, typically the set of positive integers, including zero. Transitions in

a birth and death process are only permitted between adjacent states. For example, in a one-dimensional process, the stochastic process can only increase, or decrease, by one unit during any jump of the process. Define the state space $\mathcal{S}$ to be the set of positive integers including zero ($\mathcal{S}$ may also be finite with largest state N). Then a stochastic process $\{\mathbb{X}(t)\}$, $t \in [0, \infty)$, with transition probabilities defined as

$$\begin{aligned} p_{j,i}(\Delta t) &= \text{Prob}\{\mathbb{X}(t+\Delta t) = j \mid \mathbb{X}(t) = i\} \\ &= \begin{cases} \lambda_i \Delta t + o(\Delta t), & \text{if } j = i+1, \\ \mu_i \Delta t + o(\Delta), & \text{if } j = i-1, \\ 1 - (\lambda_i + \mu_i)\Delta t + o(\Delta t), & \text{if } j = i, \\ o(\Delta t), & \text{if } j \neq -1, 0, 1, \end{cases} \end{aligned} \tag{2.51}$$

is called a birth and death process. The notation $o(\bullet)$ is the Landau order symbol. For a function f, we say $f(\Delta t) = o(\Delta t)$ if, as $\Delta t \to 0^+$, f satisfies

$$\lim_{\Delta t \to 0^+} \frac{f(\Delta t)}{\Delta t} = 0. \tag{2.52}$$

The corresponding transition rates for a birth and death process are then

$$q_{j,i} = \begin{cases} \lambda_i, & \text{if } j = i+1, \\ \mu_i, & \text{if } j = i-1, \\ -(\lambda_i + \mu_i), & \text{if } j = i, \\ 0, & \text{if } j \neq -1, 0, 1, \end{cases} \tag{2.53}$$

The Chapman-Kolmogorov equations for a birth and death process are

$$\begin{aligned} p_{j,i}(t+\Delta t) &= p_{j-1,i}(t)[\lambda_{j-1}\Delta t + o(\Delta t)] + p_{j+1,i}(t)[\mu_{j+1}\Delta t + o(\Delta t)] \\ &\quad + p_{j,i}(t)[1 - (\lambda_j + \mu_j)\Delta t + o(\Delta t)] + \sum_{k \neq j-1, j, j+1} p_{k,i}(t) o(\Delta t). \end{aligned} \tag{2.54}$$

Dividing by Δt and taking the limit $\Delta t \to 0^+$, we derive

$$\frac{\mathrm{d}p_{j,i}(t)}{\mathrm{d}t} = p_{j-1,i}(t)\lambda_{j-1} + p_{j+1,i}(t)\mu_{j+1} - p_{j,i}(t)(\lambda_j + \mu_j). \tag{2.55}$$

Let us assume the initial state of the process is fixed in the state x_0, such that $\text{Prob}\{\mathbb{X}(0) = x_0\} = 1$. From the law of total probability and the definition of conditional probability, we may express the state probabilities as

$$\begin{aligned} p_n(t) = \text{Prob}\{\mathbb{X}(t) = n\} &= \sum_k \text{Prob}\{\mathbb{X}(t) = n \text{ and } \mathbb{X}(0) = k\} \\ &= \text{Prob}\{\mathbb{X}(t) = n \text{ and } \mathbb{X}(0) = x_0\} \\ &= \text{Prob}\{\mathbb{X}(t) = n \mid \mathbb{X}(0) = x_0\}\text{Prob}\{\mathbb{X}(0) = x_0\} \\ &= \text{Prob}\{\mathbb{X}(t) = n \mid \mathbb{X}(0) = x_0\} = p_{n,x_0}(t). \end{aligned} \tag{2.56}$$

It therefore follows from (2.55), that the state probabilities satisfy

$$\frac{\mathrm{d}p_n(t)}{\mathrm{d}t} = p_{n-1}(t)\lambda_{n-1} + p_{n+1}(t)\mu_{n+1} - p_n(t)(\lambda_n + \mu_n). \tag{2.57}$$

The above equation is commonly referred to as the *master equation* for a birth and death process.

2.3.5 Inter-event times

Define the continuous random variable, $T > 0$, to be the time the process waits in the state n, before jumping to the next state. From the definition of the transition probabilities of a birth and death process, the probability that the process remains in the state n, after a small time Δt, is

$$p_{n,n}(\Delta t) = 1 - (\lambda_n + \mu_n)\Delta t + o(\Delta t). \tag{2.58}$$

Let $G(t)$ be the probability that the process remains in state n at time t, then

$$G(t) = \text{Prob}\{T > t\}. \tag{2.59}$$

From the condition $T > 0$, it follows that $G(0) = \text{Prob}\{T > 0\} = 1$. If Δt is sufficiently small then (Allen, 2003),

$$G(t + \Delta t) = G(t)[1 - (\lambda_n + \mu_n)\Delta t + o(\Delta t)]. \tag{2.60}$$

Dividing by Δt and letting $\Delta t \to 0^+$, we derive the differential equation

$$\frac{\mathrm{d}G(t)}{\mathrm{d}t} = -(\lambda_n + \mu_n)G(t), \quad G(0) = 1, \tag{2.61}$$

which has the specific solution

$$G(t) = \mathrm{e}^{-(\lambda_n+\mu_n)t}. \tag{2.62}$$

From the definition of G, it follows that

$$\mathrm{Prob}\{t \geq T\} = 1 - \mathrm{e}^{-(\lambda_n+\mu_n)t}. \tag{2.63}$$

This is the cumulative density function of an exponentially distributed random variable, T, whose probability distribution is specified by the parameter $\lambda_n + \mu_n$. Waiting times in a birth and death process are, therefore, exponentially distributed with mean $(\lambda_n + \mu_n)^{-1}$ and variance $(\lambda_n + \mu_n)^{-2}$.

2.3.6 The Gillespie algorithm

The *Gillespie algorithm* allows numerical simulations of stochastic processes with exponentially distributed waiting times (Gillespie, 1977). The algorithm follows the procedure given below:

- Define two counters to represent time, t, and the state of the process, n. Set $t = 0$ and $n = n_0$, where n_0 is the initial condition for the quantity of interest. Choose a time to end the process, T_{end}.
- Repeat the following sub-procedure until $t > T_{\mathrm{end}}$.
    1. Calculate the transition rate to each state that can be reached from n in a single jump. Let α be the sum of these transition rates.
    2. Draw a random time, τ, from an exponential distribution with parameter α^{-1}.
    3. Update time t, to $t + \tau$.
    4. Draw a uniformly distributed random number, r, from the interval $[0, \alpha]$.
    5. Partition the interval $[0, \alpha]$ by the relative size of each transition probability.
    6. Determine which sub-interval r falls within.

7. Update n based on the corresponding transition probability determined by r.
8. Record the time and state of the process as a pair, (t, n).

- Algorithm ends.

In practice, the Gillespie algorithm allows one to produce a vector, which has as components, the times at which the process undergoes a transition. A corresponding vector composed of the states of the process following each jump, is also produced.

2.3.7 A simple example of cellular division

Consider a single cell which undergoes repeated divisions. We assume the time each cell takes to divide, is exponentially distributed with parameter λ. This simple example is known as a birth process for which the transition probabilities are

$$\begin{aligned} p_{j,i}(\Delta t) &= \text{Prob}\{\mathbb{X}(t+\Delta t) = j \mid \mathbb{X}(t) = i\} \\ &= \begin{cases} \lambda i \Delta t + o(\Delta t), & \text{if } j = i+1 \\ 1 - \lambda i \Delta t + o(\Delta t), & \text{if } j = i \\ o(\Delta t), & \text{if } j \neq -1, 0, 1 \end{cases} \end{aligned} \tag{2.64}$$

The master equations for this process are

$$\frac{\mathrm{d}p_n(t)}{\mathrm{d}t} = p_{n-1}(t)\lambda(n-1) - p_n(t)\lambda n, \quad n \geq 1,\ p_n(0) = \delta_{n,1}, \tag{2.65}$$

where $\delta_{n,1}$ is the Kronecker delta[1]. Since this is a linear system of first order ODEs, there exists a unique solution (Coddington & Levinson, 1955). Furthermore, the specific solution given initial conditions, $p_n(0) = \delta_{n,1}$, is

$$p_n(t) = \sum_{k=0}^{n-1} (-1)^k \frac{(n-1)!}{k!(n-k)!} \mathrm{e}^{-\lambda(k+1)t}. \tag{2.67}$$

To verify this is indeed the unique solution, one may take the derivative of (2.67) and recover (2.65).

[1]The Kronecker delta function is defined

$$\delta_{i,j} = \begin{cases} 0 & \text{if } i \neq j, \\ 1 & \text{if } i = j. \end{cases} \tag{2.66}$$

Proof. Taking derivatives of (2.67) we have,

$$\begin{aligned}
\frac{\mathrm{d}p_n(t)}{\mathrm{d}t} =& -\lambda\sum_{k=0}^{n-1}(-1)^k\frac{(n-1)!}{k!(n-k-1)!}(k+1)\mathrm{e}^{-\lambda(k+1)t} \\
=&\lambda(n-1)p_{n-1}(t) - \lambda(n-1)p_{n-1}(t) - \lambda\sum_{k=0}^{n-1}(-1)^k\frac{(n-1)!}{k!(n-k-1)!}(k+1)\mathrm{e}^{-\lambda(k+1)t} \\
=&\lambda(n-1)p_{n-1}(t) - \lambda(n-1)\sum_{k=0}^{n-2}(-1)^k\frac{(n-2)!}{k!(n-k-2)!}(k+1)\mathrm{e}^{-\lambda(k+1)t} \\
&-\lambda\sum_{k=0}^{n-1}(-1)^k\frac{(n-1)!}{k!(n-k-1)!}(k+1)\mathrm{e}^{-\lambda(k+1)t} \\
=&\lambda(n-1)p_{n-1}(t) - \lambda\sum_{k=0}^{n-2}(-1)^k\frac{(n-1)!}{k!(n-k-1)!}(n-k-1)(k+1)\mathrm{e}^{-\lambda(k+1)t} \\
&-\lambda\sum_{k=0}^{n-1}(-1)^k\frac{(n-1)!}{k!(n-k-1)!}(k+1)\mathrm{e}^{-\lambda(k+1)t} \\
=&\lambda(n-1)p_{n-1}(t) - \lambda\sum_{k=0}^{n-1}(-1)^k\frac{(n-1)!}{k!(n-k-1)!}(n-k-1)(k+1)\mathrm{e}^{-\lambda(k+1)t} \\
&-\lambda\sum_{k=0}^{n-1}(-1)^k\frac{(n-1)!}{k!(n-k-1)!}(k+1)\mathrm{e}^{-\lambda(k+1)t} \\
=&\lambda(n-1)p_{n-1}(t) - \lambda\sum_{k=0}^{n-1}(-1)^k\frac{(n-1)!}{k!(n-k-1)!}(n)(k+1)\mathrm{e}^{-\lambda(k+1)t} \\
=&\lambda(n-1)p_{n-1}(t) - \lambda np_n(t).
\end{aligned}$$

□

In the top panel of Figure 2.3 we plot the time evolution of the state probabilities for $n \in \{1, 2, 5, 10, 20, 40\}$, where $\lambda = 1$. Looking at the plot for $n = 1$, we see that the probability the initial cell remains undivided is an exponentially decreasing function of time. The probability of observing a finite number of cells peaks at some later time. The position in time of this peak shifts to the right as the number of cells increases.

In the bottom panel of Figure 2.3 we plot a single stochastic trajectory realised using the Gillespie algorithm. The blue line is the theoretical mean number of cells at time t ($\mu(t) = \mathrm{e}^{\lambda t}$), and the red area is the mean $\pm$ 1.96 standard deviations, as calculated from the theoretical variance ($\sigma^2(t) = \mathrm{e}^{2\lambda t} - \mathrm{e}^{\lambda t}$).

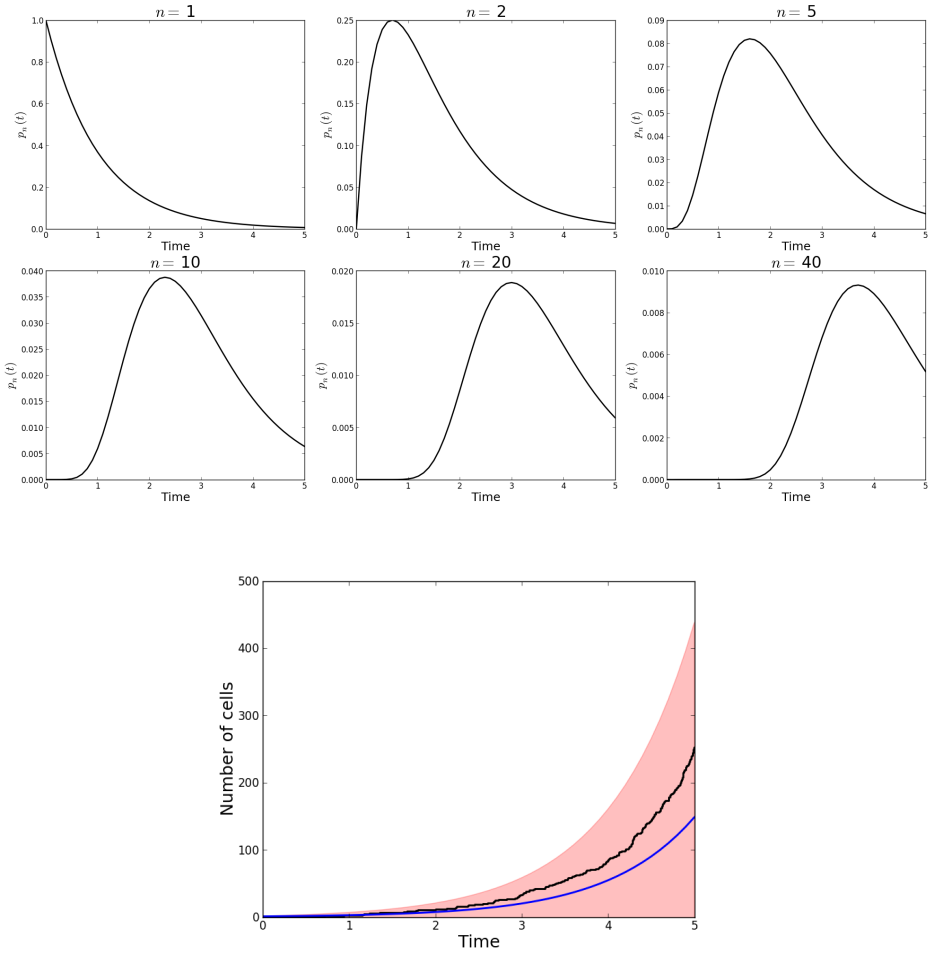

Figure 2.3: Top: time evolution of the state probabilities for $n \in \{1, 2, 5, 10, 20, 40\}$. Bottom: One stochastic realisation (black), mean number of cells (blue) and mean $\pm$ 1.96 standard deviations (red).

The code used to produce the realisation in Figure 2.3 was implemented in the programming language Python. The section of code which implements the Gillespie algorithm is presented below:

```
# Define time course
T_end = 10.0

# Define parameters & initial conditions
lam = 1.0

# Gillespie algorithm

n = 1
t = 0
time = [0]
cells = [n]
while t < T_end:

    # Choose next event from random variable r2
    if t != 0:
        s = 0
        s_ = s
        s += birth_rate
        if s_ <= r2 <= s:
            n += 1

        cells.append(n)
        time.append(t)

    # Calculate transition rates & sum over all rates

    birth_rate = lam * n

    sum_rates = sum([birth_rate])

    # Draw random variables to determine next event
    # and corresponding time to event
```

```
r1 = random.random()
tau = math.log(1/r1) / sum_rates
t += tau
cells.append(n)

if t < T_end:
    time.append(t)
else:
    time.append(T_end)

r2 = random.random() * sum_rates
```

Chapter 3

Modelling naive T cell homeostasis

A population of T cells in homeostasis is able to adapt to changes in various features of the population. An example of such a change could be a loss of cells within the population; in which case homeostatic mechanisms serve to replace the lost cells, returning the population to its original number. Another example may be a loss in the diversity of TCR specificities within a population; a homeostatically regulated population should be able to reconstitute its original diversity. Many examples of homeostatically regulated systems, not necessarily restricted to T cells, can be found in the biological literature. Some of these examples the reader is no doubt familiar with, such as blood pressure or body temperature.

For the next three chapters we shall be considering the homeostasis of the peripheral naive T cell pool. Introduced in Chapter 1, the periphery of the mammalian immune system is made up of the lymph nodes, spleen and mucosa-associated lymphoid tissues. Mature naive T cells which have egressed from the thymus circulate through these tissues, wherein their survival (and hence population size) is regulated by the availability of trophic factors required for survival such as IL-7 or access to sp:MHC. In the periphery, naive T cells may die or divide, depending on the signals available. Furthermore, in healthy mice and humans, there is output of recently matured T cells from the thymus throughout life. Understanding the relative contribution each of these factors has to regulating the absolute number of naive T cells is non-trivial. It is our hope that mathematical modelling can aid this understanding.

In this chapter we introduce deterministic mathematical models which describe naive T cell homeostasis. We begin with a very simple description, which, whilst mathematically easy to analyse, does a poor job of describing the number of T cells in steady state conditions. The limitations of the simple model are discussed, following which we present some examples which have been taken in the literature to improve

it. In the final section of this chapter we introduce a deterministic description in which T cell homeostasis is assumed to be dependent on the availability of a resource, included as a variable within the model.

3.1 A simple model of a peripheral naive T cell population

We introduce a simple model to describe a population of naive T cells in the periphery. The model is described by a pair of coupled ordinary differential equations with constant coefficients. The steady state behaviour of the model is analysed, and then we discuss how this model compares against qualitative biological observations.
Naive T cells are assumed to either be resting or cycling (undergoing a round of cell division). Let $R(t)$ be the number of resting naive T cells. Formally $R(t)$ corresponds to the number of cells in the G0 phase of the cell cycle (Cooper, 2000). Furthermore, we define $C(t)$ to be the number of naive T cells in either one of the G1, S, G2 and M phases of the cell cycle (Cooper, 2000). The assumptions of the model are presented forthwith.

Thymic production of naive T cells Naive T cells are assumed to mature within the thymus. Following maturation, we assume naive T cells leave the thymus and enter the peripheral lymphatic tissue. At this point we assume that naive T cells are resting. We let the rate of thymic export of naive T cells be constant. We introduce the parameter ν to denote this rate.

Cell death We assume resting naive T cells may undergo cell death due to apoptosis. We further assume cycling cells may experience cell death as a consequence of induced apoptosis and mechanistic failures during the division process. The rates of T cell death are assumed to be proportional to the respective population sizes. We denote the constants of proportionality as μ_R and μ_C, respectively.

Entry into the cell cycle We assume resting naive T cells may be induced to undergo division in response to the cytokine IL-7 and TCR interactions with sp:MHC presented by APCs. The availability of these stimuli is assumed to be constant. We model entry into division as a transition term from the pool of resting T cells to the pool of cycling T cells. This transition occurs at a rate proportional to the

number of resting T cells. The constant of proportionality for the rate at which this transition occurs is denoted by the parameter ρ.

Cell division We assume cycling T cells take a fixed length of time to complete division. Following division, we assume a cycling T cell produces two daughter T cells in the resting state. In reference (Reynolds *et al.*, 2012) we consider alternative possibilities for the location of daughter T cells in this model. Here however, we restrict ourselves to assuming both daughter T cells are produced in the resting state. The rate of production of daughter T cells is defined to be proportional to the number of T cells in cycle, with rate constant λ.

Deterministic model As stated earlier, we describe the model as a pair of coupled ordinary differential equations. Based on the assumptions introduced above, the equations are expressed as follows:

$$\frac{\mathrm{d}R(t)}{\mathrm{d}t} = \nu - (\mu_R + \rho)\, R(t) + 2\lambda C(t), \tag{3.1}$$

$$\frac{\mathrm{d}C(t)}{\mathrm{d}t} = \rho R(t) - (\mu_C + \lambda)\, C(t). \tag{3.2}$$

Initial conditions are specified as $R(t=0) = R_0$ and $C(t=0) = C_0$. We note that functionally similar versions of this model have been proposed to describe naive T cells previously. One example of mention is give in reference (Ribeiro & de Boer, 2008).

3.1.1 Exact solutions of the simple model

Let us define

$$\bar{X}(t) = \begin{pmatrix} R(t) \\ C(t) \end{pmatrix}. \tag{3.3}$$

Then, the system of ODEs given by equations (3.1) and (3.2) can be expressed as

$$\frac{\mathrm{d}}{\mathrm{d}t}\bar{X}(t) = \begin{pmatrix} -(\mu_R + \rho) & 2\lambda \\ \rho & -(\mu_C + \lambda) \end{pmatrix} \bar{X}(t) + \begin{pmatrix} \nu \\ 0 \end{pmatrix} = A\bar{X}(t) + \begin{pmatrix} \nu \\ 0 \end{pmatrix}. \tag{3.4}$$

The eigenvalues of the matrix A are

$$\epsilon_{1,2} = \frac{1}{2}\left(-(\mu_R + \rho + \mu_C + \lambda) \pm \sqrt{(\mu_R + \rho + \mu_C + \lambda)^2 + 8\rho\lambda - 4(\mu_R + \rho)(\mu_C + \lambda)}\right), \tag{3.5}$$

where we let ϵ_1, ϵ_2 correspond to the positive and negative root, respectively. The eigenvectors associated with the above eigenvalues are

$$\bar{V_1} = \begin{pmatrix} v_{11} \\ v_{12} \end{pmatrix} = \begin{pmatrix} 1 \\ \dfrac{\epsilon_1 + \mu_R + \rho}{2\lambda} \end{pmatrix}, \tag{3.6}$$

$$\bar{V_2} = \begin{pmatrix} v_{21} \\ v_{22} \end{pmatrix} = \begin{pmatrix} 1 \\ \dfrac{\epsilon_2 + \mu_R + \rho}{2\lambda} \end{pmatrix}. \tag{3.7}$$

We let

$$h_1 = \frac{v_{22}\nu}{v_{11}v_{22} - v_{12}v_{21}}, \tag{3.8}$$

$$h_2 = -\frac{v_{12}\nu}{v_{11}v_{22} - v_{12}v_{21}}. \tag{3.9}$$

The exact solution of the simple model is then

$$\bar{X}(t) = \left(C_1 \mathrm{e}^{\epsilon_1 t} - \frac{h_1}{\epsilon_1}\right)\bar{V_1} + \left(C_2 \mathrm{e}^{\epsilon_2 t} - \frac{h_2}{\epsilon_2}\right)\bar{V_2}, \tag{3.10}$$

where

$$C_1 = \frac{\left(R_0 + \frac{h_1 v_{11}}{\epsilon_1} + \frac{h_2 v_{21}}{\epsilon_2}\right)(v_{11}v_{22} - v_{12}v_{21} + v_{11}v_{12}) - \left(C_0 + \frac{h_1 v_{12}}{\epsilon_1} + \frac{h_2 v_{22}}{\epsilon_2}\right)v_{11}^2}{v_{11}\left(v_{11}v_{22} - v_{12}v_{21}\right)}, \tag{3.11}$$

$$C_2 = \frac{\left(C_0 + \frac{h_1 v_{12}}{\epsilon_1} + \frac{h_2 v_{22}}{\epsilon_2}\right)v_{11} - \left(R_0 + \frac{h_1 v_{11}}{\epsilon_1} + \frac{h_2 v_{21}}{\epsilon_2}\right)v_{12}}{v_{11}v_{22} - v_{12}v_{21}}. \tag{3.12}$$

For stationary solutions we require $\epsilon_1, \epsilon_2 < 0$, which is true if and only if

$$2\rho\lambda < (\mu_R + \rho)(\mu_C + \lambda). \tag{3.13}$$

In the event that the parameters satisfy the above inequality, solutions asymptotically converge to the pair of stationary solutions $X^* = (R^*, S^*)$, where

$$R^* = \frac{\nu(\mu_C + \rho)}{(\mu_R + \rho)(\mu_C + \lambda) - 2\rho\lambda}, \tag{3.14}$$

$$C^* = \frac{\nu\rho}{(\mu_R + \rho)(\mu_C + \lambda) - 2\rho\lambda}. \tag{3.15}$$

If the parameters are such that equation (3.13) is not satisfied, then solutions grow exponentially as t tends to infinity.

3.1.2 Simple model discussion

Homeostasis of T cells is characterised by a population that is not only of constant size in time, but that will also return to its original size following perturbations in the number of T cells. For this simple model, only parameters that satisfy (3.13) give rise to deterministic trajectories that approximate T cell homeostasis. Parameters not satisfying this condition result in deterministic trajectories tending towards infinity, which clearly does not represent in vivo T cell dynamics. For the simple model introduced above, steady state solutions are proportional to the rate of thymic output. This implies that the number of T cells will tend to zero if thymic output (ν) is zero. This prediction contradicts observations from experimental mouse studies and clinical studies in humans. Children undergoing cardiothoracic surgery routinely have the thymus removed (thymectomy). Despite removal of the thymus, in later life, these individuals maintain a peripheral T cell population; however, the total number of cells may be different to a non-thymectomised individual (Halnon *et al.*, 2005). Thymectomised mice maintain steady populations of T cells. Indeed, such mice may even reconstitute the peripheral compartment following acute T cell depletion (Jameson, 2005). An in vivo environment characterised by low numbers of T cells is referred to as being lymphopenic. It is widely reported in the literature that T cell populations expand in response to an abundance of homeostatic stimuli such as TCR signalling induced by recognition of sp:MHC and cytokine signalling (Martin *et al.*, 2003; Min *et al.*, 2003; Seddon & Zamoyska, 2002). Parameter values may be chosen such that the simple model captures the early expansion phase of T cell population dynamics, but since it cannot possess a steady state that is not maintained by thymic output, the model cannot capture the plateau at which an expanding T cell population reaches equilibrium. This motivates a modification to

the simple model: we introduce a carrying capacity to limit the expansion of the T cell population.

3.2 Introducing a carrying capacity

From a mathematical perspective, there exist many possible modifications one can make to the simple model, such that solutions tend to some equilibrium for any choice of parameters. For each of the possible modifications, the dynamics of the model may behave differently. Choosing a particular method should then be motivated by the biology. In the simple model, we have assumed that self-peptide and cytokine availability is constant, where availability is encoded in the parameter governing the rate of entry into division, ρ, and the respective death rates, μ_R and μ_C. One possible modification is to assume that the availability of self-peptide and cytokines decreases as the population of T cells expand. Mathematically, we could choose to replace the parameter ρ by a decreasing function of the number of T cells ($R(t)$) competing for self-peptide and cytokine induced signals. That is, one might replace ρ by the term

$$\rho \exp\left(-\frac{R(t)}{\kappa}\right), \tag{3.16}$$

where κ corresponds to the population size. The parameter κ governs the degree to which this function tends to zero, as the population of cells increases. Specifically, at $R(t) = \kappa$, this function decreases by approximately 63%. Recently, a model incorporating such a term to describe the rate of entry into the cell cycle has been published. In reference (Hapuarachchi *et al.*, 2013), the authors publish a two compartment model of resting and cycling $CD4^+$ naive T cells in the periphery. The rate of entry into the cell cycle is described by a term similar to that above. However, this model also includes a similar term to describe the death rate of resting naive T cells, as well as a non-linear term to describe the rate of thymic output.

Allowing for a decrease in the availability of self-peptide and cytokines, as the population of T cells expand, is however only one of many modifications we could make. Under specific conditions, T cells have been observed to induce apoptosis in other T cells within the population. Apoptosis induced in this manner is a result of interactions between the Fas receptor and Fas-ligand (FasL) (Brunner *et al.*, 1995). This approach has been taken in the literature previously (Callard *et al.*, 2003; Yates *et al.*, 2000). We note that in these studies, the class of T cells being modelled is assumed to be activated in response to immunisation. This approach then may not

be suitable to modelling, for example, the naive T cell population. T cell activation may be a requirement for expression of Fas/FasL (Suda *et al.*, 1995). Despite this, a simple method in which these assumptions may be realised within the model is to include a second order death term to model cell-cell contact resulting in Fas-FasL interactions. One might modify the ODE describing the time dynamics of the resting population to include a quadratic death term of the form

$$-\xi R(t)R(t). \tag{3.17}$$

Alternatively, one could assume only cycling cells express Fas/FasL receptor/ligand. We could include a similar term in the ODE describing the time dynamics of the cycling population. In the following sections we analyse the simple model with these modifications.

3.2.1 Self-peptide and cytokine availability decreases as a population expands

We assume the rate of entry into cell cycle is a decreasing function of the number of resting T cells. The model is then fully described by the pair of ODEs

$$\frac{\mathrm{d}R(t)}{\mathrm{d}t} = \nu - \left(\mu_R + \rho \exp\left(-\frac{R(t)}{\kappa}\right)\right) R(t) + 2\lambda C(t), \tag{3.18}$$

$$\frac{\mathrm{d}C(t)}{\mathrm{d}t} = \rho \exp\left(-\frac{R(t)}{\kappa}\right) R(t) - (\mu_C + \lambda)\, C(t). \tag{3.19}$$

Due to the exponential term, we cannot express stationary solutions by means of regular analytic functions. The stationary number of resting T cells, R^*, is found by solving the relation

$$f(R^*) = \frac{\nu}{R^*} = \rho \left(\frac{\mu_C - \lambda}{\mu_C + \lambda}\right) \exp\left(-\frac{R^*}{\kappa}\right) + \mu_R = g(R^*). \tag{3.20}$$

Notice that $\lim_{x\to 0^+} f(x) = +\infty > g(0) = \rho\left(\frac{\mu_C - \lambda}{\mu_C + \lambda}\right) + \mu_R$ and $\lim_{x\to+\infty} f(x) = 0 < \lim_{x\to+\infty} g(x) = \mu_R$. Since both f and g are continuous functions on the open interval $(0, \infty)$, it follows from the intermediate value theorem (Truss, 1997), that there exists at least one solution R^* such that $f(R^*) = g(R^*)$. The stationary solution $R^* > 0$ is unique if $\lambda > \mu_C$, however, for $\lambda < \mu_C$, we may find multiple solutions.

Proof. Suppose $\lambda > \mu_C$. Assume there exist two solutions $x_1^* < x_2^*$ such that $f(x_1^*) = g(x_1^*)$ and $f(x_2^*) = g(x_2^*)$. Given that $\lambda > \mu_C$, the derivatives satisfy $f'(x) < 0$ and $g'(x) > 0$. It follows

$$f(x_1^*) > f(x_2^*) = g(x_2^*) > g(x_1^*). \tag{3.21}$$

This contradiction implies $x_1^* = x_2^*$. That is, any stationary solution is unique.

□

A numerical exploration of the trajectories[1] has revealed, for the case $\lambda > \mu_C$, that the model either tends to the unique fixed point or exhibits periodic solutions. For $\lambda < \mu_C$, we could find parameter sets for which there exists multiple fixed points, which could be concurrently stable. Late time trajectories, were then dependent on the choice of initial conditions. We cannot claim however, that these are the only behaviours for late times.
Consider that as $R(t) \to +\infty$, the rate of entry into division, $\rho \exp\left(-\frac{R(t)}{\kappa}\right) R(t) \to 0^+$. This ensures that solutions cannot grow to infinity, even if $2\rho\lambda < (\mu_R + \rho)(\mu_C + \lambda)$, which is the stability criterion for the simple model, presented in Section 3.1.

If thymic output, ν, is zero

Suppose now we assume no thymic output, that is, we set $\nu = 0$. There exist two possible sets of steady solutions. Respectively, these are

$$R^* = 0, \quad C^* = 0, \tag{3.22}$$

$$R^* = \kappa \log\left(\frac{\rho(\lambda - \mu_C)}{\mu_R(\lambda + \mu_C)}\right), \quad C^* = \frac{\mu_R \kappa}{\lambda - \mu_C} \log\left(\frac{\rho(\lambda - \mu_C)}{\mu_R(\lambda + \mu_C)}\right). \tag{3.23}$$

The second set exists if and only if $\lambda > \mu_C$. The Jacobian for the system, evaluated at stationary solution (R^*, C^*), is

$$J = \begin{pmatrix} -\mu_R - \rho \exp\left(-\frac{R^*}{\kappa}\right)\left(1 - \frac{R^*}{\kappa}\right) & 2\lambda \\ \rho \exp\left(-\frac{R^*}{\kappa}\right)\left(1 - \frac{R^*}{\kappa}\right) & -\mu_C - \lambda \end{pmatrix}. \tag{3.24}$$

The Jacobian J, has negative eigenvalues if and only if $\text{trace}(J) < 0$ and $\det(J) > 0$. For the first set of stationary solutions ($R^* = C^* = 0$), these conditions are satisfied

[1] We used a 4^{th} order Runge-Kutta scheme to compute deterministic trajectories.

if and only if

$$\frac{\rho(\lambda - \mu_C)}{\mu_R(\lambda + \mu_C)} < 1. \tag{3.25}$$

The second set of stationary solutions is stable if and only if $\lambda > \mu_C$ and

$$1 < \frac{\rho(\lambda - \mu_C)}{\mu_R(\lambda + \mu_C)} < \exp\left(1 + \frac{(\mu_R + \lambda + \mu_C)(\lambda - \mu_C)}{\mu_R(\lambda + \mu_C)}\right). \tag{3.26}$$

If the right hand side of the above inequality is not satisfied, we observe periodic solutions which neither decay to the steady state nor grow to infinity. In Figure 3.1 we show example trajectories for the cases when (3.25) holds (left panel), (3.26) holds (middle panel) and when neither hold (right panel).

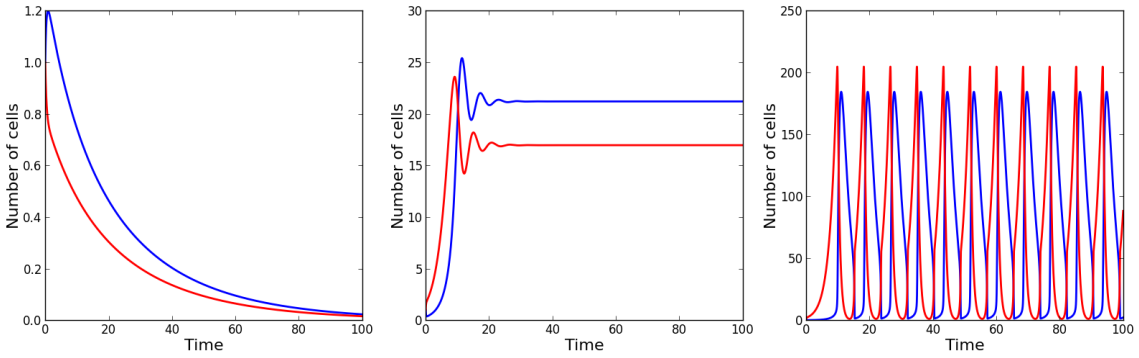

Figure 3.1: Numerical solution of equations (3.18) and (3.19) for the parameter set $\nu = 0$, $\mu_R = 0.4$, $\mu_C = 0.5$, $\lambda = 1$, $\kappa = 10$ and $\rho = 1$ (left), 10 (middle) and 100 (right). Initial conditions are $R(0) = C(0) = 1$.

3.2.2 Fas-FasL induced apoptosis as a consequence of cell-cell interactions

We modify the simple model such that we include a second order death term. The appearance of this term is motivated by the observation that T cells may induce apoptosis in other T cells due to Fas-FasL interactions (Ju *et al.*, 1999). In this section we assume Fas-FasL interactions are mediated between resting T cells. The modified pair of ODEs governing the time evolution of the model are:

$$\frac{\mathrm{d}R(t)}{\mathrm{d}t} = \nu - (\mu_R + \rho)\, R(t) + 2\lambda C(t) - \xi R(t)R(t), \tag{3.27}$$

$$\frac{\mathrm{d}C(t)}{\mathrm{d}t} = \rho R(t) - (\mu_C + \lambda)\, C(t). \tag{3.28}$$

Stationary solutions R^* satisfy the equation

$$\frac{1}{2}R^* - \Gamma R^* - \frac{\nu}{2\xi} = 0, \tag{3.29}$$

where

$$\Gamma = \frac{2\lambda\rho - (\mu_R + \rho)(\mu_C + \lambda)}{2\xi(\mu_C + \lambda)}. \tag{3.30}$$

It follows that solutions R^* satisfy

$$R^* = \Gamma \pm \sqrt{\Gamma^2 + \frac{\nu}{\xi}}. \tag{3.31}$$

For solutions satisfying R^* greater than zero we are required to take the positive square root and thus

$$R^* = \left(\Gamma + \sqrt{\Gamma^2 + \frac{\nu}{\xi}}\right), \tag{3.32}$$

$$C^* = \frac{\rho}{(\mu_C + \lambda)}\left(\Gamma + \sqrt{\Gamma^2 + \frac{\nu}{\xi}}\right). \tag{3.33}$$

The Jacobian of this system is given by

$$J = \begin{pmatrix} -\mu_R - \rho - 2\xi R^* & 2\lambda \\ \rho & -\mu_C - \lambda \end{pmatrix}. \tag{3.34}$$

The trace of the Jacobian is,

$$\text{trace}(J) = -\mu_R - \rho - 2\xi R^* - \mu_C - \lambda \tag{3.35}$$

which, for positive solutions R^*, is negative. The determinant of the Jacobian is

$$\det(J) = (\mu_C + \lambda)(\mu_R + \rho) + 2\xi R^*(\mu_C + \lambda) - 2\lambda\rho. \tag{3.36}$$

The determinant is strictly positive for positive solutions R^*.

Proof. Assume $\det(J) < 0$. Then,

$$\begin{aligned} & (\mu_C + \lambda)(\mu_R + \rho) + 2\xi R^*(\mu_C + \lambda) < 2\lambda\rho \\ \Rightarrow \quad & R^* < \Gamma \end{aligned}$$

$$\Rightarrow \quad \Gamma + \sqrt{\Gamma^2 + \frac{\nu}{\xi}} < \Gamma$$
$$\Rightarrow \quad \sqrt{\Gamma^2 + \frac{\nu}{\xi}} < 0.$$

This contradiction implies $\det(J) > 0$ for positive solutions R^*. □

It follows then that the positive solution (R^*, C^*) is stable. Note, if we assume $R^* < 0$ (by taking the negative square root), it is easily proved in the same manner as above that $\det(J) < 0$ for all parameters. Hence, negative solutions are unstable.

If thymic output, ν, is zero

In the event that thymic output is zero, the single set of steady solutions above splits into the two solutions:

$$R^* = 0, \quad C^* = 0, \tag{3.37}$$
$$R^* = 2\Gamma, \quad C^* = \frac{2\rho\Gamma}{\mu_C + \lambda}. \tag{3.38}$$

This first set of solutions, corresponding to extinction of both populations, exists unconditionally. The second set of solutions is positive if $\Gamma > 0$. The Jacobian for this system is the same as when $\nu > 0$, that is, the Jacobian is given by (3.35). For the first set of solutions, $\text{trace}(J) < 0$ and the determinant is positive provided $\Gamma < 0$; that is, provided

$$2\lambda\rho < (\mu_R + \rho)(\mu_C + \lambda). \tag{3.39}$$

The second set of solutions exists and is stable provided this inequality does not hold.

If Fas-FasL interactions are mediated by cycling cells

Suppose now that Fas-FasL interactions are mediated between cycling T cells, rather than resting T cells. The model is described by the pair of ODEs

$$\frac{\mathrm{d}R(t)}{\mathrm{d}t} = \nu - (\mu_R + \rho)\, R(t) + 2\lambda C(t), \tag{3.40}$$
$$\frac{\mathrm{d}C(t)}{\mathrm{d}t} = \rho R(t) - (\mu_C + \lambda)\, C(t) - \xi C(t)C(t). \tag{3.41}$$

The positive stationary solution for $\nu > 0$ is

$$R^* = \frac{\nu}{\mu_R + \rho} + \frac{2\lambda}{\mu_R + \rho}\left(\Gamma + \sqrt{\Gamma^2 + \frac{\rho\nu}{\xi(\mu_R + \rho)}}\right), \tag{3.42}$$

$$C^* = \Gamma + \sqrt{\Gamma^2 + \frac{\rho\nu}{\xi(\mu_R + \rho)}}. \tag{3.43}$$

In a completely analogous method as before, it is readily shown that these solutions are stable. For $\nu = 0$, there again exist two stationary solutions:

$$R^* = 0, \quad C^* = 0, \tag{3.44}$$

$$R^* = \frac{4\lambda\Gamma}{\mu_R + \rho}, \quad C^* = 2\Gamma. \tag{3.45}$$

The first one is stable provided the inequality

$$2\lambda\rho < (\mu_R + \rho)(\mu_C + \lambda), \tag{3.46}$$

holds, whilst the second one is positive and stable provided this inequality does not hold.

3.2.3 Discussion on including a carrying capacity

Consider the modified simple model in which the rate of transition into the cell cycle is a decreasing function of the number of resting cells. If $\nu > 0$, the model either tends to a fixed-point (which may not be unique if $\lambda < \mu_C$), or exhibits periodic solutions. If $\nu = 0$, then there exist two stationary solutions, one characterised by extinction of the T cell population, and one in which population growth is limited by the availability of self-peptide and cytokines. In both cases, if parameters are such that the positive stationary solutions are stable, this model can be used to describe T cell populations in equilibrium and during expansion in lymphopenic environments. The model is limited with respect to capturing changes in the lifetimes of resting cells, corresponding to μ_R^{-1}. Lifetimes of resting cells are invariant during lymphopenia and lymphocyte populations in equilibrium. Such a prediction may not match the biology, since the survival of naive T cells is dependent on both the availability of signals from cytokines and TCR induced signals through recognition of self-peptides presented by APCs. The availability of these trophic factors is presumably limited in homeostatic environments when compared to lymphopenic ones.

Now consider the modified simple models in which we assume a cell-cell contact term to describe Fas-FasL interactions. For $\nu > 0$ we observe a single steady state, which is stable for all choices of parameters. When $\nu = 0$ we observe a pair of steady states, one corresponding to extinction of the T cell population, and one in which population growth is balanced against T cell death due to T cell induced apoptosis. This second modified model does not possess periodic solutions. One can make similar criticisms as before for this approach, the most obvious being the rate of entry into cell cycle. This model assumes this rate is constant for both lymphopenic and homeostatic environments. This is likely to be not the case due to the change in availability of self-peptides and cytokines, from which entry into cell cycle may be induced. Additionally, whilst it has been reported in the literature that activated T cells induce cell death by Fas-FasL interactions, the same may not be true for naive T cells.

For the simple models presented, analysis of the model behaviour is relatively straightforward. However it is unreasonable to use these simple approaches to make predictions on the more nuanced details of T cell population dynamics such as the lifetimes of individual T cells. In the next section we expand the simple model to include an equation modelling the availability of some resource. Furthermore, the rates of entry into the cell cycle and death are described by functions of a resource.

3.3 Modelling a resource

Naive T cells in the periphery require signals induced from trophic factors such as IL-7 and recognition of self-peptides. In vitro studies have shown that the survival of $CD8^+$ naive T cells is dependent on the concentration of available IL-7 (Palmer *et al.*, 2011). For low concentrations of IL-7, the amount of signalling naive $CD8^+$ T cells receive is sufficient to promote cell survival, whereas the same cells have been shown to proliferate in excess IL-7 (Palmer *et al.*, 2011). Studies show that the ability of a naive T cell to survive, or undergo division, is dependent on the amount of signalling a cell receives with respect to signalling thresholds for survival and proliferation. The threshold for proliferation has been shown to be at least an order of magnitude greater than the signalling threshold for survival (Palmer *et al.*, 2011). We use these observations to construct functions that describe the respective loss rates and rates of entry into cell cycle for naive T cells. These functions are then included in the simple model to refine the previously discussed weak assumptions of constant rates of entry into cell cycle and death.

In this model we assume the amount of signalling naive T cells receive is a function of some global resource, the amount of which is encoded in the variable $I(t)$. We introduce a variable to describe the amount of signal each T cell in the population receives. This variable is denoted by $S(t)$, and is assumed to be some function of the resource, $I(t)$. Each naive T cell within the population is assumed to experience the same amount of signal for a given amount of the resource.

3.3.1 Rate of cell loss

Suppose that we consider each T cell as a distinct object, rather than considering the population as some continuous density. We assume each T cell within this population receives, at resource availability I, an amount of signal S. Further suppose that each T cell, labelled by index j, possesses some threshold θ_j^s, above which signalling is required for survival of the cell. Let $f_j^s(S, \theta_j^s)$ be the rate of cell death for each T cell j and define:

$$f_j^s(S, \theta_j^s) = \begin{cases} \mu_R & \text{if } S < \theta_j^s, \\ 0 & \text{if } S > \theta_j^s. \end{cases} \tag{3.47}$$

Thus, we assume that T cell j may survive indefinitely if the amount of signal remains above this cell's signalling threshold θ_j^s. If the amount of signal is below this threshold, we assume this cell will be lost due to cytokine deprivation. If cytokine signalling is insufficient to promote survival, the average time for the loss of this cell is given by μ_R^{-1}.

We assume each T cell j possesses its individual survival threshold θ_j^s. We assume no T cell can survive indefinitely, independently of the resource I, thus we choose a distribution such that each signalling threshold is greater than zero. Furthermore, the survival threshold for each T cell is finite, that is, there exists some finite amount of signalling which is sufficient to maintain the cell. We are taking a deterministic approach to modelling the population of cells, therefore we approximate the discrete distribution of cells by a continuous distribution. Let Θ be a continuous random variable defined on the state space of all possible survival thresholds. We assume Θ is log normally distributed. That is, we define $\Theta \sim \log \mathcal{N}(\log \theta_s, \frac{1}{2\alpha^2})$. The choice of a log normal distribution ensures that all survival thresholds are positive. Furthermore, the probability of Θ taking a survival threshold for which no finite amount of signalling can promote cell survival is vanishingly small. This implies that no T cell can survive independently of IL-7. Lastly, log normal distributions have been used

in the literature to describe receptor densities on the surface of T cells, therefore it seems reasonable to assume other quantities may be described by these distributions. By definition, the probability density of Θ is given by

$$p_\Theta(\theta_j^s) = \frac{\alpha}{\theta_j^s} \exp\left(-\left(\alpha\left(\log\theta_j^s - \log\theta_s\right)\right)^2\right). \tag{3.48}$$

From equations (3.47) and (3.48), we derive the average rate of loss of T cells from this population. We denote the average rate of resting T cell loss due to death as $\bar{\mu}_R(S(t))$. Then,

$$\begin{aligned}\bar{\mu}_R(S(t)) &= \int_0^{+\infty} f_j^s(S(t), \theta_j^s) p_\Theta(\theta_j^s)\, \mathrm{d}\theta_j \\ &= \int_{S(t)}^{+\infty} \mu_R p_\Theta(\theta_j^s)\, \mathrm{d}\theta_j^s \\ &= \frac{1}{2}\mu_R\left(1 - \operatorname{erf}\left(\alpha\left(\log S(t) - \log\theta_s\right)\right)\right).\end{aligned} \tag{3.49}$$

The average rate of cell loss is a monotonically decreasing function of the amount of signalling S. As $S \to +\infty$, the average rate of cell loss tends to zero. Furthermore, $\bar{\mu}_R(S)$ obtains a maximum equal to μ_R when $S = 0$. We assume the distribution of signalling thresholds does not change with changes in the size of the naive population.

3.3.2 Rate of entry into the cell cycle

We derive the average rate of entry into the cell cycle in a similar manner to the derivation of the average rate of cell loss. This time we assume each cell possesses a signalling threshold, which signalling must exceed to enter division, denoted by θ_j^p. The rate of entry into division for each individual cell j is then assumed to be given by

$$f_j^p(S, \theta_j^p) = \begin{cases} \rho & \text{if } S > \theta_j^p, \\ 0 & \text{if } S < \theta_j^p. \end{cases} \tag{3.50}$$

As before, we assume the distribution of each threshold θ_j^p can be approximated by some continuous distribution, which we again choose to be log normal. Let

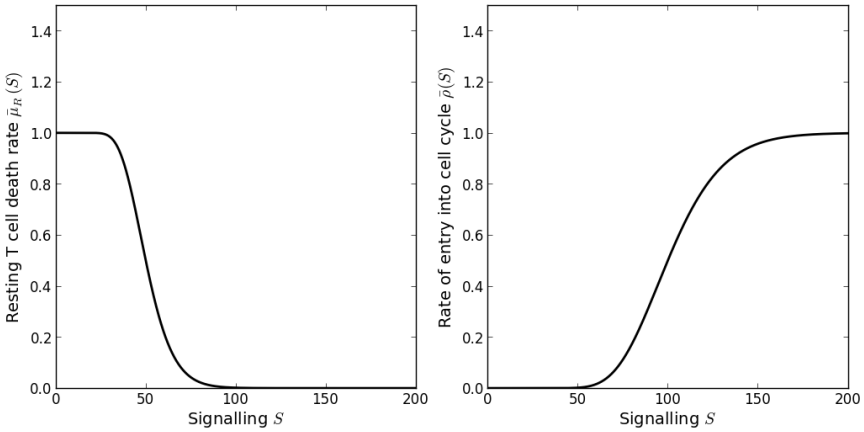

Figure 3.2: Example plots of $\bar{\mu}_R(S(t))$ (left panel) and $\bar{\rho}(S(t))$ (right panel). Parameter values used: $\mu_R = 1$, $\rho = 1$, $\alpha = 2$, $\theta_s = 50$ and $\theta_p = 100$.

$\Theta \sim \log \mathcal{N}(\log \theta_p, \frac{1}{2\alpha^2})$. Then the average rate of entry into the cell cycle is

$$\begin{aligned}
\bar{\rho}(S(t)) &= \int_0^{+\infty} f(S(t), \theta_j^p) p_\Theta(\theta_j^p)\, \mathrm{d}\theta_j^p \\
&= \int_0^{S(t)} \rho p_\Theta(\theta_j^p)\, \mathrm{d}\theta_j^p \\
&= \rho \left(1 - \int_{S(t)}^{+\infty} p_\Theta(\theta_j^p)\, \mathrm{d}\theta_j^p\right) \\
&= \rho \left(1 - \frac{1}{2}\left(1 - \operatorname{erf}\left(\alpha\left(\log S(t) - \log \theta_p\right)\right)\right)\right) \\
&= \frac{1}{2}\rho\left(1 + \operatorname{erf}\left(\alpha\left(\log S(t) - \log \theta_p\right)\right)\right). \qquad (3.51)
\end{aligned}$$

The rate of entry into the cell cycle is then an increasing function of the amount of signal S. This function is equal to zero when $S = 0$ and tends to ρ as $S \to +\infty$. We plot examples of both $\bar{\mu}_R(S(t))$ and $\bar{\rho}(S(t))$ in Figure 3.2.

3.3.3 Modelling changes in resources

Changes in the concentration of resource, denoted by $I(t)$, are encoded in a differential equation. The resource is assumed to be produced by cells not of the T cell population; therefore, we assume production occurs at some constant rate independent of the size of the T cell population. Let β denote the rate of resource production. We assume that in the absence of a T cell population, the resource reaches some equilibrium, at which, production of the resource is balanced against

the loss of the resource. The simplest approach to encoding this within an ODE, is to assume the rate of loss of the resource is proportional to the amount of the resource. The constant of proportionality for this relation is denoted by δ. We lastly assume the resource is consumed by the T cell population. The rate of this consumption is assumed to be proportional to the product of the amount of signal each T cell receives and the number of T cells. We denote the constant of proportionality by γ. The rate of change of resource is then

$$\frac{\mathrm{d}I(t)}{\mathrm{d}t} = \beta - \gamma S(t)R(t) - \delta I(t). \tag{3.52}$$

Initial conditions are chosen to be $I(0) = I_0$. We do not assume cycling cells consume the resource.

3.3.4 Signalling as a function of the resource

In this first approach, we make the simple assumption that the amount of signal depends linearly on the availability of the resource. That is,

$$S(t) = \eta I(t). \tag{3.53}$$

In Chapter 4 of this thesis, we derive a signalling relation from a consideration of the events occurring at the molecular level.

3.3.5 Resource model

Combining the simple model with the equation describing changes in resources and the rate functions (3.49) and (3.51), we may write a down a system of ODEs to describe the model. The system of ODEs is:

$$\frac{\mathrm{d}I(t)}{\mathrm{d}t} = \beta - \gamma S(t)R(t) - \delta I(t), \tag{3.54}$$

$$\frac{\mathrm{d}R(t)}{\mathrm{d}t} = \nu - \left(\bar{\mu}_R(S(t)) + \bar{\rho}(S(t))\right) R(t) + 2\lambda C(t), \tag{3.55}$$

$$\frac{\mathrm{d}C(t)}{\mathrm{d}t} = \bar{\rho}(S(t))R(t) - \left(\mu_C + \lambda\right) C(t). \tag{3.56}$$

The rates of cell death and entry into the cell cycle, $\bar{\mu}_R(S(t))$, $\bar{\rho}(S(t))$ are respectively given by equations (3.49) and (3.51), and the signalling relation is given by (3.53).

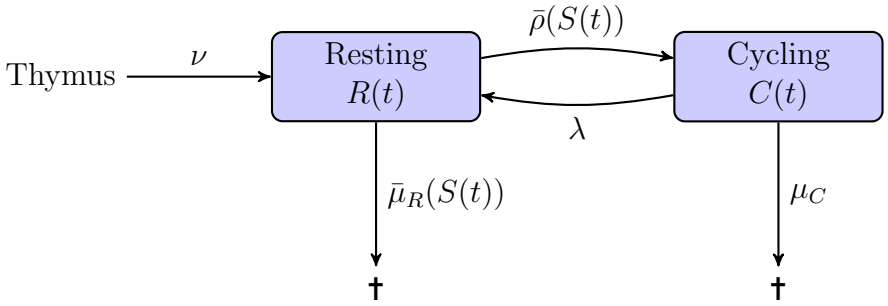

Figure 3.3: Diagrammatic illustration of the resource model. T cells leaving the thymus enter the resting state. Cells in either a resting state or cycling state may die; the rate of death from the resting state is dependent on the availability of the resource. Resting cells enter the cell cycle at a rate dependent on the resource. Cycling cells produce two daughter cells in the resting state upon completion of the cell cycle.

3.3.6 Steady state analysis of the resource model

Setting the derivative in equations (3.54) and (3.56) equal to zero, we derive the steady state solutions I^* and C^* as functions of R^*. Respectively these are:

$$I^* = \frac{\beta}{\gamma\eta R^* + \delta}, \tag{3.57}$$

$$C^* = \frac{\bar{\rho}(S^*)R^*}{\mu_C + \lambda}, \tag{3.58}$$

where $S^* = S(I^*)$. Setting the derivative in equation (3.55) equal to zero and substituting the above two expressions for I^* and C^*, we find

$$\frac{\nu}{R^*} = \bar{\mu}_R(S^*) + \bar{\rho}(S^*)\left(1 - \frac{2\lambda}{\mu_C + \lambda}\right), \tag{3.59}$$

where

$$S^* = \frac{\eta\beta}{\gamma\eta R^* + \delta}. \tag{3.60}$$

Let us define $\bar{S}(x) = \dfrac{\eta\beta}{\gamma\eta x + \delta}$. Consider the functions

$$f(x) = \frac{\nu}{x}, \tag{3.61}$$

$$g(x) = \bar{\mu}_R\left(\bar{S}(x)\right) + \bar{\rho}\left(\bar{S}(x)\right)\left(1 - \frac{2\lambda}{\mu_C + \lambda}\right). \tag{3.62}$$

Letting $x \to 0^+$ we have $f(x) \to +\infty$ and $g(0) = c_1$, where c_1 is some real number.

Furthermore, considering the limit $x \to +\infty$, we find $f(x) \to 0$ and $g(x) \to c_2$, where c_2 is a positive real number. It follows from the intermediate value theorem that there exists at least one solution $x^* > 0$ such that $f(x^*) = g(x^*)$. Suppose $\lambda \geq \mu_C$, then $g'(x) > 0$. Since $f'(x) < 0$, the solution x^* is unique when $\lambda \geq \mu_C$. For $\lambda < \mu_C$, there exists at least one solution, however this solution may not be unique since $g'(x)$ can be either positive or negative, allowing multiple intersections between f and g. Numerically, we observed up to three solutions, however, there may be more for some parameter sets.
In the case that $\lambda > \mu_C$, it cannot be proved that the unique stationary solution is stable for all parameter values, indeed, numerical exploration reveals the model exhibits periodic solutions in some region of the parameter space.

3.3.7 If thymic output, ν, is zero

Suppose now that we set $\nu = 0$, stationary solutions are found by solving the system of equations

$$\beta - \gamma S^* R^* - \delta I^* = 0, \tag{3.63}$$

$$-\left(\bar{\mu}_R(S^*) + \bar{\rho}(S^*)\right) R^* + 2\lambda C^* = 0, \tag{3.64}$$

$$\bar{\rho}(S^*)R^* - (\mu_C + \lambda)C^* = 0. \tag{3.65}$$

From (3.65) we find $C^* = \dfrac{\bar{\rho}(S^*)}{\mu_C + \lambda} R^*$. Substituting this into (3.64) we find

$$-\left(\bar{\mu}_R(S^*) + \bar{\rho}(S^*)\right) R^* + \frac{2\lambda\bar{\rho}(S^*)}{\mu_C + \lambda} R^* = 0. \tag{3.66}$$

One solution is $R^* = 0$, which implies $I^* = \frac{\beta}{\gamma}$ and $C^* = 0$. Alternatively, if $R^* > 0$, then the resource satisfies

$$\bar{\mu}_R(S^*)(\mu_C + \lambda) + (\mu_C - \lambda)\bar{\rho}(S^*) = 0, \tag{3.67}$$

from which R^* is found from (3.63) and $C^* > 0$ is found from (3.65). The second solution satisfying $I^*, R^*, C^* > 0$ exists if and only if $\lambda > \mu_C$. The Jacobian for this

system is

$$J = \begin{pmatrix} -\gamma\eta R^* - \delta & -\gamma\eta I^* & 0 \\ -\eta(\bar{\mu}_R'(S^*) + \bar{\rho}'(S^*))R^* & -(\bar{\mu}_R(S^*) + \bar{\rho}(S^*)) & 2\lambda \\ \eta\bar{\rho}'(S^*)R^* & \bar{\rho}(S^*) & -(\mu_C + \lambda)) \end{pmatrix}. \tag{3.68}$$

The characteristic polynomial of $\det(J - \xi I)$, evaluated at the set of stationary solutions $I^* = \frac{\beta}{\delta}$, $R^* = C^* = 0$, is

$$\xi^3 + a_1\xi^2 + a_2\xi + a_3 = 0, \tag{3.69}$$

where

$$a_1 = \delta + \bar{\mu}_R(s) + \bar{\rho}(s) + \mu_C + \lambda, \tag{3.70}$$

$$a_2 = \delta\left(\bar{\mu}_R(s) + \bar{\rho}(s) + \mu_C + \lambda\right) + (\mu_C + \lambda)\bar{\mu}_R(s) + (\mu_C - \lambda)\bar{\rho}(s), \tag{3.71}$$

$$a_3 = \delta\left((\mu_C + \lambda)\bar{\mu}_R(s) + (\mu_C - \lambda)\bar{\rho}(s)\right), \tag{3.72}$$

$$s = \frac{\eta\beta}{\delta}. \tag{3.73}$$

The stationary solution $I^* = \frac{\beta}{\delta}$, $R^* = C^* = 0$ is stable if and only if $a_i > 0$ for $i = 1, 2, 3$ and $a_1 a_2 > a_3$. Since both $\bar{\mu}_R$ and $\bar{\rho}$ are strictly positive, $a_1 > 0$. Consider that we can write $a_2 = \delta(a_1 - \delta) + \delta^{-1}a_3$. Then $a_1 a_2 = \delta a_1(a_1 - \delta) + \delta^{-1}a_1 a_3 = \delta a_1(a_1 - \delta) + a_3 + \delta^{-1}(a_1 - \delta)a_3 > a_3$. Thus, a necessary and sufficient condition for stability is $a_3 > 0$, which holds if and only if

$$\delta\left((\mu_C + \lambda)\bar{\mu}_R(s) + (\mu_C - \lambda)\bar{\rho}(s)\right) > 0. \tag{3.74}$$

Clearly, a sufficient condition for stability is $\lambda < \mu_C$. The stationary solution $I^* = \frac{\beta}{\delta}$ represents the maximum possible amount of resource at equilibrium. Thus, any solution S^* satisfying equation (3.67) is less than s. Given $S^* < s$, we have $\bar{\mu}_R(s) < \bar{\mu}_R(S^*)$ and $\bar{\rho}(s) > \bar{\rho}(S^*)$, therefore, for $\lambda > \mu_C$, it follows $a_3 < 0$. Therefore $\lambda < \mu_C$ is also a necessary condition for stability of solutions $I^* = \frac{\beta}{\delta}$, $R^* = C^* = 0$.

3.3.8 Resource model discussion

In healthy individuals, from energy considerations alone, it seems reasonable to expect that T cells which enter division are more likely to survive and produce daughter cells than fail to complete the cycle and die. Mathematically, within the resource model this corresponds to the condition $\lambda > \mu_C$. We have shown that if this parameter relation holds, then there exists a unique fixed point representing the number of T cells at equilibrium. This fixed point, however, is not necessarily stable, indeed, during numerical explorations we observed periodic solutions.

Under conditions favouring stability, the resource model may approximately describe the homeostasis of T cell numbers for healthy individuals. We may also use this model to describe T cell populations expanding in a lymphopenic environment. If initial conditions are such that I_0 is equal to I^* evaluated at $R^* = 0$ (i.e., the maximum possible stable resource) and further, we set R_0 to be some small value relative to R^* for a given parameter (also, set $C_0 = 0$), then the resource model predicts the rate of entry into the cell cycle is sufficient enough to allow the T cell population to expand. As the trajectories of the model approach the steady value R^*, we see a drop in the number of cycling cells, the balance of total cell numbers shifts to a greater fraction of quiescent, resting cells (see Figure 3.4).

The resource model is of greater interest in the case $\lambda < \mu_C$. Under this restriction the model may possess either one positive fixed point or a set of three positive fixed points. In the case of three fixed points, ordered by their size, within some region of the parameter space, the smallest and largest fixed points are stable whilst the middle point is unstable. A change in various parameters of the model can result in a saddle-node bifurcation, moving through which can cause a significant change in the number of T cells at equilibrium. In Figure 3.5 we give an example of this for changes in the parameter ν. We note however, that the parameters used to produce Figures 3.4 and 3.5 are somewhat arbitrary. Later in this thesis we introduce a parameter set representative of in vivo time-scales for T cell dynamics.

In humans the thymus is atrophic (Haynes & Hale, 1998; Simpson *et al.*, 1975). As a consequence, there is a reduction in the number of thymocytes entering the periphery as an individual ages. In healthy individuals, this reduction is relatively slow compared to the time scales of T cell dynamics (Bains *et al.*, 2009b). In the resource model this reduction could be included by defining the parameter ν to be a continuous function of time, with the condition that ν changes slowly compared to the model dynamics. This allows us to assume that after some initial time period,

the model is in quasi-equilibrium for a given time, and corresponding rate of thymic output $\nu(t)$. This implies that when cell division is impaired, a reduction in thymic output can cause the model to bifurcate.

In equation 3.53 we chose a linear relationship between the extra-cellular concentration of IL-7 ($I(t)$) and the amount in IL-7 induced signalling ($S(t)$). This relationship however has no biological basis, rather, it was chosen to be simple here for the purposes of introducing the resource model. In the next chapter we consider IL-7R dynamics during IL-7 signalling, from which we derive a signalling relation to improve upon the one used here. This signalling relation is then used in Chapter 5 to refine the model shown in this section.

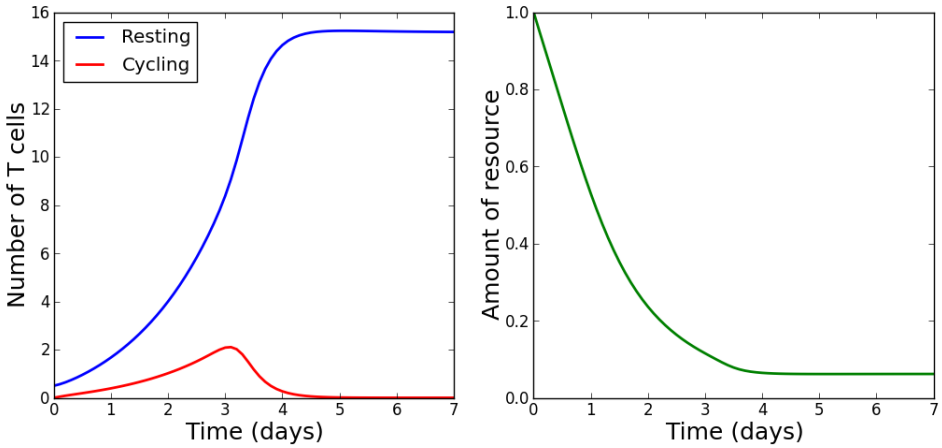

Figure 3.4: Left: Example solutions for a population of resting and cycling cells during lymphopenic expansion. As the number of cells approaches the fixed point we see the balance of cell numbers shifts to favour a greater a proportion of resting cells representing a more quiescent repertoire. Right: The density of resource. The resource is at its maximum stable value at time zero, during the expansion the resource density is reduced. The parameters used to produce this plot were chosen to be non-representative of the biology. In Chapter 5 we revisit the issue of the parameter estimation. The parameter values chosen are: $\beta = 1$, $\gamma = 1$, $\delta = 1$, $\eta = 1$, $\nu = 1$, $\mu_R = 1$, $\mu_C = 0.1$, $\rho = 1$, $\lambda = 3$, $\alpha = 5$, $\theta_s = 0.05$, $\theta_p = 0.1$.

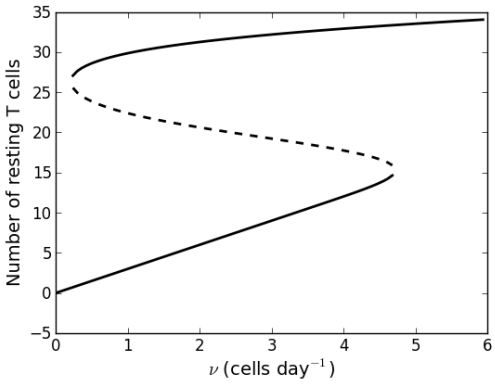

Figure 3.5: A reduction in thymic output will cause a modest reduction in the number of T cells at equilibrium. Near the critical value of $\nu = 0.2$ cells day^{-1}, a small reduction in thymic output can cause a drop of several orders of magnitude in the number of T cells in equilibrium. The parameter values used are given in the caption of Figure 3.4.

Chapter 4

A stochastic model of interleukin-7 signalling

In Section 3.3.4 we related the average signalling S and the resource availability I by the linear function (3.53). This choice was motivated by little more than the fact that such a relationship is simple to work with when analysing the the model. However, one problem with this choice is that it predicts that the amount of signalling a T cell can receive is unbounded. Consider that T cells internalise IL-7 following its binding to the IL-7 receptor (Henriques *et al.*, 2010). Furthermore, note that the maximum number of IL-7R receptors a T cell can express is finite, therefore it follows that there should be an upper limit to the amount of signalling a T cell can receive.

Exactly what functional form the signalling relation should take is unclear. To address this issue, in this chapter we consider the molecular dynamics of IL-7 signalling. We develop a stochastic Markov model in which we introduce random variables to represent the number of IL-7 receptors on the surface of a cell, the amount of signal internal to the cell, and, in the latter part of this chapter, also consider internalised receptors which may or may not be bound to IL-7. This chapter is split into two sections. In Section 4.1 we introduce a basic model of the molecular events of IL-7 signalling. This model possesses non-linear transition terms. This first section is used to explain the methods we use to deal with the non-linear terms in the derivation of the moments of the stochastic model. In Section 4.2 we introduce a more detailed stochastic model of IL-7 signalling. The methods developed in the first section are then used to analyse the second, more complicated, model. At the end of Section 4.2 we derive functions which respectively describe the relationship between the concentration of IL-7 external to the T cell and the amount of signalling the

T cell receives. In addition, we derive a relationship between the external concentration of IL-7 and the rate of internalisation of IL-7. These relationships are then used in Chapter 5, in which redefine the model presented in Section 3.3.

4.1 Simple signalling relation

We consider a single T cell which is assumed to be suspended in some well-mixed medium containing the resource. The resource is assumed to be IL-7 and we let the concentration be fixed. The availability of IL-7 is denoted by the parameter I. IL-7 signals through the IL-7 receptor (IL-7R) and activates several signal transduction pathways. IL-7 signalling through the JAK and STAT pathways results primarily in the production of anti-apoptotic proteins such as Bcl-2 (Jiang *et al.*, 2005). Many of the proteins in these pathways are essential for the development of T cells in the thymus (Fry & Mackall, 2005). IL-7 further activates the PI3 kinase and Src kinase pathways (Dadi *et al.*, 1994; Seckinger & Fougereau, 1994). These pathways promote the survival and growth of lymphocytes both during development and during peripheral maintenance (Bradley *et al.*, 2005; Datta *et al.*, 1999; Rathmell *et al.*, 2001). T cell survival depends on a large number of distinct proteins, in particular the ratio of pro and anti-apoptotic proteins, which respectively promote or retard apoptosis. IL-7 signalling has been shown to promote JAK3 activity which is required for production of Bcl-2 (Eynon *et al.*, 1999; Suzuki *et al.*, 2000), however this is by no means the only mechanism by which IL-7 promotes cell survival. The aim of this work is not to model each individual intra-cellular pathway IL-7 activates. Instead, we introduce a pair of discrete random variables which describe the numbers of IL-7 receptors on the surface of the cell, and the number of signalling units inside the cell. We introduce the idea of signalling units as an abstraction to describe the amount of pathway activation resulting from internalisation of IL-7:IL-7R complexes. Studies of $CD8^+$ T cells support the notion that $CD8^+$ T cells require a minimum amount of IL-7 signalling to prevent death by apoptosis (Palmer *et al.*, 2011). The same studies highlighted the need for a minimum, but greater, amount of IL-7 signalling for proliferation of $CD8^+$ T cells. The behaviour of the single cell in this model is assumed to be determined by the amount of signalling units the cell possesses relative to thresholds for survival and division. As in the simple resource model, we assume thresholds in signalling must be surpassed to promote either cell survival or entry into the cell cycle.

We introduce the family of pairs of discrete random variables $\{\mathbb{X}_1(t), \mathbb{X}_2(t)\}_{t\geq 0}$, where $\mathbb{X}_1(t)$ denotes the number of IL-7 receptors on the surface of the cell and $\mathbb{X}_2(t)$ denotes the number of signalling units inside the cell. Time, t, is measured in hours. Both random variables take values on the space of positive integers (including zero) with probabilities

$$p_{n_1,n_2}(t) = \text{Prob}\{\mathbb{X}_1(t) = n_1, \mathbb{X}_2(t) = n_2 \mid \mathbb{X}_1(0) = n_{1,0}, \mathbb{X}_2(0) = n_{2,0}\}, \quad n_1, n_2 \in \mathbb{N}\cup\{0\}. \tag{4.1}$$

The pair of random variables take the values $(n_{1,0}, n_{2,0})$ at time $t = 0$. Formally the family of pairs of random variables $\{\mathbb{X}_1(t), \mathbb{X}_2(t)\}_{t\geq 0}$ are a continuous-time homogeneous Markov process. Denote by $\boldsymbol{n}$ the pair of states (n_1, n_2), then the infinitesimal transition probabilities of this Markov process are defined as

$$p_{\boldsymbol{m},\boldsymbol{n}}(\Delta t) = \text{Prob}\{\mathbb{X}_1(t+\Delta t) = m_1, \mathbb{X}_2(t+\Delta t) = m_2 \mid \mathbb{X}_1(t) = n_1, \mathbb{X}_2(t) = n_2\}. \tag{4.2}$$

In the following section we outline the biological assumptions from which the transition probabilities of this stochastic process are defined.

4.1.1 Transition probabilities

Transcription of IL-7R

We assume in the absence of signalling the IL-7 receptor is transcribed and expressed at a constant rate, denoted by the parameter ν. We furthermore assume IL-7 signalling induces negative feedback on the rate of transcription of the receptor (Jiang *et al.*, 2005). The amount of negative feedback is a function of the number of signalling units. This function takes the form $\mathrm{e}^{-n_2/\kappa}$, where κ is the number of signalling units required to retard the expression rate by approximately 63%. The transition probability is encoded as

$$p_{(n_1+1,n_2),\boldsymbol{n}}(\Delta t) = \nu \mathrm{e}^{-n_2/\kappa}\Delta t + o(\Delta t), \quad n_1, n_2 \geq 0. \tag{4.3}$$

Internalisation of IL-7R

IL-7 receptor is assumed to be internalised. The rate of internalisation is denoted by the parameter μ. The transition probability encoding this is

$$p_{(n_1-1,n_2),\boldsymbol{n}}(\Delta t) = \mu n_1 \Delta t + o(\Delta t), \quad n_1 \geq 1, n_2 \geq 0. \tag{4.4}$$

Production of signal

We assume signalling units are generated at a rate proportional to the number of receptors bound to IL-7. In this first approach, we assume generation of signal is described by a cross-product term between the number of IL-7Rs and the external concentration of IL-7, $\gamma I n_1$. The concentration of IL-7, I, is assumed to measured in the units ng ml^{-1}, in keeping with commonly reported units in the literature. The parameter γ therefore takes the units ng^{-1}ml hour^{-1}. The transition probability is written as

$$p_{(n_1,n_2+1),\boldsymbol{n}}(\Delta t) = \gamma I n_1 \Delta t + o(\Delta t), \quad n_1, n_2 \geq 0. \tag{4.5}$$

Decay of signal

We assume the IL-7 signal decays at a rate proportional to the number of signalling units. This rate is specified by the parameter ρ. The transition probability encoding decay of signal is

$$p_{(n_1,n_2-1),\boldsymbol{n}}(\Delta t) = \rho n_2 \Delta t + o(\Delta t), \quad n_1 \geq 0, n_2 \geq 1. \tag{4.6}$$

Conservation of probabilities

Probabilities should be conserved, therefore we introduce the probability that no transition occurs in a small time interval Δt as:

$$p_{\boldsymbol{n},\boldsymbol{n}}(\Delta t) = 1 - \left(\nu \mathrm{e}^{-n_2/\kappa} + \mu n_1 + \gamma I n_1 + \rho n_2\right) \Delta t + o(\Delta t), \quad n_1, n_2 \geq 0. \tag{4.7}$$

4.1.2 Master equation

Based on the defined transition probabilities, we write down the system of forward Kolmogorov equations governing the time evolution of the transition probabilities of the Markov process (Allen, 2003):

$$\begin{aligned}\frac{\mathrm{d}p_{\boldsymbol{n}}(t)}{\mathrm{d}t} =& \nu \mathrm{e}^{-n_2/\kappa} p_{(n_1-1,n_2)}(t) + \mu(n_1+1) p_{(n_1+1,n_2)}(t) \\ &+ \gamma I n_1 p_{(n_1,n_2-1)}(t) + \rho(n_2+1) p_{(n_1,n_2+1)}(t) \\ &- \left(\nu \mathrm{e}^{-n_2/\kappa} + \mu n_1 + \gamma I n_1 + \rho n_2\right) p_{\boldsymbol{n}}(t).\end{aligned} \tag{4.8}$$

The state space for this model is defined as the set of pairs of positive integers, that is, $(n_1, n_2) \in \mathbb{N}_0 \times \mathbb{N}_0$. Therefore, we define $p_{(n_1-1,n_2)}(t) = p_{(n_1,n_2-1)}(t) = 0$, such that

these equations are consistent at the lower limits of the state space. The stochastic process cannot take either a negative number of receptors or signalling units.

4.1.3 Time evolution of the moment generating function

The moment generating function for the stochastic process is defined as

$$M(\theta_1, \theta_2, t) \stackrel{\text{def}}{=} \sum_{n_1=0}^{+\infty} \sum_{n_2=0}^{+\infty} \mathrm{e}^{n_1\theta_1 + n_2\theta_2} p_{\boldsymbol{n}}(t), \quad \boldsymbol{n} = (n_1, n_2),\ \theta_1, \theta_2 \in \mathbb{R}^+. \tag{4.9}$$

We use the moment generating function technique (described in reference (Allen, 2003)) to derive a partial differential equation describing the time evolution of the moment generating function. From this PDE we then derive ordinary differential equations governing the time evolution of the moments of the stochastic process. The moment generating function technique is outlined in the remainder of this section. First multiply equation (4.8) by $\mathrm{e}^{n_1\theta_1 + n_2\theta_2}$. We next sum over all probabilities in the state space. Note that in the summations of terms encoding loss of receptor and decay of signal, we sum from $n_1 = -1$ and $n_2 = -1$, respectively. This ensures we count the terms containing the probabilities $p_{(0,0)}(t)$. Thus, equation (4.8) becomes

$$\begin{aligned}
\sum_{n_1=0}^{+\infty} \sum_{n_2=0}^{+\infty} \frac{\mathrm{d}p_{\boldsymbol{n}}(t)}{\mathrm{d}t} \mathrm{e}^{n_1\theta_1 + n_2\theta_2} = &\sum_{n_1=1}^{+\infty} \sum_{n_2=0}^{+\infty} \nu \mathrm{e}^{-n_2/\kappa} p_{(n_1-1,n_2)}(t) \mathrm{e}^{n_1\theta_1 + n_2\theta_2} \\
&+ \sum_{n_1=-1}^{+\infty} \sum_{n_2=0}^{+\infty} \mu(n_1+1) p_{(n_1+1,n_2)}(t) \mathrm{e}^{n_1\theta_1 + n_2\theta_2} \\
&+ \sum_{n_1=0}^{+\infty} \sum_{n_2=1}^{+\infty} \gamma I n_1 p_{(n_1,n_2-1)}(t) \mathrm{e}^{n_1\theta_1 + n_2\theta_2} \\
&+ \sum_{n_1=0}^{+\infty} \sum_{n_2=-1}^{+\infty} \rho(n_2+1) p_{(n_1,n_2+1)}(t) \mathrm{e}^{n_1\theta_1 + n_2\theta_2} \\
&- \sum_{n_1=0}^{+\infty} \sum_{n_2=0}^{+\infty} \left(\nu \mathrm{e}^{-n_2/\kappa} + \mu n_1 + \gamma I n_1 + \rho n_2\right) p_{\boldsymbol{n}}(t) \mathrm{e}^{n_1\theta_1 + n_2\theta_2}.
\end{aligned} \tag{4.10}$$

We next rewrite the summations such that they are expressed over the same limits and collect terms by the parameter coefficients. Assume the moment generating function exists and hence the summation on the left hand side of the above equation converges absolutely, then, we can interchange the derivative and summation. This

gives

$$\begin{aligned}\frac{\partial}{\partial t}\sum_{n_1=0}^{+\infty}\sum_{n_2=0}^{+\infty}p_{\boldsymbol{n}}(t)\mathrm{e}^{n_1\theta_1+n_2\theta_2} =&\nu(\mathrm{e}^{\theta_1}-1)\sum_{n_1=0}^{+\infty}\sum_{n_2=0}^{+\infty}\mathrm{e}^{-n_2/\kappa}p_{\boldsymbol{n}}(t)\mathrm{e}^{n_1\theta_1+n_2\theta_2}\\ &+\mu(\mathrm{e}^{-\theta_1}-1)\sum_{n_1=0}^{+\infty}\sum_{n_2=0}^{+\infty}n_1p_{\boldsymbol{n}}(t)\mathrm{e}^{n_1\theta_1+n_2\theta_2}\\ &+\gamma I(\mathrm{e}^{\theta_2}-1)\sum_{n_1=0}^{+\infty}\sum_{n_2=0}^{+\infty}n_1p_{\boldsymbol{n}}(t)\mathrm{e}^{n_1\theta_1+n_2\theta_2}\\ &+\rho(\mathrm{e}^{-\theta_2}-1)\sum_{n_1=0}^{+\infty}\sum_{n_2=0}^{+\infty}n_2p_{\boldsymbol{n}}(t)\mathrm{e}^{n_1\theta_1+n_2\theta_2}.\end{aligned}\tag{4.11}$$

A Taylor expansion of the function $f(x)=\mathrm{e}^{-x/\kappa}$ about the point $x=0$ gives the relation

$$f(x)=\sum_{j=0}^{+\infty}\frac{(-1)^j}{j!\kappa^j}x^j,\tag{4.12}$$

which holds for all $x\in\mathbb{R}$. Using this relation, we express our equation in terms of the partial derivatives of the moment generating function with respect to θ_i. Therefore equation (4.11) may be written as

$$\begin{aligned}\frac{\partial M(\theta_1,\theta_2,t)}{\partial t} =&\nu(\mathrm{e}^{\theta_1}-1)\sum_{j=0}^{+\infty}\frac{(-1)^j}{j!\kappa^j}\frac{\partial^j M(\theta_1,\theta_2,t)}{\partial\theta_2^j}+\mu(\mathrm{e}^{-\theta_1}-1)\frac{\partial M(\theta_1,\theta_2,t)}{\partial\theta_1}\\ &+\gamma I(\mathrm{e}^{\theta_2}-1)\frac{\partial M(\theta_1,\theta_2,t)}{\partial\theta_1}+\rho(\mathrm{e}^{-\theta_2}-1)\frac{\partial M(\theta_1,\theta_2,t)}{\partial\theta_2}.\end{aligned}\tag{4.13}$$

Taking derivatives of the moment generating function with respect to θ_i and evaluating at $\theta_i=0$, $i=1,2$, we derive expressions for the moments of the stochastic process. For a general bivariate process, we can write

$$m^{(i,j)}\overset{\text{def}}{=}\mathbb{E}[\mathbb{X}_1^i(t)\mathbb{X}_2^j(t)]=\left.\frac{\partial^{i+j}M(\theta_1,\theta_2,t)}{\partial\theta_1^i\partial\theta_2^j}\right|_{\theta_1=\theta_2=0}.\tag{4.14}$$

The moments $m^{(i,j)}$ depend on time and should be written as $m^{(i,j)}(t)$, from now on however, we drop the dependence on time for notational convenience. Therefore, finding the derivatives of equation (4.13) with respect to θ_1 and θ_2 and evaluating the resulting expressions at $\theta_1=\theta_2=0$, we derive dynamical equations for the first

moments of the stochastic process. We have

$$\frac{\mathrm{d}m^{(1,0)}}{\mathrm{d}t} = \nu \sum_{j=0}^{+\infty} \frac{(-1)^j}{j!\kappa^j} m^{(0,j)} - \mu m^{(1,0)}, \tag{4.15}$$

$$\frac{\mathrm{d}m^{(0,1)}}{\mathrm{d}t} = \gamma I m^{(1,0)} - \rho m^{(0,1)}. \tag{4.16}$$

Finding the second derivatives of equation (4.13) allows us to write down ODEs for the second moments of the process. Doing so gives the set of equations:

$$\frac{\mathrm{d}m^{(2,0)}}{\mathrm{d}t} = \nu \sum_{j=0}^{+\infty} \frac{(-1)^j}{j!\kappa^j} m^{(0,j)} + 2\nu \sum_{j=0}^{+\infty} \frac{(-\kappa^{-1})^j}{j!} m^{(1,j)} + \mu m^{(1,0)} - 2\mu m^{(2,0)} \tag{4.17}$$

$$\frac{\mathrm{d}m^{(1,1)}}{\mathrm{d}t} = \nu \sum_{j=0}^{+\infty} \frac{(-1)^j}{j!\kappa^j} m^{(0,j+1)} - \mu m^{(1,1)} + \gamma I m^{(2,0)} - \rho m^{(1,1)}, \tag{4.18}$$

$$\frac{\mathrm{d}m^{(0,2)}}{\mathrm{d}t} = \gamma I m^{(1,0)} + 2\gamma I m^{(1,1)} + \rho m^{(0,1)} - 2\rho m^{(0,2)}. \tag{4.19}$$

4.1.4 Mean field approximation

In this section we derive a mean field approximation to the stochastic process. Assume that the variance and higher moments of the process are zero, then, for a discrete random variable, $\mathbb{Y}$, we have from Lemma 3 in Appendix B:

$$\mathbb{E}[\mathbb{Y}^k] = \mathbb{E}[\mathbb{Y}]^k, \quad \text{for } k \geq 2. \tag{4.20}$$

The infinite series in equation (4.15) can be expressed as

$$\sum_{j=0}^{+\infty} \frac{(-1)^j}{j!\kappa^j} m^{(0,j)} = \sum_{j=0}^{+\infty} \frac{(-\kappa^{-1})^j}{j!} \left(m^{(0,1)}\right)^j = \mathrm{e}^{-m^{(0,1)}/\kappa}. \tag{4.21}$$

Letting $m_1(t) = m^{(1,0)}$, $m_2(t) = m^{(0,1)}$, the mean field approximation to the stochastic process is given by the following pair of ODEs:

$$\frac{\mathrm{d}m_1(t)}{\mathrm{d}t} = \nu \mathrm{e}^{-m_2(t)/\kappa} - \mu m_1(t), \tag{4.22}$$

$$\frac{\mathrm{d}m_2(t)}{\mathrm{d}t} = \gamma I m_1(t) - \rho m_2(t). \tag{4.23}$$

4.1.5 First order approximation

The coupled pair of ODEs describing the time evolution of the stochastic process, (4.15) and (4.16)), constitute an open set of equations. The solution of this set of equations depends on an infinite number of higher moments. We require a closed system of equations when computing the first two moments of the process, namely the mean and variance. We derive a closed system of equations by truncating the infinite summation. We may choose to truncate the sum at $j = 0$. However, in doing so we lose the dependence on the number of signalling units in the term representing the rate of expression of the IL-7 receptor, ν. Let us define a first order approximation as one in which we take $j = 1$. This gives the following system of equations, which describe the time evolution of the first and second moments of the process:

$$\frac{\mathrm{d}m^{(1,0)}}{\mathrm{d}t} = \nu\left(1 - \frac{m^{(0,1)}}{\kappa}\right) - \mu m^{(1,0)}, \tag{4.24}$$

$$\frac{\mathrm{d}m^{(0,1)}}{\mathrm{d}t} = \gamma I m^{(1,0)} - \rho m^{(0,1)}, \tag{4.25}$$

$$\frac{\mathrm{d}m^{(2,0)}}{\mathrm{d}t} = \nu\left(1 - \frac{m^{(0,1)}}{\kappa}\right) + 2\nu\left(1 - \frac{m^{(1,1)}}{\kappa}\right) + \mu m^{(1,0)} - 2\mu m^{(2,0)} \tag{4.26}$$

$$\frac{\mathrm{d}m^{(1,1)}}{\mathrm{d}t} = \nu\left(m^{(0,1)} - \frac{m^{(0,2)}}{\kappa}\right) - \mu m^{(1,1)} + \gamma I m^{(2,0)} - \rho m^{(1,1)}, \tag{4.27}$$

$$\frac{\mathrm{d}m^{(0,2)}}{\mathrm{d}t} = \gamma I m^{(1,0)} + 2\gamma I m^{(1,1)} + \rho m^{(0,1)} - 2\rho m^{(0,2)}. \tag{4.28}$$

The linear approximation gives a system of closed equations which can be solved to find the first and second moments of the process. Furthermore, under this approximation, if we are interested in the higher moments of the system, we are free derive the equations describing their time evolution by taking further derivatives of equation (4.13). There is no complication from the linear approximation. For the linear approximation, notice that the term representing the rate of expression of the IL-7 receptor becomes negative as the average number of signalling units exceeds κ. From a biological perspective we cannot have a negative expression rate and so this approximation is only valid when $m^{(0,1)} < \kappa$.

4.1.6 Second order approximation

Let us define the second order approximation as one in which we set $j = 2$ in the infinite summation of moments in 4.13. This gives the system of equations:

$$\frac{\mathrm{d}m^{(1,0)}}{\mathrm{d}t} = \nu\left(1 - \frac{m^{(0,1)}}{\kappa} + \frac{m^{(0,2)}}{2\kappa^2}\right) - \mu m^{(1,0)}, \tag{4.29}$$

$$\frac{\mathrm{d}m^{(0,1)}}{\mathrm{d}t} = \gamma I m^{(1,0)} - \rho m^{(0,1)}, \tag{4.30}$$

$$\frac{\mathrm{d}m^{(2,0)}}{\mathrm{d}t} = \nu\left(1 - \frac{m^{(0,1)}}{\kappa} + \frac{m^{(0,2)}}{2\kappa^2}\right) + 2\nu\left(m^{(1,0)} - \frac{m^{(1,1)}}{\kappa} + \frac{m^{(1,2)}}{2\kappa^2}\right) + \mu m^{(1,0)} - 2\mu m^{(2,0)}, \tag{4.31}$$

$$\frac{\mathrm{d}m^{(1,1)}}{\mathrm{d}t} = \nu\left(m^{(0,1)} - \frac{m^{(0,2)}}{\kappa} + \frac{m^{(0,3)}}{2\kappa^2}\right) - \mu m^{(1,1)} + \gamma I m^{(2,0)} - \rho m^{(1,1)}, \tag{4.32}$$

$$\frac{\mathrm{d}m^{(0,2)}}{\mathrm{d}t} = \gamma I m^{(1,0)} + 2\gamma I m^{(1,1)} + \rho m^{(0,1)} - 2\rho m^{(0,2)}. \tag{4.33}$$

This set of equations is not a closed system; that is, there exist terms with third order moments in equations (4.31) and (4.32). To allow solutions of the system to be computed we must use a moment closure technique. Moment closure techniques allow closed systems of equations to be formed by expressing higher order moments as polynomial functions of the lower order moments of the system. One chooses such a dependence by making assumptions on the distribution of the fluctuations of the process. For example, one might assume fluctuations are normally distributed. In a normal distribution, third order and higher order moments are zero. Correspondingly, for a random variable $\mathbb{Y} \sim \mathcal{N}(\mu, \sigma^2)$, one may derive the relation

$$\mathbb{E}[\mathbb{Y}^3] = 3\mathbb{E}[\mathbb{Y}]\mathbb{E}[\mathbb{Y}^2] - 2\mathbb{E}[\mathbb{Y}]^3. \tag{4.34}$$

In reference (Singh & Hespanha, 2006b), Singh and Hespanha suggest matching the first derivatives of the approximations to the $(n+1)$th moments of the stochastic system, to the first derivatives of the true $(n+1)$th moments, when attempting to close a system for the first nth moments. Specifically, the authors consider closing a system for the first two moments. This entails introducing a polynomial to express third moments in terms of the first and second moments. Borrowing from

reference (Singh & Hespanha, 2006b), let us define

$$m^{(0,3)} = \begin{cases} \left(\frac{m^{(0,2)}}{m^{(0,1)}}\right)^3, & \text{if } m^{(0,1)} > 0, \\ 0, & \text{if } m^{(0,1)} = 0, \end{cases} \tag{4.35}$$

$$m^{(1,2)} = \begin{cases} \frac{m^{(0,2)}}{m^{(1,0)}}\left(\frac{m^{(1,1)}}{m^{(0,1)}}\right)^2, & \text{if } m^{(1,0)} > 0 \text{ and } m^{(0,1)} > 0, \\ 0, & \text{if } m^{(1,0)} = 0 \text{ or } m^{(0,1)} = 0. \end{cases} \tag{4.36}$$

These polynomials are symmetric with respect to the indices of the moments. Thus, one may easily derive $m^{(3,0)}$ and $m^{(2,1)}$ by replacing $m^{(i,j)}$ by $m^{(j,i)}$ in the above equations. This moment closure approach is equivalent to assuming fluctuations are distributed log-normally (Singh & Hespanha, 2006a). For a log-normally distributed random variable $\mathbb{Y}$, the probability that $\mathbb{Y}$ takes the value zero is zero. Therefore the log-normal approximation is only valid when $\mathbb{X}_i \geq 1$, $i = 1, 2$. However, for the stochastic process we have introduced, there is a non-zero probability that $\mathbb{X}_i = 0$, $i = 1, 2$, for some time $t \geq 0$. Suppose however, that we assume the random variables $\mathbb{X}_i$, $i = 1, 2$ have a multi-variate log-normal distribution. In Theorem 1 in Appendix A we show that in the limit $\mathbb{E}[\mathbb{X}_i] \to 0$, we have $\mathbb{E}[\mathbb{X}_1^j \mathbb{X}_2^k] \to 0$ for any $j, k \geq 0$ such that $j + k > 1$. Therefore, setting the above polynomials equal to zero when either $m^{(1,0)}$ or $m^{(0,1)}$ is zero, is consistent with the log-normal assumption as the first moments become vanishingly small. Under this moment closure method, the first two moments are described by the system of equations:

$$\frac{\mathrm{d}m^{(1,0)}}{\mathrm{d}t} = \nu\left(1 - \frac{m^{(0,1)}}{\kappa} + \frac{m^{(0,2)}}{2\kappa^2}\right) - \mu m^{(1,0)}, \tag{4.37}$$

$$\frac{\mathrm{d}m^{(0,1)}}{\mathrm{d}t} = \gamma I m^{(1,0)} - \rho m^{(0,1)}, \tag{4.38}$$

$$\begin{aligned} \frac{\mathrm{d}m^{(2,0)}}{\mathrm{d}t} =& \nu\left(1 - \frac{m^{(0,1)}}{\kappa} + \frac{m^{(0,2)}}{2\kappa^2}\right) + 2\nu\left(m^{(1,0)} - \frac{m^{(1,1)}}{\kappa} + \frac{1}{2\kappa^2}\frac{m^{(0,2)}}{m^{(1,0)}}\left(\frac{m^{(1,1)}}{m^{(0,1)}}\right)^2\right) \\ &+ \mu m^{(1,0)} - 2\mu m^{(2,0)}, \end{aligned} \tag{4.39}$$

$$\frac{\mathrm{d}m^{(1,1)}}{\mathrm{d}t} = \nu\left(m^{(0,1)} - \frac{m^{(0,2)}}{\kappa} + \frac{1}{2\kappa^2}\left(\frac{m^{(0,2)}}{m^{(0,1)}}\right)^3\right) - \mu m^{(1,1)} + \gamma I m^{(2,0)} - \rho m^{(1,1)}, \tag{4.40}$$

$$\frac{\mathrm{d}m^{(0,2)}}{\mathrm{d}t} = \gamma I m^{(1,0)} + 2\gamma I m^{(1,1)} + \rho m^{(0,1)} - 2\rho m^{(0,2)}. \tag{4.41}$$

If we truncate the infinite summation in equation (4.13) at $j = k$, the derivative matching method for moment closure allows us to express moments of order $k+1$ in terms of moments up to order k. However, we must find derivatives of (4.13) up to order k such that we derive a closed system of equations. Therefore, whilst we may truncate at arbitrary order, we are required to derive increasingly larger numbers of equations to close the system. Here we truncate at $j = 2$. Consider that the infinite summation of moments is approximated by a second order polynomial. If for example $m^{(0,2)}$ grows too large, this polynomial may dominate the terms of the ODEs and trajectories may tend to infinity. Therefore, this method is only valid when parameters are such that the random variable $\mathbb{X}_2$ takes values typically less than κ. The accuracy of this method is explored in the following sections, however, first, in the next section, we derive parameters for this model from the literature.

4.1.7 Choice of parameter values

In this section we use the mean field approximation derived in Subsection 4.1.4 to estimate parameter values from published experimental data. We use reference (Park *et al.*, 2004) to derive our parameter values since this paper presents extensive studies of the effect IL-7 has on IL-7Rα expression. The mean field model is given by equations (4.22) and (4.23). Whilst exact solutions for the fixed points of these equations cannot be expressed in terms of regular functions, the fixed points satisfy

$$m_2^* = \frac{\gamma I}{\rho} m_1^*, \tag{4.42}$$

where m_1^* is the unique solution of the following equation:

$$\nu \exp\left(-\frac{\gamma I}{\kappa \rho} m_1^*\right) = \mu m_1^*. \tag{4.43}$$

It is easily proved m_1^* exists and is unique. Furthermore, the solution (m_1^*, m_2^*) is asymptotically stable. In reference (Park *et al.*, 2004), $CD4^+$ T cells were found to express approximately 3.6×10^4 IL-7Rα chains on the surface of the cell in IL-7 free medium, whilst $CD8^+$ T cells were found to express approximately 4.1×10^4 IL-7Rα chains. In our model of IL-7 receptor dynamics we shall ignore this modest difference between $CD4^+$ and $CD8^+$ expression and assume T cells express 4×10^4 IL-7Rα chains at steady state in IL-7 free medium. Therefore, using equation (4.43)

we have

$$m_1^*|_{I=0} = \frac{\nu}{\mu} = 4 \times 10^4 \text{ receptors.} \tag{4.44}$$

Surface expression of IL-7Rα was assessed for T cells left overnight in 6 ng ml^{-1} culture of IL-7. After overnight treatment, IL-7Rα expression was approximately 2% of control T cells left in IL-7 free medium. Assuming steady state numbers of receptors after overnight culture, we have

$$m_1^*|_{I=6} = 0.02\frac{\nu}{\mu} = 8 \times 10^2 \text{ receptors.} \tag{4.45}$$

Substituting this expression into relation (4.43) we find

$$\begin{aligned} & \exp\left(-\frac{6\gamma}{\kappa\rho}m_1^*\right) = 0.02, \\ \Rightarrow \quad & -4.8 \times 10^3 \frac{\gamma}{\rho\kappa} = \log(0.02), \\ \Rightarrow \quad & \rho\kappa \approx 1.2 \times 10^3 \gamma. \end{aligned} \tag{4.46}$$

T cells left in overnight culture of 6 ng ml^{-1} IL-7 were placed in IL-7 free medium and the abundance of IL-7Rα mRNA was measured relative to controls over a 12 hour period. After 12 hours, IL-7 mRNA levels were approximately 99% of control levels (Park *et al.*, 2004). These observations allow us to obtain an estimate for the rate of signal decay. We shall assume that over the 12 hour period, the IL-7Rα transcription rate, $T(m_2(t)) \stackrel{\text{def}}{=} \nu \exp(-m_2(t)/\kappa)$, returns to approximately that of the transcription rate of an uninhibited ($m_2(t) = 0$) cell. We let

$$T(m_2(12)) = 0.99\nu. \tag{4.47}$$

The ODE describing the change in the number of signalling units is given by equation (4.23). Note that without IL-7 stimulus ($I = 0$ ng ml^{-1}), this ODE has solution $m_2(t) = S_0 \exp(-\rho t)$, where $S_0 = m_2(t = 0)$. Combining this solution with the above expression for T, we find

$$\begin{aligned} & T(m_2(12)) = \nu \exp\left(-\frac{m_2(12)}{\kappa}\right) = \nu \exp\left(-\frac{S_0 \exp(-12\rho)}{\kappa}\right) = 0.99\nu, \\ \Rightarrow \quad & \frac{S_0}{\kappa} \mathrm{e}^{-12\rho} = -\log(0.99). \end{aligned} \tag{4.48}$$

Assume the number of signalling units reach equilibrium during overnight culture in 6ng ml^{-1} IL-7, then $S_0 = m_2^*|_{I=6}$. Combining relations (4.42) and (4.43), $m_2^*|_{I=6}$ satisfies

$$\frac{\nu}{\mu} \mathrm{e}^{-m_2^*|_{I=6}/\kappa} = \frac{\rho}{6\gamma}\, m_2^*|_{I=6}\,. \tag{4.49}$$

Substituting our previously derived parameter relations ($\nu/\mu = 4 \times 10^4$, $\rho/\gamma = 1.2 \times 10^3/\kappa$), this equation reduces to

$$2 \times 10^2 \mathrm{e}^{S_0/\kappa} \approx \frac{S_0}{\kappa}. \tag{4.50}$$

We solve this equation numerically for S_0/κ, from which we find $S_0/\kappa \approx 3.9$. Therefore, from equation (4.48) we find

$$\rho \approx 0.5 \text{ hours}^{-1}. \tag{4.51}$$

T cells rested overnight in IL-7 free medium were placed in 6 ng ml^{-1} IL-7 culture for 6 hours, following which the expression of IL-7Rα was found to be approximately 10% of controls for CD8$^+$ T cells and 16% of controls for CD4$^+$ T cells. Let us assume after 6 hours in IL-7 culture, IL-7Rα expression drops to 13% of initial expression. This observation allows us to determine a value for the rate of internalisation of IL-7R, μ. However, the calculation requires the full solution of equations (4.43) and (4.42) and a known value of κ. Due to the non-linearity of these equations, we omit an analytical calculation, and instead carry out a numerical study. Prior to this, we must choose a value for κ.

We have introduced the idea of signalling units as an abstraction to avoid modelling a myriad of downstream signalling pathways inside the T cell. Since we are working with an abstraction, rather than a measurable quantity, we have one degree of freedom in choosing a typical value for the number of signalling units. The decisions a cell makes, for example, whether to undergo apoptosis or enter the cell cycle, are assumed to be dependent on the number of signalling units relative to thresholds for survival and division. In particular, if the number of signalling units is below a threshold given, θ_s, we assume the cell will die due to apoptosis at some fixed rate. Likewise, if the number of signalling units is greater than a threshold, θ_p, the cell will enter the cell cycle at some fixed rate. In reference (Palmer *et al.*, 2011), T cells placed in in vitro cultures of IL-7 were assessed for cell viability and markers of proliferation. Results show a significant drop in cell viability for concentrations below, approximately, 10^{-2} ng ml^{-1} IL-7, whereas markers for proliferation were

observed for IL-7 concentrations above 0.1 ng ml^{-1}. Let us choose 10^{-2} ng ml^{-1} IL-7 as a typical value for a low concentration of IL-7. We choose κ such that in low concentrations, stochastic fluctuations in the number of signalling units typically remain above zero. This should minimise any issues arising from the log-normal moment closure method for the stochastic moments when the moment $m^{(0,1)}$ is close to zero. A numerical exploration of different values of κ reveals this condition is met for values of κ greater than 100 signalling units. Reducing κ to 10 signalling units produces stochastic realisations under which $\mathbb{X}_2$ frequently visits the state $n_2 = 0$. Therefore, let us choose $\kappa = 10^2$ signalling units.

It should be noted that the choice to define a typical number of signalling units for a given concentration is somewhat arbitrary. However, for the results derived at the end of this chapter, this choice is not important, provided the signalling thresholds θ_s and θ_p (introduced in Section 3.3 and reintroduced in Section 5.2) are chosen appropriately.

Based on this value chosen value for κ, and the observations of an 87% drop in receptor expression after 6 hours in IL-7 culture of 6 ng ml^{-1}, we numerically determine a suitable value for internalisation rate to be $\mu = 0.4$ hours^{-1}. Table 4.1 summarises our chosen parameter set.

Based on our chosen parameter set and the observations at which significant changes occur in cell viability and proliferation in reference (Palmer *et al.*, 2011) we choose the respective thresholds for survival and proliferation to be the equilibrium numbers of signalling units for $I = 10^{-2}$, $I = 0.1$, respectively. Graphical inspection of the mean field trajectories shows $m_2^* \approx 25$ when $I = 10^{-2}$ and $m_2^* \approx 1.1 \times 10^2$ when $I = 0.1$. In Figure 4.1 we show numerical solutions to the mean field approximation for our chosen parameter set for $I = 10^{-2}$ ng ml^{-1} and $I = 0.1$ ng ml^{-1}.

Parameter	Value	Units
ν	1.6×10^4	rec hour^{-1}
μ	0.4	hour^{-1}
κ	10^2	signalling units
γ	4×10^{-2}	signalling units rec^{-1} ng^{-1} ml hour^{-1}
ρ	0.5	hour^{-1}
θ_s	25	signalling units
θ_p	1.1×10^2	signalling units

Table 4.1: Parameter set for mean field approximation. We let *rec* be the units for the number of surface receptors.

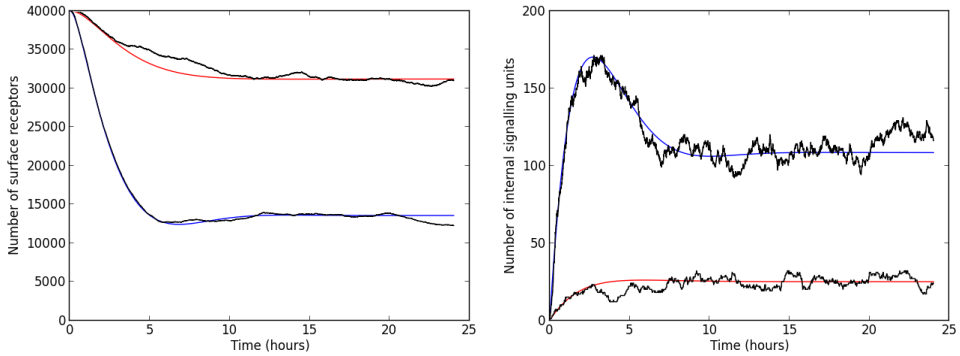

Figure 4.1: Trajectories of mean field approximation over a 24 hour period. We show one stochastic trajectory (black). The stochastic trajectory was realised using the Gillespie algorithm wherein the transition rates are defined by equations (4.3)-(4.7). Initial conditions are 4×10^4 receptors and zero signalling units. The parameter set used is given in Table 4.1. Blue: $I = 10^{-1}$ ng ml^{-1}. Red: $I = 10^{-2}$ ng ml^{-1}.

4.1.8 Comparison of approximations

We use the Gillespie algorithm to produce 10^4 realisations of the stochastic process over a time interval of 24 hours. We discretise the 24 hour period into 2.4×10^3 time intervals of length 10^{-2} hours. For each time interval, the state of the stochastic process following the first jump in the time interval, is recorded. Thus, we produce 10^4 observations of the stochastic process during each time interval. The mean and sample standard deviation for each time interval is computed, both for the number of receptors and the number of signalling units. This is done for $I = 10^{-2}$ ng ml^{-1} and $I = 0.1$ ng ml^{-1}, we compare the statistics obtained from the simulated data sets with the approximations discussed in Sections 4.1.4, 4.1.5 and 4.1.6.

First order approximation, $I = 10^{-2}$ ng ml^{-1}. Figure 4.2, first row. The first moments from the theoretical approximation and simulated trajectories agree under this approximation. However, the first order approximation completely fails to reproduce the second moments of the process. Indeed, numerical solutions for the second moments predict $\mathbb{E}[\mathbb{X}_1^2] < (\mathbb{E}[\mathbb{X}_1])^2$, this does not make mathematical sense, since this would imply the variance is negative.

First order approximation, $I = 0.1$ ng ml^{-1}. Figure 4.2, second row. For $I = 0.1$ ng ml^{-1}, the first order approximation performs worse than when $I = 10^{-2}$ ng ml^{-1}. Not only does the approximation predict the variance is negative, but for both the number of receptors and the number of signalling units, there is a significant

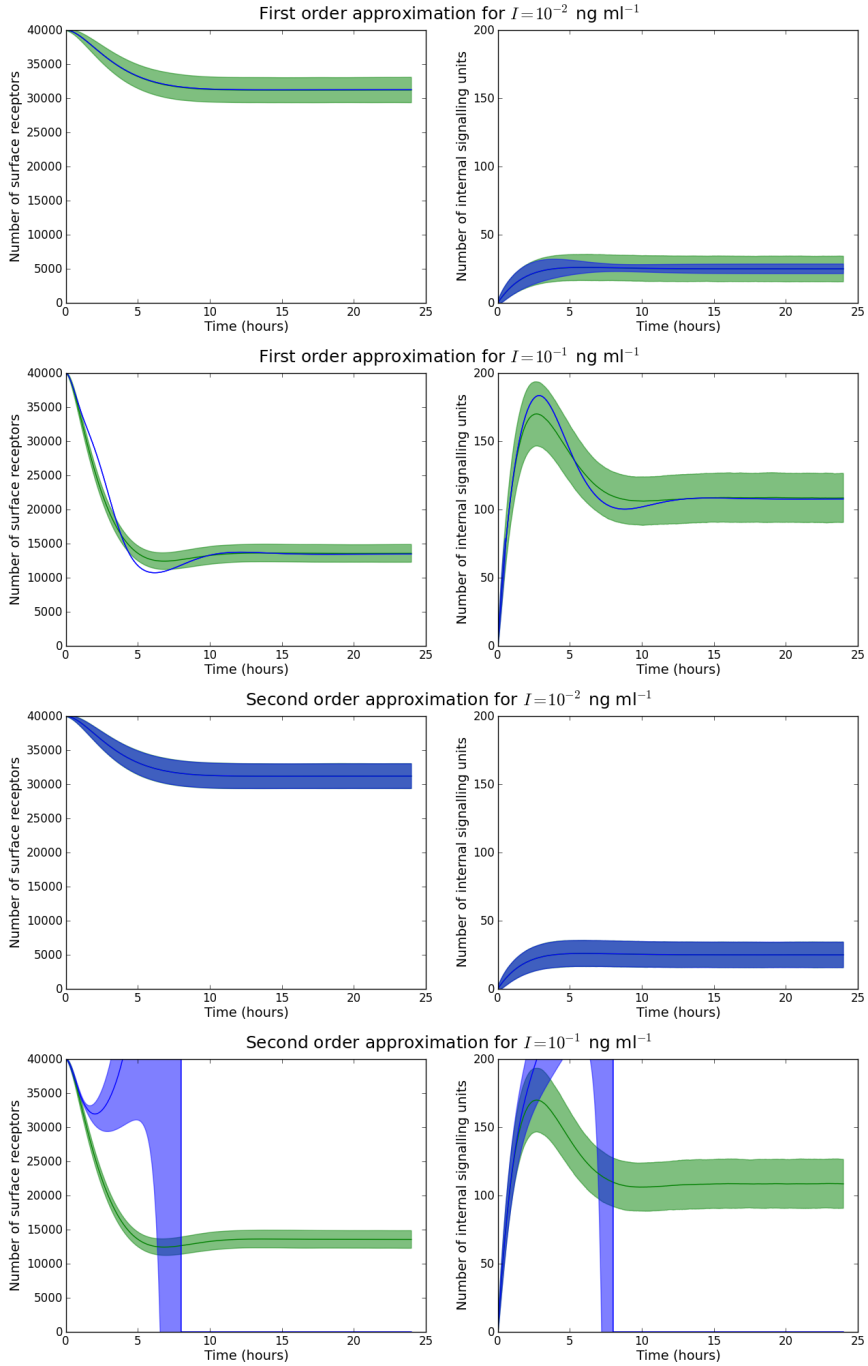

Figure 4.2: Green areas represent the mean ± 1.96 standard deviations of 10^4 realisations produced using the Gillespie algorithm. Blue areas represent the mean ± 1.96 standard deviations computed from the various approximations. From top to bottom, we present in each row, the first order approximation for $I = 10^{-2}$ ng ml^{-1}, the first order approximation for $I = 10^{-1}$ ng ml^{-1}, the second order approximation for $I = 10^{-2}$ ng ml^{-1}, and finally, the second order approximation for $I = 10^{-1}$ ng ml^{-1}.

deviation in the prediction of the first moments from the numerically simulated observations. The issue arises since when I takes this larger value, because, at this larger value we typically observe the number of signalling units exceeding the parameter κ. This implies the approximation to the exponential in Section 4.1.1 is negative.

Second order approximation, $I = 10^{-2}$ ng ml^{-1}. Figure 4.2, third row. The second order approximation for the lower value of I closely matches the simulated observations for both the first and second moments. It is difficult to see any discrepancy between outputs at the scale shown in Figure 4.2.

Second order approximation, $I = 0.1$ ng ml^{-1}. Figure 4.2, fourth row. The second order approximation completely fails to capture both the first and second moments for the greater value of I. Typically, for this value of I, the number of signalling units exceeds κ. In the second order approximation this implies quadratic growth terms dominate all other terms in the system of ODEs. The result is rapidly increasing trajectories for which the numerical schemes (4^{th}-order Runge-Kutta) used to produce solutions quickly break down. These schemes break because the variables representing the number of receptors and signalling units quickly become so large, Python returns the object "Nan", that is, an object used to represent numbers beyond what the limits of what can be stored in memory.

Neither the first order or second order approximations satisfyingly predict the first two moments for $I = 0.1$ ng ml^{-1}. Two options present themselves when considering improvements upon the approximations. The first option is to derive and solve ODEs for the higher order moments of the process. Suppose we wish to derive a system of ODEs up to and including the third order moments of the stochastic process. The dynamical equations governing the third order moments now contain terms which are dependent on the fourth and fifth order moments. In reference (Singh & Hespanha, 2006a) the approaches outlined in reference (Singh & Hespanha, 2006b) are extended to stochastic processes with multiple populations. In particular, for a system of two populations, the authors suggest the polynomial approximations to the fourth order moments given in Table 4.2. As for the polynomial approximations presented in Section 4.1.6, these polynomials are symmetric with respect to the indices. That is, we can find $m^{(j,i)}$ from $m^{(i,j)}$ by replacing all terms $m^{(k,l)}$ by the terms $m^{(l,k)}$ in the corresponding polynomial. These polynomials were derived

using the derivative matching techniques outlined in (Singh & Hespanha, 2006b). However, these methods are equivalent to assuming the random variables of the process corresponding to a given time t are distributed log-normally. For a simple example, consider the univariate log-normally distributed random variable $\mathbb{Y}$ with log-mean and shape parameters (μ, σ^2). For such a random variable, the moments can be expressed as (Johnson *et al.*, 1970)

$$\mathbb{E}[\mathbb{Y}^s] = \mathrm{e}^{s\mu + \frac{1}{2}s^2\sigma^2}. \tag{4.52}$$

From this expression and the first polynomial in Table 4.2, we see that

$$\begin{aligned}
\frac{\left(\mathbb{E}[\mathbb{Y}]\mathbb{E}[\mathbb{Y}^3]\right)^4}{\left(\mathbb{E}[\mathbb{Y}^2]\right)^6} &= \frac{\left(\mathrm{e}^{\mu+\frac{1}{2}\sigma^2}\mathrm{e}^{3\mu+\frac{1}{2}\times 9\sigma^2}\right)^4}{\left(\mathrm{e}^{2\mu+\frac{1}{2}\times 4\sigma^2}\right)^6} \\
&= \frac{\mathrm{e}^{16\mu+\frac{1}{2}\times 40\sigma^2}}{\mathrm{e}^{12\mu+\frac{1}{2}\times 16\sigma^2}} \\
&= \mathrm{e}^{4\mu+\frac{1}{2}\times 16\sigma^2} \\
&= \mathbb{E}[\mathbb{Y}^4].
\end{aligned} \tag{4.53}$$

Using the general method outlined in (Singh & Hespanha, 2006b), we derived the equivalent results for a set of fifth order moments. These polynomials are expressed in Table 4.3. We nested the polynomials for the fourth order moments inside the polynomials for the fifth order moments to derive polynomials with which we can close the system of equations describing the third and lower order moments. We omit the presentation of this nine-equation system. However, the numerical solution of this system for $I = 0.1$ ng ml^{-1} is presented in the top row of Figure 4.3.

The second approach we take is to reconsider the expansion described by equation (4.12). In this series we expanded about the point $x = 0$. This implies the expansion is most accurate for x in some neighbourhood about 0. From the mean of the Gillespie realisations presented in Figure 4.2, we see, for $I = 0.1$ ng ml^{-1}, the number of signalling units in equilibrium is approximately 1.1×10^2, which is reasonably close to $\kappa = 10^2$ signalling units. We may improve the accuracy of the expansion for $I = 0.1$ ng ml^{-1} by expanding about a value close to the number of signalling units in equilibrium. In this case we expand about κ. Equation (4.12)

Moment	Polynomial approximation
$m^{(0,4)}$	$\frac{\left(m^{(0,1)}m^{(0,3)}\right)^4}{\left(m^{(0,2)}\right)^6}$
$m^{(1,3)}$	$\left(\frac{m^{(1,2)}}{m^{(1,1)}}\right)^3\left(\frac{m^{(0,1)}}{m^{(0,2)}}\right)^3 m^{(0,3)}m^{(1,0)}$
$m^{(2,2)}$	$\frac{\left(m^{(1,2)}m^{(2,1)}m^{(1,0)}m^{(0,1)}\right)^2}{\left(m^{(1,1)}\right)^4 m^{(0,2)}m^{(2,0)}}$

Table 4.2: Polynomial approximations to the fourth moments of a two species Markov process.

Moment	Polynomial approximation
$m^{(0,5)}$	$\left(\frac{m^{(0,2)}}{m^{(0,3)}}\right)^{10}\left(\frac{m^{(0,4)}}{m^{(0,1)}}\right)^5$
$m^{(1,4)}$	$\left(\frac{m^{(0,2)}}{m^{(1,2)}}\right)^6\left(\frac{m^{(1,1)}m^{(1,3)}}{m^{(0,1)}m^{(0,3)}}\right)^4\frac{m^{(0,4)}}{m^{(1,0)}}$
$m^{(2,3)}$	$\left(\frac{m^{(1,1)}}{m^{(1,2)}}\right)^6\left(\frac{m^{(0,2)}m^{(2,2)}}{m^{(0,1)}m^{(0,3)}}\right)^3\left(\frac{m^{(1,3)}}{m^{(1,0)}}\right)^2\frac{m^{(2,0)}}{m^{(0,3)}}$

Table 4.3: Polynomial approximations to the fifth moments of a two species Markov process.

therefore becomes

$$f(x) = \mathrm{e}^{-1}\sum_{j=0}^{+\infty}\frac{(-1)^j}{j!\kappa^j}(x-\kappa)^j = \mathrm{e}^{-1}\sum_{j=0}^{\infty}\sum_{k=0}^{j}\frac{(-\kappa)^{-k}}{k!(j-k)!}x^k, \tag{4.54}$$

where we have used a binomial expansion[1] to expand the term $(x-\kappa)^j$. Using such an expansion, equation (4.13) becomes

$$\begin{aligned}\frac{\partial M(\theta_1,\theta_2,t)}{\partial t} =& \nu\mathrm{e}^{-1}(\mathrm{e}^{\theta_1}-1)\sum_{j=0}^{+\infty}\sum_{k=0}^{j}\frac{(-\kappa)^{-k}}{k!(j-k)!}\frac{\partial^k M(\theta_1,\theta_2,t)}{\partial\theta_2^k}\\ &+\mu(\mathrm{e}^{-\theta_1}-1)\frac{\partial M(\theta_1,\theta_2,t)}{\partial\theta_1}+\gamma I(\mathrm{e}^{\theta_2}-1)\frac{\partial M(\theta_1,\theta_2,t)}{\partial\theta_1}\\ &+\rho(\mathrm{e}^{-\theta_2}-1)\frac{\partial M(\theta_1,\theta_2,t)}{\partial\theta_2}.\end{aligned} \tag{4.55}$$

From this equation we again derive a second order approximation using the same

[1] We define $\binom{j}{k} = \begin{cases}\frac{j!}{k!(j-k)!} & \text{if j} \geq \text{k}\\ 0 & \text{if j} < \text{k.}\end{cases}$

methods discussed in Section 4.1.6. Numerical solutions of the second order approximation are shown in the bottom row of Figure 4.3. It can be clearly seen that the second order approximation derived by first expanding about κ rather than 0 is in closer agreement with the simulated moments than the third order approximation when expanding about 0. We surmise that the dominant factor limiting the accuracy of the approximations is the agreement between the term $\exp(-n_2/\kappa)$ and its polynomial expansion. The point about which we expand should be chosen to be representative of a typical value any given stochastic realisation may take. When considering the process in equilibrium this choice is clear: to obtain the best approximations to the fluctuations in equilibrium, we should expand about a point equal to the mean value of the fluctuations, which may be estimated from the mean field approximation.

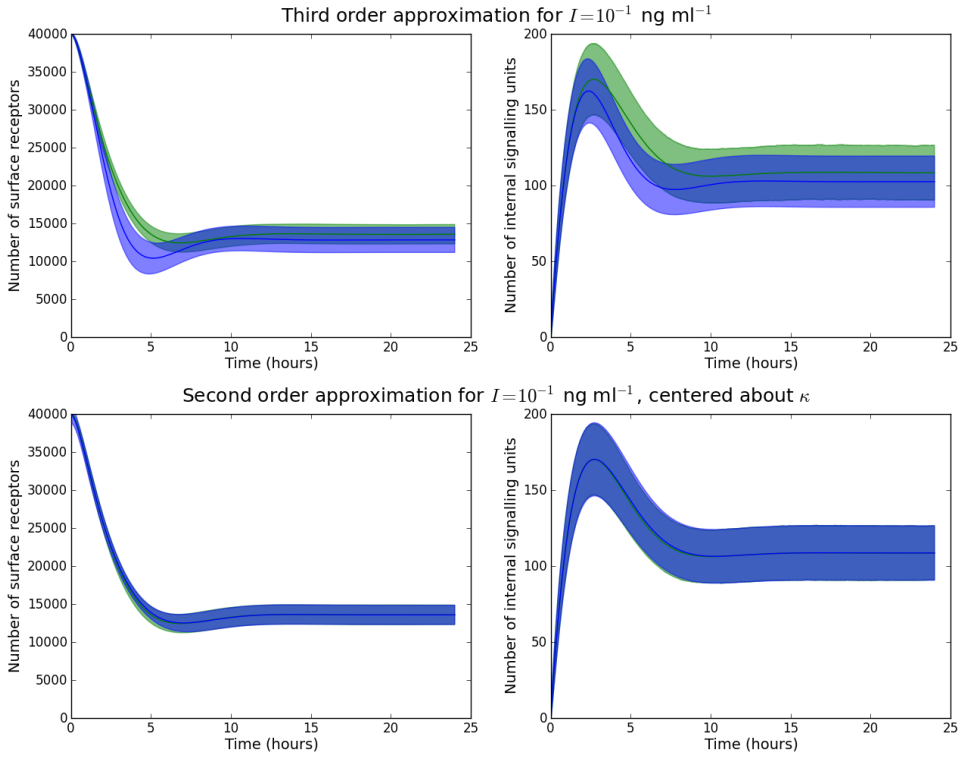

Figure 4.3: As in Figure 4.2, green areas represent the mean ± 1.96 standard deviations of 10^4 realisations produced using the Gillespie algorithm, and blue areas represent the mean ± 1.96 standard deviations computed from the approximations. In the top row we present the third order approximations to the stochastic model for $I = 10^{-1}$ ng ml^{-1}. In the bottom row we present second order approximations where we have expanded about κ.

4.1.9 Fluctuations in equilibrium

Let m_2^* be the steady state solution of equation (4.23). We define

$$\epsilon = \frac{m_2^*}{\kappa}. \tag{4.56}$$

In this section we present a second order approximation to the stochastic model in which we replace equation (4.12) by an expansion about the point $\epsilon\kappa$. Omitting the derivation, which follows exactly the same procedure as shown in previous sections, the system of ODEs governing the time evolution of the first and second moments is given by

$$\frac{\mathrm{d}m^{(1,0)}}{\mathrm{d}t} = \nu \mathrm{e}^{-\epsilon}\left(1+\epsilon+\frac{\epsilon^2}{2}-(1+\epsilon)\frac{m^{(0,1)}}{\kappa}+\frac{m^{(0,2)}}{2\kappa^2}\right)-\mu m^{(1,0)}, \tag{4.57}$$

$$\frac{\mathrm{d}m^{(0,1)}}{\mathrm{d}t} = \gamma I m^{(1,0)} - \rho m^{(0,1)}, \tag{4.58}$$

$$\begin{aligned}\frac{\mathrm{d}m^{(2,0)}}{\mathrm{d}t} =& 2\nu \mathrm{e}^{-\epsilon}\left(\left(1+\epsilon+\frac{\epsilon^2}{2}\right)m^{(1,0)}-(1+\epsilon)\frac{m^{(1,1)}}{\kappa}+\frac{1}{2\kappa^2}\frac{m^{(0,2)}}{m^{(1,0)}}\left(\frac{m^{(1,1)}}{m^{(0,1)}}\right)^2\right)\\ &+\nu \mathrm{e}^{-\epsilon}\left(1+\epsilon+\frac{\epsilon^2}{2}-(1+\epsilon)\frac{m^{(0,1)}}{\kappa}+\frac{m^{(0,2)}}{2\kappa^2}\right)+\mu m^{(1,0)}-2\mu m^{(2,0)},\end{aligned} \tag{4.59}$$

$$\begin{aligned}\frac{\mathrm{d}m^{(1,1)}}{\mathrm{d}t} =& \nu \mathrm{e}^{-\epsilon}\left(\left(1+\epsilon+\frac{\epsilon^2}{2}\right)m^{(0,1)}-(1+\epsilon)\frac{m^{(0,2)}}{\kappa}+\frac{1}{2\kappa^2}\left(\frac{m^{(0,2)}}{m^{(0,1)}}\right)^3\right)\\ &-\mu m^{(1,1)}+\gamma I m^{(2,0)}-\rho m^{(1,1)},\end{aligned} \tag{4.60}$$

$$\frac{\mathrm{d}m^{(0,2)}}{\mathrm{d}t} = \gamma I m^{(1,0)} + 2\gamma I m^{(1,1)} + \rho m^{(0,1)} - 2\rho m^{(0,2)}. \tag{4.61}$$

As a verification that this approach accurately approximates the fluctuations of the process in equilibrium, Figure 4.4 shows numerical solutions of these ODEs for $I = 1$ ng ml^{-1} (top row) and $I = 10$ ng ml^{-1} (bottom row). Since this approximation is only valid when the number of signalling units takes values in some neighbourhood of m_2^*, we choose initial conditions to be close to the equilibrium to ensure the process stays within this neighbourhood. If initial conditions are not suitably chosen, the process may enter a regime where typically $m^{(0,1)} \gg \epsilon\kappa$. In this situation, quadratic growth terms dominate the remaining terms, and solutions grow sufficiently fast that the numerical schemes used to solve the system of ODEs break down. The choice was made by reducing initial conditions until the numerical scheme used to

solve the ODEs completed successfully. The numerical scheme breaks down more readily for larger values of I (the average amount of signalling, $m^{(0,1)}$, is more likely to exceed $\epsilon\kappa$), hence, the initial conditions for $I = 10$ ng ml^{-1} had to be chosen closer to the equilibrium.

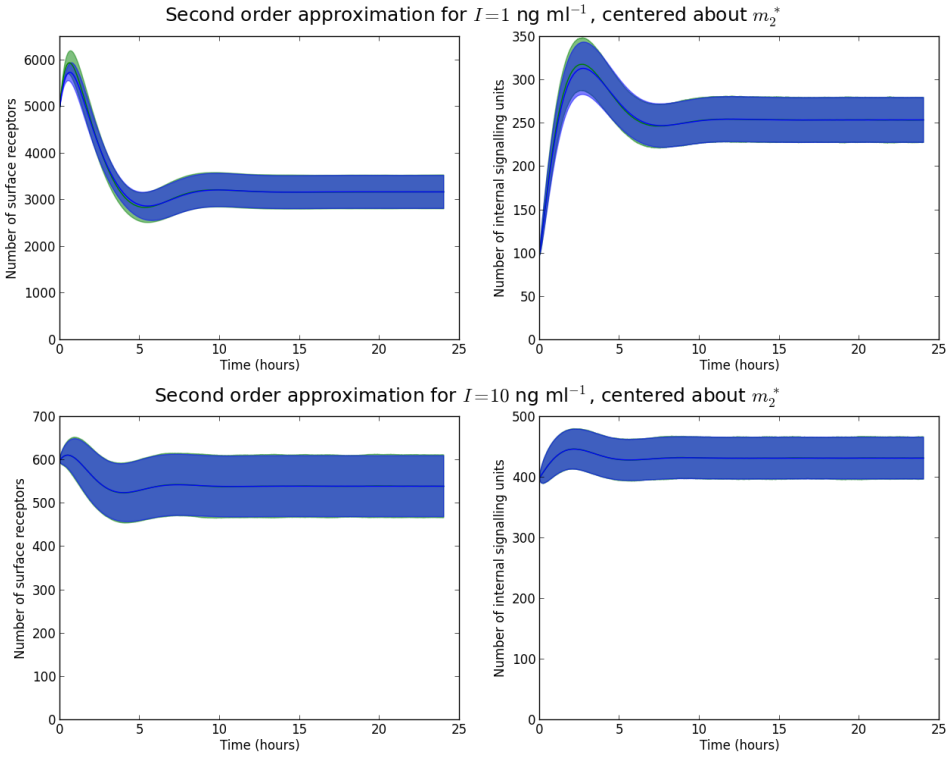

Figure 4.4: As in Figures 4.2 and 4.3, green areas represent the mean ± 1.96 standard deviations of 10^4 realisations produced using the Gillespie algorithm, and blue areas represent the mean ± 1.96 standard deviations computed from the approximations. In the top row we present the second second order approximation centred on the mean field solution m_2^* for $I = 1$ ng ml^{-1}. In the bottom row we present the second order approximation centred on m_2^* for $I = 10$ ng ml^{-1}. Initial conditions were reduced relative to those chosen in Figures 4.2 and 4.3 to ensure trajectories stay within a suitable neighbourhood of m_2^*.

4.1.10 Signalling in equilibrium

We look for fixed point solutions of the system of equations (4.57)-(4.61). To determine a value of ϵ, we find fixed point solutions of equations (4.22) and (4.23), from which we use equation (4.56) to find ϵ. For values of I less than approximately $I_c = 8.4 \times 10^2$ ng ml^{-1} there exist three stationary solutions. Ordered by size, the

middle of these solutions is unstable, whilst the remaining two are stable. For concentrations of IL-7 greater than I_c, there exists a single stationary solution which, at the bifurcation point, matches the largest of three solutions for concentrations less than I_c. For clarity, we plot these solutions in Figure 4.5. Note that, the uppermost line should continue as the concentration decreases, however, these solutions are computationally expensive to obtain and so are not displayed.
Mean field solutions qualitatively concur with the lowest line in Figure 4.5, for concentrations up to the I_c. For concentrations above I_c, the mean field solutions differ from the second order approximation obtained from expanding about m_2^*. This be-

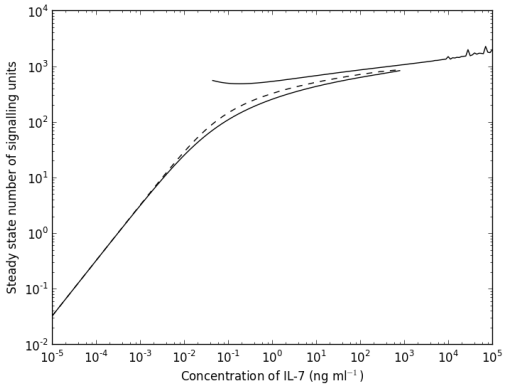

Figure 4.5: We plot the steady state solutions for the number of signalling units as a function of the concentration of IL-7.

haviour can be understood intuitively by considering a realisation simulated for a value of I greater than I_c. In Figure 4.6 we show one such realisation for $I = 10^4$ ng ml^{-1}. For IL-7 at this concentration, the model predicts a single receptor present on the surface of the cell, over a period of several hours, is able to increase the number of signalling units by several hundred. Typically, at this concentration, after some time we observe few receptors present on the surface of the cell (less than 10). Stochastic effects from the varying number of receptors produce dramatic changes in the number of signalling units. We discussed earlier that the second order approximation is valid only when $\mathbb{X}_2$ takes values in some neighbourhood around $\epsilon\kappa$. If the concentration of IL-7 is sufficiently high, fluctuations are large enough that a typical trajectory does not stay within this neighbourhood, resulting in a breakdown of the approximation (the breakdown in this case being the disappearance of a representative solution). Whilst we may increase the size of the neighbourhood by taking higher order approximations, we conjecture that there exists some value of I for which the approximation will break down due to fluctuations in equilibrium

deviating far enough away from $\epsilon\kappa$. The relatively large fluctuations observed in the right panel of Figure 4.6 also explain why the number of signalling units at equilibrium becomes erratic for high concentrations, as observed for $I > 10^4$ ng ml^{-1} in Figure 4.5.

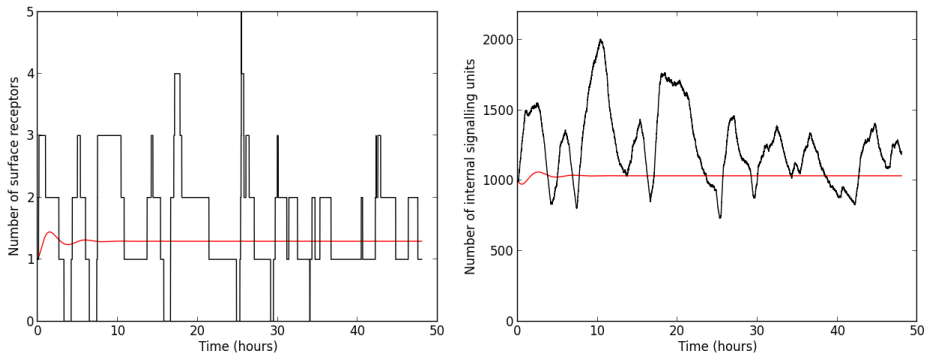

Figure 4.6: Black: realisation simulated using the Gillespie algorithm for $I = 10^4$ ng ml^{-1}. Red: numerical solution of the mean field approximation.

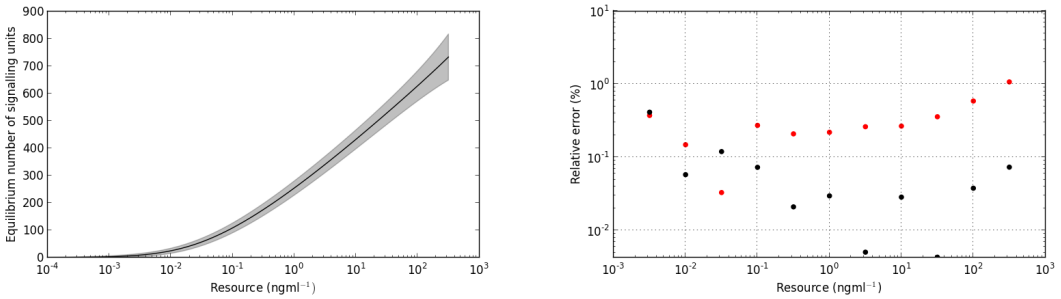

Figure 4.7: Left panel: average number of signalling units ± 1.96 standard deviations, derived using the second order approximation where we have expanded about $\epsilon\kappa$. Parameters used are given in Table 4.1. Right panel: we computed 10^4 Gillespie realisations from which we calculated an estimate for the average number of signalling units when the process is in equilibrium. Red: relative error of the mean field approximation. Black: relative error of the second order approximation derived by expanding about $\epsilon\kappa$.

In Figure 4.7 (right plot) we present comparisons of the mean field estimates versus the second order estimates (expanded about $\epsilon\kappa$) of the first moments of the stochastic process. We computed 10^4 realisations of the stochastic process and recorded the number of signalling units at the 48 hour time point. The average number of

signalling units at 48 hours was then computed. We defined the relative error by the following formula:

$$\text{relative error} = \frac{\text{approximaton estimate}}{\text{Gillespie estimate}} \times 100\%. \tag{4.62}$$

In the right panel of Figure 4.7 we plot the relative error between the mean field and second order approximations and the statistics of the stochastic simulations. As can be seen, with the exception of two points, the second order approximation (black dots) consistently performs better than the mean field approximation (red dots) when computing the first moments of the stochastic process. Indeed, for larger values of I we observe approximately an order of magnitude reduction in the relative error.

4.1.11 Discussion

At the start of this chapter we introduced a simple model to describe changes in IL-7 receptor numbers in response to IL-7 signalling. In this model, we introduced a non-linear transition term (equation (4.3)) to describe the probability of expressing a receptor on the surface of the cell in some small time interval Δt. Due to the presence of this non-linear term, we cannot find exact expressions for the time evolution of the moments of the stochastic process. Instead, we have presented a method to devise a system of ODEs whose solutions approximate the nth moment of the stochastic process. In particular, we have demonstrated this method generally performs better than the mean field approximation when considering stationary solutions of the first moments of the process.

The simple model analysed here predicts the number of signalling units at equilibrium is an increasing function of the availability of the resource. In particular, the number of signalling units at equilibrium grows like the logarithm of the resource. Let this quantity be denoted by S, and let the resource be denoted by I, then the dependence may be approximated by introducing the relationship

$$S = a \log(bI + 1), \tag{4.63}$$

for some appropriate values of a and b. We note that this function was chosen by inspection of the numerical trajectory given in Figure 4.7. The function above is given by the red line. Considering I in the range $[10^{-4}, 10^{2.5}]$ ng ml^{-1}, we determine S at the end points of this interval via the second order approximation, centred on

$\epsilon\kappa$. Using this pair of values, S_1, S_2, with corresponding values $I_1 = 10^{-4}, I_2 = 10^{2.5}$, we solve for a and b in equation (4.63), giving $a \approx 77.3$ signalling units and $b \approx 41.4$ ng^{-1} ml. In Figure 4.8 we plot the number of signalling units at equilibrium over this interval (black line). We also plot the above function $S(I)$ for I in the range $[I_1, I_2]$ (red line). As can be seen, the signalling relation defined by (4.63) does a reasonably good job at approximating the number of signalling units at equilibrium for I in this range.

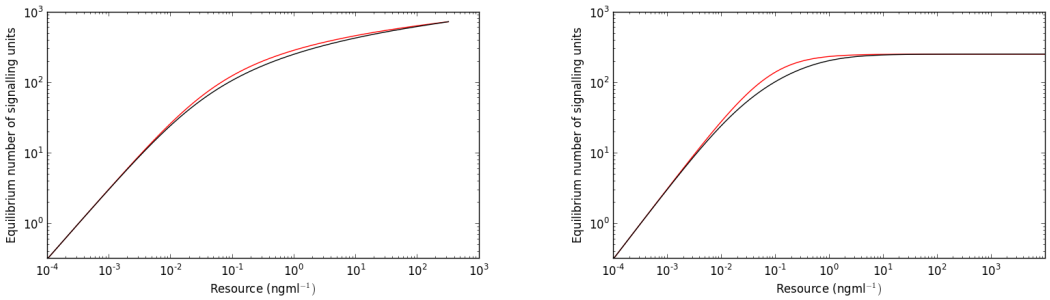

Figure 4.8: Left panel: Black: number of signalling units at equilibrium, calculated from the second order approximation centred on $\epsilon\kappa$. Red: plot of relation (4.63). Right panel: Black: reproduction of left plot where we have replaced equation (4.5) by equation (4.64). Red: approximate description of this solution using the functional form $S = aI/(b + I)$. The parameters γ and ϕ were chosen to be 0.2 hours^{-1} and 1 ng ml^{-1}, respectively. All other parameters as listed in Table 4.1.

As discussed earlier, the second order approximation breaks down when the resource exceeds the value I_c, introduced in Section 4.1.10. Fortunately, this area of the parameter space is not representative of the biology. For IL-7 at these concentrations, the model predicts a single receptor can increase the signalling intensity by several hundred units in a few hour hours. Taking a biological viewpoint, once a single IL-7 ligand binds to the IL-7Rα/γc heterodimer, it seams reasonable that the same heterodimer cannot be stimulated by further IL-7, since its binding site is occupied (Jiang *et al.*, 2005). This should presumably place an upper bound on the amount of signal each IL-7:IL-7R complex can produce. One suitable modification we can make to the model such that this upper bound is encoded would be to replace the linear term γI by some bounded function of I. The most obvious change would be to let equation (4.5) become

$$p_{(n_1,n_2+1),\boldsymbol{n}}(\Delta t) = \frac{\gamma I}{\phi + I} n_1 \Delta t + o(\Delta t), \tag{4.64}$$

where ϕ determines how quickly this probability attains its maximum with respect to increasing resource availability, for a given number of receptors. Provided $\gamma < I_c$, the inclusion of this function eliminates the possibility of the bifurcation discussed in Section 4.1.10. Such a change also qualitatively changes the form the signalling function takes as described by equation (4.63). If the probability of producing a unit of signal is now a bounded function of I, the fixed point solution to the number of signalling units in the second order approximation is also a bounded function of I. This can be seen in the right plot of Figure 4.8 where we have made this modification in the above transition probability and reproduced the left plot of Figure 4.8. Now we find

$$S = \frac{aI}{b+I} \tag{4.65}$$

is a more suitable functional form for the approximate dependence of the signal on the resource. In this modified example the approximation is valid for all $I \in \mathbb{R}^+$.

4.2 A stochastic model of IL-7R dynamics

In the simple model introduced in the previous section we presented a simple description of IL-7 receptor signalling. In this section we refine the model to take into account a little more of the biology. The simple model allowed us to introduce mathematical techniques which were used to derive the relationship between the average number of signalling units at equilibrium and the external concentration of IL-7. We apply the techniques introduced in the previous section to derive the signalling relation for the more detailed model introduced forthwith.

The IL-7 receptor is composed of the IL-7Rα-chain and the common cytokine receptor γ-chain (γ_c) (Mazzucchelli & Durum, 2007). Whilst signalling through the IL-7R has dramatic effects on the abundance of IL-7Rα on the surface of the cell, in reference (Park *et al.*, 2004), only modest changes in expression of γ_c were observed following exposure to IL-7. In the construction of the upcoming model we shall assume γ_c availability is constant and non-limiting. Signalling through the IL-7 receptor requires cross-linkage of the extracellular domains of IL-7Rα and γ_c (Mazzucchelli & Durum, 2007). We shall further assume that the time to recruit γ_c to the IL-7Rα:IL-7 complex, thereby constructing a fully functional receptor complex, is negligible. As such, when referring to the IL-7 receptor, we do not distinguish between whether γ_c is linked with IL-7Rα or not, we merely assume it is present

when required.

4.2.1 Model description

In this section we introduce the transition probabilities of the stochastic model of IL-7 receptor dynamics. We shall construct a multi-variate Markov process defined on a 4-dimensional lattice. We let $\mathbb{X}(t) = (\mathbb{X}_1(t), \mathbb{X}_2(t), \mathbb{X}_3(t), \mathbb{X}_4(t))$ be a 4-dimensional random vector for the state of the process at time t, where $n_0 = (n_{10}, n_{20}, n_{30}, n_{40})$, $n \in \mathbb{N} \cup \{0\}$, is the state of the process at time $t = 0$. We shall consider a single cell suspended in a medium of IL-7 at fixed concentration. Further, we shall define three observable variables in addition to the previously introduced description of the internal IL-7 signal. We consider changes in the numbers of receptors on the surface of the cell, the number of internalised receptors and the IL-7 signal. We make a further distinction between the number of receptors which are internalised as a consequence of binding to IL-7 and those which internalise whilst unbound.

1. We model the number of receptors on the surface of the cell, represented by the random variable $\mathbb{X}_1(t)$.

2. Also taken into account are the number of internalised-unbound receptors, described by the random variable $\mathbb{X}_2(t)$.

3. In addition to this we include the number of internalised receptors bound to IL-7, represented by the random variable $\mathbb{X}_3(t)$.

4. The number of IL-7 signalling unit is encoded by the random variable $\mathbb{X}_4(t)$.

The state probabilities of the Markov process are defined as

$$p_{\boldsymbol{n}}(t) = \text{Prob}\{\mathbb{X}(t) = \boldsymbol{n} \mid \mathbb{X}(0) = n_0\}, \tag{4.66}$$

furthermore, the transition probabilities are defined as

$$\begin{aligned} p_{\boldsymbol{m},\boldsymbol{n}}(\Delta t) &= \text{Prob}\{\mathbb{X}(t + \Delta t) = \boldsymbol{m} \mid \mathbb{X}(t) = \boldsymbol{n}\}, \\ &= q_{\boldsymbol{m},\boldsymbol{n}}\Delta t + o(\Delta t), \end{aligned} \tag{4.67}$$

where the $q_{\boldsymbol{m},\boldsymbol{n}}$ are the corresponding transition intensity functions (Allen, 2003). We define

$$q_{\boldsymbol{m},\boldsymbol{n}} = \begin{cases} \lim_{t\to\infty} \dfrac{p_{\boldsymbol{m},\boldsymbol{n}}(\Delta t)}{\Delta t}, & \text{if } \boldsymbol{m} \neq \boldsymbol{n}, \\ \lim_{t\to\infty} \dfrac{1 - p_{\boldsymbol{m},\boldsymbol{n}}(\Delta t)}{\Delta t}, & \text{if } \boldsymbol{m} = \boldsymbol{n}. \end{cases} \tag{4.68}$$

Proportion of receptors bound to IL-7

We assume the number of surface receptors bound to IL-7 is a constant fraction of the total number of surface receptors. Such an assumption comes from considering a single cell possessing a fixed number of surface receptors suspended in a medium of IL-7 at constant concentration I. Assume IL-7 binds to IL-7R with rate k_+, and furthermore, assume IL-7 unbinds from the receptor at rate k_-. Let the total number of surface receptors be R_T and define the number of bound receptors to be $R_B(t)$. Then, assuming conservation of receptors, the number of bound receptors can be described by the ODE

$$\frac{\mathrm{d}R_B(t)}{\mathrm{d}t} = k_+ I \left(R_T - R_B(t)\right) - k_- R_B(t). \tag{4.69}$$

This ODE has steady state solution

$$R_B^* = \frac{R_T I}{\dfrac{k_-}{k_+} + I} \stackrel{\text{def}}{=} f_I R_T. \tag{4.70}$$

In equilibrium the number of receptors bound to IL-7 is given by f_I which is constant for a given concentration I. We assume the time scales typical for this simple description are much shorter than the time scales typical for changes in receptor numbers due to the expression and internalisation terms, introduced below. Furthermore, we assume this process reaches equilibrium quickly given a change in the total number of surface receptors. In our stochastic model we let the fraction of bound surface receptors be approximated by

$$f_I = \frac{I}{\dfrac{k_-}{k_+} + I}. \tag{4.71}$$

Transcription of the IL-7 receptor

We assume, in an unstimulated cell, IL-7 receptors are transcribed and upregulated to the surface of the cell at a constant rate per unit time, ν. A key study examining the effect of cytokine signalling on transcription of the IL-7 receptor found IL-7 signalling suppresses transcription of the α-chain of the IL-7 receptor (Jiang *et al.*, 2005). Based on this study we shall assume the rate of receptor transcription is a decreasing function of the number of signalling units. Our particular choice of function shall be an exponential akin to the function introduced in Section 4.1.1. We let

$$q_{(n_1+1,n_2,n_3,n_4),\boldsymbol{n}} = \nu \mathrm{e}^{-n_4/\kappa}, \quad n_i \geq 0,\ i = 1,2,3,4. \tag{4.72}$$

In the above expression, ν represents the maximal rate of expression of receptors and κ governs the magnitude of suppression due to signalling. Specifically, larger values of κ imply IL-7 signalling effects the expression rate to a lesser degree.

Internalisation of the IL-7 receptor

The study given in (Henriques *et al.*, 2010) presents results showing that, in unstimulated cells, the pool of IL-7 receptors on the surface of the cell internalises. We assume the rate of internalisation of unbound receptors is constant with parameter μ_U. Letting f_I denote the fraction of bound surface receptors, the transition intensity function for the internalisation of unbound surface receptors is defined to be

$$q_{(n_1-1,n_2+1,n_3,n_4),\boldsymbol{n}} = \mu_U(1-f_I)n_1, \quad n_1 \geq 1, n_i \geq 0,\ i = 2,3,4. \tag{4.73}$$

Correspondingly, we define the transition intensity function representing internalisation of the bound receptor as

$$q_{(n_1-1,n_2,n_3+1,n_4),\boldsymbol{n}} = \mu_B f_I n_1, \quad n_1 \geq 1, n_i \geq 0,\ i = 2,3,4. \tag{4.74}$$

Recycling of internalised receptors

Reference (Henriques *et al.*, 2010) presents further results showing internalised receptors recycle back to the surface of the cell. This was observed to occur in both unstimulated and stimulated cells, however the fraction of recycled receptor was shown to be less for stimulated cells. We define the pair of transition intensity functions denoting the rates at which internalised receptors are recycled back to the cell

surface as

$$q_{(n_1+1,n_2-1,n_3,n_4),\boldsymbol{n}} = \xi_U n_2, \quad n_2 \geq 1, n_i \geq 0,\ i = 1,3,4, \tag{4.75}$$

$$q_{(n_1+1,n_2,n_3-1,n_4),\boldsymbol{n}} = \xi_B n_3, \quad n_3 \geq 1, n_i \geq 0,\ i = 1,2,4. \tag{4.76}$$

Degradation of internalised receptors

In reference (Henriques *et al.*, 2010) it was also observed that internalised receptor is degraded by at least two distinct pathways. The two pathways reported were the ubiquitin-proteasome and pH-dependent lysosomal pathways. The rate of receptor degradation was observed to be enhanced for bound internalised receptors. The transition intensity functions encoding degradation of unbound receptors are given as

$$q_{(n_1,n_2-1,n_3,n_4),\boldsymbol{n}} = \delta_U n_2, \quad n_2 \geq 1, n_i \geq 0,\ i = 1,3,4, \tag{4.77}$$

$$q_{(n_1,n_2,n_3-1,n_4),\boldsymbol{n}} = \delta_B n_3, \quad n_3 \geq 1, n_i \geq 0,\ i = 1,2,4. \tag{4.78}$$

Signal generation and decay

It is further reported in reference (Henriques *et al.*, 2010) that internalisation of the bound receptor is required for signal transduction. We assume the rate of signal generation is proportional to the number of internalised and bound receptors. Furthermore, we assume the signal decays at a linear rate. The pair of transition intensity functions encoding generation and decay of IL-7 induced signal are given by

$$q_{(n_1,n_2,n_3,n_4+1),\boldsymbol{n}} = \gamma n_3, \quad n_i \geq 0,\ i = 1,2,3,4, \tag{4.79}$$

$$q_{(n_1,n_2,n_3,n_4-1),\boldsymbol{n}} = \rho n_4, \quad n_4 \geq 1, n_i \geq 0,\ i = 1,2,3. \tag{4.80}$$

4.2.2 Time evolution of the moment generating function

The same techniques outlined in Section 4.1 are used to derive a PDE describing the time evolution of the moment generating function for this stochastic process. The

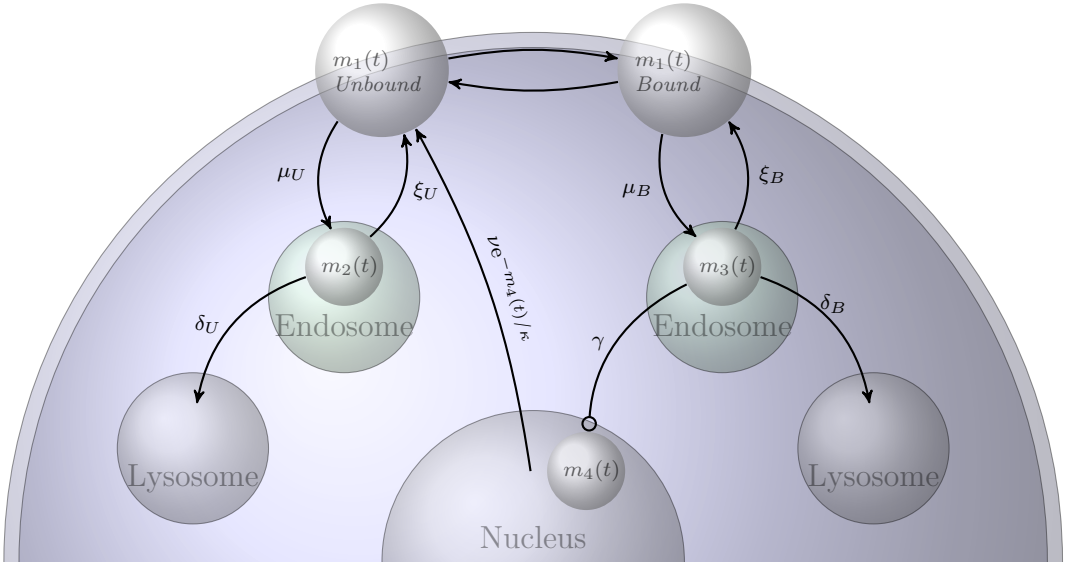

Figure 4.9: Diagrammatic representation of the transition probabilities of the stochastic model for the IL-7 and IL-7 receptor system.

moment generating function is defined

$$M(\boldsymbol{\theta}, t) = \mathbb{E}[\mathrm{e}^{\boldsymbol{\theta}\cdot\mathbb{X}(t)}] = \sum_{n_1=0}^{+\infty}\sum_{n_2=0}^{+\infty}\sum_{n_3=0}^{+\infty}\sum_{n_4=0}^{+\infty} p_{\boldsymbol{n}}(t)\mathrm{e}^{\boldsymbol{\theta}\cdot\boldsymbol{n}}, \tag{4.81}$$

where $\boldsymbol{\theta} = (\theta_1, \theta_2, \theta_3, \theta_4)$. We perform a Taylor expansion about the point $\epsilon\kappa$ to express the exponential in equation (4.72) as a series of polynomials. The resulting terms $(n_4 - \epsilon\kappa)^j$, $j \in \mathbb{Z}$ are expanded using the Binomial Theorem (Brualdi, 1992), giving

$$\mathrm{e}^{-n_4/\kappa} = \mathrm{e}^{-\epsilon}\sum_{i=0}^{+\infty}\sum_{j=0}^{i}\frac{(-\kappa)^{-j}\epsilon^{i-j}}{j!(i-j)!}n_4^j, \quad n_4 \in \mathbb{R}. \tag{4.82}$$

Omitting the derivation which proceeds exactly as in the previous section for the simple model of the IL-7 receptor, the PDE governing the time evolution of the moment generating function is given by

$$\begin{aligned}\frac{\partial M(\boldsymbol{\theta}, t)}{\partial t} &= \nu\mathrm{e}^{-\epsilon}\left(\mathrm{e}^{\theta_1} - 1\right)\sum_{i=0}^{+\infty}\sum_{j=0}^{i}\frac{(-\kappa)^{-j}\epsilon^{i-j}}{j!(i-j)!}\frac{\partial^j M(\boldsymbol{\theta}, t)}{\partial\theta_4^j} \\ &\quad + \left(\mu_U(1-f_I)\left(\mathrm{e}^{-\theta_1}\mathrm{e}^{\theta_2} - 1\right) + \mu_B f_I\left(\mathrm{e}^{-\theta_1}\mathrm{e}^{\theta_3} - 1\right)\right)\frac{\partial M(\boldsymbol{\theta}, t)}{\partial\theta_1} \\ &\quad + \left(\xi_U\left(\mathrm{e}^{\theta_1}\mathrm{e}^{-\theta_2} - 1\right) + \delta_U\left(\mathrm{e}^{-\theta_2} - 1\right)\right)\frac{\partial M(\boldsymbol{\theta}, t)}{\partial\theta_2}\end{aligned}$$

$$+\left(\xi_B\left(\mathrm{e}^{\theta_1}\mathrm{e}^{-\theta_3}-1\right)+\delta_B\left(\mathrm{e}^{-\theta_3}-1\right)+\gamma\left(\mathrm{e}^{\theta_4}-1\right)\right)\frac{\partial M(\boldsymbol{\theta},t)}{\partial\theta_3}$$
$$+\rho\left(\mathrm{e}^{-\theta_4}-1\right)\frac{\partial M(\boldsymbol{\theta},t)}{\partial\theta_4}. \tag{4.83}$$

The nth order moment of the stochastic process is defined by

$$m^{(i,j,k,l)}=\mathbb{E}\left[\left(\mathbb{X}_1(t)\right)^i\left(\mathbb{X}_2(t)\right)^j\left(\mathbb{X}_3(t)\right)^k\left(\mathbb{X}_4(t)\right)^l\right]=\left.\frac{\partial^{i+j+k+l}M(\boldsymbol{\theta},t)}{\partial\theta_1^i\partial\theta_2^j\partial\theta_3^k\partial\theta_4^l}\right|_{\theta_1=\theta_2=\theta_3=\theta_4=0}, \tag{4.84}$$

where $n=i+j+k+l$. In the next section we present a mean field approximation to describe the time evolution of the first order moments of the stochastic process. In the section following the mean field approximation, we present a system of ODEs which approximately describe the time evolution of the first two moments.

4.2.3 Mean field approximation

To derive the mean field approximation we assume all central moments of the process are zero. Let us define $\boldsymbol{s}_i$ to be a 1-dimensional vector of length 4 containing a 1 in the ith position and zeros elsewhere. Then the first order moment of the ith random variable of the stochastic moment is given by $m^{\boldsymbol{s}_i}$, $i=1,2,3,4$. We let

$$\mathbb{E}\left[\prod_{i=1}^{4}(\mathbb{X}_i(t)-m^{\boldsymbol{s}_i})^{n_i}\right]=0,\quad 1\leq i\leq 4. \tag{4.85}$$

From Lemma 3 in Appendix B, it follows that

$$\mathbb{E}\left[\prod_{i=1}^{4}\left(\mathbb{X}_i(t)\right)^{n_i}\right]=\prod_{i=1}^{4}\left(m^{\boldsymbol{s}_i}\right)^{n_i}. \tag{4.86}$$

Combining this result with definition (4.84) implies

$$m^{(i,j,k,l)}=\left(m^{\boldsymbol{s}_1}\right)^i\left(m^{\boldsymbol{s}_2}\right)^j\left(m^{\boldsymbol{s}_3}\right)^k\left(m^{\boldsymbol{s}_4}\right)^l \tag{4.87}$$

in the mean field approximation. Taking derivatives of (4.83) with respect to θ_i, $i=1,\ldots 4$ and evaluating the expression at $\boldsymbol{\theta}=\mathbf{0}$ allows us to derive the system of ODEs constituting the mean field approximation. Equation (4.86) allows us to collapse the expansion in the resulting equations back into an exponential. The

mean field approximation is then given by

$$\frac{\mathrm{d}m_1(t)}{\mathrm{d}t} = \nu \mathrm{e}^{-m_4(t)/\kappa} + \xi_U m_2(t) + \xi_B m_3(t) - \left(\mu_U(1-f_I) + \mu_B f_I\right) m_1(t), \tag{4.88}$$

$$\frac{\mathrm{d}m_2(t)}{\mathrm{d}t} = \mu_U(1-f_I) m_1(t) - \left(\xi_U + \delta_U\right) m_2(t), \tag{4.89}$$

$$\frac{\mathrm{d}m_3(t)}{\mathrm{d}t} = \mu_B f_I m_1(t) - \left(\xi_B + \delta_B\right) m_3(t), \tag{4.90}$$

$$\frac{\mathrm{d}m_4(t)}{\mathrm{d}t} = \gamma m_3(t) - \rho m_4(t). \tag{4.91}$$

Finally, let us define

$$\epsilon = \frac{m_4^*}{\kappa}, \tag{4.92}$$

where m_4^* is the stationary solution corresponding to $\lim_{t\to+\infty} m_4(t)$, which exists and is unique (proved below). Numerical exploration suggests the unique solution is also stable.

Proof. Stationary solutions of the system of ODEs (4.88)-(4.91) are found from solving the system

$$0 = \nu \mathrm{e}^{-m_4^*/\kappa} + \xi_U m_2^* + \xi_B m_3^* - \left(\mu_U(1-f_I) + \mu_B f_I\right) m_1^*, \tag{4.93}$$

$$0 = \mu_U(1-f_I) m_1^* - \left(\xi_U + \delta_U\right) m_2^*, \tag{4.94}$$

$$0 = \mu_B f_I m_1^* - \left(\xi_B + \delta_B\right) m_3^*, \tag{4.95}$$

$$0 = \gamma m_3^* - \rho m_4^*. \tag{4.96}$$

After some algebra, it is easily shown that m_4^* satisfies

$$\Gamma m_4^* = \nu \mathrm{e}^{-m_4^*/\kappa}, \tag{4.97}$$

where

$$\Gamma = \frac{\rho\left[\mu_B f_I(\xi_U + \delta_U)\delta_B + \mu_U(1-f_I)(\xi_B + \delta_B)\delta_U\right]}{\gamma \mu_B f_I(\xi_U + \delta_U)}. \tag{4.98}$$

Since $\Gamma > 0$ over the entire parameter space, it follows that there exists a unique solution to equation (4.97). Thus there exists a unique solution to the number of signalling units at equilibrium. □

4.2.4 Second order approximation

We replicate the methods used in Section 4.1 to derive a second order approximation describing the time evolution of the first two moments of the stochastic process.

That is, we truncate the infinite summation in equation (4.83) at $j = 2$, and use the moment closure methods outlined in (Singh & Hespanha, 2006b) to express third order moments in terms of the first and second order moments. The second order approximation to the time evolution of the first two moments is given by:

$$\begin{aligned}
\frac{\mathrm{d}m^{(1,0,0,0)}}{\mathrm{d}t} =& \nu \mathrm{e}^{-\epsilon} \left(\left(1 + \epsilon + \frac{\epsilon^2}{2} \right) + \frac{1+\epsilon}{\kappa} m^{(0,0,0,1)} + \frac{1}{2\kappa^2} m^{(0,0,0,2)} \right) \\
& - \left(\mu_U (1 - f_I) + \mu_B f_I \right) m^{(1,0,0,0)} + \xi_U m^{(0,1,0,0)} + \xi_B m^{(0,0,1,0)}, && (4.99) \\
\frac{\mathrm{d}m^{(0,1,0,0)}}{\mathrm{d}t} =& \mu_U (1 - f_I) m^{(1,0,0,0)} - \left(\xi_U + \delta_U \right) m^{(0,1,0,0)}, && (4.100) \\
\frac{\mathrm{d}m^{(0,0,1,0)}}{\mathrm{d}t} =& \mu_B f_I m^{(1,0,0,0)} - \left(\xi_B + \delta_B \right) m^{(0,0,1,0)}, && (4.101) \\
\frac{\mathrm{d}m^{(0,0,0,1)}}{\mathrm{d}t} =& \gamma m^{(0,0,1,0)} - \rho m^{(0,0,0,1)}, && (4.102) \\
\frac{\mathrm{d}m^{(2,0,0,0)}}{\mathrm{d}t} =& \nu \mathrm{e}^{-\epsilon} \left(\left(1 + \epsilon + \frac{\epsilon^2}{2} \right) + \frac{1+\epsilon}{\kappa} m^{(0,0,0,1)} + \frac{1}{2\kappa^2} m^{(0,0,0,2)} \right) \\
& + 2\nu \mathrm{e}^{-\epsilon} \left(\left(1 + \epsilon + \frac{\epsilon^2}{2} \right) m^{(1,0,0,0)} + \frac{1+\epsilon}{\kappa} m^{(1,0,0,1)} + \frac{1}{2\kappa^2} \frac{m^{(0,0,0,2)}}{m^{(1,0,0,0)}} \left(\frac{m^{(1,0,0,1)}}{m^{(0,0,0,1)}} \right)^2 \right) \\
& + \left(\mu_U (1 - f_I) + \mu_B f_I \right) \left(m^{(1,0,0,0)} - 2m^{(2,0,0,0)} \right) \\
& + \xi_U \left(m^{(0,1,0,0)} + 2m^{(1,1,0,0)} \right) + \xi_B \left(m^{(0,0,1,0)} + 2m^{(1,0,1,0)} \right), && (4.103) \\
\frac{\mathrm{d}m^{(1,1,0,0)}}{\mathrm{d}t} =& \nu \mathrm{e}^{-\epsilon} \left(\left(1 + \epsilon + \frac{\epsilon^2}{2} \right) m^{(0,1,0,0)} + \frac{1+\epsilon}{\kappa} m^{(0,1,0,1)} + \frac{1}{2\kappa^2} \frac{m^{(0,0,0,2)}}{m^{(0,1,0,0)}} \left(\frac{m^{(0,1,0,1)}}{m^{(0,0,0,1)}} \right)^2 \right) \\
& + \mu_U (1 - f_I) \left(m^{(2,0,0,0)} - m^{(1,0,0,0)} \right) - \left(\mu_U (1 - f_I) + \mu_B f_I + \xi_U + \delta_U \right) m^{(1,1,0,0)} \\
& + \xi_U \left(m^{(0,2,0,0)} - m^{(0,1,0,0)} \right) + \xi_B m^{(0,1,1,0)}, && (4.104) \\
\frac{\mathrm{d}m^{(1,0,1,0)}}{\mathrm{d}t} =& \nu \mathrm{e}^{-\epsilon} \left(\left(1 + \epsilon + \frac{\epsilon^2}{2} \right) m^{(0,0,1,0)} + \frac{1+\epsilon}{\kappa} m^{(0,0,1,1)} + \frac{1}{2\kappa^2} \frac{m^{(0,0,0,2)}}{m^{(0,0,1,0)}} \left(\frac{m^{(0,0,1,1)}}{m^{(0,0,0,1)}} \right)^2 \right) \\
& + \mu_B f_I \left(m^{(2,0,0,0)} - m^{(1,0,0,0)} \right) - \left(\mu_U (1 - f_I) + \mu_B f_I + \xi_B + \delta_B \right) m^{(1,0,1,0)} \\
& + \xi_U m^{(0,1,1,0)} + \xi_B \left(m^{(0,0,2,0)} - m^{(0,0,1,0)} \right), && (4.105) \\
\frac{\mathrm{d}m^{(1,0,0,1)}}{\mathrm{d}t} =& \nu \mathrm{e}^{-\epsilon} \left(\left(1 + \epsilon + \frac{\epsilon^2}{2} \right) m^{(0,0,0,1)} + \frac{1+\epsilon}{\kappa} m^{(0,0,0,2)} + \frac{1}{2\kappa^2} \left(\frac{m^{(0,0,0,2)}}{m^{(0,0,0,1)}} \right)^3 \right) \\
& - \left(\mu_U (1 - f_I) + \mu_B f_I + \rho \right) m^{(1,0,0,1)} + \xi_U m^{(0,1,0,1)} + \xi_B m^{(0,0,1,1)} + \gamma m^{(1,0,1,0)}, \\
& && (4.106)
\end{aligned}$$

$$\frac{\mathrm{d}m^{(0,2,0,0)}}{\mathrm{d}t} = \mu_U(1-f_I)\left(m^{(1,0,0,0)} + 2m^{(1,1,0,0)}\right) + (\xi_U+\delta_U)\left(m^{(0,1,0,0)} - 2m^{(0,2,0,0)}\right), \tag{4.107}$$

$$\frac{\mathrm{d}m^{(0,1,1,0)}}{\mathrm{d}t} = \mu_U(1-f_I)m^{(1,0,1,0)} + \mu_B f_I m^{(1,1,0,0)} - (\xi_U+\xi_B+\delta_U+\delta_B)\, m^{(0,1,1,0)}, \tag{4.108}$$

$$\frac{\mathrm{d}m^{(0,1,0,1)}}{\mathrm{d}t} = \mu_U(1-f_I)m^{(1,0,0,1)} + \gamma m^{(0,1,1,0)} - (\xi_U+\delta_U+\rho)\, m^{(0,1,0,1)}, \tag{4.109}$$

$$\frac{\mathrm{d}m^{(0,0,2,0)}}{\mathrm{d}t} = \mu_B f_I\left(m^{(1,0,0,0)} + 2m^{(1,0,1,0)}\right) + (\xi_B+\delta_B)\left(m^{(0,0,1,0)} - 2m^{(0,0,2,0)}\right), \tag{4.110}$$

$$\frac{\mathrm{d}m^{(0,0,1,1)}}{\mathrm{d}t} = \mu_B f_I m^{(1,0,0,1)} + \gamma m^{(0,0,2,0)} - (\xi_B+\delta_B+\rho)\, m^{(0,0,1,1)}, \tag{4.111}$$

$$\frac{\mathrm{d}m^{(0,0,0,2)}}{\mathrm{d}t} = \gamma\left(m^{(0,0,1,0)} + 2m^{(0,0,1,1)}\right) + \rho\left(m^{(0,0,0,1)} - 2m^{(0,0,0,2)}\right). \tag{4.112}$$

4.2.5 Parameter estimates

In this section we use the mean field approximation to obtain parameter estimates from the literature.

Reduced model in the case when $I = 0$. Consider a T cell in an IL-7 free medium with initial conditions such that the IL-7 induced signalling is zero and the number of IL-7:IL-7R internal complexes is zero. Then the mean field model can be reduced to the following set of ODEs:

$$\begin{aligned}\frac{\mathrm{d}m_1(t)}{\mathrm{d}t} &= \nu + \xi_U m_2(t) - \mu_U m_1(t)\,,\\ \frac{\mathrm{d}m_2(t)}{\mathrm{d}t} &= \mu_U m_1(t) - (\xi_U+\delta_U)\, m_2(t)\,.\end{aligned}$$

This reduced system is governed by four parameters ν, ξ_U, μ_U and δ_U, and possesses the following stable steady state:

$$\begin{aligned}m_1^* &= \frac{\nu\,(\xi_U+\delta_U)}{\mu_U\delta_U}\,,\\ m_2^* &= \frac{\nu}{\delta_U}\,.\end{aligned}$$

Let us assume in the reduced model 10% of the total number of receptors are internalised in equilibrium. We note however, that we could not find any evidence in the literature to support this value. We set $m_1^* = 9m_2^*$. Based on the measurements of Park *et al.* (2004), we shall assume 4×10^4 receptors in total when the reduced model is in steady state. Therefore, we let

$$\frac{\nu\left(\xi_U + \delta_U\right)}{\mu_U \delta_U} = 3.6 \times 10^4 \,, \tag{4.113}$$

$$\frac{\nu}{\delta_U} = 4 \times 10^3 \,. \tag{4.114}$$

In the study by (Henriques *et al.*, 2010), cells were cultured with the translation inhibitor cycloheximide (CHX) to prevent transcription of the IL-7 receptor. Total expression of the IL-7 receptor was measured over several time points, from which the authors estimate the half-life of the receptor in an unstimulated cell to be approximately 24 hours.

In the reduced model, all receptors are guaranteed to be degraded in a finite amount of time. The expected time for a receptor, that is initially on the cell surface, to be degraded in the lysosome is given by

$$\tau_1 = \frac{\delta_U + \mu_U + \xi_U}{\mu_U \delta_U} \,.$$

For the derivation of this equation see Appendix C .

Assuming exponential decay, the half-life for a receptor to undergo lysosomal degradation, starting on the cell surface, is then given by

$$t_{\frac{1}{2}} = \frac{\delta_U + \mu_U + \xi_U}{\mu_U \delta_U} \log 2 \,.$$

Thus, we can write

$$\frac{\delta_U + \mu_U + \xi_U}{\mu_U \delta_U} \log 2 = 24 \text{ hour} \,. \tag{4.115}$$

Combining (4.113), (4.114) and (4.115) we find

$$\delta_U \approx 0.29 \text{ hour}^{-1} \,,$$

$$\nu \approx 1.2 \times 10^3 \text{ receptors hour}^{-1} \,,$$

$$\xi_U + 0.29 \text{ hour}^{-1} \approx 9\mu_U \,.$$

The value of ξ_U relative to δ_U effectively dictates the ratio of receptors which are degraded to those recycled back to the cell surface. We assume the system has evolved to minimise waste of functional proteins and tentatively let $\xi_U > \delta_U$. That is, we assume that a greater fraction of unbound receptors are recycled back to the surface of the cell than are degraded. We somewhat arbitrarily set

$$\xi_U = 1 \text{ hour}^{-1} \quad \Rightarrow \quad \mu_U \approx 0.14 \text{ hour}^{-1} .$$

Receptor ligand kinetics Suppose the number of surface receptors is constant and denoted by R_T. Let us also assume the extra-cellular concentration of IL-7 is constant and denoted by I. Define $R_B(t)$ to be the number of IL-7 receptors bound to IL-7. Note that we assume the time to recruit the common gamma chain, γ_c, is negligible. Then, we can describe changes in the number of bound complexes by the following ODE

$$\frac{\mathrm{d}R_B(t)}{\mathrm{d}t} = k_+ \left[R_T - R_B(t)\right] I - k_- R_B(t) ,$$

where k_+ and k_- are, respectively, the binding and unbinding rates of the IL-7:IL-7R receptor-ligand system. We assume the time scales for this reaction are shorter than the time scales for changes in total membrane receptor numbers, such that we can consider these reactions to be in equilibrium. This ODE has a unique stable steady state:

$$R_B^* = \frac{R_T I}{\frac{k_-}{k_+} + I} \stackrel{\text{def}}{=} f_I R_T . \tag{4.116}$$

The Supplementary Material for reference (Palmer *et al.*, 2008) provides estimates for k_+ and k_-, from which we set $k_+ = 1$ nM min^{-1} and $k_- = 0.1$ min^{-1}. It is reported IL-7 has a molecular mass of around 17 kDa, from which we estimate the ratio $k_-/k_+ \approx 1.7$ ng ml^{-1}.

Early internalisation events In reference (Henriques *et al.*, 2010), surface receptor expression was assessed in human thymocytes. It is reported, cells in 50 ng ml^{-1} IL-7 culture down-regulated IL-7R expression. A 20% reduction was observed after 10 minutes. Using the above estimate for k_-/k_+, we find $f_I|_{I=50} \approx 0.97$. Based on this, we can neglect internalisation of the unbound receptor. In the first ten minutes, we shall also neglect recycling and inhibition of receptor transcription. We assume surface receptor expression loss is modelled by the ODE

$$\frac{\mathrm{d}m_1(t)}{\mathrm{d}t} = \nu - \mu_B m_1(t) .$$

Given initial surface expression levels equal to $m_1(0)$, this ODE has solution

$$m_1(t) = \frac{\nu}{\mu_B} + \left[m_1(0) - \frac{\nu}{\mu_B} \right] \mathrm{e}^{\mu_B t} \, . \tag{4.117}$$

We assume the previous estimates obtained from the reduced model for $m_1(0)$ and ν. That is, we let $m_1(0) = 3.6 \times 10^4$ receptors and $\nu = 1.2 \times 10^3$ receptors hour^{-1}. Then using the above expression for $m_1(t)$, (4.117), we obtain an estimate for μ_B. We find $\mu_B \approx 1.4$ hour^{-1}. The authors of reference (Henriques *et al.*, 2010) estimate the half-life of the IL-7 receptor in cells treated with CHX, cultured in 50 ng ml^{-1}, to be approximately three hours. Derived in a similar manner to the calculation presented in Appendix C, the expected time to degradation in the lysosome for a surface receptor is given by

$$\begin{aligned} \tau_2 &= \frac{\left[\mu_U \left(1 - f_I \right) + \left(\xi_U + \delta_U \right) \right] \left(\xi_B + \delta_B \right) + \mu_B f_I \left(\xi_U + \delta_U \right)}{\mu_U \left(1 - f_I \right) \delta_U \left(\xi_B + \delta_B \right) + \mu_B f_I \left(\xi_U + \delta_U \right) \delta_B} \\ &\approx \frac{1.3 \text{ hour}^{-1} \left(\xi_B + \delta_B \right) + 1.7 \text{ hour}^{-2}}{4.6 \times 10^3 \text{ hour}^{-2} \left(\xi_B + \delta_B \right) + 1.7 \text{ hour}^{-2} \delta_B} \, . \end{aligned}$$

Assuming exponential decay, with a half-life of three hours, we find $\xi_B \approx 0.2\delta_B + 0.3$ hour^{-1}. Again, without a direct measurement, let us set $\xi_B = 1$ hour^{-1}, to obtain an estimate for $\delta_B \approx 3.5$ hour^{-1}.

Remaining parameters Consider the observation of an approximately 98% reduction in surface receptor expression following overnight culture in 6 ng ml^{-1} IL-7 made in reference (Park *et al.*, 2004). We let $m_1^*|_{I=6} = 0.02 \, m_1^*|_{I=0} = 0.02 \dfrac{\nu \left(\xi_U + \delta_U \right)}{\mu_U \delta_U} \approx$ 763 receptors. We set the derivatives equal to zero in the system of ODEs (4.88)-(4.91), and manipulate the resulting system of equations to obtain

$$\nu \exp\left(-\frac{\gamma \mu_B f_I}{\rho \kappa \left(\xi_B + \delta_B \right)} m_1^* \right) = \left[\mu_U \left(1 - f_I \right) + \mu_B f_I - \frac{\mu_U (1 - f_I) \xi_U}{\xi_U + \delta_U} - \frac{\mu_B f_I \xi_B}{\xi_B + \delta_B} \right] m_1^* \, , \tag{4.118}$$

$$\Rightarrow \quad \exp\left(-1.9 \times 10^2 \left(\frac{\gamma}{\rho \kappa} \right) \right) \approx 0.54 \, ,$$

$$\Rightarrow \quad \frac{\gamma}{\rho \kappa} \approx 3.2 \times 10^{-3} \text{ receptors}^{-1} \, .$$

From the steady solutions of ODEs (4.90) and (4.91), we find

$$m_4^* = \frac{\gamma \mu_B f_I}{(\xi_B + \delta_B)\,\rho} m_1^* \approx 1.9 \times 10^2 \left(\frac{\gamma}{\rho}\right) \text{ receptors } .$$

We use this expression to rearrange (4.118) in terms of m_4^*. This gives

$$\exp\left(-\frac{m_4^*}{\kappa}\right) \approx 9.1 \frac{m_4^*}{\kappa} .$$

Solving the above expression numerically, we find $m_4^*/\kappa \approx 0.1$. We estimate a value for ρ based on the observation that following culture in 6 ng ml^{-1} IL-7, mRNA levels took approximately twelve hours to return to 99% of the control levels (Park *et al.*, 2004). The transcription rate is given by $\nu \exp(-m_4(t)/\kappa)$. We again assume the IL-7 induced signal decays according to the equation $m_4(t) = m_4(0)\mathrm{e}^{-\rho t}$, where $m_4(0) = 0.1\kappa$, as found from m_4^* above. Combining these assumptions with the experimental observations, we have

$$\nu \exp\left[-\frac{m_4(0)\exp\left(-12\rho\right)}{\kappa}\right] = 0.99\nu ,$$

from which we find $\rho \approx 0.19$ hour^{-1} $\Rightarrow \gamma \approx 6.1 \times 10^{-4}$ receptors^{-1} hour^{-1} κ. The parameter κ was chosen to be 1000. This choice was made from the stochastic model: $\kappa = 1000$ is the minimum value (to the nearest power of 10) such that fluctuations in the signalling quantity are typically greater than zero in low (10^{-2} ng ml^{-1}) concentrations of IL-7. Using this value for κ, we find $\gamma \approx 0.61$ hour^{-1}. The parameter estimates are summarised in Table 4.4.

4.2.6 Signalling in equilibrium

The parameter set established in the previous section allows us to numerically evaluate the number of signalling units and surface receptors at equilibrium. Equilibrium solutions are found from numerically solving equations (4.99)-(4.112) when the derivatives are set to zero. We may numerically calculate the number of signalling units and surface receptors for a range of values of the resource. By inspection, we choose analytic functions to approximate the dependence these quantities have on the resource. Let $\mathcal{S}(I)$ be the approximate number of signalling units and $\mathcal{R}(I)$ be

Parameter	Value	Units
ν	1.2×10^3	rec hour^{-1}
κ	10^3	signalling units
ξ_U	1	hour^{-1}
ξ_B	1	hour^{-1}
μ_U	0.14	hour^{-1}
μ_B	1.4	hour^{-1}
k_-/k_+	1.7	ng ml^{-1}
δ_U	0.29	hour^{-1}
δ_B	3.5	hour^{-1}
γ	0.61	signalling units rec^{-1} hour^{-1}
ρ	0.19	hour^{-1}

Table 4.4: Parameter estimates obtained from the mean field model of IL-7 receptor dynamics.

the number of surface receptors. Then we choose

$$\mathcal{S}(I) = \frac{c_1 I}{c_2 + I}, \tag{4.119}$$

$$\mathcal{R}(I) = c_3 + \frac{c_4}{c_5 + I}, \tag{4.120}$$

where the constants c_i, $i = 1, \ldots 5$ are to be determined.

Signalling units Equation (4.119) possesses two constants to be determined. We pin this function to the numerical solution at the end points of our interval of consideration for the resource. We are interested in an approximation for I in the interval $[10^{-5}, 10^3]$ ng ml^{-1}, since this interval encompasses the concentrations typically reported in the literature. Numerically, we find m_4^* evaluated at $I = 10^{-5}$ and $I = 10^3$ is approximately 0.223 and 603 signalling units, respectively. Solving for c_1 and c_2 we find $c_1 \approx 600$ signalling units and $c_2 \approx 0.027$ ng ml^{-1}. Figure 4.10 shows the numerical solution and analytic approximation along with the relative error for the approximation. As can be seen in Figure 4.10, the analytic approximation lies within two standard deviations of the numerical mean. Based on this, we deem the function $\mathcal{S}(I)$ to be a reasonable approximation to the number of signalling units in equilibrium as a function of the resource.

Surface receptors Considering equation (4.120), there exist three constants to be determined. Looking at the numerical solution as the resource tends to zero and

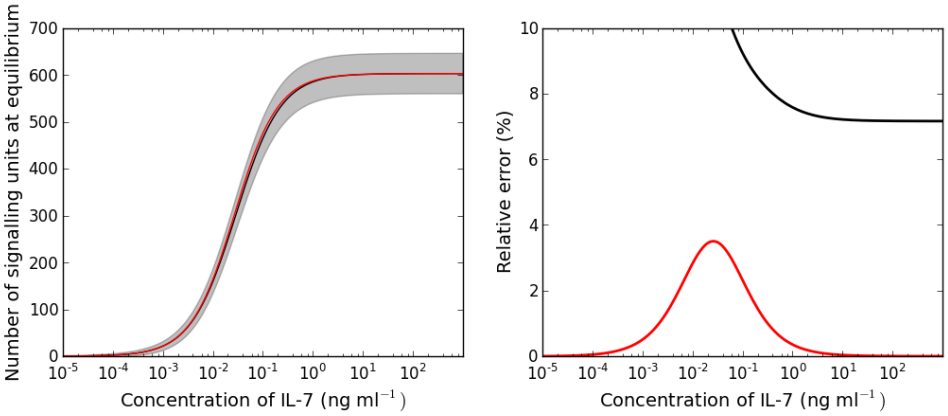

Figure 4.10: Left panel: The black line and grey area show the numerical mean number of signalling units with a boundary of 1.96 standard deviations. The red line is the analytical approximation to the numerical mean, derived from equations (4.99)-(4.112). Right panel: Black dots represent the relative error between the numerical mean and the mean + 1.96 standard deviations. Red dots represent the relative error between the numerical mean and analytic approximation.

infinity we find that the number of surface receptors is 38128 and 603, to the nearest integer, respectively. Noting that $\lim_{I\to+\infty}\mathcal{R}(I) = c_3$, we choose $c_3 = 600$ receptors. Letting $\mathcal{R}(0) = 38128$, we find $c_4 = 37525c_5$. For the remaining constant, we may pin the function at an arbitrary choice of I. We chose I such that the relative error between the analytical approximation and the numerical mean is smaller than the relative error between the numerical mean and the numerical mean plus two standard deviations. Using this choice we find $c_4 \approx 960$ receptors ng ml^{-1} and $c_5 \approx 0.026$ ng ml^{-1}. The numerical solution and analytic approximation, along with the relative error, is presented in Figure 4.11.

The analytical approximations established in this section are used in the following chapter to refine the simple resource model.

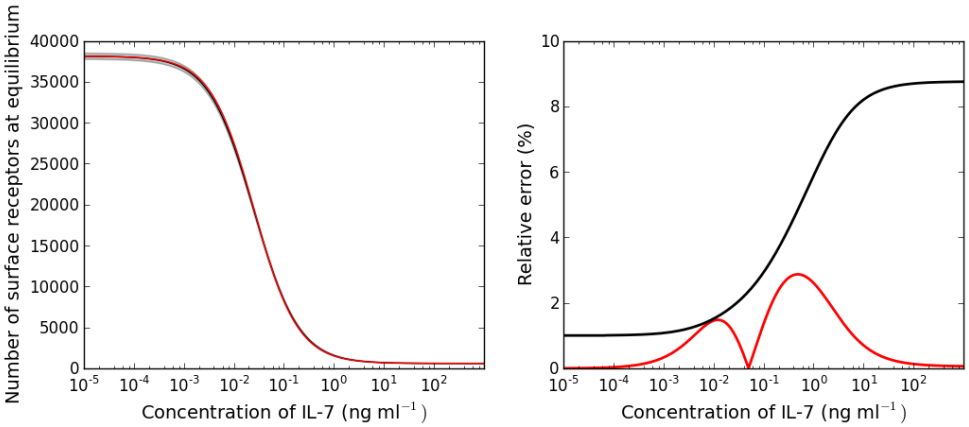

Figure 4.11: Left panel: The black line and grey area show the numerical mean number of surface receptors with a boundary of 1.96 standard deviations. The red line is the analytical approximation to the numerical mean. Right: The black line represents the relative error between the numerical mean and mean + 1.96 standard deviations. The red line shows the relative error between the numerical mean and the analytic approximation.

Chapter 5

The resource model revisited: IL-7 dependent dynamics

In this chapter we revisit the resource model in which we assume naive T cell survival is dependent on IL-7, introduced in Chapter 3, Section 3.3. In the resource model, we assumed the per cell IL-7 internalisation rate to be linearly proportional to the signalling strength (see equation 3.52). Furthermore, in equation 3.53, the signalling strength is linearly related to the external concentration of IL-7. We make use of the functions derived at the conclusion of Chapter 4 to revise these assumptions.
The main content of this chapter is divided into three sections. In the first of these sections (Section 5.2), we reintroduce the resource model in light of our derived functions for the IL-7 signalling strength and internalisation rate. Furthermore, we present the assumptions made to model considering the peripheral compartment of both mice and humans. In the second section (Section 5.3) we make use of experimental data provided by Ben Seddon [1] to estimate parameters of the model as applied to the murine periphery. In the final section (Section 5.4) we discuss the model in the context of a human periphery, investigating the homeostasis of T cells. Before delving once again into the assumptions of the model, we present a brief biological introduction taken from reference (Reynolds *et al.*, 2013b).

5.1 Introduction

The number of T cells in the periphery is determined by a balance of cell loss (death or differentiation) and cell renewal due to cell division and thymic export (Almeida

[1]University College London, benedict.seddon@ucl.ac.uk

et al., 2005; Surh & Sprent, 2008). Survival of the naive T cell population in the periphery depends on both common gamma chain cytokines and weak "tonic" signals induced by recognition of self-peptides by the T cell receptor (TCR) (Sprent & Surh, 2011; Takada & Jameson, 2009). IL-7 is required for homeostatic expansion of naive $CD8^+$ and $CD4^+$ T cells in lymphopenic hosts. This is established from the observation that naive T cells disappear over a one-month period upon adoptive transfer into IL-7 deficient (IL-7^-) hosts (Fry & Mackall, 2005; Schluns *et al.*, 2000; Tan *et al.*, 2001).

Signals from recognition of self-peptides bound to major histocompatibility complex (sp:MHC), and IL-7, promote cell survival. Naive T cell survival is impaired when removing access to one of these signals (Brocker, 1997; Kondrack *et al.*, 2003; Markiewicz *et al.*, 2003; Martin *et al.*, 2006; Vivien *et al.*, 2001). Of interest are the mechanisms by which these signals are regulated, resulting in a stable number of naive T cells throughout the lifetimes of mice and humans. IL-7 is produced by stromal cells in the tissues of the lymphatic architecture, including fibroblastic reticular cells, marginal reticular cells and lymphatic endothelial cells (Mueller & Germain, 2009). These cells produce very small amounts of IL-7 messenger RNA (mRNA), consistent with IL-7 protein levels limiting T cell expansion. IL-7 is a heparin-sulphate binding protein and, as such, it will bind extracellular matrix surrounding stromal cells. Thus, the interaction between naive T cells and stroma controls their homeostasis (Kang & Coles, 2012). Recognition of higher affinity, non-self-peptides by the T cell receptor induces naive T cells to undergo an alternative, IL-7 independent, survival program dependent on IL-2 (Koenen *et al.*, 2013).

Naive $CD8^+$ T cell responses depend on the amount of IL-7 the cells are exposed to (Palmer *et al.*, 2011). The experiments in (Palmer *et al.*, 2011) demonstrated that at low IL-7 concentrations ($< 10^{-2}$ ng ml^{-1}), cell viability was impaired; at higher concentrations (> 1 ng ml^{-1}) cells were observed to proliferate in response to IL-7. This difference might arise from changes in the strength of the IL-7R induced signal the cell receives. For an individual cell, IL-7R mediated signalling must be greater than some threshold to prevent the cell death (Palmer *et al.*, 2011). A sufficient amount of signalling is likely required to prevent the accumulation of pro-apoptotic proteins and also regulate glucose uptake (Jiang *et al.*, 2005; Wofford *et al.*, 2008). Similarly, IL-7R signalling must be greater than a second, higher, threshold to induce cell division. Heterogeneity at the single cell level in IL-7 signalling thresholds, a property reported to depend on expression of IL-7R, resulted in differential survival and division (Palmer *et al.*, 2011). Although these observations are based on two

different $CD8^+$ T cell receptor transgenic mice, it is assumed in this study that the mechanisms for T cell survival are the same for both naive $CD4^+$ and $CD8^+$ T cells. We introduce a deterministic mathematical description of the naive T cell population in the peripheral compartment of both the human and mouse immune system. Parameters are estimated for the model in the context of the murine periphery. For the human immune system, we describe changes in the homeostasis of naive T cells, as the body ages from childhood to adulthood. We assume cell survival depends on the availability of IL-7. We do not include availability of sp:MHC as a variable within the model, but assume sp:MHC availability is sufficient to allow cell survival and proliferation in conjunction with sufficient IL-7 stimulus. We also make the approximation that the distribution of signalling thresholds does not depend on the age of an individual. For a mathematical study of the impact sp:MHC availability has on clonal diversity, the reader is referred to Stirk *et al.* (Stirk *et al.*, 2010a,b). Our model is a mathematical description of the homeostasis of the naive T cell repertoire, but does not consider stimulation by foreign antigens.

5.2 A mathematical description of the size of the peripheral naive T cell population

Stochastic processes provide a method of treating each cell as a distinct, countable object and permit a more realistic model than a deterministic characterisation. Fluctuations in the number of cells can be considered, but, in a non-linear stochastic model, approximations are often made to facilitate the analysis. In the linear noise approximation (Wallace, 2010), for example, fluctuations are assumed to be of order $\Omega^{\frac{1}{2}}$ for a system of size Ω. The human peripheral T cell compartment is estimated to contain of the order of 10^{11} naive T cells (Bains *et al.*, 2009b), whilst the murine immune system is estimated to contain of the order of 10^7 naive T cells. Letting the system size be the average number of naive T cells in humans (mice), we find $\mathcal{O}(\Omega) = 10^{11}$ (10^7) cells, and correspondingly, fluctuations are expected to be typically $10^5 - 10^6$ $(10^3 - 10^4)$ cells in magnitude. That is, we expect fluctuations of approximately 0.001% (0.1%) in the size of the human (mouse) naive T cell pool due to stochasticity in the per cell division and death rates. Based on these considerations, adopting a deterministic approach to describe the total human (mouse) peripheral naive T cell population is reasonable.

5. THE RESOURCE MODEL REVISITED: IL-7 DEPENDENT DYNAMICS

We assume peripheral naive T cells are either in a resting state, or proceeding through the cell cycle. The deterministic variables $R(t)$ and $C(t)$ are introduced to model the total number of T cells in the resting and cycling states, respectively. The variable $I(t)$ is introduced to model the concentration of IL-7. The deterministic approach we take assumes a volume for the periphery. However, it is assumed that T cells are spaced uniformly across this space. Indeed, this approach is tantamount to assuming the resource, IL-7, is shared equally amongst all cells. Competition for the resource is introduced only so far as each cell acts to reduce the global concentration of the resource. Resting cells may receive a signal which induces them to proceed through one round of division. Upon completion of the cell cycle, a cycling cell produces two daughter cells in the resting compartment. Resting cells are assumed to die if the IL-7 induced survival signal is insufficient; cells may also die during the cell cycle. The input of naive T cells from the thymus into the resting compartment, in keeping with observations in humans, is a decreasing function of time (Mitchell *et al.*, 2006; Steinmann, 1986). Production of IL-7 is assumed to occur at a constant rate per unit volume of the immune system. In the absence of T cells, IL-7 is assumed to be degraded and/or consumed by other cell types at a constant rate. Upon signal induction through the IL-7 receptor, IL-7 is assumed to be internalised by the T cell. A diagrammatic representation of the model is given in Figure 5.1.

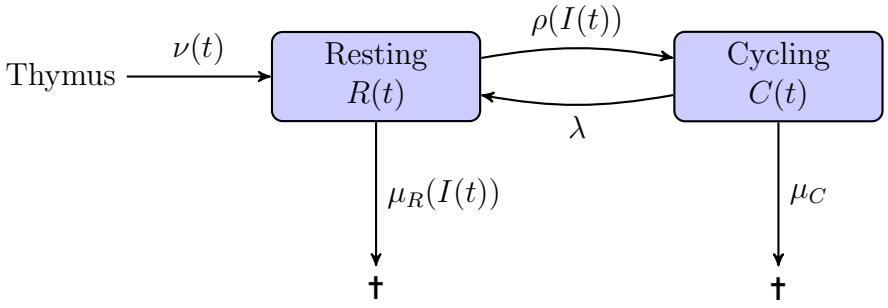

Figure 5.1: Diagrammatic illustration of the resource model. T cells leaving the thymus enter the resting naive peripheral pool. Cells in either a resting or cycling state may die. The rate of death from the resting state depends on the availability of the resource (IL-7), whereas the death rate for cycling cells is constant. Resting cells enter the cell cycle at a rate that depends on the concentration of IL-7. Cycling T cells produce two daughter cells in the resting state upon completion of the cell cycle.

5.2.1 IL-7 signalling and heterogeneity in signalling thresholds

In the model, the amount of signalling each T cell receives is assumed to be the same for all cells in the population. Yet, we introduce heterogeneity in the signalling thresholds for survival and proliferation. This introduces differences in the death and cell cycle entry rates for any two cells receiving the same amount of IL-7 signalling. Let $S(t)$ be the average amount of IL-7 signalling across the naive T cell population. We assume each T cell experiences the same amount of IL-7 induced signalling for a given concentration of IL-7, $I(t)$. We relate this amount of signalling to the extra-cellular concentration of IL-7 by equation (4.119), derived at the conclusion of Chapter 4:

$$S(t) = \frac{600I(t)}{0.027 + I(t)} \, . \tag{5.1}$$

We assume each individual cell possesses a unique pair of signalling thresholds for survival and proliferation. Furthermore, we assume, in the continuous limit, that these thresholds are distributed log-normally across the entire population of resting T cells residing in the periphery. Let the random variable Θ_s represent the survival threshold, and let Θ_p represent the proliferation threshold. We let

$$\Theta_s \sim \log \mathcal{N}\left(\log \theta_s, \frac{1}{2\alpha^2}\right) \, , \quad \Theta_p \sim \log \mathcal{N}\left(\log \theta_p, \frac{1}{2\alpha^2}\right) , \quad \alpha \in \mathbb{R}^+ \, . \tag{5.2}$$

The respective probability density functions for these distributions are

$$p_{\Theta_x}(\theta) = \frac{\alpha}{\sqrt{\pi}\theta} \exp\left[-\left(\alpha\left(\log\theta - \log\theta_x\right)\right)^2\right] \, , \quad x = s, p \, . \tag{5.3}$$

Death rate of resting cells Suppose each T cell in the naive population is a distinct member possessing a unique signalling threshold for survival. As in the previous section, we assume these signalling thresholds are distributed log-normally (in the continuous limit). We suppose the death rate of an individual cell is Boolean, in the sense that if the global amount of IL-7 signalling is greater than the cell's individual survival threshold, then the cell can survive indefinitely. Otherwise, if the amount of signalling is below the survival threshold, the cell will undergo apoptosis

at rate μ_R. The death rate for cell i with survival threshold $\theta_s^{(i)}$, is given by

$$f_s(S(t), \theta_s^{(i)}) = \begin{cases} \mu_R & \text{if } S(t) < \theta_s^{(i)} \ , \\ 0 & \text{if } S(t) \geq \theta_s^{(i)} \ . \end{cases} \tag{5.4}$$

In the continuous limit (assuming signalling thresholds are distributed log-normally), the average death rate for the population of naive T cells is given by

$$\begin{aligned} \bar{\mu}_R(S(t)) &= \int_0^{+\infty} f_s(S(t), \theta) p_{\Theta_s}(\theta) \, \mathrm{d}\theta \\ &= \int_{S(t)}^{+\infty} \mu_R \, p_{\Theta_s}(\theta) \, \mathrm{d}\theta \ , \\ &= \frac{1}{2}\mu_R \left[1 - \mathrm{erf}\left(\alpha \left(\log S(t) - \log \theta_s\right)\right)\right] \ , \end{aligned} \tag{5.5}$$

where $p_{\Theta_s}(\theta)$ is the probability density function of the random variable Θ_s, defined by (5.3) with $x = s$.

Rate of entry into cell cycle Analogous to Section 5.2.1, we assume each T cell in the naive population is a distinct member possessing a unique signalling threshold for proliferation. We let the individual rate of entry into the cell cycle be given by

$$f_p(S(t), \theta_p^{(i)}) = \begin{cases} 0 & \text{if } S(t) < \theta_p^{(i)} \ , \\ \rho & \text{if } S(t) \geq \theta_p^{(i)} \ . \end{cases} \tag{5.6}$$

Assume, in the continuous limit, the signalling threshold for entry into the cell cycle is represented by the random variable Θ_p, defined in equation (5.2), with probability density function $p_{\Theta_p}(\theta)$ (equation (5.3), $x = p$). The average rate of entry into cell cycle is given by

$$\begin{aligned} \bar{\rho}(S(t)) &= \int_0^{+\infty} f_p(S(t), \theta) \, p_{\Theta_p}(\theta) \, \mathrm{d}\theta \\ &= \int_0^{S(t)} \rho \, p_{\Theta_p}(\theta) \, \mathrm{d}\theta \ , \\ &= \frac{1}{2}\rho \left[1 + \mathrm{erf}\left(\alpha \left(\log S(t) - \log \theta_p\right)\right)\right] \ . \end{aligned} \tag{5.7}$$

5.2.2 Internalisation of IL-7

At the conclusion of Chapter 4, we derived a relationship to describe the total number of IL-7 receptors, at equilibrium, on the surface of a T cell exposed to IL-7 at concentration I ng ml^{-1}. This relation is given by equation (4.120):

$$\mathcal{R} = 600 + \frac{960}{0.026 + I} \quad \text{receptors cell}^{-1}. \tag{5.8}$$

Allowing receptor dynamics to occur with time scales faster than changes in the concentration of IL-7, one can assume the relation holds as the concentration varies with time. Let us define

$$\mathcal{R}(t) = 600 + \frac{960}{0.026 + I(t)} \quad \text{receptors cell}^{-1}. \tag{5.9}$$

In Chapter 4 we found the fraction of surface receptors bound to IL-7 in equilibrium is

$$\mathcal{F}(I) = \frac{I}{1.7 + I}. \tag{5.10}$$

In the above equation the concentration I is assumed to be constant. As above, we again assume receptor dynamics reach equilibrium in shorter time scales than changes in the concentration of IL-7. From this assumption, we let the above expression for $\mathcal{F}(I)$ hold when I is non-constant. Therefore $\mathcal{F}(I) \to \mathcal{F}(I(t))$. It follows that the number of IL-7:IL-7R complexes internalised into the cell in a 24 hour time period, starting at time t, is given by

$$\begin{aligned}\gamma_{\text{complexes}}(I(t)) &= \int_t^{t+24 \text{ hours}} \mu_B \mathcal{F}(I(s))\mathcal{R}(s)\, \mathrm{d}s \quad \text{complexes day}^{-1}\ \text{cell}^{-1} \\ &= \int_t^{t+24 \text{ hours}} \frac{1.4I(s)}{1.7 + I(s)} \left(600 + \frac{960}{0.026 + I(s)}\right) \mathrm{d}s \quad \text{complexes day}^{-1}\ \text{cell}^{-1},\end{aligned} \tag{5.11}$$

where μ_B takes the value given in Table 4.4. It is reported that IL-7 has a molecular mass of 17 kDa ($\approx 2.8 \times 10^{-11}$ ng) (Haugen *et al.*, 2010). Based on this, the per cell rate of IL-7 internalisation is given by

$$\gamma_{\text{mass}}(I(t)) = \int_t^{t+24 \text{ hours}} \frac{3.9I(s)}{1.7 + I(s)} \left(6.0 + \frac{9.6}{0.026 + I(s)}\right) \times 10^{-9}\, \mathrm{d}s \quad \text{ng day}^{-1}\ \text{cell}^{-1}. \tag{5.12}$$

Our aim is to estimate the rate at which a T cell internalising IL-7 reduces the concentration of IL-7. It follows that we must choose a volume for the model. Such a volume must be chosen with respect to the animal model being considered. In the experiments introduced in the next section, we assume the volume of the murine immune system is constant. Considering the homeostasis of naive T cells in the human immune system during ageing, the volume should reflect growth from childhood to adulthood. Naive T cells are generally assumed to be found only in the lymphoid tissues and the blood, however studies have suggested this may not be strictly true (Cose, 2007). The choice of an appropriate volume is difficult and due to the lack of studies specifically motivated with this in aim, we are forced to make a guess. For simplicity, we shall assume a volume of 1 ml for the murine immune system. A typical laboratory mouse weighs around 20 grams (0.02 kg), which, assuming mammalian tissue has a similar density to water, implies a total volume of around 20 ml. Thus, our assumed peripheral volume is around 5% of the total volume of a mouse.

To estimate the average body mass of a human we use the model for males given by Burmaster and Crouch (Burmaster & Crouch, 1997). The explicit relationship between mass (kg) and age (years) is given by the function $M(y)$ as follows

$$M(y) = \exp\Big[4.1 + 1.4\times10^{-2}y - 1.5\times10^{-4}y^2 - 2.0\exp\left[-y\left(0.15 - 1.4\times10^{-2}y + 9.8\times10^{-4}y^2\right)\right]\Big] \text{ kg}, \tag{5.13}$$

where y is age measured in years. A plot of this function is given in the left panel of Figure 5.2. Assuming the volume (ml) is 5% of total body mass (grams), we let the volume of the human immune system be given by

$$V(t) = 0.05M(t/365)\times10^3 \text{ ml}, \tag{5.14}$$

where t is time in days. The rate of IL-7 concentration reduction due to internalisation of IL-7 is then defined as

$$\gamma_{\text{conc}}(I(t)) = \frac{\gamma_{\text{mass}}(I(t))}{V(t)}. \tag{5.15}$$

To simplify this expression, we assume that for a homeostatic environment, the concentration of IL-7 is approximately constant over a period of one day. Using this

assumption the integral in equation (5.12) reduces to

$$\begin{aligned}
&\int_t^{t+24 \text{ hours}} \frac{3.9I(s)}{1.7+I(s)}\left(6.0+\frac{9.6}{0.026+I(s)}\right)\times 10^{-9}\,\mathrm{d}s \\
&= 24\frac{3.9I(t)}{1.7+I(t)}\left(6.0+\frac{9.6}{0.026+I(t)}\right)\times 10^{-9} \\
&\approx \frac{9.4I(t)}{1.7+I(t)}\left(6.0+\frac{9.6}{0.026+I(t)}\right)\times 10^{-8}. \qquad (5.16)
\end{aligned}$$

Finally, we define the IL-7 internalisation rate to be

$$\gamma(I(t)) \stackrel{\text{def}}{=} \frac{9.4I(t)}{1.7+I(t)}\left(6.0+\frac{9.6}{0.026+I(t)}\right)\times 10^{-8}(V(t))^{-1} \quad \text{ngml}^{-1}\ \text{cell}^{-1}\ \text{day}^{-1}, \qquad (5.17)$$

where $V(t)$ is given by equation (5.14) for humans and $V(t) = 1$ ml for mice. A plot of this function for a human volume with t in the range 0 - 60 years and $I(t)$ in the range 0 - 1 ng ml^{-1} is shown in the middle panel of Figure 5.2.

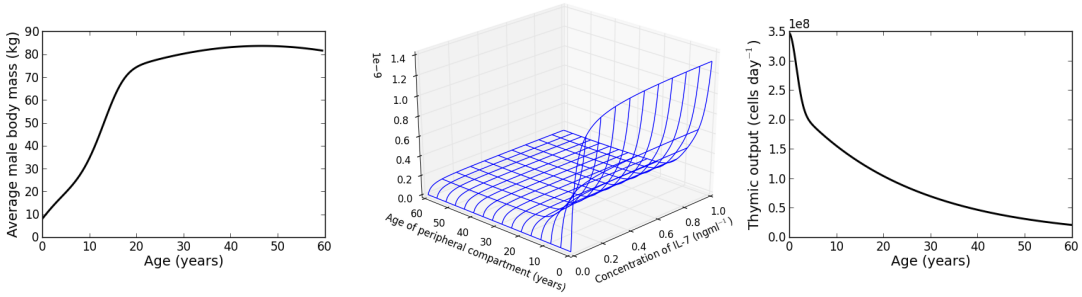

Figure 5.2: Left panel: Average body mass of males (equation (5.13)) between ages 0 and 60 years. Middle panel: Plot of the function $\gamma(I(t))$ (equation (5.17)) for a human immune volume with t in the range 0 - 60 years and $I(t)$ in the range 0 - 1 ng ml^{-1}. Right panel: rate of export of thymocytes for human individuals aged 0 - 60 years (equation (5.18)).

5.2.3 Export of thymocytes

In the experiments described in the next section, host mice were Rag1 knock-outs, for which we assume thymic export is zero. For humans we let the rate of export of thymocytes to the periphery be a decreasing function of time. In particular, we use the functional form given by Bains *et al.* (Bains *et al.*, 2009b). Let us introduce the thymic output function, $\nu(t)$, as follows

$$\nu(t) = 2.32\times 10^8 \exp(-1.1\times 10^4 t) + 1.15\times 10^8 \exp(-1.6\times 10^7 t^2)\ , \qquad (5.18)$$

where t corresponds to the age of the individual, measured in days. A plot of this function is shown in the left panel of Figure 5.2. The function was chosen by Bains *et al.* to describe the rate of thymic export of $CD4^+$ T cells. We use the same function to describe the export rate of all naive T cells ($CD4^+$ or $CD8^+$ T cells). This approximation is justified since we require the absolute cell count to roughly approximate the cell count observed in humans (indeed, such an observation is likely subject to large differences). Of interest later in this chapter is the relative variation of cell numbers with different choices of parameter values. For our purposes, the important feature of $\nu(t)$ is that it is a decreasing function of time.

5.2.4 Production and degradation of IL-7

We assume IL-7 is produced at a constant rate per unit time. This rate is encoded by the parameter β, which has units ng ml^{-1} day^{-1}. Furthermore, we assume IL-7 is degraded and internalised by other cell types at a constant rate per unit time. We let the degradation rate of IL-7 be denoted by the parameter δ, which has units day^{-1}.

5.2.5 Cell cycle progression

Cycling cells take on average λ^{-1} days to complete the cell cycle. After a cell divides, both daughter cells are produced in the resting state and require a second signal before they can progress through another round of cell division. Cell cycle may be interrupted resulting in the death of the cell. Such death events occur at a rate μ_C, which has units days^{-1}.

5.2.6 Deterministic equations for the resource model

From the above assumptions, the system of differential equations governing the behaviour of the naive T cells (resting and cycling) and the concentration of IL-7 is given by

$$\frac{\mathrm{d}I(t)}{\mathrm{d}t} = \beta - \gamma(I(t))R(t) - \delta I(t) \,, \tag{5.19}$$

$$\frac{\mathrm{d}R(t)}{\mathrm{d}t} = \nu(t) - \left[\bar{\rho}(S(t)) + \bar{\mu}_R(S(t))\right] R(t) + 2\lambda C(t) \,, \tag{5.20}$$

$$\frac{\mathrm{d}C(t)}{\mathrm{d}t} = \bar{\rho}(S(t))R(t) - (\mu_C + \lambda)\, C(t) \,. \tag{5.21}$$

The model expressed in these equations is assumed to describe naive T cell survival for both humans and mice. However, the parameter choices, functional form of $\nu(t)$ and volume used in the function $\gamma(I(t))$ differ between humans and mice. This system is subject to the initial conditions I_0, R_0, and C_0 at time $t = 0$.

5.3 Inferring parameters from experimental data

An immune system possessing an abnormally low number of lymphocytes is referred to as being lymphopenic. Lymphopenia induced proliferation (LIP) is defined as the expansion of a population of lymphocytes in response to such an environment. Expansion in this manner is not a response to antigenic stimulation, such as in the case of an infection. Rather, it has been suggested that during LIP, the signals normally regulating homeostasis of lymphocyte populations are in excess due to the low numbers of lymphocytes competing for these signals (Goldrath *et al.*, 2004). In this section we use measurements of an expanding population of T cells in a mouse, to estimate the parameters of our model.

The abundance of IL-7 and sp:MHC induces T cells to divide, thereby increasing the size of the population. After expansion, it is assumed the availability of trophic factors required to induce proliferation returns to levels found in lymphoreplete environments (Fry & Mackall, 2005). We restrict ourselves to assuming the rate of expansion is controlled by the effective concentration at which IL-7 is available. Availability of sp:MHC is not considered.

In an experimental setting, T cells may be induced to undergo LIP by creating a lymphopenic environment in mice. The gene Rag-1 is expressed during development of the T cell receptor. Mice, genetically engineered such that they do not express the Rag-1 gene, do not generate T cells. Such mice are lymphopenic and have been used to study the expansion of lymphocytes in response to lymphopenic environments (Mombaerts *et al.*, 1992). Rag1 knock-out OT-I T Cell Receptor mice are engineered to produce $CD8^+$ T cells which possess only the OT-1 TCR. Similarly, Rag1 knock-out F5 T Cell Receptor mice are engineered to produce $CD8^+$ T cells possessing the F5 TCR. Such mice are used for adoptive transfer experiments. In the experiments performed by Hogan *et al.*, OT-1 and F5 T cells were adoptively transferred from transgenic mice into Rag-1 knock-out mice to study the mechanisms controlling the lymphopenic expansion of these two T cell clonotypes (Hogan *et al.*, 2013). In these experiments, both T cell clonotypes proliferate in lymphopenic

hosts. Measuring the number of T cells at various time points allows the acquisition of time course data. In reference (Hogan *et al.*, 2013) the authors present a deterministic mathematical model, sharing features of the model presented in Section 3.2.1. The authors conclude that the underlying mechanisms regulating LIP are the same for both OT-1 and F5 T cells. The authors kindly agreed to share the experimental data obtained through these experiments. In this section, we fit the model introduced in this chapter (in the context of a mouse) to this data, allowing us to make an estimate for the parameters of the model.

Prior to adoptive transfer into Rag-1 deficient hosts, the two transgenic T cell clonotypes were stained with carboxyfluorescein succinimidyl ester (CFSE). CFSE is a fluorescent green dye which can be used to track the division history of a population of T cells. A cell stained with CFSE will, upon division, produce two daughter cells which fluoresce at half the intensity of the parent. If one labels a population of T cells using CFSE, one can, at later time points, count the total number of cells that have undergone n divisions. The population of cells having undergone n divisions fluoresces, on average, at half the intensity of the population which has undergone $n-1$ divisions. After about 8 divisions, CFSE is practically indistinguishable from background fluorescence. In the experiments performed by Hogan *et al.*, mice were sacrificed at days 3, 4, 5, 6, 7, 10, 12 and 18. At these time points, CFSE labelled cells were recovered from the spleens and lymph nodes of recipient mice. The total number of recovered donor transgenic T cells was determined by flow cytometry.

5.3.1 Generational model

Our model presented thus far describes the average number of resting T cells and the average number of cells in the cell cycle. In this section we extend the model to record the average number of T cells which have divided n times for both the resting and cycling compartments. The approach we take bears similarity to the approaches taken by Schittler *et al.* (2013), and Ganusov and De Boer (2013) in modelling lymphocytes populations for BrdU labelling experiments.

To avoid introducing more parameters, we assume the parameters governing the dynamics of the total population also govern the dynamics of each generation. Let us denote by N the generation at which CFSE fluorescence is indistinguishable from the background. Furthermore, denote by $R_n(t)$, the number of resting cells which have divided n times and by $C_n(t)$, the number of cycling cells which have gone through n divisions previously. Then, assuming dividing cells enter the resting pool

in the next generation, the generational model is described by the following system of ordinary differential equations:

- The number of cells internalising IL-7 is now summed over the number of resting cells in each generation. We also assume host mice produce IL-7 at a constant rate for the time course of the experiment:

$$\frac{\mathrm{d}I(t)}{\mathrm{d}t} = \beta - \gamma(I(t)) \sum_{k=0}^{N} R_k(t) - \delta I(t). \tag{5.22}$$

- Since the host mice in the experiments are Rag-1 knock-outs, no T cells are produced by the host and therefore we set $\nu = 0$. The ODEs describing the number of cells which have not divided are given by:

$$\frac{\mathrm{d}R_0(t)}{\mathrm{d}t} = -\left[\bar{\rho}(S(t)) + \bar{\mu}_R(S(t))\right] R_0(t), \tag{5.23}$$
$$\frac{\mathrm{d}C_0(t)}{\mathrm{d}t} = \bar{\rho}(S(t))R_0(t) - (\mu_C + \lambda)C_0(t). \tag{5.24}$$

- Cycling cells in generation n produce two resting cells in generation $n+1$. The ODEs describing the model for $n = 1 \ldots ...N-1$ are given by:

$$\frac{\mathrm{d}R_n(t)}{\mathrm{d}t} = 2\lambda C_{n-1}(t) - \left[\bar{\rho}(S(t)) + \bar{\mu}_R(S(t))\right] R_n(t), \tag{5.25}$$
$$\frac{\mathrm{d}C_n(t)}{\mathrm{d}t} = \bar{\rho}(S(t))R_n(t) - (\mu_C + \lambda)C_n(t). \tag{5.26}$$

- At generation N, we assume CFSE fluorescence is indistinguishable from the background and therefore, collect all subsequent generations of cells into a single variable. The ODEs describing the model beyond CFSE detectability are given by:

$$\frac{\mathrm{d}R_N(t)}{\mathrm{d}t} = 2\lambda \left(C_{N-1}(t) + C_N(t)\right) - \left[\bar{\rho}(S(t)) + \bar{\mu}_R(S(t))\right] R_N(t), \tag{5.27}$$
$$\frac{\mathrm{d}C_N(t)}{\mathrm{d}t} = \bar{\rho}(S(t))R_N(t) - (\mu_C + \lambda)C_N(t). \tag{5.28}$$

Summing over all generations, the generational model gives identical results to the model presented in Section 5.2.6. That is,

$$\sum_{k=0}^{N} R_k(t) = R(t) \quad \text{and} \quad \sum_{k=0}^{N} C_k(t) = C(t). \tag{5.29}$$

5.3.2 Initial parameter guesses

The model possesses 9 parameters, $\{\alpha, \beta, \delta, \theta_s, \theta_p, \lambda, \rho, \mu_R, \mu_C\}$, which we aim to estimate. Furthermore, the initial conditions are unknown. We let the in vivo concentration of IL-7 prior to T cell transfer be equal to the equilibrium solution of equation (5.22), subject to setting the internalisation rate equal to zero ($\gamma(I(t)) = 0$). We define

$$I(t = 0) = I_0 = \frac{\beta}{\delta}. \tag{5.30}$$

In the experiments, 1.5×10^6 T cells were adoptively transferred to host mice (Hogan *et al.*, 2013). Following transfer, T cells must migrate to the lymphoid tissue to access IL-7. We assume approximately 5% of cells survive the transfer, however, we treat the initial number of resting cells as a further parameter to be estimated, with 7.5×10^4 cells as the initial guess. We assume no cells are in cycle following transfer. In the experiments, host mice receiving OT-1 T cells are the same as those receiving F5 T cells. Due to this, we assume the rates of IL-7 production and degradation due to non-T cell sources are the same in both sets of experiments. Thus, rather than performing parameter estimation for the OT-1 and F5 data independently, we combine data sets, such that β and δ can be fixed between data sets.

A rough estimate for the total number of T cells in a lymphoreplete mouse is around 10^7 cells. We guess that in a lymphoreplete mouse, the effective concentration of IL-7 is limiting and close to the mean survival threshold. The studies of Palmer *et al.* (Palmer *et al.*, 2011) indicate cell viability becomes impaired at around 10^{-2} ng ml^{-1} IL-7 in vitro. We use this value as the effective concentration of IL-7 in a lymphoreplete mouse containing around 10^7 T cells. Equation (5.17), subject to choosing a volume for the mouse of 1 ml, is given by

$$\gamma(I(t)) = \frac{9.4 I(t)}{1.7 + I(t)} \left(6.0 + \frac{9.6}{0.026 + I(t)} \right) \times 10^{-8} \, . \tag{5.31}$$

From (5.31), we estimate the rate of IL-7 internalisation ($\gamma(I(t))R(t)$) in a lymphoreplete mouse to be approximately 1.5 ng ml^{-1} day^{-1}. Let us choose $\beta = 2$ ng

ml^{-1} day^{-1}. Furthermore, we let the difference between β and $\gamma(I(t))$ be accounted for by δ, which we initially guess is 40 days^{-1}.

The parameter λ encodes the average length of time a cell takes to complete the cell cycle, we guess λ^{-1} to be half a day ($\lambda = 2$ days^{-1}). The parameter μ_C encodes the rate at which cells fail to complete the cell cycle resulting in cell death. We choose $\mu_C = 0.5$ days^{-1}. The rate of resting cell death due to IL-7 starvation is encoded by the parameter μ_R. We guess T cells may survive on average for 2 days without IL-7 stimulus, hence $\mu_R = 0.5$ days^{-1}. We note that this represents the minimum lifetime of a T cell, in the absence of any survival signals. In IL-7 deficient hosts, trasferred T cell survive for approximately a month. However, in vivo these cells may have access to other pro-survival cytokines and TCR signals. Lastly, we guess the rate of entry into cell cycle is of the order of a few hours, we choose $\rho = 4$ days^{-1}. Assuming signalling thresholds are an order of magnitude apart, as suggested by Palmer *et al.* (2011), and noting that the average number of signalling units is, by construction, bounded between 0 and 600, we guess $\theta_s = 50$ signalling units and $\theta_p = 500$ signalling units. Given the above parameter choices, an initial exploration of the numerical solutions suggests a suitable value for α is 3 $(\text{log signalling units})^{-1}$.

5.3.3 Parameter optimisation

Data obtained at days 3, 4, 5, 6, 7, 10, 12 and 18 was processed such that the average number of cells per day per generation was recorded for generations 0 - 8. This was done for both the OT-1 and F5 data sets. No distinction was made between resting and cycling cells within the experiments, therefore data is compared to $R_i(t)+C_i(t)$, $i = 0, \ldots, 8$. Data for both sets of experiments was stored in a matrix X^{obs} of size 8 (number of days) $\times$ 9 (number of generations). Model output was formatted to simulate observations at the equivalent time points and stored in the matrix X^{sim}, for both the model subject to the OT-1 and F5 parameter sets. For each data set, the discrepancy between model output and experimental data was quantified using the measure

$$D(X^{\text{sim}}, X^{\text{obs}}) = \sum_{i,j} \left(\frac{x_{ij}^{\text{sim}} - x_{ij}^{\text{obs}}}{x_{ij}^{\text{sim}} + x_{ij}^{\text{obs}}} \right)^2, \quad 1 \leq i \leq 8,\ 1 \leq j \leq 9. \tag{5.32}$$

Parameter optimisation was performed using the function fmin_tnc, available within the *scipy.optimize* package for Python. The parameter vector passed to this function

was

$$\{\beta, \delta, \alpha^{\mathrm{OT-1}}, \theta_s^{\mathrm{OT-1}}, \theta_p^{\mathrm{OT-1}}, \lambda^{\mathrm{OT-1}}, \rho^{\mathrm{OT-1}}, \mu_R^{\mathrm{OT-1}}, \mu_C^{\mathrm{OT-1}},$$
$$R_0^{\mathrm{OT-1}}, \alpha^{\mathrm{F5}}, \theta_s^{\mathrm{F5}}, \theta_p^{\mathrm{F5}}, \lambda^{\mathrm{F5}}, \rho^{\mathrm{F5}}, \mu_R^{\mathrm{F5}}, \mu_C^{\mathrm{F5}}, R_0^{\mathrm{F5}}\}. \tag{5.33}$$

Note that we have assumed β and δ are the same for both sets of experiments, but in principle all other parameters are intrinsic to the cell type being transferred to the host. We therefore obtain two values of D, one for the OT-1 data set and one for the F5 data set. These two values are summed to give the total distance the model output and the experimental data.

The measure above was minimised using the initial guesses given in the second column of Table 5.1. In this table we also present the parameters obtained post optimisation. In Figures 5.3 and 5.4 we present bar charts showing each component of X^{obs} against the simulated observation in X^{sim}, for the OT-1 and F5 data, respectively. The aggregate simulated number of cells ($\sum_{i=0}^{8} R_i(t) + C_i(t)$) is shown alongside the observed number of cells (aggregate) recorded for each mouse, in the left panel of Figure 5.5.

Parameter	β	δ	α	θ_s	θ_p	λ	ρ	μ_R	μ_C	R_0
Initial Guess	2	40	3	50	500	2	4	0.5	0.5	7.5×10^4
Best Fit OT-1	1.83	41.5	3.33	50.0	483	3.20	4.38	0.500	0.396	7.69×10^4
Best Fit F5	1.83	41.5	3.19	50.0	555	2.37	3.54	0.500	0.279	8.42×10^4
Units	ng ml^{-1} day^{-1}	days^{-1}	(log signalling units)$^{-1}$	signalling units	signalling units	days^{-1}	days^{-1}	days^{-1}	days^{-1}	cells

Table 5.1: Initial guesses and optimised parameters.

5.3.4 Testing the model

To test the model, further data was obtained from Hogan *et al.* (2013). The original experiments were repeated; however this time, observations were recorded at days 1, 20, 42 and 48. These time points lie outside the range of the time points used to estimate the parameters of the model. In the right panel of Figure 5.5 we plot the

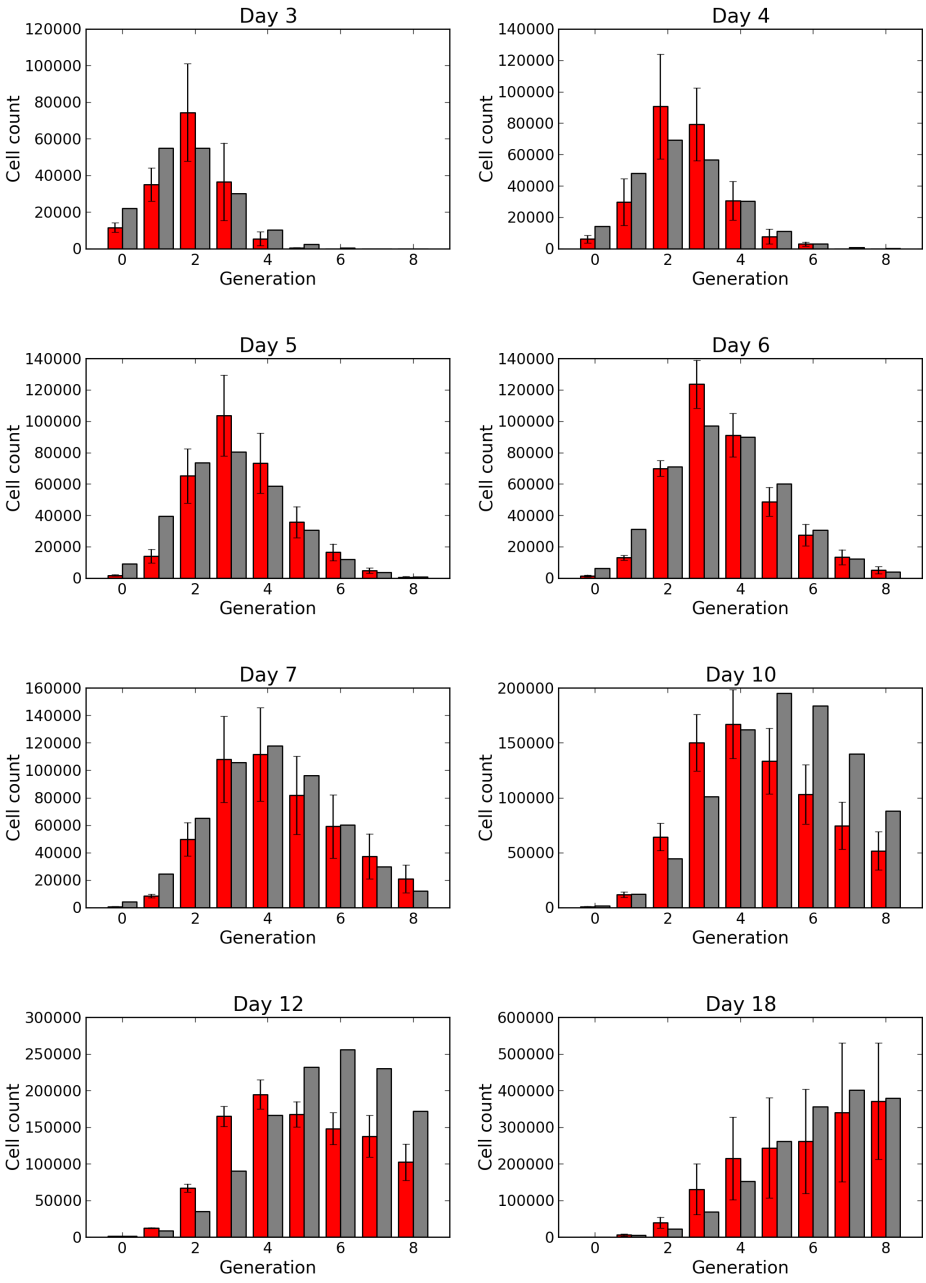

Figure 5.3: Red: Experimental cell counts obtained from mice receiving OT-1 T cells. Grey: model output using best fit parameter set.

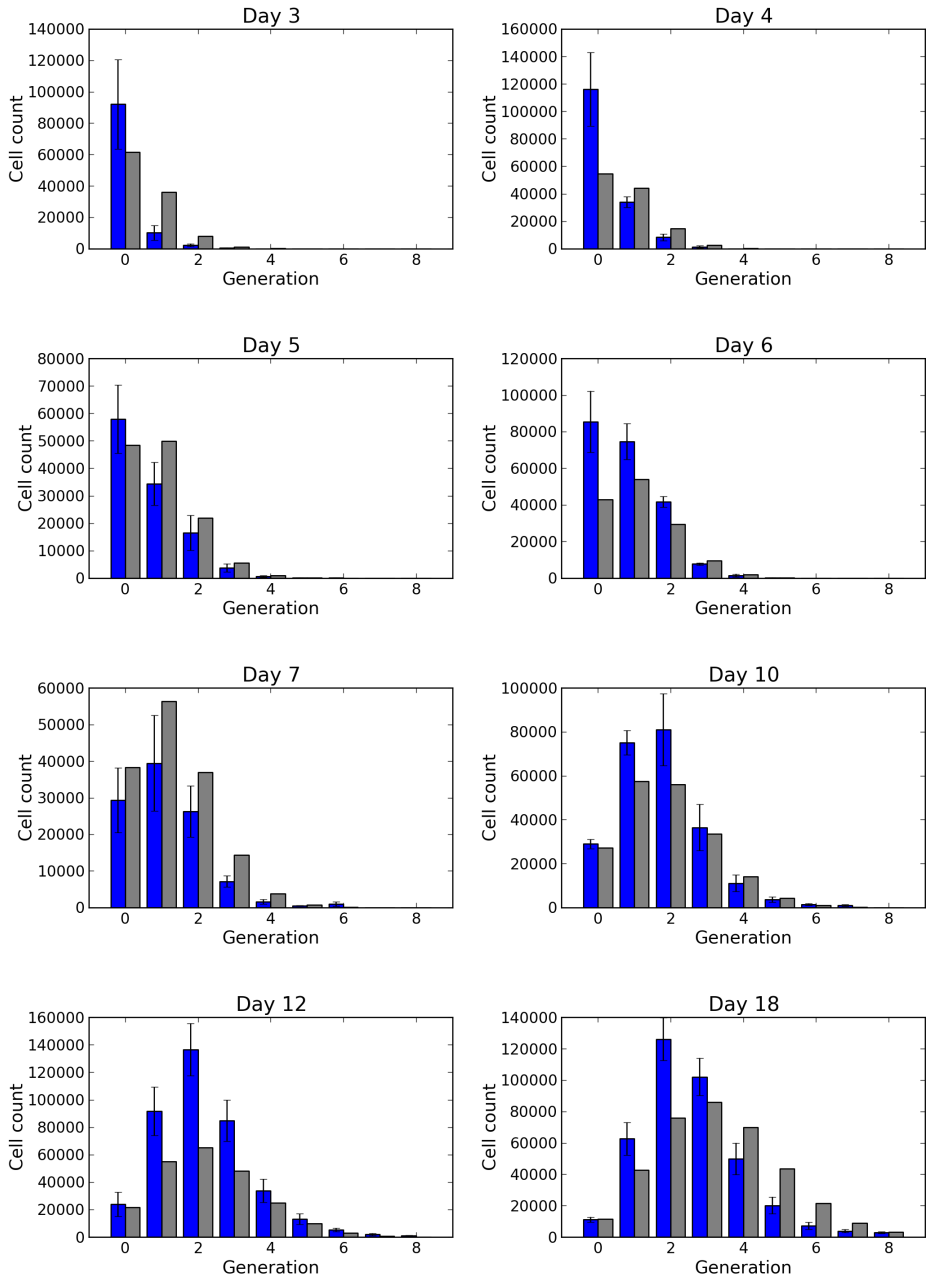

Figure 5.4: Blue: Experimental cell counts obtained from mice receiving F5 T cells. Grey: model output using best fit parameter set.

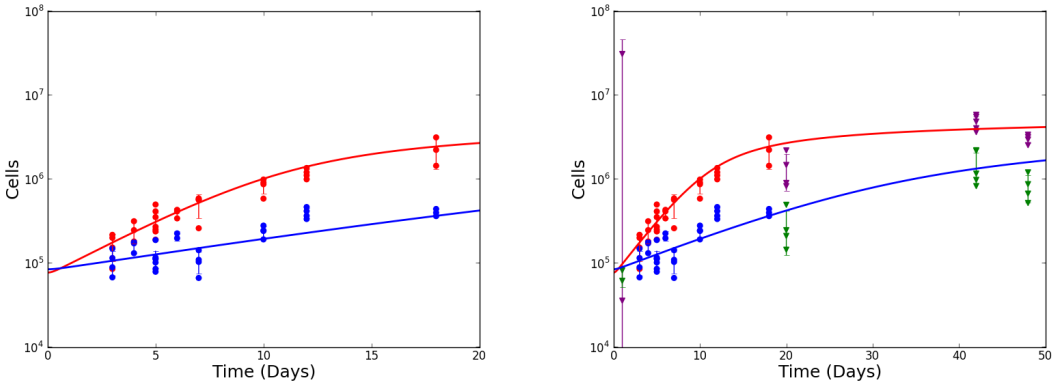

Figure 5.5: Left: Solid lines show the aggregate number of T cells calculated using equations (5.19)-(5.21) and the parameter set given in the third column of Table 5.1. Each point represents the total number of cells recorded from a mouse. OT-1 data shown in red, F5 data shown in blue. Right: Purple markers show experimental test data for OT1 T cells. Green markers indicate experimental test data for F5 T cells.

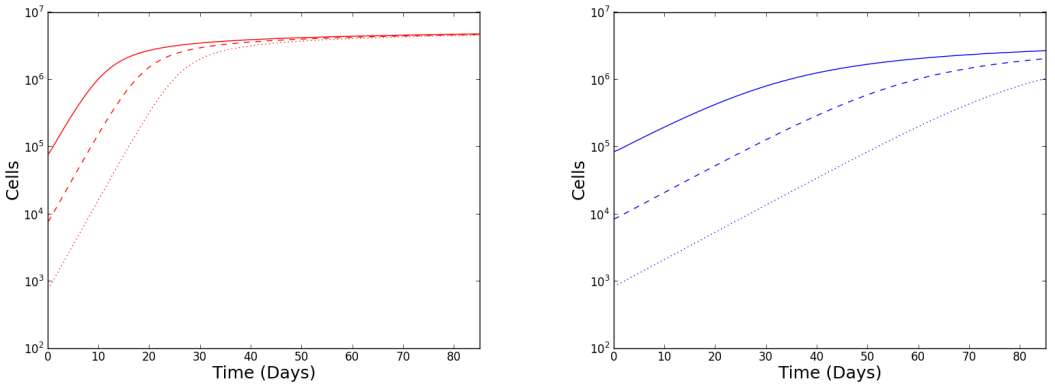

Figure 5.6: Left panel: model output computed with best fit parameter set for OT-1 data. Solid lines are produced with R_0 as obtained from parameter estimation (presented in the third column of Table 5.1 for both the OT-1 and F5 varieties). Dashed lines simulated with $R_0/10$, dotted lines simulated with $R_0/100$. Right panel: model output computed with best fit parameter set for F5 data. Solid lines are produced with R_0 as obtained from parameter estimation. Dashed lines simulated with $R_0/10$, dotted lines simulated with $R_0/100$.

additional observations (triangles) against model predictions. The model extrapolated to later times matches the new time points reasonably well for both the OT-1 and F5 cell types.

To further test the model we emulated tests made by Hogan *et al.* In these tests, model parameters were used to estimate the rate of T cell expansion from different initial numbers of cells. Using our model, we reduced the initial number of resting cells (R_0) by a factor of 10 and 100. In Figure 5.6 solid lines correspond to taking R_0 as estimated from the parameter optimisation, dashed lines were produced using the initial condition $R_0/10$, and dotted lines were simulated with $R_0/100$ resting cells. The model realised using the OT-1 parameter set predicts that solid and dotted trajectories converge to within 2×10^5 cells of each other within the experimental time course of 86 days. In contrast to this, the model realised using the F5 parameter set predicts a lesser degree of convergence over the 86 day time window. Indeed, the closest approach between solid and dotted trajectories is approximately 1.6×10^6 cells, nearly an order of magnitude larger than the closest approach for the OT-1 trajectories. These predictions are reflected remarkably well in the experimental data shown in the middle panel of Figure 7B in reference (Hogan *et al.*, 2013). The agreement between these model predictions and the experimental observations suggests our model is good at describing the rate of expansion of a population of T cells in a lymphopenic environment.

5.3.5 Stability analysis of the mouse model

The analysis of steady states of the resource model in the context of an experimental mouse is similar to the analysis presented in Section 3.3.7. Stationary solutions are found from solving the system of equations

$$0 = \beta - \gamma(I^*)R^* - \delta I^* \,, \tag{5.34}$$

$$0 = -\left[\bar{\rho}(S^*) + \bar{\mu}_R(S^*)\right] R^* + 2\lambda C^* \,, \tag{5.35}$$

$$0 = \bar{\rho}(S^*)R^* - (\mu_C + \lambda)\, C^* \,, \tag{5.36}$$

where $S^* = S(I^*)$. Combining (5.35) and (5.36) we find

$$\left((\mu_C + \lambda)\bar{\mu}_R(S^*) + (\mu_C - \lambda)\bar{\rho}(S^*)\right) R^* = 0. \tag{5.37}$$

Therefore, either $R^* = 0$, in which case $C^* = 0$ and $I^* = \frac{\beta}{\delta}$, or the signalling at equilibrium satisfies

$$(\mu_C + \lambda)\bar{\mu}_R(S^*) + (\mu_C - \lambda)\bar{\rho}(S^*) = 0. \tag{5.38}$$

Note, that by construction, $\bar{\mu}_R(0) = \mu_R > 0 = \bar{\rho}(0)$ and $\lim_{x\to+\infty} \bar{\mu}_R(x) = 0 < \lim_{x\to+\infty} \bar{\rho}(x)$. Given that $\bar{\mu}_R(x)$ and $\bar{\rho}(x)$ are respectively, strictly decreasing and increasing, there exists a unique solution S^* satisfying (5.38), on the semi-open interval $[0, \infty)$. It follows then that I^*, R^* and C^* are unique if $R^* > 0$. The Jacobian for this system is

$$J = \begin{pmatrix} -\gamma'(I^*)R^* - \delta & -\gamma(I^*) & 0 \\ -S'(I^*)R^* \left(\bar{\rho}'(S^*) + \bar{\mu}'_R(S^*)\right) & -\left(\bar{\rho}(S^*) + \bar{\mu}_R(S^*)\right) & 2\lambda \\ S'(I^*)\bar{\rho}(S^*)R^* & \bar{\rho}(S^*) & -(\mu_C + \lambda) \end{pmatrix}. \tag{5.39}$$

The characteristic polynomial for this system is $\det(J - \xi I) = 0$:

$$\xi^3 + a_1\xi^2 + a_2\xi + a_3 = 0, \tag{5.40}$$

where

$$a_1 = \bar{\rho}(S^*) + \bar{\mu}_R(S^*) + \mu_C + \lambda + \gamma'(I^*)R^* + \delta, \tag{5.41}$$

$$\begin{aligned} a_2 = &\left(\bar{\rho}(S^*) + \bar{\mu}_R(S^*) + \mu_C + \lambda\right)\left(\gamma'(I^*)R^* + \delta\right) + (\mu_C + \lambda)\bar{\mu}_R(S^*) + (\mu_C - \lambda)\bar{\rho}(S^*) \\ &- \gamma(I^*)S'(I^*)R^*\left(\bar{\rho}'(S^*) + \bar{\mu}'_R(S^*)\right), \end{aligned} \tag{5.42}$$

$$\begin{aligned} a_3 = &\left(\gamma'(I^*)R^* + \delta\right)\left((\mu_C + \lambda)\bar{\mu}_R(S^*) + (\mu_C - \lambda)\bar{\rho}(S^*)\right) \\ &- \gamma(I^*)S'(I^*)R^*\left((\mu_C + \lambda)\bar{\mu}'_R(S^*) + (\mu_C - \lambda)\bar{\rho}'(S^*)\right). \end{aligned} \tag{5.43}$$

All eigenvalues ξ, are negative if and only if, $a_i > 0$, $i = 1, 2, 3$, and $a_1 a_2 > a_3$. If these conditions are met, then stationary solutions I^*, R^*, C^* are stable (Hurwitz, 1964).

5. THE RESOURCE MODEL REVISITED: IL-7 DEPENDENT DYNAMICS

Stationary solutions of the form $I^* = \frac{\beta}{\delta}$, $R^* = C^* = 0$

Consider stationary solutions of the form $I^* = \frac{\beta}{\delta}$, $R^* = C^* = 0$. The coefficients a_i, $i = 1, 2, 3$ reduce to

$$a_1 = \bar{\rho}(\hat{S}) + \bar{\mu}_R(\hat{S}) + \mu_C + \lambda + \delta, \tag{5.44}$$

$$a_2 = \left(\bar{\rho}(\hat{S}) + \bar{\mu}_R(\hat{S}) + \mu_C + \lambda\right)\delta + (\mu_C + \lambda)\bar{\mu}_R(\hat{S}) + (\mu_C - \lambda)\bar{\rho}(\hat{S}) \tag{5.45}$$

$$a_3 = \delta\left((\mu_C + \lambda)\bar{\mu}_R(\hat{S}) + (\mu_C - \lambda)\bar{\rho}(\hat{S})\right), \tag{5.46}$$

$$\tag{5.47}$$

where $\hat{S} = S(\frac{\beta}{\delta})$. The functions $\bar{\rho}$ and $\bar{\mu}_R$, are, by definition, strictly positive. Therefore, $a_1 > 0$ (as is $a_1 - \delta$). We may write $a_2 = (a_1 - \delta)\delta + \delta^{-1}a_3$. From which it follows, $a_1 a_2 = a_1(a_1 - \delta)\delta + \delta^{-1}a_1 a_3 = a_1(a_1 - \delta)\delta + \delta^{-1}(a_1 - \delta)a_3 + a_3 > a_3$. Stability is thus ensured if $a_3 > 0$, which is true if and only if

$$(\mu_C + \lambda)\bar{\mu}_R(S^*) + (\mu_C - \lambda)\bar{\rho}(S^*) > 0. \tag{5.48}$$

The above inequality holds if $\mu_C > \lambda$. Consider that, for non-zero stationary solutions R^*, C^*, any corresponding stationary solution I^* must be less than $\frac{\beta}{\delta}$. It follows that any solution S^* paired with non-zero stationary solutions R^*, C^* is less than $\hat{S}$. Thus, $\bar{\mu}_R(S^*) > \bar{\mu}_R(\hat{S})$ and $\bar{\rho}(S^*) < \bar{\rho}(\hat{S})$ and from (5.38) we have

$$(\mu_C + \lambda)\bar{\mu}_R(\hat{S}) + (\mu_C - \lambda)\bar{\rho}(\hat{S}) < 0 \tag{5.49}$$

when $\lambda > \mu_C$. Therefore, if $\lambda > \mu_C$, a_3 is negative. Thus, $\lambda < \mu_C$ is a necessary and sufficient condition for stability of stationary solutions corresponding to extinction of the T cell population.

Stationary solutions of the form $I^*, R^*, C^* > 0$

Consider now non-zero stationary solutions. From (5.38) the coefficients a_i, $i = 1, 2, 3$ reduce to

$$a_1 = \bar{\rho}(S^*) + \bar{\mu}_R(S^*) + \mu_C + \lambda + \gamma'(I^*)R^* + \delta, \tag{5.50}$$

$$a_2 = (\bar{\rho}(S^*) + \bar{\mu}_R(S^*) + \mu_C + \lambda)(\gamma'(I^*)R^* + \delta)$$

Stationary solution	Value	Stability coefficient	Value
I^*	8.98×10^{-3} ng ml^{-1}	a_1	1.56×10^2
R^*	1.30×10^7 cells	a_2	5.50×10^2
C^*	1.30 cells	a_3	1.73×10^{-3}
I^*	9.90×10^{-3} ng ml^{-1}	a_1	1.38×10^2
R^*	1.21×10^7 cells	a_2	3.58×10^2
C^*	1.90×10^{-1} cells	a_3	5.84×10^{-4}

Table 5.2: Top: Stationary solutions and stability coefficients for the OT-1 parameter set. Bottom: Stationary solutions and stability coefficients for the F5 parameter set.

$$- \gamma(I^*)S'(I^*)R^* \left(\bar{\rho}'(S^*) + \bar{\mu}_R'(S^*)\right), \tag{5.51}$$

$$a_3 = - \gamma(I^*)S'(I^*)R^* \left((\mu_C + \lambda)\bar{\mu}_R'(S^*) + (\mu_C - \lambda)\bar{\rho}'(S^*)\right). \tag{5.52}$$

The rate of IL-7 internalisation is an increasing function of the concentration and so $\gamma'(I^*) > 0$, therefore $a_1 > 0$. In general, parameters may be chosen such that a_2 and a_3 are negative. Note, if $\lambda > \mu_C$ then $a_3 > 0$ but, for example, ρ may be chosen such that $a_2 < 0$. The stationary solutions and stability coefficients are given in Table 5.2 for both the OT-1 and F5 parameter sets. In both cases, the parameters lead to trajectories tending to non-zero stationary solutions which are stable. Notice that at steady state, practically zero cells are undergoing division.

5.3.6 Numerical exploration of the mouse model

The optimised parameter set represents optimisation with respect to a local minimum, rather than a global minimum. This is because there is insufficient explanatory power in the data to uniquely estimate all parameters. Despite this, over the next section we explore the numerical behaviour of the model given this parameter set.

Negligible resting cell death rate One may have noticed that the best fit parameters for μ_R and θ_s are identical to the initial guesses. Looking at the reduction in the average signalling per T cell, $S(t)$, for both parameter sets the signalling is far above the guessed threshold for survival ($\theta_s = 50$ signalling units). To see this, consider Figure 5.7, the range of signalling observed lies between the two dashed green lines. Between the green lines, the function $\bar{\mu}_R(S(t))$ is approximately zero. As such, we cannot say with any certainty that θ_s and μ_R represent the true values. We predict that during LIP, T cell death due to lack of IL-7 stimulus is negligible.

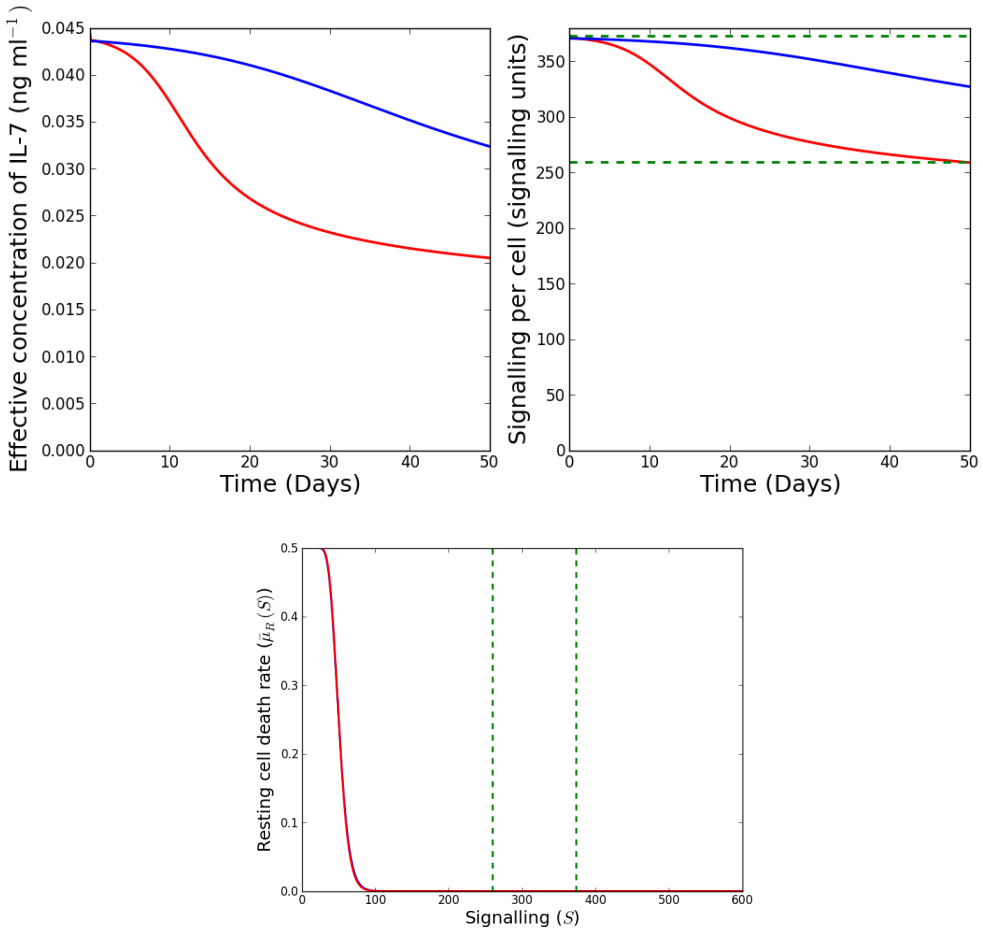

Figure 5.7: Top panels: Reduction in concentration of IL-7 and average signalling per T cell for both the OT-1 (red) and F5 (blue) parameter sets. Bottom panel: The death rate of resting cells $\bar{\mu}_R(S)$, as a function of the signalling S. Blue and red curves correspond to the F5 and OT-1 parameter sets respectively. The dashed green lines indicate the range of signalling observed from days 0 - 18.

Rates of entry into the cell cycle In the left panel of Figure 5.8 we plot the average rate of entry into the cell cycle, $\bar{\rho}(S)$. From this plot it is clear why the signalling does not fall lower than 260 signalling units for the OT-1 parameter set (330 for F5). Below these values, the rate of entry into the cell cycle is approximately 0, and so below these amounts of signalling we observe a relatively slow increase in the population size and hence a slow decrease in the amount of IL-7.

Given that the resting T cell death rate is negligible, this suggests that resting T cells are becoming quiescent, that is, these cells are remaining in the resting pool for a relatively long period of time. Since, in this model, the concentration of IL-7 is determined by the number of T cells sharing it, a slow increase in the number of T cells results in a slow decrease in the IL-7 concentration and hence, the amount of signalling.

In the right panel of Figure 5.8 we plot the probability distributions of the signalling thresholds for entry into the cell cycle. The distribution for OT-1 T cells has a peak to the left of the peak for the F5 distribution. This suggests that on average OT-1 T cells require less IL-7 to enter cell cycle than F5 T cells. For both transgenic T cell types, the distributions predict a significant proportion of cells cannot enter division even when receiving the maximum amount of signalling at equilibrium, indicated by the vertical dashed line.

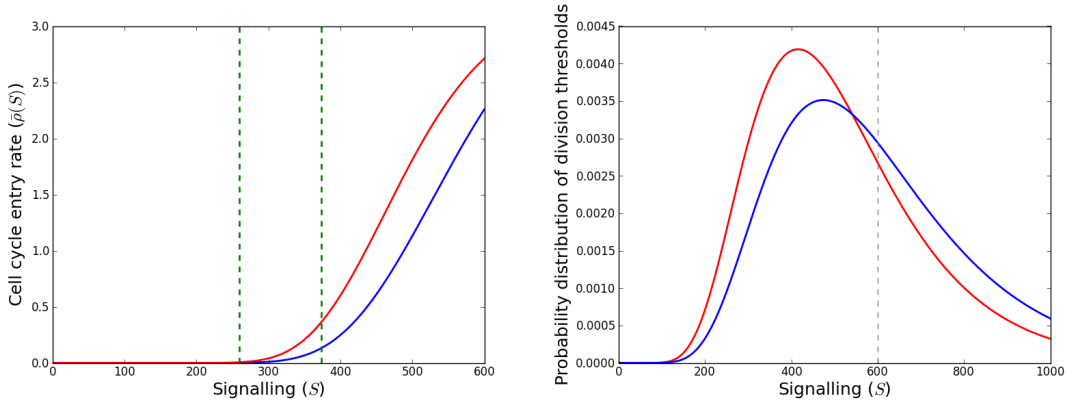

Figure 5.8: Left panel: rate of entry into cell cycle as a function of the number of IL-7 signalling units. The dashed green lines indicate the range of signalling observed from days 0 - 18. Right panel: probability distribution of thresholds for entry into cell cycle. The vertical dashed line indicates the theoretical maximum number of signalling units (in equilibrium) a T cell can possess. Blue and red curves correspond to the F5 and OT-1 parameter sets, respectively.

Convergence to fixed points Another interesting feature is the model's propensity to approach an equilibrium value. Over the 86 day time window shown in the right panel of Figure 5.5, the total number of cells is still increasing, albeit slowly, even after 86 days. Simulating the model for a longer time, it is evident that even after 2 years, a time scale comparable with the lifetime of a mouse, the total number of T cells is slowly increasing (Figure 5.9). It should be noted that the increase is slight enough that in an experimental setting it would be practically impossible to distinguish such an observation from a true equilibrium, due to the inherent noise in these types of observations. We shall classify trajectories showing such modest increase in the number of cells over time as quasi-fixed-points.

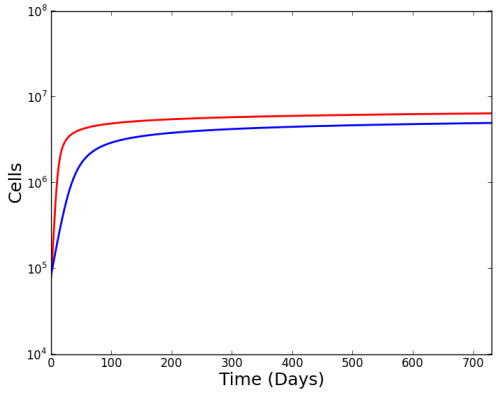

Figure 5.9: Model output simulated over a two year time course. Red, OT-1 and blue, F5.

Theoretically, there exists a single fixed point solution to the model for the estimated parameter set, which is independent of initial conditions. For the estimated parameter sets this fixed point is stable. The markedly slow convergence to the fixed point implies the existence of quasi-fixed-points (defined as trajectories wherein the rate of change of cell numbers is negligible relative to the lifespan of a mouse) which are dependent on initial conditions. In Figure 5.10 we simulate the model for 80 days for various choices of R_0 in the range 10^3-10^8 T cells. In a region near the theoretical fixed point, we observe a number of quasi-fixed-points dependent on the choice of R_0. We note that the upper boundary of this region depends on the lower signalling threshold θ_s. Since we could not infer a true value for θ_s, we cannot reliably infer where the upper part of this boundary lies. When the total number of T cells is within this region, the average amount of IL-7 signalling lies to the left of the distributions in the right panel of Figure 5.8 and to the right of equivalent distributions

for the survival thresholds. For signalling in this range (see the area between the dashed vertical lines in Figure 5.11), resting T cells are largely quiescent, hardly undergoing death or entering the cell cycle. The total number of quiescent resting cells is dependent on the number of cells at the time in which the signalling enters this zone for quiescence, ranging from roughly 5 - 20 million T cells.

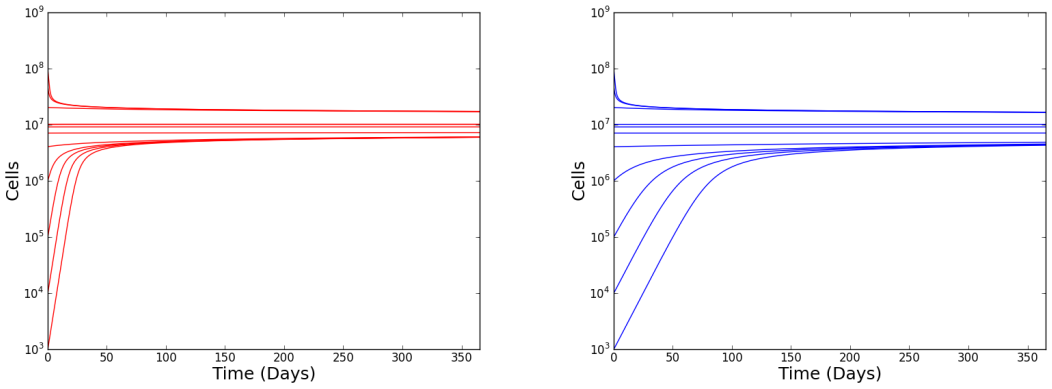

Figure 5.10: Illustration of quasi-fixed-points reached from various initial conditions.

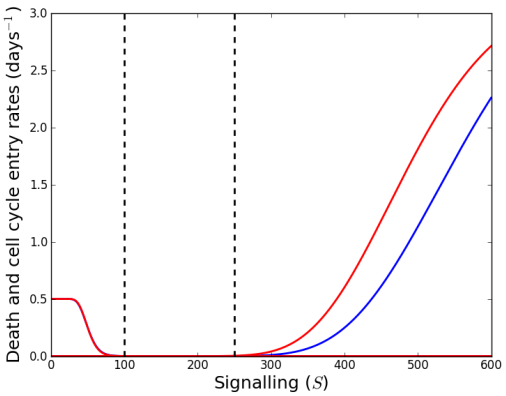

Figure 5.11: The rates of resting cell death and entry into the cell cycle as a function of the concentration of IL-7. The black lines indicate the boundaries of the region in which IL-7 signalling results in resting T cell quiescence.

Thymic output Suppose we now simulate the model using the OT-1 parameter set, but introduce the parameter $\nu > 0$ to describe thymic output. In Figure 5.12 we compute trajectories with the OT-1 parameter set with thymic output set at a rate of 10^6 T cells per day. Inclusion of thymic output predicts a faster reconstitution of the T cell population, furthermore, the total number of cells at equilibrium is higher

(relative to setting $\nu = 0$). It is also clear that inclusion of thymic output drives the model to converge to the fixed-point at a much faster rate. In the example shown, it takes about a week to reconstitute the number of T cells to the quiescent zone discussed in the previous paragraph. It then takes about a month of slower expansion for the model to converge to the set point. To reinforce this point, we repeated the computation used to produce Figure 5.10, however this time we included thymic output at a rate of 10^6 cells per day (right panel, Figure 5.12). It is clear that the extra competition from the new T cells drives the model to a fixed-point at a markedly faster rate than peripheral homeostatic expansion or contraction of the T cell population alone.

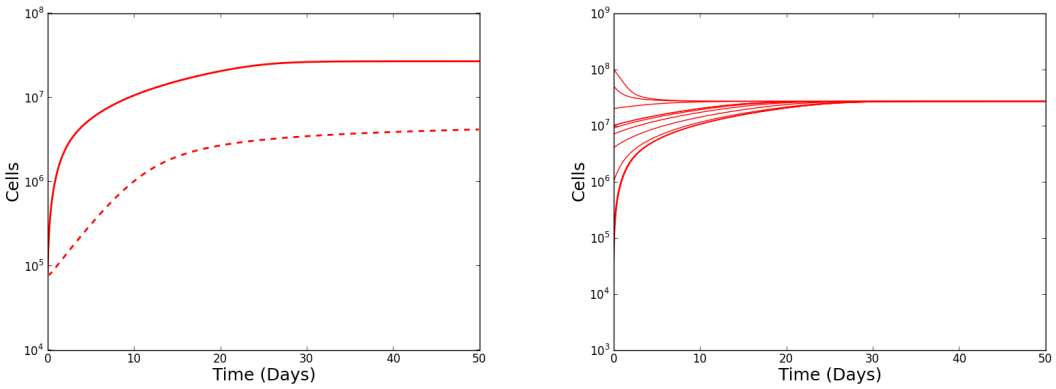

Figure 5.12: Left panel: Model computed with the OT-1 parameter set with thymic output set at 10^6 cells per day (solid line) and zero cells per day (dashed line). Right panel: Trajectories from various initial conditions subject to setting thymic output at a rate of 10^6 cells per day.

5.3.7 Discussion of the mouse model

The model is over parameterised for the available data set. Starting with different initial guesses, the optimisation scheme presented above will converge to different local minimum. Despite this, we have demonstrated that the model is able to reproduce the experimental data. In our exploration of different initial guesses, we consistently observed that the death rate of resting T cells was negligible, and further observed the tendency of the model to exhibit quasi-fixed-point solutions. We note though that the model does not possess these types of trajectories when $\alpha \ll 1$. However, one immediate implication of this is that the distributions of signalling thresholds significantly overlap, which contradicts the statement by Palmer *et al.*

(2011) that the thresholds are significantly distinct. We conclude that the observation of quasi-fixed-points is a robust feature of the model, and not a peculiarity of the local minimum we have found.

Parameter values could be uniquely determined if the number of cells undergoing division, as well as the amount of IL-7, is measured, in addition to the data presented. Exactly how one would measure the amount of IL-7 is not easy, since IL-7 is not uniformly distributed throughout the lymphatic architecture. One possible method is to measure the amount of IL-7 in the serum. However, this measurement is most likely not equal to the effective concentration at which IL-7 is available to T cells. Even so, measuring the amount of IL-7 in the serum over time could indicate the relative changes in its availability following expansion of the T cell population. From information about the relative changes, it should be possible to infer the rate at which the effective concentration changes as the size of the population increases. Despite the limitations in our ability to uniquely estimate the parameters of the model, we have demonstrated that the model is capable of reproducing the experimental observations made in reference (Hogan *et al.*, 2013).

The model, simulated under the parameter sets estimated from experimental data, predicts the existence of quasi-fixed-point solutions at which resting T cell death and entry into cell cycle rates are small. Quasi-fixed-points were observed for T cell population sizes in the range $5 - 20$ million cells. Population sizes smaller than 5 million cells expand over a few weeks to about 5 million T cells. A T cell population with more than 20 million cells contracts until it reaches around 20 million cells. For populations whose size is between these values, the rate of change of the size of the population is sufficiently slow that the population does not reach true equilibrium within the expected lifetime of a mouse. Inclusion of thymic output at a rate of 10^6 cells per day (den Braber *et al.*, 2012) predicted an equilibrium of around 27 million cells. Interestingly these observations are in agreement with a previous study which found that transferred T cells are unable to reconstitute the entire naive T cell pool in mice lacking a thymus (Tanchot *et al.*, 2002).

Consider the following scenario: a healthy mouse undergoes thymectomy, leaving the mouse with approximately 27 million naive T cells in the periphery. Initially, from the model, we would expect a modest reduction in the total number of T cells. Suppose at some later time, the mouse experiences acute T cell loss, losing say, 90% of the peripheral population. Our model predicts that the mouse is unable to reconstitute the entire T cell pool. Indeed, for our estimated parameters the transgenic mouse can only reconstitute approximately 20% of the peripheral population

following acute loss of T cells. However, this figure is very sensitive to the value of α, which we could not determine uniquely. For a polyclonal population, we would expect α to be smaller, as it is reasonable to expect a polyclonal population of cells has more variability in IL-7 signalling thresholds than a population of a single specificity. Thus, for a polyclonal mouse, we would make the same predictions as above, but would expect a greater fraction of the population to be reconstituted.
The numerical values given in this discussion are dependent on the choice of parameters, which as discussed above, we were not able to determine uniquely. However, the qualitative predictions stand provided there is a noticeably flat region between the functions describing the resting cell death rate and rate of entry into division. That is, there exists a region of signalling between thresholds at which rates of apoptosis of resting cells and rates of entry into cell cycle are relatively small. This region is shown in Figure 5.11 by the area between the vertical dashed black lines. This region is maintained provided $\theta_p \gg \theta_s$ and α is such that the distributions of signalling thresholds do not significantly overlap in the regions in which there is a significant probability density.

5.4 Resource model in the context of the human periphery

In this section we explore the resource model in the context of the human periphery. Changes between the mouse model presented in the previous section and the human model are as follows: we let the volume of the system be defined by equation (5.14), wherein, the term $M(y)$ represents the average body mass of American males between ages 0-60 years, specified by (5.13). Also, the rate of export of thymocytes into the periphery is defined by equation (5.18), taken from reference (Bains *et al.*, 2009a). The rate of thymic export, specified by this function, decreases with the age of an individual. The non-linearity of these functions further complicates the analysis of the steady states of the model. Therefore, in this section, we restrict ourselves to exploring the model numerically. To that end, we require a parameter set representative of a polyclonal population of naive T cells in the periphery.

5.4.1 Human parameters

OT-1 and F5 T cells are commonly used in experiments because they are reported to represent opposite ends of the spectrum of responsiveness to stimuli. We guess

then that the average signalling threshold for division lies somewhere between the the thresholds for the OT-1 and F5 parameter sets, respectively 482 and 554. Let us choose $\theta_p = 520$ signalling units to represent the average signalling threshold for division in a human polyclonal naive T cell population. The signalling threshold for survival is 50 in both the OT-1 and F5 parameter sets. We also choose $\theta_s = 50$ signalling units in the human parameter set. Given that we are considering a polyclonal population, it is reasonable to assume a greater degree of variability in the signalling thresholds than was found for the monoclonal OT-1 and F5 populations. This is done by choosing α to be smaller than the inferred values in Table 5.1. Let us choose $\alpha = 2$ (log signalling units)$^{-1}$. In addition to the above parameter choices, we let $\beta = 2$ ng ml^{-1} day^{-1} and $\delta = 40$ day^{-1}. For the remaining parameters, we choose a rough average between the inferred parameters for the OT-1 and F5 parameter sets. The full parameter set for the human model is given in Table 5.3.

Parameter	Value	Units
α	2.0	(log signalling units)$^{-1}$
β	2.0	ng ml^{-1} day^{-1}
δ	40	day^{-1}
θ_s	50	signalling units
θ_p	520	signalling units
λ	2.5	day^{-1}
ρ	4.0	day^{-1}
μ_R	0.50	day^{-1}
μ_C	0.30	day^{-1}

Table 5.3: Parameter set for the human model.

5.4.2 Adiabatic solutions

Let us assume changes in T cell numbers and the concentration of IL-7 occur on faster time scales than changes in body mass and rate of thymic output. Under this assumption we define adiabatic solutions to be solutions of the following system of equations:

$$0 = \beta - \gamma(\hat{I}(t))\hat{R}(t) - \delta\hat{I}(t) \,, \tag{5.53}$$

$$0 = \nu(t) - \left[\bar{\rho}(\hat{S}(t)) + \bar{\mu}_R(\hat{S}(t))\right]\hat{R}(t) + 2\lambda\hat{C}(t) \,, \tag{5.54}$$

$$0 = \bar{\rho}(\hat{S}(t))\hat{R}(t) - (\mu_C + \lambda)\,\hat{C}(t) \,. \tag{5.55}$$

This system is derived by simply setting the derivatives in (5.19)-(5.21) equal to zero. Adiabatic solutions are found by numerically solving the above system for $\hat{I}(t)$, $\hat{R}(t)$, $\hat{C}(t)$, given a fixed time t. We use the programming language Python in conjunction with the package *scipy.optimize* to find numerical solutions. In the left panel of Figure 5.13 we plot the relative error between the adiabatic solution and the numerical solution of the system (5.19)-(5.21), where initial conditions have been fixed to be equal to the adiabatic solutions at $t = 0$. The relative error for the number of resting cells and concentration of IL-7 is less than 1% for nearly all times in the interval 0-60 years. For the number of cycling cells, the relative error peaks at approximately 10%. However, since this population is small relative to the resting population, the relative error between solutions for the total number of cells remains less than 1% over the period 0-60 years, see the right panel of Figure 5.13.

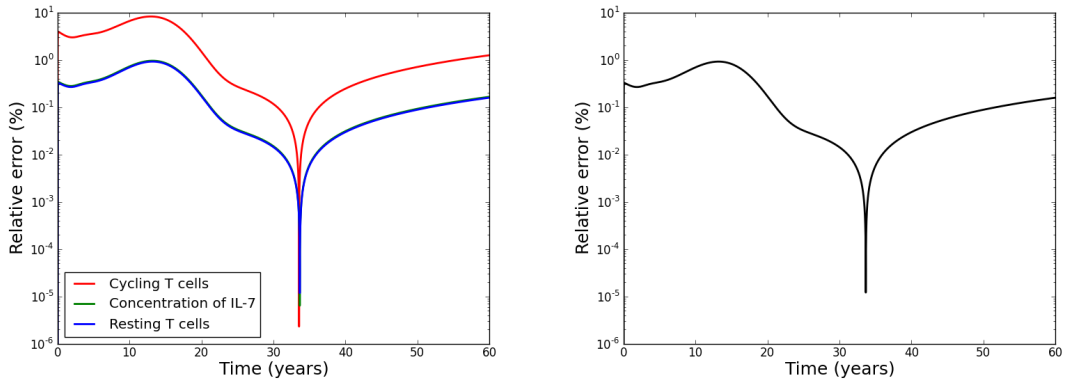

Figure 5.13: Left panel: Relative error between adiabatic solutions of equations (5.53)-(5.55) and numerical solutions to equations (5.19)-(5.21) computed using a 4-th order Runge-Kutta scheme, subject to initial conditions equal to adiabatic solutions at $t = 0$. Right panel: relative error for the total number of T cells $(R(t) + C(t))$.

5.4.3 Changing the IL-7 production rate

Adiabatic solutions for the parameter set presented in Table 5.3 are shown in Figure 5.14. We see that for this parameter set the total number of naive T cells is an increasing function of age up until about age 20, then approximately stationary thereafter. Qualitatively, this trajectory appears superficially similar to the increase in body mass, as shown in the left panel of Figure 5.2. The number of cycling cells increases with age. However, the number of cycling cells is only a small proportion of the total number of cells, ranging from $1.7 \times 10^{-5}\%$ at age 0 years to $1.7 \times 10^{-2}\%$

at age 60.

Of interest is the effect of varying the parameter describing the rate of IL-7 production. In Figure 5.15 we plot the total number of T cells (adiabatic solution) for values of β in the set $\{10^{-1.5}, 10^{-1.4}, \ldots, 10^{0.9}, 10^{1.0}\}$. For the lower values of β in this set, the shape of the curves qualitatively resemble the curve representing the rate of thymic output (green line). However, for larger values of β the shape of the curves resemble the curve representing body mass (black line, equal to $10^{10}M(t/365)$). For intermediate values of β there is a continuous transition between these two qualitatively different behaviours.

The difference between the lowest trajectory and the curve representing thymic output (in Figure 5.15) is determined by the parameter μ_R. This parameter specifies how long a naive T cell will survive if starved of IL-7. For the smallest value of β in the above set, the amount of IL-7 is sufficiently small that the resting cell death rate $\bar{\mu}_R(t)$ is approximately equal to its maximum, μ_R. This implies that trajectories, for which the total number of T cells resemble thymic output, do so, because the behaviour of an individual T cell is to leave the thymus, live for approximately μ_R^{-1} days, then die. The small value of β implies that the maximum adiabatic concentration of IL-7 (equal to β/δ) is insufficient to promote cell survival, hence the dominance of the resting T cell death term.

In contrast to this, for the largest values of β in the above set, adiabatic solutions qualitatively resemble the change in body mass. For the higher values of β, the maximum stable concentration of IL-7, given by β/δ, is sufficient to promote cell division. This causes the T cell population to expand. As it does so, the rate of internalisation of IL-7 increases, which in turn decreases the concentration of IL-7. The adiabatic solution is representative of the equilibrium point for this expansion, for a given age t. Trajectories for the larger values of β are qualitatively similar to body mass because the equation for this is encoded in the IL-7 internalisation rate.

5.4.4 Comparisons with clinical observations

In Section 5.3 we demonstrate that the resource model can agree well with experiments studying LIP in mice. Of interest then is whether the resource model in the context of the human periphery agrees with clinical observations or not. For ethical reasons, measuring the total number of naive T cells in humans is not practical[1].

[1]In experimental settings using mice, the mouse is typically sacrificed such that the spleen and lymphatic tissue can be removed.

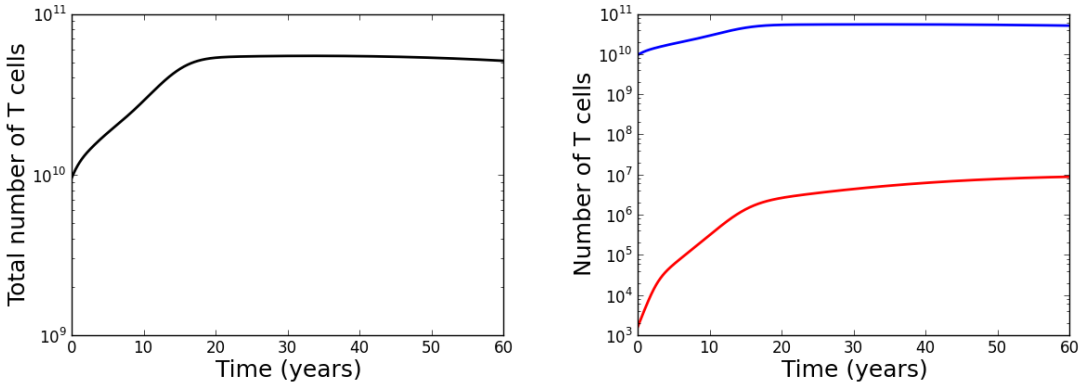

Figure 5.14: Left panel: The total number of T cells (resting plus cycling) obtained from solving equations (5.53)-(5.55) using the parameter set given in Table 5.3. Right panel: the blue line shows the adiabatic solution for the number of resting T cells and the red line indicates the number of cycling T cells.

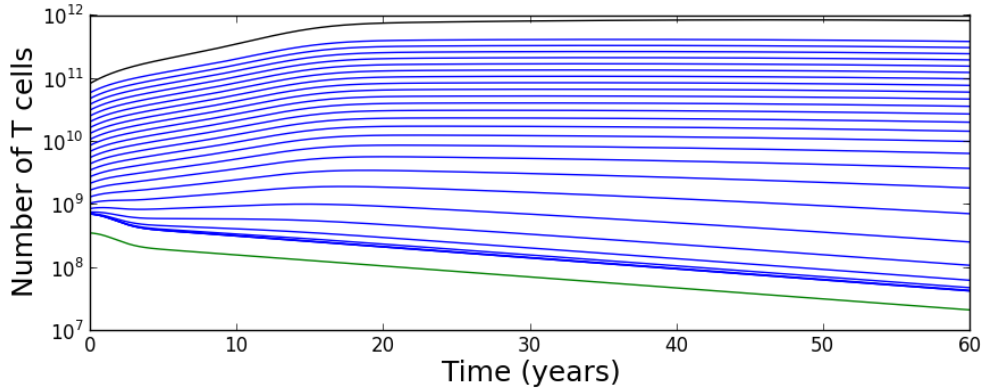

Figure 5.15: Adiabatic solutions for choices of β in the set $\{0.5, 1.0, \ldots, 9.0, 9.5\}$ ng ml^{-1}. The green line represents the number of thymocytes entering the periphery in one day (equation (5.18)), whereas the black line is a plot of body mass (equation (5.13)) multiplied by a factor of 10^{10}.

However, one can count the number of T cells in a blood sample. In reference (Prelog *et al.*, 2009), the authors published data showing observed numbers of $CD4^+$ T cells per μl of blood versus age, from 0-40 years. Figure 1 in reference (Prelog *et al.*, 2009) shows that the number of naive $CD4^+$ T cells per μl of blood decreases from around 3000 to 1000 over the first 10 years of life, then decreases at a slower rate from around 1000 to 300 over the next 25 years.

To compare our model against these observations we must first infer the number of T cells per volume of blood from the total number of T cells in the body. Let us assume a typical 70kg adult has 5 litres of blood (Taggart & Starr, 2009). Furthermore, let us assume the ratio between blood volume and body mass is constant throughout life. It is estimated that approximately 2% of the naive T cell population is found in the blood at any one time (Trepel, 1974). In our model the number of T cells per kilogram of body mass is given by

$$\frac{R(t)+C(t)}{M(t/365)}, \tag{5.56}$$

where $M(t/365)$ is defined by (5.13). Under our assumptions, 70 kg of body mass is equivalent to 5 litres of blood, (70 kg : 5×10^6 μl). Therefore 1 kg^{-1} : 1.4×10^{-5} μl^{-1}. Given that we are assuming 2% of cells are in the blood at any one time, it follows that 1 cell kg^{-1} : 2.8×10^{-7} cell μl^{-1}. Thus, in our model, the number of cells per μl of blood is given by

$$2.8\times10^{-7}\frac{R(t)+C(t)}{M(t/365)}. \tag{5.57}$$

Using the parameter set given in Table 5.3 we plot, in Figure 5.16, the number of cells per μl of blood, calculated by using the above conversion with adiabatic solutions of equations (5.53)-(5.55). We see in this plot that the number of naive T cells per μl of blood decreases from around 320 cells at age 0 to about 180 cells at age 40. This decrease is neither as pronounced as that presented in reference (Prelog *et al.*, 2009), nor is the number of cells as high.

To explain these discrepancies, first consider that our parameter set was estimated from observations made on studies of T cell population kinetics in mice. We have assumed that parameters for human naive T cells are similar but this is not necessarily true (den Braber *et al.*, 2012). A modest increase in β from 2 ng ml^{-1} day^{-1} to 5 ng ml^{-1} day^{-1} is sufficient for our model to roughly agree with observations in (Prelog *et al.*, 2009) for ages 20 to 40 years. However, we do not reproduce the sharp decline

in the number of T cells per μl of blood observed in childhood. The decline in $CD4^+$ T cells per μl of blood in childhood is also observed in reference (Hapuarachchi *et al.*, 2013). In this study the number of $CD4^+$ T cells per μl of blood is presented for healthy infants aged 0-3 years. Whilst there is a high degree of variability in the observations, the general trend is a decrease from around 3000 cells to around 1500 cells over the first 3 years of life. Consider also the estimations of absolute $CD4^+$ T cell numbers made in (Bains *et al.*, 2009b). Here, the authors estimate that the absolute number of $CD4^+$ T cells peaks to about 8×10^{10} cells at age 2, which is followed by a modest decline to around 6×10^{10} cells at age 7, and lastly followed by an increase to approximately 1.2×10^{11} cells by age 20. As can be seen from the plot in Figure 5.14, our model does not reproduce the peak in T cells observed in childhood (Bains *et al.*, 2009b). Taken together, these observations suggest that our model underestimates the number of naive T cells in childhood.

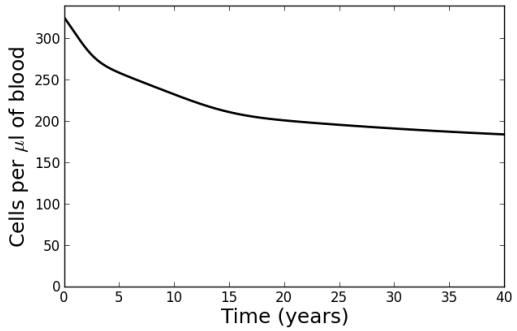

Figure 5.16: The number of cells per μl of blood calculated form solutions of (5.53)-(5.55) and the conversion given by (5.57).

The question remains as to how our model should be modified such that we can reconcile it with the above clinical observations made in childhood. For the remainder of this section, we discuss some possibilities.

Non-constant IL-7 production In the model presented thus far we have assumed the amount of IL-7 produced in a fixed volume of the peripheral immune system is constant. Suppose now we revise this assumption, specifically, let us assume IL-7 production peaks in childhood before returning to a constant in adulthood. We expect such a change to increase the number of naive T cells in childhood relative to the numbers observed in adulthood. Furthermore, given that the volume of a child's lymphatic architecture is expected to be smaller than an adult's, this

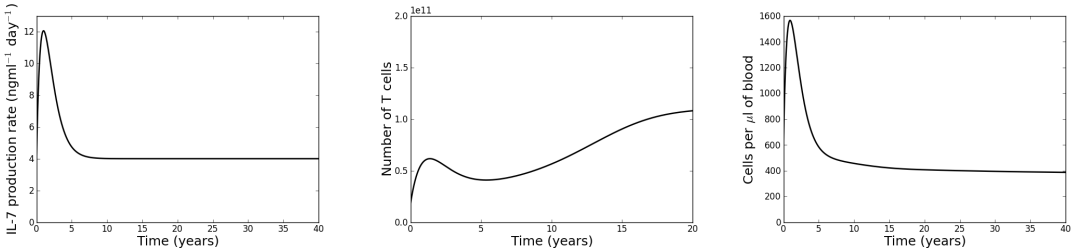

Figure 5.17: Left panel: plot of equation (5.58). Middle panel: total cell count found with IL-7 production rates specified by (5.58). Right panel: number of cells per μl of blood subject to IL-7 production being specified by (5.58).

should lead to a higher peak in the number of naive T cells per volume of blood. To explore this hypothesis, we replaced the constant term β by the function

$$\hat{\beta}(t) = 4 + 0.06te^{-t/365}. \tag{5.58}$$

This function has a base level of IL-7 production at 4 ng ml^{-1} day^{-1}. IL-7 production rises at age 0 from 4 ng ml^{-1} day^{-1} to approximately 12 ng ml^{-1} day^{-1} at age 1, before declining back to the base production level of 4 ng ml^{-1} day^{-1}. A plot of this function is shown in the left panel of Figure 5.17. Adiabatic solutions for the total number of T cells computed with this function are presented in the middle panel of Figure 5.17. Modifying the rate of IL-7 production to take this functional form allows the model to reproduce the estimated total naive CD4$^+$ T cell count presented in (Bains *et al.*, 2009b) reasonably well. The number of T cells per μl of blood is shown in the right panel of Figure 5.17. Observe that this plot shows the decrease in T cells per blood volume is more pronounced from 1 year of age, but, the cell density actually increases over the first year of life. Clinical observations suggest a modest increase in the T cell density during the first two months of life, but a decrease thereafter (Bains *et al.*, 2009b).
Using this modification we are able to reproduce the previously estimated absolute cell counts, but the predictions of cell counts per volume of blood are still unsatisfactory. Furthermore, we could find no evidence in the literature to suggest IL-7 production rates are intrinsically higher in childhood relative to adulthood.

Non-constant lymphatic volume to body mass ratio In the model presented in this chapter, we have assumed the volume of the peripheral compartment of the immune system is a constant proportion of body mass. As it stands, the model underestimates the number of naive T cells in childhood. Suppose however, that

for childhood, we assume the volume to body mass ratio is higher than it is in adulthood. Such an assumption would lead to an increase in the number of naive T cells in childhood, relative to adulthood. Likewise, the concentration of naive T cells in the blood would be more pronounced in childhood relative to adulthood, in keeping with the observations in reference (Prelog *et al.*, 2009).
In a clinical setting, it would of course be difficult to assess the volume of the peripheral immune architecture. A proxy measurement could possibly be the volume of the spleen, a major secondary lymphoid organ. However, we could not find any data for measurements of spleen volume to body mass ratios versus age of individuals. Such data, would be interesting to obtain in light of this discussion.

Non-constant distributions of signalling thresholds The parameters θ_s, θ_p and α, respectively, specify the mean survival and division thresholds and the variance in signalling thresholds. These parameters are fixed in time, implying that the distributions of signalling thresholds are the same in childhood and adulthood. Suppose now that these parameters evolve in time such that the mean survival and division thresholds are higher in adulthood relative to childhood. Under this assumption, in childhood, it follows that for a given concentration of IL-7, the amount of T cells the system could support is higher. Thus, the physically smaller space of the immune system of a child could support a proportionally larger number of T cells, because these cells require less signalling for survival and division.

Memory T cells During an infection, a population of memory T cells, specific for the antigen derived from the infection, is generated from the responding naive T cell clonotypes. Central memory T cells require IL-7 for their survival within the peripheral lymphoid organs (Kondrack *et al.*, 2003; Schluns *et al.*, 2000; Surh & Sprent, 2008). One might expect there would be a degree of competition between the naive and memory T cells for the available IL-7. Given that an individual encounters pathogens repeatedly throughout their life, it is reasonable to assume to an individual will continually be generating clonotypes of memory T cells. Indeed, studies have confirmed that the percentage of T cells which are of the central memory phenotype increases with age (Saule *et al.*, 2006). Furthermore, the rate of accumulation of memory T cells is presumably at its highest during infanthood, since it is at this age that our exposure to not yet encountered pathogens is highest. Therefore, it is in infanthood when we would expect to observe the quickest drop in the number of naive T cells per μl of blood.

In our model we have not included a term to represent the transition of naive T cells to the memory T cell pool. Memory T cells are generated from naive T cells during clonal expansion of a naive T cell population responding to a pathogen (Lanzavecchia & Sallusto, 2005). However, in mice, memory T cells are also generated through the division of naive T cells in homeostatic conditions, such as during LIP (note that this is distinct from division during a challenge since in homeostatic conditions, T cells are not responding to specific antigen) (Cho *et al.*, 2000; Schüler *et al.*, 2004). This may also be true for humans. We could reconcile the model with clinical observations with the inclusion of these considerations. However, if we were to include terms within the model to describe loss of naive T cells to the memory pool, it is unclear how significant these factors would be. During the expansion phase of an immune response, T cells undergo many IL-7 independent divisions to generate an effector population. Thus, a relatively small number of naive T cells is capable of generating a much larger population of memory T cells. To our knowledge, no reliable estimates have been made for the average number of naive T cells activated during one day. Similarly, to our knowledge there are no estimates for the rate at which memory T cells which are generated through homeostatic turnover of naive T cells. These assumptions present further avenues for modelling efforts.

5.4.5 Discussion

Throughout this chapter we have assumed naive T cell survival is dependent on the effective concentration of IL-7. In the mammalian immune system, IL-7 is produced by the stromal tissues of the lymphatic architecture (Jiang *et al.*, 2005). We expect that IL-7 availability is at its highest in the vicinity of these tissues. Naive T cells are continually circulating between the peripheral lymphoid organs, and so will regularly transit into close proximity of the stromal tissues (Bromley *et al.*, 2005). We therefore feel that modelling IL-7 availability as being uniformly distributed, over a typical time scale of a day, is a reasonable approximation.

In addition to IL-7, studies have shown that naive T cell survival is dependent on recognition of self-peptide through the TCR, where self-peptide is presented within a sp:MHC complex on the surface of an antigen presenting cell (Kieper *et al.*, 2004; Seddon & Zamoyska, 2002; Tan *et al.*, 2001). TCR signalling has not been included in the model, we have restricted ourselves to the assumption that sp:MHC availability is sufficient and non-limiting for T cell survival. We feel inclusion of TCR signalling is largely unnecessary in the context of the mouse model, since in

this model, we consider T cell populations of single specificities. The OT-1 and F5 transgenic T cell populations each possess a unique T cell receptor. It is reasonable to assume there is far less diversity with respect to TCR mediated signalling strengths for the OT-1 and F5 populations relative to a polyclonal population. Even in an expanded model in which we explicitly model self-peptide availability, it is assumed the parameters governing availability could be absorbed into the existing parameters we have introduced in this chapter.

The exclusion of modelling TCR interactions is more problematic when considering a polyclonal naive T cell population in the human model. Each clonotype present in the population presumably possesses its own death and cell cycle entry rates, which are based on the availability of self-peptide which the clonotype can recognise (Kieper *et al.*, 2004). The model we have presented does not consider the diversity of clonotypes within the naive T cell population, indeed, it is restricted to modelling the total number of resting naive T cells and the total number of naive T cells in the cell cycle. However, if the model was to be extended to include diversity of clonotypes, TCR interactions would need to be taken into account.

In the previous section we discussed how the human model fails to capture the decline in numbers of naive T cells per μl of blood, which occurs from childhood to adulthood. Of the various possibilities for this discrepancy, we feel the exclusion of modelling a population of memory T cells is the most likely candidate. In our modelling efforts, we have assumed IL-7 signalling thresholds for survival and entry into cell cycle are distributed log-normally; the parameters of these distributions are specified by θ_s, θ_p and α. Suppose now we introduce two further variables into the model which denote the number of central memory T cells which are either resting or in the cell cycle. Let us also assume that the memory population is dependent on IL-7 for the survival and division of its members (Kondrack *et al.*, 2003; Schluns *et al.*, 2000). Furthermore, suppose the distributions of IL-7 signalling thresholds for the memory T cell population are log-normal and specified by the parameters $\hat{\theta}_s$, $\hat{\theta}_p$ and $\hat{\alpha}$. For the naive population, these parameters were inferred from the mouse model. It is unclear how we should choose these parameters for the memory population. Presumably, to agree with clinical observations, where memory T cells dominate the T cell repertoire with age, memory T cells should out-compete the naive population for IL-7 (Saule *et al.*, 2006). Thus, we might require the relations $\hat{\theta}_s < \theta_s$ and $\hat{\theta}_p < \theta_p$. However, this may not be a necessary condition. Suppose the naive population requires less IL-7 for survival and entry into the cell cycle such that $\hat{\theta}_s > \theta_s$ and $\hat{\theta}_p > \theta_p$. The memory T cell population may still dominate if there

is a sufficient rate of differentiation of naive T cells into memory T cells. Further quantitative studies of the homeostasis of peripheral T cell populations in humans and mice should help elucidate these considerations.

The average time for a resting T cell to die, as well as the average waiting time before a cell enters the cell cycle, is highly sensitive to changes in the parameter α. The average time to die for resting T cells is given by $(\bar{\mu}_R(I(t)))^{-1}$. Similarly, the average time to enter the cell cycle is given by $(\bar{\rho}(I(t)))^{-1}$. We compute these quantities for times in the range 0-60 years from adiabatic solutions, for values of α in the set $\mathcal{S} = \{1.0, 1.5, 2.0, 2.5\}$. Plots of these quantities are shown in Figure 5.18. We see that varying α has little effect on the number of resting T cells. However, these small changes in α have an enormous effect on the number of cycling T cells and the times to die and enter the cell cycle. The number of T cells in the cell cycle varies from 10^4 to 10^9 cells for values of α in this range. The time to die for resting T cells varies from roughly 18 days to 7 years, whereas the time to enter the cell cycle varies from 15 days to 10^6 years.

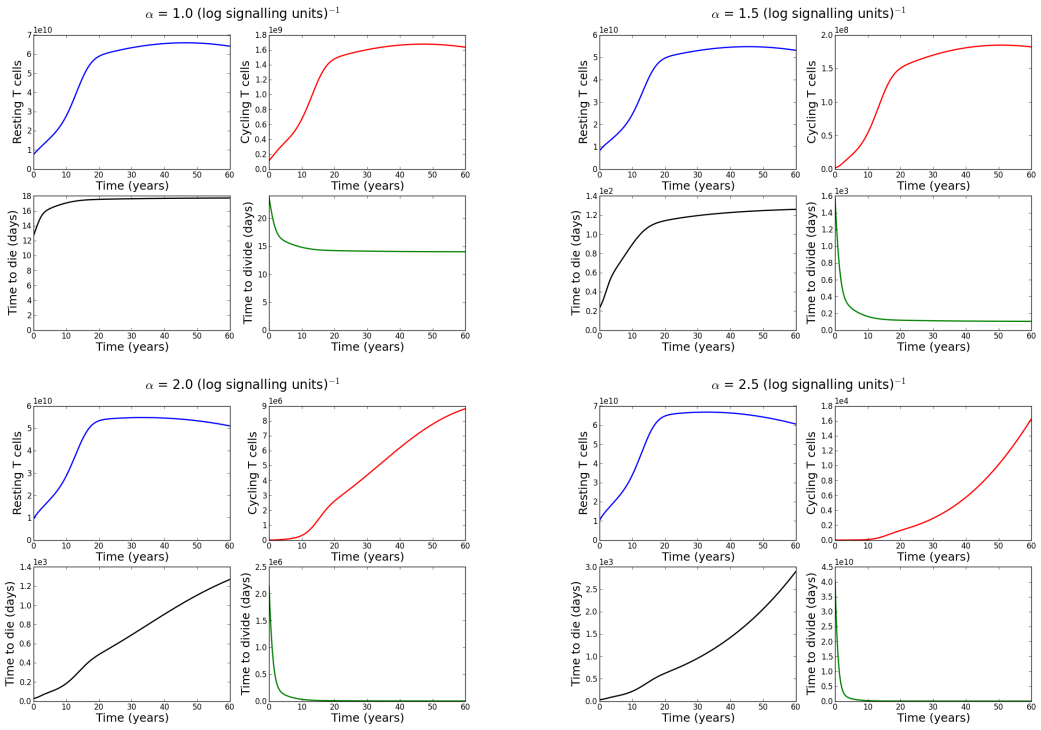

Figure 5.18: We plot the number of resting (blue) and cycling (red) T cells. We also plot the average time to die (black) for resting T cells and the average time to enter the cell cycle (green) for resting T cells. This is done for values of α in the set $\{1.0, 1.5, 2.0, 2.5\}$.

As discussed previously, due to the model being over parameterised, we were unable to uniquely estimate the parameters of the mouse model. Since the parameters for the human model were inferred from the mouse model parameters, it follows that our parameter set for the human model is largely a guess. A previous study suggested that in humans, the peripheral T cell population is largely maintained by cellular division, especially post childhood (den Braber *et al.*, 2012). Thus, it seems to be the case that times to divide are of the time scale of days (true for $\alpha < 1.5$), rather than millennia ($\alpha > 2.0$). In the same study, a mathematical model was postulated for peripheral T cell survival in mice (den Braber *et al.*, 2012). In this model, the death rate of peripheral T cells was assumed to be dependent on the number of T cells, in contrast to this, it was assumed that these cells undergo no division in the periphery. This model was found to fit the data reasonably well. We note that these findings are consistent with the mouse model for which we have chosen a larger value of α to model the OT-1 and F5 data sets. That is, for a larger value of α, inclusion of thymic output within the model implies that peripheral T cell division is negligible.

For the OT-1 parameter set, in equilibrium, with thymic output set at 10^6 T cells per day, resting T cells take approximately 24 days to die; the rate of entry into the cell cycle is effectively zero. This death rate is comparable with the rates reported for the model in which T cells do not divide in reference (den Braber *et al.*, 2012). Considering that for this value of α, we were able to model the LIP data in reference (Hogan *et al.*, 2013), we conclude that a larger value of α is appropriate for the mouse model. In contrast, we find that we must choose a smaller value of α for the human model (relative to the mouse model) such that the human model is consistent with the observation that the peripheral naive T cell population is maintained by peripheral division (den Braber *et al.*, 2012). From these findings, we conclude that while the distributions of signalling thresholds for survival and cell cycle entry may be distinct for a given clonotype, for a polyclonal repertoire, this distinction is blurred. A more suitable value of α for the human model would be $\alpha = 1$ (log signalling units)$^{-1}$. For this value, the distribution of IL-7 signalling thresholds for survival overlaps significantly (for regions in which there is non-negligible probability density) with the distribution of signalling thresholds for entry into the cell cycle. The overlap between distributions is shown in Figure 5.19. We note that this implies, for the human parameter set, that we do not observe resting T cells which are quiescent as discussed for the mouse model in Section 5.3.6.

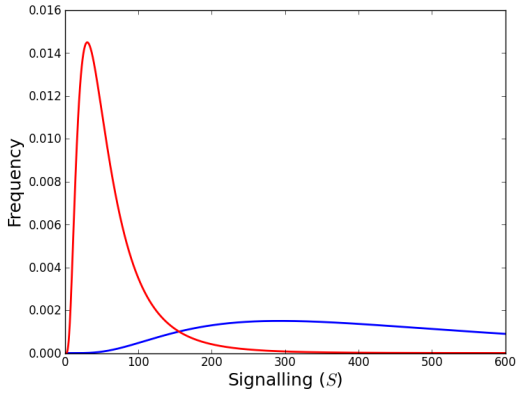

Figure 5.19: Probability density functions of IL-7 signalling thresholds for resting T cell survival (red) and entry into cell cycle (blue).

In reference (Reynolds *et al.*, 2013b) we published an earlier version of the model presented in this chapter. One difference between the earlier version and the current one is in the function representing the rate of decrease in the concentration of IL-7 due to internalisation. In the earlier version, the volume of the space of occupied by naive T cells was assumed to be constant, whereas in the current version, the volume is proportional to the mass of the animal being considered (either mouse or human). Rather, the model in reference (Reynolds *et al.*, 2013b) assumed IL-7 production increased with age, thus the parameter β was a function of time. In the model presented in this chapter, β is a constant. Also, the parameter set for the earlier model was not supported by any experimental data, whereas the parameter set for the current version is guided by the data in reference (Hogan *et al.*, 2013).
In our previously published model, we explored adiabatic solutions of the model under the assumption that $\lambda < \mu_C$. This parameter relation implies the probability that a naive T cell will complete division, given that it has entered the cell cycle, is less than one half. Under this condition, for thymic output in the approximate range of 6.2×10^7-1.2×10^8 T cells per day, there exist three adiabatic solutions to the number of resting T cells (and hence the concentration of IL-7 and the number of cycling T cells). This is illustrated in Figure 5.20, taken directly from (Reynolds *et al.*, 2013b).
In humans, the thymus is atrophic, and so the rate of export of thymocytes declines with age (Bains *et al.*, 2009b). Therefore, for the hypothetical scenario where $\lambda < \mu_C$, we naturally traverse along the curve from the right to the left in Figure 5.20. Note, in producing the figure in (Reynolds *et al.*, 2013b), for a given value of ν, we

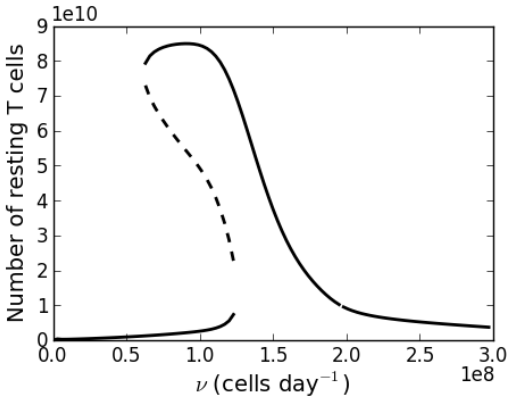

Figure 5.20: Adiabatic solutions for the number of resting T cells when $\lambda < \mu_C$ for the model presented in reference (Reynolds *et al.*, 2013b).

computed the corresponding age from equation (5.18). For this age, we computed the corresponding rate of IL-7 production, as defined by equation (12) in (Reynolds *et al.*, 2013b). The rate of IL-7 production was then used for the computation of adiabatic solutions. Since the rate of IL-7 production was defined to increase with age, the number of naive T cells initially increases as we traverse along adiabatic solutions in Figure 5.20 to the left. However, when thymic output drops to about 6.2×10^7 T cells per day, corresponding to roughly 33 years of age, the number of resting naive T cells drops nearly two orders in magnitude from around 10^{11} T cells to around 10^9 T cells. What was interesting about these findings is that a contracted condition (in early age), in which the ability of naive T cells to complete the cell cycle is impaired, initially would not have much of an effect on the number of resting naive T cells in the peripheral pool. However, at some later age, an individual could be left severely immunocompromised as a result of declining thymic output.

The same behaviour can also be observed in the model presented in this chapter. In the middle panel of Figure 5.21 we plot the adiabatic solution for the number of resting T cells against the parameter ν, where we have chosen $\mu_C = 5$ days^{-1}, such that $\mu_C < \lambda$. For our estimated parameter set, the discussion in the previous paragraph is applicable, however a quantitative difference is that the bifurcation point occurs at about 36 years of age rather than 33. This result is however, like times to die or enter the cell cycle, highly dependent on the choice of the parameter α. If we choose α to be equal to 1 (log signalling unit)$^{-1}$, then the number of resting T cells is largely proportional to thymic output over the biological range for humans ($\approx 2.3 \times 10^7$-3.5×10^8 cells per day). If we increase α to 3 (signalling units)$^{-1}$, then

we still observe the bifurcation, however it occurs much later, at around 55 years of age. See the left and right panels of Figure 5.21.

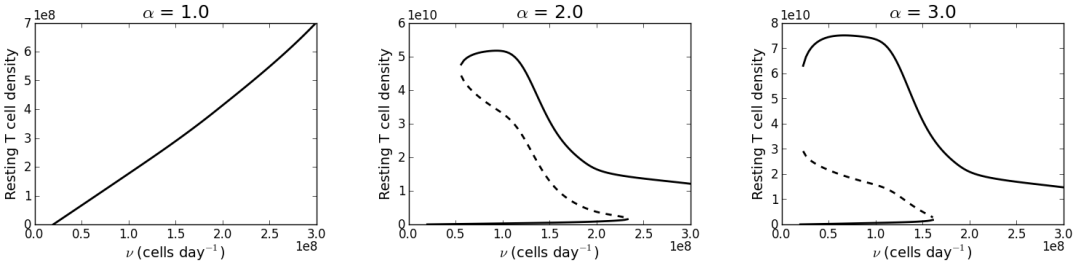

Figure 5.21: Adiabatic solutions for the number of resting T cells. We have used the parameters given in Table 5.3 with the exception that $\mu_C = 5.0$ days^{-1} and from left to right we plot solutions for α in the set $\{1.0, 2.0, 3.0\}$.

5.5 Summary

In summary, we have developed a model of naive T cell homeostasis which assumes resting T cell survival and entry into division is dependent on the effective concentration of IL-7 available to the population. Whilst over parameterised for the available data, the mouse version of this model was able to describe the expansion of a transgenic T cell population in a lymphopenic environment. The model also accurately predicted the rates of expansion of OT-1 and F5 T cells for different transferred numbers of cells. The human version of the model reasonably agreed with clinical observation of blood T cell counts in elderly individuals (with a modest change in the rate of IL-7 production), but failed to predict the fall in T cell numbers per volume of blood observed through childhood. This was most likely because we have not modelled a central memory T cell population. Not including a memory population within the model implies there is no competition for IL-7 with central memory T cells, or loss of naive T cells to the central memory T cell pool through homeostatic division. Both models are highly sensitive to changes in the parameter α, which describes the spread in signalling thresholds across the population of T cells. However, we predict that the spread is greater for human populations relative to murine populations. Further modelling efforts with this approach would require careful support from biological observations.

Chapter 6

A mathematical perspective on $CD4^+$ T cell quorum-sensing

6.1 Introduction

Regulatory T cells, characterised by the expression of the transcription factor FOXP3, make up 5-10% of the peripheral $CD4^+$ T cell pool in humans and mice (Feuerer *et al.*, 2010; Josefowicz *et al.*, 2012; Powrie & Maloy, 2003; Sakaguchi, 2000; Sakaguchi *et al.*, 1995; Seddon & Mason, 2000; Walker & Sansom, 2011). They are able to regulate disease in adoptive transfer models, and prevent unconstrained proliferation of $CD4^+$ T cells (Sakaguchi, 2004). While a sufficient number of regulatory T cells is required to prevent the onset of autoimmune disease (Almeida *et al.*, 2002; Fontenot *et al.*, 2003), regulatory T cells have also been shown to suppress beneficial immune responses against tumours and viral infections (Antony *et al.*, 2005; Belkaid & Rouse, 2005). These experimental findings suggest that there exists an ideal size for the regulatory T cell pool, which allows for both the prevention of autoimmunity and the effective mounting of adaptive immune responses.

Mathematical and computational models have been developed to propose potential cellular (or molecular) mechanisms that control the size of the regulatory T cell population. León *et al.* (Carneiro *et al.*, 2007; León *et al.*, 2000, 2001, 2003; Sepúlveda & Carneiro, 2011) have developed the cross-regulation model, based of the interactions between populations of regulatory and effector $CD4^+$ T cells. This model is built on experimental studies that support the cell-cell contact hypothesis (Tang *et al.*, 2005). That is, that interactions between regulatory and effector T cells occur at conjugation sites present on the surface of antigen presenting cells (APCs). The

cross-regulation model predicts that the peripheral CD4$^+$ T cell repertoire is comprised of two distinct subsets (Carneiro *et al.*, 2007; León *et al.*, 2000, 2001, 2003; Sepúlveda & Carneiro, 2011): small clones of auto-reactive effector T cells, which are highly suppressed by their T cell receptor (TCR) related regulatory T cells, and effector T cell clones which barely recognise self-antigen, but have the potential to strongly recognise non-self-antigen. Thus, an effective immune response can take place, without autoimmunity. Other approaches include that of Fouchet and Regoes, who analysed the interaction between antigen and six populations of APCs and regulatory T cells (Fouchet & Regoes, 2008). Kim *et al.* (Kim *et al.*, 2007) introduced a comprehensive model of immune responses, that includes populations of CD4$^+$ T cells, CD8$^+$ T cells, APCs, virus infected cells and antigen. Feinerman *et al.* provided a model in which binding of IL-2 leads to the up-regulation of IL-2Rα (CD25) in both effector and regulatory T cells, favouring their subsequent ability to bind IL-2 (Feinerman *et al.*, 2010). Other mathematical models, based on the idea of bystander T cell activation (Burroughs *et al.*, 2011; Kim *et al.*, 2007), predict that an autoimmune state can arise following an immune response.

According to the recent quorum-sensing (QS) hypothesis (Almeida *et al.*, 2012), homeostasis of CD4$^+$ T cell numbers can be achieved by the ability of the regulatory T cell population to sense the number of interleukin-2 (IL-2) producing CD4$^+$ T cells (Almeida *et al.*, 2012). Quorum-sensing, thus, is a mechanism whereby an optimum ratio between CD4$^+$ effector and regulatory T cells can be established and maintained (Almeida *et al.*, 2005, 2006a, 2012). The mechanism resembles that observed in species of bacteria, in which gene expression is regulated in response to the density of the bacterial population (Diggle *et al.*, 2007; Miller & Bassler, 2001). Rather, control is mediated by the regulatory T cell subset, which responds to the size of the peripheral CD4$^+$ population; the mechanism does not involve a change in gene expression. Furthermore, the CD4$^+$ T cell QS mechanism considered here also controls the dynamics of the regulatory T cell population itself.

Here, we use a mathematical model of four interacting CD4$^+$ T cell subsets to explore the dynamics in the absence and in the presence of specific antigen. It is assumed that all subsets are specific for the same antigen, furthermore, we assume no interaction with T cells not specific for the same antigen. In the absence of antigen, we study the establishment of the peripheral CD4$^+$ T cell pool from thymic output, and its return to homeostasis after an immune challenge. In the presence of antigen, we make use of the QS mathematical model to understand the steady state of the IL-2 producing and regulatory T cell populations and how to avoid autoimmunity.

We divide the $CD4^+$ T cell pool into four subsets. The first, population 1, is the set of $CD4^+$ naive T cells, defined as not having yet encountered their specific antigen. The second subset, population 2, is the set of $CD4^+$ T cells which have encountered their specific antigen. These cells exhibit effector (or helper) function, such as the production of various cytokines to promote immune responses (Banchereau *et al.*, 2012). In particular, we assume that effector cells produce the cytokine interleukin-2 (IL-2) (Wan & Flavell, 2009), and we refer to this population as the effector or the IL-2 producing population. The third subset, population 3, is the set of $CD4^+$ T cells, assumed to have encountered their specific (or cognate) antigen, but not to be producing IL-2. Lastly, population 4 is the set of $CD4^+$ regulatory T cells. These cells are assumed to suppress the activity of the effector T cell population (Almeida *et al.*, 2006b), but to depend on the IL-2 produced by the effector T cells for their survival (Cheng *et al.*, 2011; Malek & Castro, 2010) and proliferation. Proliferation, death and differentiation of cells within these populations will be introduced as transition probabilities of a stochastic Markov model. The quorum-sensing hypothesis will be implemented as follows:

- the (per cell) death rate of regulatory T cells depends on the number of IL-2 producing cells (Almeida *et al.*, 2012), and
- in the absence of antigen, and due to the fact that regulatory T cells constitutively express the IL-2Rα chain, IL-2 induced proliferation only takes place in the regulatory T cell pool (Almeida *et al.*, 2012).

The regulatory T cell suppression mechanism (Sakaguchi, 2004; von Boehmer, 2005) will be implemented mathematically as follows:

- the rate at which an IL2-producing cell becomes a non-IL2 producing cell is proportional to the number of regulatory T cells.

The initial stages of an immune response are characterised by the presence of antigen, that perturbs the homeostatic equilibrium of the $CD4^+$ T cell population, and leads to proliferation of the antigen specific T cells and thus, to an increase in the number of IL-2 producing T cells. This, in turn, leads to regulatory T cell proliferation. Eventually, $CD4^+$ T cell homeostasis is re-established due to the suppression of the IL-2 producing $CD4^+$ T cell subset by the regulatory T cell population. We assume that the level of IL-2 is proportional to the number of IL-2 producing $CD4^+$ T cells.

The structure of the chapter is as follows. In Section 6.2, we introduce the stochastic quorum-sensing model and the transition probabilities that describe the dynamics of the four different CD4$^+$ T cell subsets. The deterministic approximation in the absence of specific antigen is discussed in Section 6.2.2. Two scenarios of immunological relevance are considered. In the first, we study how CD4$^+$ T cells establish themselves in the periphery (see Section 6.3.1). In the second, we study how the CD4$^+$ T cell population returns to its homeostatic equilibrium after antigenic challenge (see Section 6.3.2). In Section 6.4 we discuss, from a deterministic perspective, how the homeostatic equilibrium of the CD4$^+$ T cell population will change in the case of specific antigen presentation (see Section 6.4). In Section 6.5, we study the stochastic dynamics of the CD4$^+$ T cell population after antigenic challenge and its return to homeostasis. Given the potentially small number of specific CD4$^+$ T cells involved, we consider extinction of either regulatory T cells or IL-2 producing cells. We show that extinction takes place with probability one, and compute the temporal order in which extinction occurs. We also compute the probability of extinction and the expected time to extinction as a function of the parameter values. We finish the chapter with a summary of our results and a discussion.

6.2 Stochastic model of CD4$^+$ T cell quorum-sensing

The stochastic model will be defined in terms of the transition probabilities of a multi-variate Markov process. The state space of this Markov process, S, is the four-dimensional lattice $\mathbb{N} \times \mathbb{N} \times \mathbb{N} \times \mathbb{N}$, with $\mathbb{N} = \{0, 1, 2, \ldots\}$. The transition probabilities describe the jumps the process may take on this lattice in a small time interval Δt. Note that, in this immunological context, jumps correspond to either cell proliferation, death, differentiation or migration (thymic export). Let $\{\mathbb{X}(t)\}$ be a four-dimensional Markov process, where each sub-chain $\{\mathbb{X}_i(t)\}$, $i = 1, 2, 3, 4$, is a uni-variate Markov chain that describes one of the four subsets of the CD4$^+$ T cell population. Let the four-dimensional vector $\mathbf{n}(t) \in S$ be a realisation of the multi-variate Markov process at time t, and assume the process starts at $\mathbf{N} \in S$, that is,

$$\text{Prob}\{\mathbb{X}(0) = \mathbf{N}\} = 1 \, . \tag{6.1}$$

The state probabilities of the Markov process are denoted by $p_{\mathbf{n}}(t)$ and are defined as follows (Allen, 2003):

$$p_{\mathbf{n}}(t) = \text{Prob}\{\mathbb{X}(t) = \mathbf{n} \mid \mathbb{X}(0) = \mathbf{N}\} \, . \tag{6.2}$$

The transition probabilities of the Markov process are derived from the assumed possible cellular fates (proliferation, death, differentiation or migration) of the four different CD4$^+$ T cell subsets (Almeida *et al.*, 2012). We describe these cellular events and their associated transition probabilities in the following section.

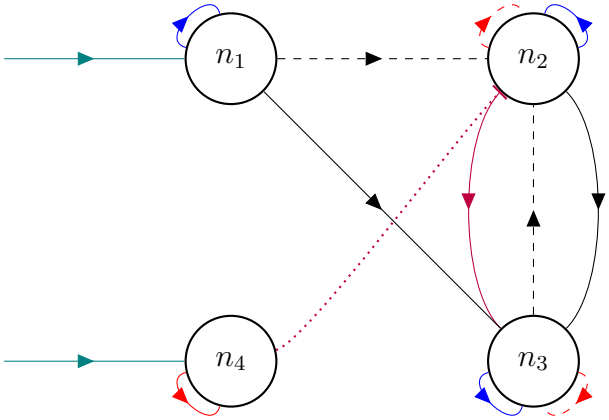

Figure 6.1: Representation of the cellular birth events that can increase the number of T cells in any of the four CD4$^+$ pools. Dashed lines indicate the events that depend on recognition of specific antigen. Not shown are cell death processes that occur in each T cell pool. The death rate of regulatory T cells, n_4, depends on the number of IL-2 producing cells, n_2 (QS mechanism). Thymocytes are exported to the periphery into naive, n_1, and regulatory, n_4, T cells (teal arrows). Homeostatic proliferation takes place for naive, n_1, IL-2 producing, n_2, and IL-2 non-producing, n_3, T cells (blue arrows). IL-2 induced proliferation takes place for IL-2 producing, n_2, IL-2 non-producing, n_3, and regulatory, n_4, T cells (red arrows). The solid red arrow of IL-2 induced proliferation for n_4 is a QS mechanism. Differentiation and activation processes are shown in black. Suppression of effector T cells by regulatory T cells is shown in purple.

6.2.1 Transition probabilities: immunological background

The transition probabilities are denoted by $p_{\mathbf{m},\mathbf{n}}(\Delta t)$ and defined as (Allen, 2003):

$$p_{\mathbf{m},\mathbf{n}}(\Delta t) = \text{Prob}\{\mathbb{X}(t + \Delta t) = \mathbf{m} \mid \mathbb{X}(t) = \mathbf{n}\} \, . \tag{6.3}$$

We shall adopt the following notation for the transition probabilities in order to simplify the expressions. Let us introduce the state vector $\mathbf{n} = (n_1, n_2, n_3, n_4) \in S$. By writing $\{\mathbf{n} : n_i \pm k\}$ we refer to the new state vector in which the entry n_i is replaced by $n_i \pm k$. For example, $\{\mathbf{n} : n_1 - 1\} = (n_1 - 1, n_2, n_3, n_4)$. In a similar manner, if we refer to changes in two entries of $\mathbf{n}$, we shall write, for example $\{\mathbf{n} : n_1 - 1, n_2 + 1\} = (n_1 - 1, n_2 + 1, n_3, n_4)$.

Specific antigen presentation We do not consider specific antigen a dynamical variable. However, we introduce a function, $f(t)$, to represent presentation of specific antigen by APCs, where t denotes time. In the case of a successful immune response (which entirely clears antigen), $f(t) \to 0^+$ as $t \to +\infty$.

IL-2 level We assume that IL-2 availability is proportional to the number of IL-2 producing cells, that is, n_2.

Thymic export We assume both naive T cells and regulatory T cells develop in the thymus and upon thymic maturation migrate to the periphery (Almeida *et al.*, 2005). We shall assume this occurs at a constant rate, ν_i $(i = 1, 4)$. In a small time interval Δt, the transition probability encoding the influx of thymocytes into the peripheral CD4$^+$ T cell pool is

$$p_{\{\mathbf{n}:n_i+1\},\mathbf{n}}(\Delta t) = \nu_i \Delta t + o(\Delta t) \ , \qquad i = 1, 4 \ . \tag{6.4}$$

Death In a small time interval Δt, it is assumed that for each CD4$^+$ T cell subset, a cell belonging to that subset may die. The probability of a natural death event occurring for all subsets, with the exception of the regulatory subset, is assumed to be proportional to the number of cells in that subset. The expression for the transition probability for such a death event is

$$p_{\{\mathbf{n}:n_i-1\},\mathbf{n}}(\Delta t) = \mu_i n_i \Delta t + o(\Delta t) \ , \qquad i = 1, 2, 3 \ , \tag{6.5}$$

with μ_i the (per cell) death rate for $i = 1, 2, 3$. The survival of regulatory T cells is assumed to depend on the available level of IL-2, and thus the number of IL-2 producing cells (Cheng *et al.*, 2011; Malek & Castro, 2010). This is one of the hypotheses of the QS mechanism. The transition probability modelling the death

of regulatory T cells is

$$p_{\{\mathbf{n}:n_4-1\},\mathbf{n}}(\Delta t) = \mu_4 \frac{\kappa_4}{\kappa_4 + n_2} n_4 \Delta t + o(\Delta t) , \tag{6.6}$$

where μ_4 is the (per cell) death rate of regulatory T cells, and κ_4 is the number of IL-2 producing cells at which the probability of death of a regulatory T cell is half the value of the probability when there are no IL-2 producing cells.

Homeostatic proliferation We assume cells from the first three subsets may proliferate in response to homeostatic signals. A number of different signals constitute the full set of signals a CD4$^+$ T cell requires under homeostatic conditions. The main signals regulating homeostasis of T cells are believed to be self-peptide/MHC signals mediated via the T cell receptor (TCR), and the cytokine interleukin-7 (IL-7) (Kimura *et al.*, 2012; Seddon *et al.*, 2003). We assume that each population (naive, IL-2 producing, and IL-2 non-producing) has a different niche for homeostatic signals. Thus, we consider these signals are limiting in the sense that as a population of T cells of subset i grows larger than a carrying capacity κ_i, $i = 1, 2, 3$, the probability of a cell receiving a signal to proliferate decreases. For cell subsets smaller than κ_i, we assume the probability of a proliferation event occurring in that subset is an increasing function of the subset size. The homeostatic proliferation rate is denoted by λ_{i_H}. We encode these assumptions into the transition probabilities as follows:

$$p_{\{\mathbf{n}:n_i+1\},\mathbf{n}}(\Delta t) = \lambda_{i_\mathrm{H}} n_i \mathrm{e}^{-n_i/\kappa_i} \Delta t + o(\Delta t) . \tag{6.7}$$

Specific antigen/IL-2 induced proliferation We assume all T cells, except naive T cells, may proliferate in response to the cytokine IL-2. We assume that IL-2 and IL-2 non-producing T cells first require recognition of specific antigen mediated via TCR:peptide/MHC (T cell:APC) interactions, to up-regulate the α chain of the IL-2 receptor. Upon recognition of specific antigen, it has been shown naive T cells proceed through a small number of divisions before exhibiting markers typical of effector T cells (Jelley-Gibbs *et al.*, 2000). However, we simplify the model by assuming antigenic stimulation of naive T cells causes them to differentiate to effector T cells, without proliferating first. CD4$^+$ effector T cells up-regulate the IL-2 receptor α chain (IL-2Rα or CD25) in response to their specific antigen (Feinerman *et al.*, 2010). Therefore, it is reasonable to assume effector cells become more sensitive to IL-2 following specific antigenic stimulation. We also assume this is the case for

CD4$^+$ IL-2 non-producing cells. For IL-2 producing and IL-2 non-producing cells, we assume the IL-2 derived signals are only able to induce proliferation when specific antigen is being presented. Hence, the transition probabilities for IL-2 induced proliferation for these two subsets will depend on the function $f(t)$ introduced above. Regulatory T cells up-regulate the α chain of the IL-2 receptor in larger numbers at the basal (pre-antigen stimulation) level and, unlike IL-2 producing cells and IL-2 non-producing cells, are critically dependent on IL-2 for their survival and proliferation (Malek *et al.*, 2002). This is the second hypothesis of the QS mechanism. For this reason, for the regulatory T cell subset: (i) we neglect TCR and/or IL-7 induced proliferation, and (ii) we we assume IL-2 induced proliferation does not depend on specific antigen levels encoded by $f(t)$. The specific antigen/IL-2 induced proliferation rate is denoted by $\lambda_{i_{\mathrm{A}}}$ for $i = 2, 3, 4$. The transition probabilities for specific antigen/IL-2 induced proliferation are

$$p_{\{\mathbf{n}:n_i+1\},\mathbf{n}}(\Delta t) = \lambda_{i_{\mathrm{A}}} f(t)\, n_2\, n_i \Delta t + o(\Delta t)\,, \qquad i = 2, 3\,, \tag{6.8}$$

$$p_{\{\mathbf{n}:n_4+1\},\mathbf{n}}(\Delta t) = \lambda_{4_{\mathrm{A}}} n_2\, n_4 \Delta t + o(\Delta t)\,. \tag{6.9}$$

Differentiation of naive T cells We assume naive CD4$^+$ T cells may become activated and start exhibiting effector (helper) functions in response to signals resulting from TCR interaction with their specific antigen (Jenkins *et al.*, 2001). This transition probability will then depend on $f(t)$, and is given by

$$p_{\{\mathbf{n}:n_1-1,n_2+1\},\mathbf{n}}(\Delta t) = \alpha_{12} f(t) n_1 \Delta t + o(\Delta t)\,, \tag{6.10}$$

where α_{12} is the naive T cell differentiation rate into IL-2 producing T cells.
We additionally assume naive T cells can differentiate directly into IL-2 non-producing cells through homeostatic-driven proliferation. This event is considered to be independent of TCR recognition of specific antigen (Ge *et al.*, 2002). The transition probability for this differentiation event is

$$p_{\{\mathbf{n}:n_1-1,n_3+1\},\mathbf{n}}(\Delta t) = \alpha_{13} n_1 \Delta t + o(\Delta t)\,, \tag{6.11}$$

where α_{13} is the naive T cell differentiation rate into IL-2 non-producing T cells.

Differentiation of IL-2 producing T cells We assume IL-2 producing cells may stop producing IL-2 and become IL-2 non-producing cells (Pepper & Jenkins, 2011).

The transition probability is

$$p_{\{\mathbf{n}:n_2-1,n_3+1\},\mathbf{n}}(\Delta t) = \alpha_{23} n_2 \Delta t + o(\Delta t) \ , \tag{6.12}$$

where α_{23} is the IL-2 producing cell differentiation rate into IL-2 non-producing T cells.

Activation of IL-2 non-producing T cells We assume IL-2 non-producing T cells can become activated and start producing IL-2 in secondary responses to specific antigen (Berard & Tough, 2002). This transition probability will then depend on $f(t)$, and is

$$p_{\{\mathbf{n}:n_2+1,n_3-1\},\mathbf{n}}(\Delta t) = \alpha_{32} f(t) n_3 \Delta t + o(\Delta t) \ , \tag{6.13}$$

where α_{32} is the IL-2 non-producing cell differentiation rate into IL-2 producing T cells.

Suppression of IL-2 producing T cells We assume regulatory T cells suppress the ability of IL-2 producing T cells to secrete IL-2 (Sakaguchi, 2004; von Boehmer, 2005). This cellular process is introduced as a contact term: an IL-2 producing T cell will become a IL-2 non-producing T cell, if it receives a suppressive signal from a regulatory T cell. This transition probability is given by

$$p_{\{\mathbf{n}:n_2-1,n_3+1\},\mathbf{n}}(\Delta t) = \beta n_2 n_4 \Delta t + o(\Delta t) \ , \tag{6.14}$$

with β the suppression parameter.

Remaining probabilities In a small time interval Δt, it is possible that none of the above transitions may occur (Allen, 2003). The probability of no event occurring within a time interval Δt is

$$\begin{aligned} p_{\mathbf{n},\mathbf{n}}(\Delta t) = 1 - \Bigg[& \nu_1 + \nu_4 + \sum_{i=1}^{3} \mu_i n_i + \mu_4 \frac{\kappa_4}{\kappa_4 + n_2} n_4 + \sum_{i=1}^{3} \lambda_{i_{\mathrm{H}}} n_i \mathrm{e}^{-n_i/\kappa_i} \\ & + \sum_{i=2}^{3} \lambda_{i_{\mathrm{A}}} f(t) n_2 n_i + \lambda_{4_{\mathrm{A}}} n_2 n_4 + \alpha_{12} f(t) n_1 + \alpha_{13} n_1 \\ & + \alpha_{23} n_2 + \alpha_{32} f(t) n_3 + \beta n_2 n_4 \Bigg] \Delta t + o(\Delta t) \ . \end{aligned}$$

The probability of any other transition occurring within the proposed Markov process in a small time interval Δt is assumed to be $o(\Delta t)$ (Allen, 2003).

6.2.2 Deterministic approximation of the QS mathematical model

Throughout this chapter we assume the CD4$^+$ T cell population being modelled is the subset of CD4$^+$ T cells specific to a given antigen. We write down a system of ordinary differential equations (ODEs) which approximate the average behaviour of the stochastic model. That is, we let $m_i(t)$ be an approximation to the first moments of the Markov chain $\{\mathbb{X}_i(t)\}$ for $i = 1, 2, 3, 4$. One may derive these equations from the stochastic model using the generating function technique and assuming the kth central moment is zero for $k \geq 2$ (Allen, 2003). The system of ODEs is given by the following equations:

$$\frac{\mathrm{d}m_1}{\mathrm{d}t} = \nu_1 - \mu_1 m_1 + \lambda_{1_{\mathrm{H}}} m_1 \mathrm{e}^{-m_1/\kappa_1} - \alpha_{12} f(t) m_1 - \alpha_{13} m_1 \ , \tag{6.15}$$

$$\begin{aligned}\frac{\mathrm{d}m_2}{\mathrm{d}t} &= -\mu_2 m_2 + \lambda_{2_{\mathrm{H}}} m_2 \mathrm{e}^{-m_2/\kappa_2} + \lambda_{2_{\mathrm{A}}} f(t) m_2^2 + \alpha_{12} f(t) m_1 \\ &\quad - \alpha_{23} m_2 + \alpha_{32} f(t) m_3 - \beta m_2 m_4 \ ,\end{aligned} \tag{6.16}$$

$$\begin{aligned}\frac{\mathrm{d}m_3}{\mathrm{d}t} &= -\mu_3 m_3 + \lambda_{3_{\mathrm{H}}} m_3 \mathrm{e}^{-m_3/\kappa_3} + \lambda_{3_{\mathrm{A}}} f(t) m_2 m_3 + \alpha_{13} m_1 \\ &\quad + \alpha_{23} m_2 - \alpha_{32} f(t) m_3 + \beta m_2 m_4 \ ,\end{aligned} \tag{6.17}$$

$$\frac{\mathrm{d}m_4}{\mathrm{d}t} = \nu_4 - \mu_4 \frac{\kappa_4}{\kappa_4 + m_2} m_4 + \lambda_{4_{\mathrm{A}}} m_2 m_4 \ . \tag{6.18}$$

6.2.3 Deterministic approximation of the model without the QS hypothesis

If we do not make use of the QS hypothesis, we need to modify the system of ODEs as follows:

$$\frac{\mathrm{d}m_1}{\mathrm{d}t} = \nu_1 - \mu_1 m_1 + \lambda_{1_{\mathrm{H}}} m_1 \mathrm{e}^{-m_1/\kappa_1} - \alpha_{12} f(t) m_1 - \alpha_{13} m_1 \ , \tag{6.19}$$

$$\frac{\mathrm{d}m_2}{\mathrm{d}t} = -\mu_2 m_2 + \lambda_{2_{\mathrm{H}}} m_2 \mathrm{e}^{-m_2/\kappa_2} + \lambda_{2_{\mathrm{A}}} f(t) m_2^2 + \alpha_{12} f(t) m_1$$

$$- \alpha_{23} m_2 + \alpha_{32} f(t) m_3 - \beta m_2 m_4 \ , \tag{6.20}$$

$$\frac{\mathrm{d}m_3}{\mathrm{d}t} = - \mu_3 m_3 + \lambda_{3_\mathrm{H}} m_3 \mathrm{e}^{-m_3/\kappa_3} + \lambda_{3_\mathrm{A}} f(t) m_2 m_3 + \alpha_{13} m_1 + \alpha_{23} m_2 - \alpha_{32} f(t) m_3 + \beta m_2 m_4 \ , \tag{6.21}$$

$$\frac{\mathrm{d}m_4}{\mathrm{d}t} = \nu_4 - \mu_4 m_4 + \lambda_{4_\mathrm{A}} \sigma_{\mathrm{IL}-2} m_4 \ , \tag{6.22}$$

where we have introduced the parameter $\sigma_{\mathrm{IL}-2}$, which represents an external source of IL-2 (which is, of course, independent of the population n_2). In the absence of the QS hypothesis, one needs to assume that the death rate of regulatory T cells does not depend on the IL-2 producing cells. Inspection of (6.22) allows us to infer that the dynamics of the regulatory T cell population does not depend on any other population, in particular the population of IL-2 producing cells, n_2. Thus, the steady state that characterises the population of regulatory T cells is given by

$$m_4^* = \frac{\nu_4}{(\mu_4 - \lambda_{4_\mathrm{A}} \sigma_{\mathrm{IL}-2})} \ , \tag{6.23}$$

with the condition $\mu_4 > \lambda_{4_\mathrm{A}} \sigma_{\mathrm{IL}-2}$. Given the experimental observations that support the indexation of regulatory T cell numbers to the size of the IL-2 producing $\mathrm{CD4}^+$ T cells (Almeida *et al.*, 2005, 2006b), we conclude that a mathematical description of the $\mathrm{CD4}^+$ T cell population requires a QS mechanism, as the one proposed earlier and analysed here (Almeida *et al.*, 2012).

6.3 Deterministic approximation in the absence of specific antigen

We start the mathematical analysis of the deterministic model in the case when specific antigen is not being presented by APCs, by setting $f(t) = 0$. The system of ODEs simplifies to

$$\frac{\mathrm{d}m_1}{\mathrm{d}t} = \nu_1 - \mu_1 m_1 + \lambda_{1_\mathrm{H}} m_1 \mathrm{e}^{-m_1/\kappa_1} - \alpha_{13} m_1 \ , \tag{6.24}$$

$$\frac{\mathrm{d}m_2}{\mathrm{d}t} = -\mu_2 m_2 + \lambda_{2_\mathrm{H}} m_2 \mathrm{e}^{-m_2/\kappa_2} - \alpha_{23} m_2 - \beta m_2 m_4 \ , \tag{6.25}$$

$$\frac{\mathrm{d}m_3}{\mathrm{d}t} = -\mu_3 m_3 + \lambda_{3_\mathrm{H}} m_3 \mathrm{e}^{-m_3/\kappa_3} + \alpha_{13} m_1 + \alpha_{23} m_2 + \beta m_2 m_4 \ , \tag{6.26}$$

$$\frac{\mathrm{d}m_4}{\mathrm{d}t} = \nu_4 - \mu_4 \frac{\kappa_4}{\kappa_4 + m_2} m_4 + \lambda_{4_\mathrm{A}} m_2 m_4 \ , \tag{6.27}$$

with initial conditions $\mathbf{m}(0) = \mathbf{M}$, where $\mathbf{m}(t) = (m_1(t), m_2(t), m_3(t), m_4(t))$.

6.3.1 CD4$^+$ T cell establishment in the periphery

The first question that can be studied with the deterministic approximation of the QS model is the establishment in the periphery of the CD4$^+$ T cell pool from thymic output. That is, the homeostatic distribution of the sub-populations before any antigenic challenge has taken place.

We will analyse the steady states of the model described by equations (6.24)-(6.27). We begin with the observation that the differential equation for population $m_1(t)$ does not involve any other CD4$^+$ T cell subset and, thus, can be treated independently of the remaining equations. Let us introduce

$$g(m_1) = \nu_1 - (\mu_1 + \alpha_{13})\, m_1 + \lambda_{1_{\mathrm{H}}} m_1 \mathrm{e}^{-m_1/\kappa_1} \ . \tag{6.28}$$

Then the steady state solution of (6.24), m_1^*, is found by solving $g(m_1) = 0$. Due to the presence of the term $\mathrm{e}^{-m_1/\kappa_1}$, an analytical solution for m_1^* cannot be found. However, the existence and stability of such a steady state solution can be proved, as follows.

Existence In the limit $m_1 \to +\infty$, we have $g(m_1) \to -\infty$. Furthermore, at $m_1 = 0$, we have $g(m_1 = 0) = \nu_1 > 0$. Since g is a continuous function, by the intermediate value theorem, there exists at least one solution $m_1^* \in (0, \infty)$, such that $g(m_1^*) = 0$. That is, there exists at least one steady state solution for the population of naive T cells, such that $m_1^* > 0$.

Uniqueness Assume a solution $m_1^* > 0$, such that $g(m_1^*) = 0$, exists. We have

$$\lambda_{1_{\mathrm{H}}} \mathrm{e}^{-m_1^*/\kappa_1} = \mu_1 + \alpha_{13} - \frac{\nu_1}{m_1^*} \ . \tag{6.29}$$

Let us introduce $h_1(m) = \lambda_{1_{\mathrm{H}}} \mathrm{e}^{-m/\kappa_1}$ and $h_2(m) = \mu_1 + \alpha_{13} - \dfrac{\nu_1}{m}$ for $m > 0$. The derivatives of h_1 and h_2 with respect to m are given by $h_1'(m) = -\frac{\lambda_{1_{\mathrm{H}}}}{\kappa_1} \mathrm{e}^{-m/\kappa_1} < 0$ and $h_2'(m) = \frac{\nu_1}{m^2} > 0$, respectively, for $m > 0$. The derivatives of h_1 and h_2 are, respectively, monotonically increasing and decreasing, and continuous functions (for $m > 0$). We conclude that (6.29) has at most one solution.

Stability The steady state $m_1^* > 0$ is asymptotically stable if and only if

$$\frac{\mathrm{d}g(m_1)}{\mathrm{d}m_1}\Big|_{m_1^*} < 0\,. \tag{6.30}$$

Taking the first derivative of g we have

$$\frac{\mathrm{d}g(m_1)}{\mathrm{d}m_1} = -\left(\mu_1 + \alpha_{13}\right) + \lambda_{1_\mathrm{H}}\left(1 - \frac{m_1}{\kappa_1}\right)\mathrm{e}^{-m_1/\kappa_1}\,. \tag{6.31}$$

We also know that by definition m_1^* satisfies the following equation:

$$\nu_1 - \left(\mu_1 + \alpha_{13}\right)m_1^* + \lambda_{1_\mathrm{H}} m_1^* \mathrm{e}^{-m_1^*/\kappa_1} = 0\,. \tag{6.32}$$

Rearranging equation (6.32) we have

$$\nu_1 + m_1^*\left(\lambda_{1_\mathrm{H}}\mathrm{e}^{-m_1^*/\kappa_1} - \mu_1 - \alpha_{13}\right) = 0. \tag{6.33}$$

Since m_1^* and $\nu_1 > 0$, the term inside the parenthesis must be negative and so the following inequality must hold:

$$\mathrm{e}^{-m_1^*/\kappa_1} < \frac{\mu_1 + \alpha_{13}}{\lambda_{1_\mathrm{H}}}\,. \tag{6.34}$$

We now evaluate equation (6.31) at m_1^*:

$$\frac{\mathrm{d}g(m_1)}{\mathrm{d}m_1}\Big|_{m_1^*} = -\left(\mu_1 + \alpha_{13}\right) + \lambda_{1_\mathrm{H}}\left(1 - \frac{m_1^*}{\kappa_1}\right)\mathrm{e}^{-m_1^*/\kappa_1}\,. \tag{6.35}$$

If $m_1^* > \kappa_1$ then the RHS of (6.35) is negative, and m_1^* is stable. Now suppose $m_1^* < \kappa_1$. Then, using the inequality in equation (6.34), we have:

$$\begin{aligned}
\frac{\mathrm{d}g(m_1)}{\mathrm{d}m_1}\Big|_{m_1^*} &= -\left(\mu_1 + \alpha_{13}\right) + \lambda_{1_\mathrm{H}}\left(1 - \frac{m_1^*}{\kappa_1}\right)\mathrm{e}^{-m_1^*/\kappa_1} \\
&< -\left(\mu_1 + \alpha_{13}\right) + \lambda_{1_\mathrm{H}}\left(1 - \frac{m_1^*}{\kappa_1}\right)\frac{\mu_1 + \alpha_{13}}{\lambda_{1_\mathrm{H}}} \\
&= -\frac{\left(\mu_1 + \alpha_{13}\right)m_1^*}{\kappa_1} < 0\,.
\end{aligned}$$

Therefore, we conclude that $m_1^* > 0$ is stable for all parameter values.

IL-2 producing T cells The value $m_2^* = 0$ is a steady state of (6.25). That is, as there are no source terms for the population of IL-2 producing cells, if $m_2(t = 0) = 0$,

then $m_2(t) = 0$ for all $t \geq 0$.
We do not consider any other steady states for the IL-2 producing T cell population, since we are interested in the peripheral CD4$^+$ T cell establishment from thymus output, before any T cell activation takes places. Thus, before specific antigen has been introduced, the number of IL-2 producing cells should be zero.

IL-2 non-producing T cells In a similar manner to the naive T cells, the exponential term in equation (6.26) implies that an analytical solution for m_3^* cannot be found. However, setting the derivative equal to zero in equation (6.26), and assuming that $m_2^* = 0$, gives an equation for m_3^*, which is of exactly the same form as that for m_1^*. The same arguments used to prove existence and uniqueness of m_1^* can be invoked to show that $m_3^* > 0$ not only exists, but is unique. It is also stable, under the assumption that $m_2^* = 0$.

Regulatory T cells If $m_2(t) = 0$ then

$$\frac{\mathrm{d}m_4}{\mathrm{d}t} = \nu_4 - \mu_4 m_4 \ , \tag{6.36}$$

and the steady state population is

$$m_4^* = \frac{\nu_4}{\mu_4} \ . \tag{6.37}$$

It is easy to show that m_4^* is a stable solution in this case.

Summary The steady state analysed in this section corresponds to populations of cells that originate in the thymus and are established in the periphery. There are non-zero populations of naive, IL-2 non-producing and regulatory T cells. The steady state population of naive T cells is determined by a balance between cell death, proliferation, loss due to differentiation and an influx of new thymic emigrants. Similarly, the population of IL-2 non-producing T cells is determined by a balance between cell death, proliferation and differentiation of the naive T cell pool into IL-2 non-producing cells, which we have assumed to be due to homeostatic proliferation. The population of regulatory T cells is set by the balance between migration of new regulatory cells from the thymus to the periphery and cell death. If $\nu_4 = 0$, that is, there is no further thymic output for the CD4$^+$ regulatory T cell population, the regulatory T cell pool will eventually become extinct.

Since we have assumed there is no specific antigen presentation, there can be no differentiation from the naive pool into the IL-2 producing one. If we start with no IL-2 producing cells, this population will always be equal to zero. Thus, the above steady state represents a scenario of T cell homeostasis prior to any specific antigen challenge. That is, it represents the steady state $CD4^+$ T cell population that, from thymic export, gets homeostatically established in the periphery. Naive T cells in the periphery require TCR signals from self-peptide/MHC complexes for their survival. These TCR signals can, on rare occasions, promote activation of naive T cells to exhibit effector functions. Additionally, IL-2 produced by effector cells of a given TCR specificity (or clonotype) may produce a bystander effect, supporting the regulatory T cell populations of other TCR specificities (Burroughs *et al.*, 2011; Feinerman *et al.*, 2010).

6.3.2 Homeostasis of $CD4^+$ T cells after a specific antigenic challenge

The second question that can be studied with the deterministic approximation of the QS model is the re-establishment of peripheral homeostasis in the $CD4^+$ T cell pool after an immune challenge, and when antigen has been cleared.

In this Section, we explore a scenario in which a specific antigen challenge has already taken place. We assume that the specific antigen of the $CD4^+$ T cell population being modelled is no longer presented by APCs, and that there is no thymic output. That is, we assume sufficient time has elapsed to allow all T cells of the specificity under consideration to have egressed from the thymus (Bains *et al.*, 2009a,c; Freitas & Rocha, 2000). This approximation can be justified as follows: estimates of thymic output for mice are 2.5 $\times 10^6$ T cells per day ($CD4^+$ and $CD8^+$) (Scollay *et al.*, 1980), and the $\alpha\beta$ T cell receptor diversity for mice is of the order of 2 $\times 10^6$ (Nikolich-&Zcaron *et al.*, 2004). This means that, at most, one $CD4^+$ T cell of a given specificity is incorporated into the peripheral pool per day. The contribution from thymic output can then be neglected when compared with any of the proliferating terms in the post-challenge scenario considered in this Section (homeostatic or specific antigen/IL-2 induced).

This post-challenge scenario can be described by initial conditions, such that all T cell subsets have non-zero cell numbers at time $t = 0$. We set $\nu_1 = \nu_4 = 0$ and

$f(t) = 0$. Under these assumptions, the deterministic model is

$$\frac{\mathrm{d}m_1}{\mathrm{d}t} = -\mu_1 m_1 + \lambda_{1_\mathrm{H}} m_1 \mathrm{e}^{-m_1/\kappa_1} - \alpha_{13} m_1 \,, \tag{6.38}$$

$$\frac{\mathrm{d}m_2}{\mathrm{d}t} = -\mu_2 m_2 + \lambda_{2_\mathrm{H}} m_2 \mathrm{e}^{-m_2/\kappa_2} - \alpha_{23} m_2 - \beta m_2 m_4 \,, \tag{6.39}$$

$$\frac{\mathrm{d}m_3}{\mathrm{d}t} = -\mu_3 m_3 + \lambda_{3_\mathrm{H}} m_3 \mathrm{e}^{-m_3/\kappa_3} + \alpha_{13} m_1 + \alpha_{23} m_2 + \beta m_2 m_4 \,, \tag{6.40}$$

$$\frac{\mathrm{d}m_4}{\mathrm{d}t} = -\mu_4 \frac{\kappa_4}{\kappa_4 + m_2} m_4 + \lambda_{4_\mathrm{A}} m_2 m_4 \,, \tag{6.41}$$

with initial conditions $m_i(0) \neq 0$, $i = 1, 2, 3, 4$.

Naive T cells The steady state solution of population $m_1(t)$, denoted by m_1^*, satisfies

$$0 = -\mu_1 m_1^* + \lambda_{1_\mathrm{H}} m_1^* \mathrm{e}^{-m_1^*/\kappa_1} - \alpha_{13} m_1^* \,. \tag{6.42}$$

There are two solutions to equation (6.42): the first is given by $m_1^* = 0$ and the second by $m_1^* = \kappa_1 \log\left(\dfrac{\lambda_{1_\mathrm{H}}}{\mu_1 + \alpha_{13}}\right)$. The vanishing solution exists unconditionally and is stable provided $\lambda_{1_\mathrm{H}} < \mu_1 + \alpha_{13}$. This stability condition can be shown as follows. The steady state $m_1^* = 0$ is asymptotically stable if and only if (Edelstein-Keshet, 2005)

$$\frac{\mathrm{d}g(m_1)}{\mathrm{d}m_1}\Big|_{m_1^*} < 0 \,, \tag{6.43}$$

with $g(m_1) = -\mu_1 m_1 + \lambda_{1_\mathrm{H}} m_1 \mathrm{e}^{-m_1/\kappa_1} - \alpha_{13} m_1$. We have

$$\frac{\mathrm{d}g(m_1)}{\mathrm{d}m_1} = -\mu_1 + \lambda_{1_\mathrm{H}} \mathrm{e}^{-m_1/\kappa_1} - \tfrac{\lambda_{1_\mathrm{H}}}{\kappa_1} m_1 \mathrm{e}^{-m_1/\kappa_1} - \alpha_{13} \,, \tag{6.44}$$

which evaluated at the steady state vanishing solution, $m_1^* = 0$, yields

$$\frac{\mathrm{d}g(m_1)}{\mathrm{d}m_1}\Big|_{m_1^*=0} = -\mu_1 + \lambda_{1_\mathrm{H}} - \alpha_{13} \,. \tag{6.45}$$

Thus, in order for the vanishing solution to be stable, the condition $\lambda_{1_\mathrm{H}} < \mu_1 + \alpha_{13}$ needs to be imposed. On the other hand, the non-zero solution exists and is stable provided $\lambda_{1_\mathrm{H}} > \mu_1 + \alpha_{13}$. This condition is required to ensure that the argument of the logarithmic term is positive.

For the analysis of the remaining CD4$^+$ T cell populations, we shall assume $\lambda_{1_\mathrm{H}} > \mu_1$, but $\lambda_{1_\mathrm{H}} < \mu_1 + \alpha_{13}$, so that $m_1^* = 0$ is a stable steady state. This can be justified as follows: during an immune challenge, most, if not all, naive T cells specific to

the antigen presented will differentiate to become IL-2 producing T cells. Under the assumptions of no thymic output and antigen clearance, all naive T cells have differentiated and thus, the naive T cell population vanishes, so that this $CD4^+$ population subset is unable to reconstitute itself after the challenge.

IL-2 producing T cells and regulatory T cells The steady state solutions for populations m_2 and m_4 are found by solving the following pair of coupled equations:

$$0 = -\mu_2 m_2^* + \lambda_{2_{\mathrm{H}}} m_2^* \mathrm{e}^{-m_2^*/\kappa_2} - \alpha_{23} m_2^* - \beta m_2^* m_4^* \,, \tag{6.46}$$

$$0 = -\mu_4 \frac{\kappa_4}{\kappa_4 + m_2^*} m_4^* + \lambda_{4_{\mathrm{A}}} m_2^* m_4^* \,. \tag{6.47}$$

There exist three solutions (m_2^*, m_4^*) with $m_2^*, m_4^* \geq 0$. The first solution is $(m_2^*, m_4^*) = (0, 0)$, which always exists and is stable provided $\lambda_{2_{\mathrm{H}}} < \mu_2 + \alpha_{23}$. The second solution is

$$(m_2^*, m_4^*) = \left(\kappa_2 \log\left(\frac{\lambda_{2_{\mathrm{H}}}}{\mu_2 + \alpha_{23}} \right), 0 \right) \,, \tag{6.48}$$

which exists provided $\lambda_{2_{\mathrm{H}}} > \mu_2 + \alpha_{23}$, and is stable provided $\mu_2 + \alpha_{23} < \lambda_{2_{\mathrm{H}}} < \lambda_{2_{\mathrm{H}}}^\star$, where

$$\lambda_{2_{\mathrm{H}}}^\star = (\mu_2 + \alpha_{23}) \exp\left(\frac{\kappa_4}{2\kappa_2} \left(\sqrt{1 + \frac{4\mu_4}{\kappa_4 \lambda_{4_{\mathrm{A}}}}} - 1 \right) \right) . \tag{6.49}$$

The third solution is

$$(m_2^*, m_4^*) = \left(\frac{\kappa_4}{2} \left(\sqrt{1 + \frac{4\mu_4}{\kappa_4 \lambda_{4_{\mathrm{A}}}}} - 1 \right), \frac{\lambda_{2_{\mathrm{H}}} \mathrm{e}^{-m_2^*/\kappa_2} - \mu_2 - \alpha_{23}}{\beta} \right) \,, \tag{6.50}$$

which exists and is stable provided $\lambda_{2_{\mathrm{H}}}^\star < \lambda_{2_{\mathrm{H}}}$. The bifurcation diagram provided in Figure 6.2 illustrates the steady state analysis for the populations of IL-2 producing and regulatory T cells. We note that the existence and stability of the three steady states depends on the parameter $\lambda_{2_{\mathrm{H}}}$, which is the homeostatic proliferation rate of the effector T cell population. This parameter encodes the level of auto-reactivity of the $CD4^+$ T cell clonotype under consideration. As $\lambda_{2_{\mathrm{H}}}$ increases above $\lambda_{2_{\mathrm{H}}}^\star$, the number of regulatory T cells required to suppress the effector population also increases.

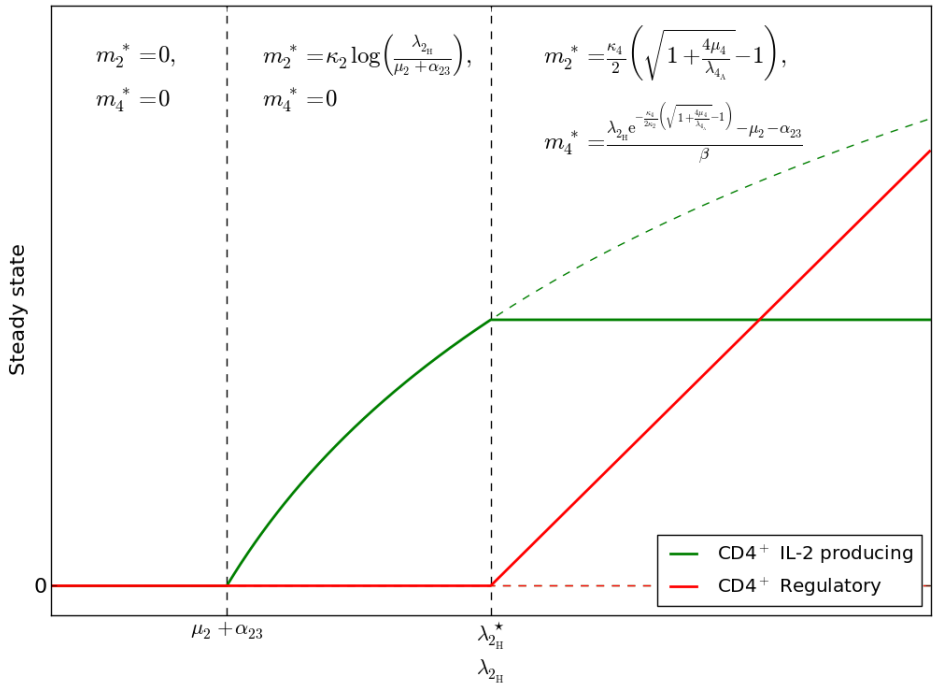

Figure 6.2: Bifurcation diagram for the IL-2 producing and regulatory T cell subsets under the assumptions $\nu_1 = \nu_4 = 0$ and $f(t) = 0$. For proliferation rates of the IL-2 producing T cells (λ_{2_H}) greater than $\lambda^\star_{2_H}$, the steady state number of IL-2 producing cells is held constant by a non-zero population of regulatory T cells. Note that in the region $\lambda_{2_H} > \lambda^\star_{2_H}$, increasing the proliferation rate of IL-2 producing cells leads to a linear increase in the number of regulatory T cells at steady state. The vertical black dashed lines at $\mu_2 + \alpha_{23}$ and $\lambda^\star_{2_H}$ have been drawn to separate the three different stability regions. The red (regulatory) and green (IL-2 producing) dashed lines in the third region ($\lambda_{2_H} > \lambda^\star_{2_H}$) indicate the unstable steady state solution.

IL-2 non-producing T cells The steady state solution for the population of IL-2 non-producing T cells is found by solving the following equation:

$$0 = -\mu_3 m_3^* + \lambda_{3_H} m_3^* e^{-m_3^*/\kappa_3} + \alpha_{23} m_2^* + \beta m_2^* m_4^* \,. \tag{6.51}$$

An analytical solution for m_3^* cannot be found. However, if we assume m_2^* and $m_4^* > 0$, a solution can be shown to exist, be unique and be unconditionally stable. This is shown in an identical manner to the proof of existence, uniqueness and stability of m_1^* provided in Section 6.3.1.

Summary The steady state, under the assumptions of no specific thymic output and antigen clearance, has no naive T cells. A steady state solution exists with non-zero population sizes of IL-2 producing and regulatory T cells. This describes a tolerant state of the $CD4^+$ population; by tolerant, we mean a state in which the steady state number of effector (IL-2 producing) T cells is less than the "natural" carrying capacity of this population in the absence of regulatory T cells. Given that effector T cells may promote the activity of some components of the innate immune system (for example, by secretion of interferon gamma), limiting the effector population number is presumably desirable (Banchereau *et al.*, 2012). When the proliferation rate of IL-2 producing T cells is low, $\mu_2 + \alpha_{23} < \lambda_{2_H} < \lambda^\star_{2_H}$, the steady state number of IL-2 producing T cells is always smaller than the corresponding steady state number of IL-2 producing cells in the parameter region $\lambda_{2_H} > \lambda^\star_{2_H}$ (see Figure 6.2). This suggests that a population of IL-2 producing cells with poor proliferative capacity does not need regulatory T cell suppression to remain tolerant, as defined above.

Another interesting feature of our analysis is the independence, both in the steady states and their stability, of the effector T cell subset on the parameter β. Varying β only affects the steady state number of regulatory T cells. This suggests that at equilibrium, regulatory T cells compensate for either a diminished or enhanced ability to suppress IL-2 producing T cells by increasing or decreasing their population size.

Finally, for values of $\lambda_{2_H} > \lambda^\star_{2_H}$, the third steady state, ($m_2^* > 0$ and $m_4^* > 0$), is globally stable. From a deterministic perspective, and unless the initial condition for the population of regulatory T cells is given by $m_4(t = 0) = 0$, we shall always observe a regulated number of IL-2 producing cells; that is, m_2^* is smaller than the carrying capacity of IL-2 producing cells. However, from a stochastic perspective, there exists a non-zero probability of a fluctuation causing the regulatory T cell population to become extinct. In Section 6.5, we shall explore both the probability of such an event occurring and the average time to extinction.

Figure 6.3 shows deterministic trajectories for a range of initial conditions and for parameter values as described in Table 6.1, in the absence of thymic output and specific antigen.

A) B)

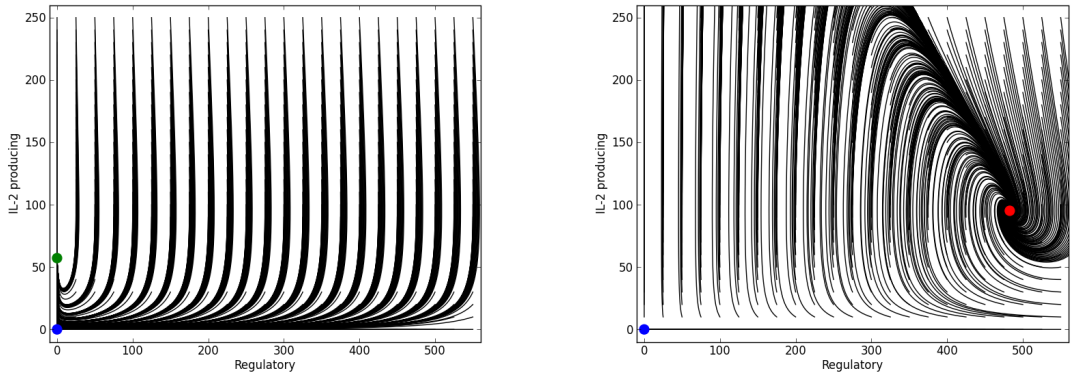

Figure 6.3: Deterministic trajectories in the absence of thymic output and specific antigen, computed from various initial conditions, and within the stochastic finite state space. Parameter values are described in Table 6.1. Blue dots represent the steady state solution that corresponds to extinction of both cell types, IL-2 producing and regulatory T cells. A) The green dot represents the stable steady state solution that exists when $\mu_2 + \alpha_{23} < \lambda_{2_H} < \lambda^\star_{2_H}$. In this case $\lambda_{2_H} = 2.2 \times 10^{-2}$ hours^{-1}. B) The red dot represents the stable steady state solution that exists when $\lambda_{2_H} > \lambda^\star_{2_H}$. In this case $\lambda_{2_H} = 8 \times 10^{-2}$ hours^{-1}.

6.4 Deterministic approximation in the presence of specific antigen

A third question that can be studied with the deterministic approximation of the QS model is the dynamics of an immune response. It is interesting to see that the QS hypothesis is not only a mechanism of CD4$^+$ T cell homeostasis, but a mechanism that allows immune responses to take place, yet avoids autoimmunity (Almeida *et al.*, 2012).

In the previous sections, we have restricted ourselves to the case $f(t) = 0$, that is, to cases where antigen specific for the CD4$^+$ T cells is not presented. In this section, however, we consider the behaviour of a clonotype of CD4$^+$ T cells when its specific antigen is presented at a constant level. We set $f(t) = c$, where $c > 0$ is constant.

Antigen is presented to T cells by professional APCs, such as dendritic cells or macrophages (Janeway *et al.*, 2001). APCs collect antigen in the lymph and tissue via phagocytosis. Inside the APC, antigen is broken down further into peptides, which are subsequently displayed on the surface of the cell as peptide/MHC complexes (MHC class II complexes in the case of CD4$^+$ T cells). A naive CD4$^+$ T cell,

Parameter	Value	Units
μ_2	1×10^{-2}	hours^{-1}
μ_3	1×10^{-2}	hours^{-1}
μ_4	1×10^{-2}	hours^{-1}
$\lambda_{2_{\mathrm{H}}}$	$2.2 \times 10^{-2}/8 \times 10^{-2}$	hours^{-1}
$\lambda_{3_{\mathrm{H}}}$	5×10^{-2}	hours^{-1}
$\lambda_{2_{\mathrm{A}}}$	1×10^{-5}	cells^{-1}hours^{-1}
$\lambda_{3_{\mathrm{A}}}$	1×10^{-5}	cells^{-1}hours^{-1}
$\lambda_{4_{\mathrm{A}}}$	1×10^{-5}	cells^{-1}hours^{-1}
κ_2	6×10^{2}	cells
κ_3	2×10^{3}	cells
κ_4	1×10^{1}	cells
α_{23}	1×10^{-2}	hours^{-1}
α_{32}	1×10^{-3}	hours^{-1}
β	1×10^{-4}	cells^{-1}hours^{-1}

Table 6.1: Parameter values used to generate numerical results. The two values given for $\lambda_{2_{\mathrm{H}}}$ are chosen to ensure stability of the types of steady solution shown in the middle and right regions of the bifurcation diagram in Figure 6.2, respectively. For the middle region the stability interval for $\lambda_{2_{\mathrm{H}}}$ is $[\mu_2 + \alpha_{23} = 0.02, \lambda^{\star}_{2_{\mathrm{H}}} \approx 0.023]$, hence the specific choice $\lambda_{2_{\mathrm{H}}} = 0.022$ hours^{-1}.

upon successful binding with a dendritic cell presenting antigen of the correct specificity, will become activated. After activation, the naive T cell will undergo a phenotypic change and elicit effector functions. For CD4$^+$ T cells, these effector functions serve to promote the functional ability of CD8$^+$ effector T cells and boost the innate components of the immune system by, for example, releasing pro-inflammatory cytokines. During a successful immune response, the target of T cells (infected cells) are destroyed and cleared from the body. In a typical response, the elimination of infected cells leads to a decrease in the amount of antigen available for uptake and presentation by APCs.

We now consider the steady state behaviour of a clonotype of CD4$^+$ T cells when its specific antigen is presented at a constant level. This implies $f(t) = c$, where $c > 0$ is constant. We further assume thymic output is zero, and that consequently there are no naive CD4$^+$ T cells. That is, all naive T cells have been activated due to the presentation of specific antigen. The deterministic equations describing the model, where c has been absorbed into the relevant parameters, are

$$\frac{\mathrm{d}m_2}{\mathrm{d}t} = -\mu_2 m_2 + \lambda_{2_{\mathrm{H}}} m_2 \mathrm{e}^{-m_2/\kappa_2} + \lambda_{2_{\mathrm{A}}} m_2 m_2 + \alpha_{32} m_3 - \alpha_{23} m_2 - \beta m_2 m_4 \ , \quad (6.52)$$

$$\frac{\mathrm{d}m_3}{\mathrm{d}t} = -\mu_3 m_3 + \lambda_{3_{\mathrm{H}}} m_3 \mathrm{e}^{-m_3/\kappa_3} + \lambda_{3_{\mathrm{A}}} m_2 m_3 + \alpha_{23} m_2 - \alpha_{32} m_3 + \beta m_2 m_4 \ , \quad (6.53)$$

$$\frac{\mathrm{d}m_4}{\mathrm{d}t} = -\mu_4 \frac{\kappa_4}{\kappa_4 + m_2} m_4 + \lambda_{4_{\mathrm{A}}} m_2 m_4 \ . \quad (6.54)$$

The non-linear system of ODEs (6.52)-(6.54) admit multiple steady state solutions. We focus on non-vanishing steady state solutions for all three populations. Other steady state solutions, which may be stable, can be found (numerically) in the following combinations: $m_2^* = m_3^* = m_4^* = 0$, and $m_2^*, m_3^* > 0, m_4^* = 0$. Although we did not observe any other vanishing steady states during numerical exploration, this may not be an exhaustive list.

Let us look for steady state solutions such that $m_2^*, m_3^*, m_4^* > 0$. The steady state m_2^* is unique and found directly from equation (6.54):

$$m_2^* = \frac{\kappa_4}{2}\left(\sqrt{1 + \frac{4\mu_4}{\kappa_4 \lambda_{4_{\mathrm{A}}}}} - 1\right) \ . \quad (6.55)$$

We can make use of (6.52), and write down an expression for m_4^*, which depends on m_2^* and m_3^*. This expression is given by

$$m_4^* = \frac{\lambda_{2_{\mathrm{H}}} \mathrm{e}^{-m_2^*/\kappa_2} - \mu_2 - \alpha_{23}}{\beta} + \frac{\lambda_{2_{\mathrm{A}}} \left(m_2^*\right)^2 + \alpha_{32} m_3^*}{\beta m_2^*} \ . \quad (6.56)$$

The above equation provides a unique value of m_4^* for a given (but fiducial) steady state value of m_3^*. The problem of determining the number of positive steady state solutions can then be reduced to determining how many stable steady state solutions can be found for m_3. Equation (6.52) can be written as

$$c_2 - \alpha_{23} m_2^* + \alpha_{32} m_3^* = \beta m_2^* m_4^* \ , \quad (6.57)$$

where

$$c_2(\mu_2, \lambda_{2_{\mathrm{H}}}, \lambda_{2_{\mathrm{A}}}, \kappa_2, \mu_4, \lambda_{4_{\mathrm{A}}}, \kappa_4) = -\mu_2 m_2^* + \lambda_{2_{\mathrm{H}}} m_2^* \mathrm{e}^{-m_2^*/\kappa_2} + \lambda_{2_{\mathrm{A}}} m_2^* m_2^* \ . \quad (6.58)$$

We substitute this expression into (6.53) to find

$$c_2 + c_3 m_3^* + \lambda_{3_{\mathrm{H}}} m_3^* \mathrm{e}^{-m_3^*/\kappa_3} = 0 \ , \quad (6.59)$$

where

$$c_3(\mu_3, \lambda_{3_{\mathrm{A}}}, \mu_4, \lambda_{4_{\mathrm{A}}}, \kappa_4) = \lambda_{3_{\mathrm{A}}} m_2^* - \mu_3 \ . \quad (6.60)$$

The constants c_2 and c_3 may be positive or negative real numbers. Let us define

$$f(m) = -\lambda_{3_{\mathrm{H}}} m \mathrm{e}^{-m/\kappa_3}, \qquad g(m) = c_2 + c_3 m \; . \tag{6.61}$$

We know that

$$\frac{\mathrm{d}m_3}{\mathrm{d}t} = g(m_3) - f(m_3) \; . \tag{6.62}$$

Stability of $m_3^* > 0$ requires that

$$\frac{\mathrm{d}g(m_3)}{\mathrm{d}m_3} - \frac{\mathrm{d}f(m_3)}{\mathrm{d}m_3}\Big|_{m_3^*} < 0 \; . \tag{6.63}$$

The definition of the derivative and the fact that $f(m_3^*) = g(m_3^*)$, allows us to conclude that $m_3^* > 0$ is a stable steady state if $g(m_3^* + \epsilon) < f(m_3^* + \epsilon)$ for $\epsilon \to 0^+$. In Figure 6.4 we provide an example plot of $f(m)$ (red curve), which for positive $\lambda_{3_{\mathrm{H}}}$ and κ_3 has a qualitatively fixed shape. Black lines give various examples of $g(m)$ for different choices of c_2 and c_3. If $c_2 > 0$, then we may either have no ($c_3 > 0$) or one ($c_3 < 0$) fixed point solution. If $c_2 < 0$, we may either have no solution or up to three solutions. For any choice of c_2 and c_3, there is at most one solution which satisfies the necessary condition for asymptotic stability. We conclude that we have at most one stable steady state solution in the case of constant specific antigen.

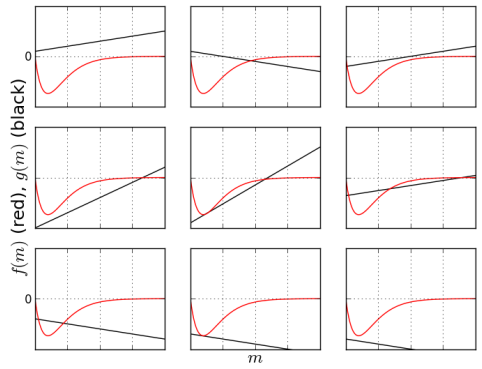

Figure 6.4: The red line gives an example plot of $f(m)$. Black lines give various examples of $g(m)$ for different choices of c_2 and c_3. If $c_2 > 0$, then we may either have no ($c_3 > 0$) or one ($c_3 < 0$) fixed point solution. If $c_2 < 0$, we may either have no solution or up to three solutions. For any choice of c_2 and c_3, there is at most one solution which satisfies the necessary condition for asymptotic stability. We conclude that we have at most one stable steady state solution.

We conclude that the model, under the assumptions listed at the start of this section

(no thymic output, no naive T cells, and constant presentation of antigen) exhibits one possible stable steady state solution, such that all populations are non-zero. The solution for m_2^* is the same as the solution for m_2^* in (6.50), found under the assumption of no specific antigen presentation. We further note that the solution for m_4^* is greater than the solution for m_4^* when $f(t) = 0$ [given by (6.50)]. The QS model predicts that, when antigen specific to the CD4$^+$ T cell population is presented at a constant level, the number of regulatory T cells at steady state is greater than the number required to maintain homeostasis is the absence of antigen. The quorum sensing hypothesis, as implemented with this model, predicts that the number of IL-2 producing T cells found at steady state (assuming parameters are such that all populations are non-zero) is the same, whether the IL-2 producing population sees specific antigen or not. In the latter case, when the IL-2 producing population is exposed to specific antigen, a greater number of regulatory T cells is required to maintain the steady state. Of further note is that the steady state solution for the IL-2 producing population does not depend on the parameter describing the rate of suppression, β. Rather, varying β has the effect of controlling the number of regulatory T cells at steady state.

In Figure 6.5 we present numerical solutions of equations (6.52)-(6.54) in the case that $f(t) = 0$ (dashed lines), and in the case that $f(t) = 1$ (solid lines). Parameters used are given in Table 6.1. If antigen is presented at a constant level, a greater number of regulatory T cells is observed, whereas the steady state number of IL-2 producing T cells remains the same. Overall, there is a modest increase in the total number of CD4$^+$ T cells in the case of constant antigen presentation.

Autoimmunity Let us assume now that the CD4$^+$ T cell clonotype being modelled is specific to self-antigen. Without loss of generality, let us also assume that self-antigen is presented by APCs at a constant rate, so that the dynamics of the clonotype are governed by equations (6.52)-(6.54).

We discuss the requirements for the QS model to be in a regime in which autoimmunity can occur. Let us use the trajectories in Figure 6.5 as an example of a self-reactive clonotype, in which autoimmunity is controlled due to the relatively small number of IL-2 producing T cells. That is, we assume tolerance can be maintained with a non-zero population of IL-2 producing T cells, provided the size of this population is relatively small (compared to the size of the regulatory T cell population). We suppose a typical feature of tolerance is an abundance of regulatory T cells relative to the number of IL-2 producing cells ($m_4^* > m_2^*$). Given this

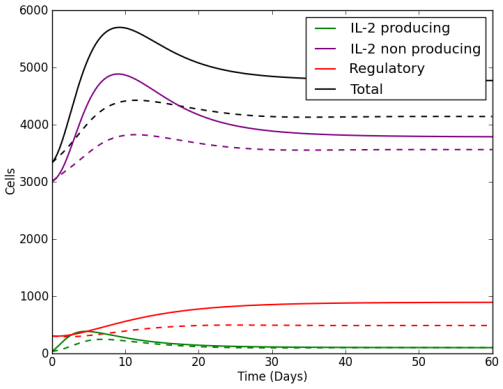

Figure 6.5: Deterministic trajectories when $f(t) = 1$ are shown by solid lines. Solutions for $f(t) = 0$ are shown by dashed lines. Initial conditions are 3×10 IL-2 producing T cells, 3×10^3 IL-2 non-producing T cells, and 3×10^2 regulatory T cells. Parameters used are given in Table 6.1. For $f(t) = 1$ and at equilibrium, we have a greater number of regulatory T cells and non-IL-2 producing T cells.

example of a tolerant state, we define an autoimmune state as one in which the number of IL-2 producing T cells is in excess relative to the number of regulatory T cells.

As discussed earlier, the steady state number of IL-2 producing T cells is a function of the parameters λ_{4_A}, μ_4 and κ_4. The question of how to increase the steady state number of IL-2 producing T cells is clear: increase κ_4, μ_4, decrease λ_{4_A}, or a combination of these. In Figure 6.6, we decrease the value of λ_{4_A} by a factor of 10 (set $\lambda_{4_A} = 10^{-7}$ cells^{-1}hours^{-1}). The number of IL-2 producing T cells increases by approximately 3-fold, whereas the number of regulatory T cells decreases by approximately 2-fold. Varying the parameters in this manner allows the ratio between m_2^* and m_4^* to approach the autoimmune scenario described above.

The findings from this model suggest that in the event that a clonotype is self-reactive, autoimmunity may arise as a consequence of poor proliferation and/or high death rate of regulatory T cells. However the mechanism by which regulatory T cell function may be impaired is unclear. Many autoimmune diseases are specific by a particular antigen, whilst the rest of the T cell pool is effectively normal in its ability to fight infection. It seems unlikely that only the regulatory T cells implicated in autoimmune disease could have their survival impaired whilst the rest of the pool does not.

Of interest in this model is the fact that the rate of suppression is irrelevant for controlling the number of IL-2 producing T cells at steady state. Indeed, if suppression

is reduced, the regulatory population expands to compensate.

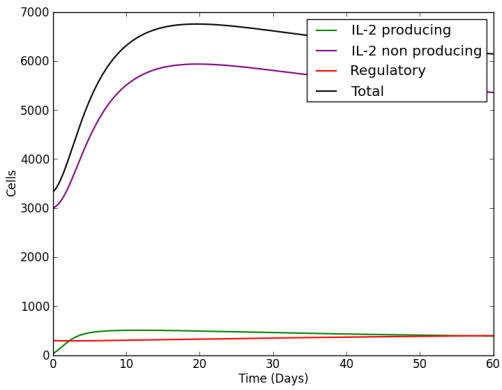

Figure 6.6: Deterministic solutions computed using the parameters given in Table 6.1, with the exception that λ_{4_A} has been reduced by a factor of 10 ($\lambda_{4_A} = 10^{-6}$). The number of IL-2 producing T cells at equilibrium has increased approximately 3-fold, whereas the number of regulatory T cells has decreased approximately 2-fold. Decreasing λ_{4_A} further (or increasing μ_4) may result in the loss of stability with trajectories tending towards infinity. This can be rectified by replacing each parameter λ_{i_A} $(i = 2, 3, 4)$ by a density dependent term in the same manner as done for parameters of the form λ_{j_H} $(j = 1, 2, 3)$.

6.5 Extinction: a stochastic analysis

In this Section, we consider the stochastic model under the assumptions that specific antigen is not presented, $f(t) = 0$, and thymic output is zero, $\nu_1 = \nu_4 = 0$. This corresponds to the scenario analysed in Section 6.3.1 from a deterministic perspective. We evaluate the probability of regulatory T cell extinction conditioned on the non-extinction of the IL-2 producing T cell population, and the average time one must wait before regulatory T cell extinction takes place (Allen, 2003). We also compute the probability of IL-2 producing T cell extinction conditioned on the non-extinction of the regulatory T cell population, and the average time to IL-2 producing T cell extinction.

In this section, we show that the ultimate fate of the CD4$^+$ T cell subsets is extinction, and present some results for general birth and death processes (Allen, 2003). It is of interest to record which population is extinguished first. We shall study whether the process visits, (before extinction takes place), the region in which the number of IL-2 producing T cells is greater than their characteristic size when regulated. We consider the problem of regulatory T cell extinction conditioned on the

non-extinction of the IL-2 producing T cell population, and then study the problem of IL-2 producing T cell extinction conditioned on the non-extinction of the regulatory T cell population.

6.5.1 Extinction for a regular birth and death process

For a regular uni-variate birth and death process $\{\mathbb{X}(t)\}$ we have (Allen, 2003)

$$p_{ji}(\Delta t) = \text{Prob}\{\mathbb{X}(t+\Delta t) = j \mid \mathbb{X}(t) = i\} \tag{6.64}$$

$$= \begin{cases} \lambda_i \Delta t + o(\Delta t) & \text{if } j = i+1 \ , \\ \mu_i \Delta t + o(\Delta t) & \text{if } j = j-1 \ , \\ 1 - (\lambda_i + \mu_i)\, \Delta t + o(\Delta t) & \text{if } j = i \ , \\ o(\Delta t) & \text{otherwise} \ , \end{cases} \tag{6.65}$$

where $\lambda_i > 0$ for $i \geq 1$, $\mu_i > 0$ for $i \geq 1$, and $\lambda_0 = \mu_0 = 0$. For such a process, the state defined by $i = 0$ is an absorbing state (Allen, 2003).
Karlin and McGregor (Karlin & McGregor, 1957) provide conditions for guaranteed absorption (or extinction) of a birth and death process of the form above, as well as giving conditions for absorption in a finite time. Let us introduce r_n as follows:

$$r_n = \frac{\lambda_1 \lambda_2 \cdots \lambda_{n-1}}{\mu_2 \mu_3 \cdots \mu_n} \quad \text{for } n \geq 1 \ . \tag{6.66}$$

A sufficient condition for guaranteed absorption of the process at state $n = 0$ is that the series

$$\sum_{n=1}^{\infty} \frac{1}{\lambda_n r_n} \tag{6.67}$$

diverges (Karlin & McGregor, 1957). A birth and death process with guaranteed absorption will be absorbed in a finite time if the series

$$\sum_{n=1}^{\infty} \lambda_n r_n \tag{6.68}$$

converges (Karlin & McGregor, 1957). Let a birth and death process be defined by the transition rates

$$\lambda_n = \lambda n \mathrm{e}^{-n/\kappa} \ , \tag{6.69}$$

$$\mu_n = \mu n \quad \text{for } n \geq 0 \,, \tag{6.70}$$

with λ, μ and $\kappa > 0$. We prove, in what follows, that for such a process, absorption at the (absorbing) state $n = 0$ is certain and occurs in a finite time.

Absorption is certain For the birth and death process defined by equations (6.69) and (6.70) we have

$$r_n = \frac{\lambda^{n-1}(n-1)! \exp\left(-\sum_{i=1}^{n-1} i/\kappa\right)}{\mu^{n-1} n!} \,. \tag{6.71}$$

Then, it follows that

$$\frac{1}{\lambda_n r_n} = \frac{\mu^{n-1}}{\lambda_n \exp\left(-\sum_{i=1}^{n} i/\kappa\right)} \,, \tag{6.72}$$

and by the ratio test we have

$$\lim_{n\to+\infty} \frac{\lambda_n r_n}{\lambda_{n+1} r_{n+1}} = \lim_{n\to+\infty} \frac{\mu \exp\left[(n+1)/\kappa\right]}{\lambda} \to +\infty \,. \tag{6.73}$$

Thus, the series $\displaystyle\sum_{n=1}^{\infty} \frac{1}{\lambda_n r_n}$ diverges and hence the process is absorbed with certainty, as we wanted to show.

Time to absorption is finite For this process we can write

$$\lambda_n r_n = \frac{\lambda_n \exp\left(-\sum_{i=1}^{n} i/\kappa\right)}{\mu^{n-1}} \,, \tag{6.74}$$

and again by the ratio test we have

$$\lim_{n\to+\infty} \frac{\lambda_{n+1} r_{n+1}}{\lambda_n r_n} = \lim_{n\to+\infty} \frac{\lambda}{\mu \exp\left[(n+1)/\kappa\right]} = 0 \,. \tag{6.75}$$

Thus, the series $\displaystyle\sum_{n=1}^{\infty} \lambda_n r_n$ converges and the process is absorbed in a finite time as we wanted to show.

Naive T cells The Markov sub-chain $\{\mathbb{X}_1(t)\}$ can be considered a birth and death process with transition rates of the type given by equations (6.69) and (6.70). For

the population of naive T cells we have

$$\lambda = \lambda_{1_{\mathrm{H}}} ,$$

$$\mu = \mu_1 + \alpha_{13} ,$$

$$\kappa = \kappa_1 .$$

Thus, the population of naive T cells will become extinct with certainty in a finite time.

IL-2 producing T cells Borrowing ideas from Iglehart (Iglehart, 1964), we can bound the Markov sub-chain $\{\mathbb{X}_2(t)\}$ by a birth and death process (with transition rates of the form given in equations (6.69) and (6.70)), which "travels to infinity" faster than $\{\mathbb{X}_2(t)\}$ (Iglehart, 1964). For such a process we have

$$\lambda = \lambda_{2_{\mathrm{H}}} ,$$

$$\mu = \mu_2 + \alpha_{23} ,$$

$$\kappa = \kappa_2 ,$$

which is absorbed at $n = 0$ in a finite time. Since this process bounds the Markov sub-chain $\{\mathbb{X}_2(t)\}$, it follows that the population of effector T cells will also become extinct with certainty in a finite time.

Regulatory T cells If sufficient time has passed for the population of effector T cells to become extinct, that is, $n_2 = 0$, the transition probabilities for the Markov sub-chain $\{\mathbb{X}_4(t)\}$ depend only on n_4. Indeed, the only non-zero transition probability for the sub-chain $\{\mathbb{X}_4(t)\}$ is

$$p_{n_4-1,n_4}(\Delta t) = \mathrm{Prob}\{\mathbb{X}_4(t+\Delta t) = n_4 - 1 \mid \mathbb{X}_4(t) = n_4\} = \mu_4 n_4 \Delta t + o(\Delta t) . \quad (6.76)$$

Such a process is a simple death process and if not already at the unique absorbing state, $n_4 = 0$, before extinction of the effector T cell population, the process will be absorbed in a finite time (Karlin & McGregor, 1957).

IL-2 non-producing T cells Lastly, suppose sufficient time has elapsed for the naive and effector T cell populations to become extinct. Following extinction of

these populations, the Markov sub-chain representing the IL-2 non-producing T cell population can be considered a birth and death process of the form (6.69) and (6.70) with

$$\lambda = \lambda_{3_{\mathrm{H}}} \ ,$$

$$\mu = \mu_3 \ ,$$

$$\kappa = \kappa_3 \ .$$

It, therefore, follows that the IL-2 non-producing T cell population will become extinct in a finite time, given populations $\{\mathbb{X}_1(t)\}$ and $\{\mathbb{X}_2(t)\}$ have already become extinct.

Let us suppose the process starts in a general state $(n_1, n_2, n_3, n_4) \in S$, where $n_i \geq 1$ for $i = 1, \ldots, 4$. By virtue of the fact that population $\{\mathbb{X}_1(t)\}$ will become extinct in a finite time, independently of the remaining three populations, the process is guaranteed to reach (in a finite time) region R_1 defined as

$$R_1 = \{(0, n_2, n_3, n_4) : n_i \geq 0 \text{ for } i = 2, 3, 4\} \ . \tag{6.77}$$

Equivalently, we have shown that population $\{\mathbb{X}_2(t)\}$ will become extinct in a finite time, independently of the other populations. Thus, the process is guaranteed to reach (in a finite time) region R_2 defined as

$$R_2 = \{(n_1, 0, n_3, n_4) : n_i \geq 0 \text{ for } i = 1, 3, 4\} \ . \tag{6.78}$$

Since both R_1 and R_2 are reached with certainty in a finite time, it follows that the intersection of these regions, R_3, defined as

$$R_3 = \{(0, 0, n_3, n_4) : n_i \geq 0 \text{ for } i = 3, 4\} \ , \tag{6.79}$$

is reached with certainty in a finite time. Given that enough time has elapsed for the populations of naive and effector T cells to have become extinct, we have shown that the population of IL-2 non-producing T cells will become extinct in a finite time. Therefore, if the process is in R_3, the region R_4 defined as

$$R_4 = \{(0, 0, 0, n_4) : n_4 \geq 0\} \ , \tag{6.80}$$

is reached with certainty in a finite time. Equivalently, we have shown that following

extinction of the population of effector T cells, the population of regulatory T cells will become extinct in a finite time. Thus, the region R_5 defined as

$$R_5 = \{(0, 0, n_3, 0) : n_3 \geq 0\} \ , \tag{6.81}$$

is reached with certainty in a finite time for a process starting in R_3. Finally, considering that R_4 and R_5 are both reached with certainty in a finite time, the intersection of these regions, namely the absorbing state $(0, 0, 0, 0)$ is reached with certainty in a finite time from region R_3. It, thus, follows the entire process becomes extinct in a finite time starting from an arbitrary state $(n_1, n_2, n_3, n_4) \in S$, with $n_i \geq 0$ for $i = 1, \ldots, 4$.

6.5.2 Probability and time to extinction of populations 2 and 4

We have shown that the populations of effector and regulatory T cells will both become extinct in a finite time. In this Section we present a numerical method to approximately calculate the probability that the regulatory T cell population will be driven to the absorbing region defined by

$$R = \{(n_2, n_4) : n_2 \neq 0, n_4 = 0\} \ , \tag{6.82}$$

before the population of effector T cells becomes extinct. In such an event, when the population of regulatory T cells becomes extinct before the effector T cell population, the $CD4^+$ T cell population is at risk of unregulated proliferation of the effector T cell subset, following a possible increase in their proliferative capacity, which for example could be induced by presentation of specific antigen. In this scenario, the probability of autoimmunity increases (Almeida *et al.*, 2012).

In this Section, we let $\{\mathbb{X}(t)\} = \{(\mathbb{X}_2(t), \mathbb{X}_4(t))\}$ be the bi-variate Markov process representing populations 2 and 4. The transition probabilities for such a process are

$$p_{\mathbf{m},\mathbf{n}}(\Delta t) = \text{Prob}\{\mathbb{X}(t + \Delta t) = \mathbf{m} \mid \mathbb{X}(t) = \mathbf{n}\}$$

$$= \begin{cases} (\mu_2 + \alpha_{23} + \beta n_4)\, n_2 \Delta t + o(\Delta t) & \text{if } \mathbf{m} = (n_2 - 1, n_4)\ , \\ \mu_4 \dfrac{\kappa_4}{\kappa_4 + n_2} n_4 \Delta t + o(\Delta t) & \text{if } \mathbf{m} = (n_2, n_4 - 1)\ , \\ \lambda_{2_{\mathrm{H}}} n_2 \mathrm{e}^{-n_2/\kappa_2} \Delta t + o(\Delta t) & \text{if } \mathbf{m} = (n_2 + 1, n_4)\ , \\ \lambda_{4_{\mathrm{A}}} n_2 n_4 \Delta t + o(\Delta t) & \text{if } \mathbf{m} = (n_2, n_4 + 1)\ , \\ 1 - \Big[(\mu_2 + \alpha_{23} + \beta n_4)\, n_2 + \mu_4 \dfrac{\kappa_4}{\kappa_4 + n_2} n_4 & \\ + \lambda_{2_{\mathrm{H}}} n_2 \mathrm{e}^{-n_2/\kappa_2} + \lambda_{4_{\mathrm{A}}} n_2 n_4 \Big] \Delta t + o(\Delta t) & \text{if } \mathbf{m} = \mathbf{n}\ , \\ o(\Delta t) & \text{otherwise}\ . \end{cases}$$

To calculate the probability that population 4 becomes extinct before population 2, we first impose that the state space of the Markov process $\{\mathbb{X}(t)\}$ is finite, such that the maximum number of cells for population 2 is N_2, and the maximum number of cells for population 4 is N_4. Imposing a finite state space implies that the calculated probabilities will be an approximation to the true ones. Since the process typically does not grow to infinity (due to the carrying capacities of the cell subsets), for increasing values of N_i, $i = 2, 4$, the likelihood of any realisation (for a given parameter set) reaching either N_i, decreases. Thus, we can increase the accuracy of the calculation to arbitrary precision by increasing N_2 and N_4. This, however, comes at a further computational cost which we discuss below.

Let $\mathcal{P}_{\mathbf{n}}$ be the probability of reaching region R from an arbitrary state $\mathbf{n} = (n_2, n_4)$. By definition we have $\mathcal{P}_{(n_2,0)} = 1$, $\mathcal{P}_{(0,n_4)} = 0$, $\mathcal{P}_{(0,0)} = 0$, and $0 < \mathcal{P}_{(n_2,n_4)} < 1$, with $n_2, n_4 > 0$. We define

$$q_{\mathbf{m},\mathbf{n}} = \begin{cases} (\mu_2 + \alpha_{23} + \beta n_4)\, n_2 & \text{if } \mathbf{m} = (n_2 - 1, n_4)\ , \\ \mu_4 \dfrac{\kappa_4}{\kappa_4 + n_2} n_4 & \text{if } \mathbf{m} = (n_2, n_4 - 1)\ , \\ \lambda_{2_{\mathrm{H}}} n_2 \mathrm{e}^{-n_2/\kappa_2} & \text{if } \mathbf{m} = (n_2 + 1, n_4)\ , \\ \lambda_{4_{\mathrm{A}}} n_2 n_4 & \text{if } \mathbf{m} = (n_2, n_4 + 1)\ , \\ (\mu_2 + \alpha_{23} + \beta n_4)\, n_2 + \mu_4 \dfrac{\kappa_4}{\kappa_4 + n_2} n_4 & \\ + \lambda_{2_{\mathrm{H}}} n_2 \mathrm{e}^{-n_2/\kappa_2} + \lambda_{4_{\mathrm{A}}} n_2 n_4 & \text{if } \mathbf{m} = \mathbf{n}\ , \end{cases} \tag{6.83}$$

and $\rho_{\mathbf{m},\mathbf{n}}$ as follows

$$\rho_{\mathbf{m},\mathbf{n}} = \frac{q_{\mathbf{m},\mathbf{n}}}{q_{\mathbf{n},\mathbf{n}}}\ . \tag{6.84}$$

Let $S_{\mathbf{n}}$ be the set of states which can be reached in a single transition from state $\mathbf{n}$. Then $S_{\mathbf{n}}$ is given by

$$S_{\mathbf{n}} = \{(n_2 - 1, n_4), (n_2 + 1, n_4), (n_2, n_4 - 1), (n_2, n_4 + 1)\} \ , \tag{6.85}$$

for $0 < n_2 < N_2$ and $0 < n_4 < N_4$. When $n_2 = N_2$, we have $S_{\mathbf{n}} = \{(N_2 - 1, n_4), (N_2, n_4 - 1), (N_2, n_4 + 1)\}$. When $n_4 = N_4$, we have $S_{\mathbf{n}} = \{(n_2 - 1, N_4), (n_2 + 1, N_4), (n_2, N_4 - 1)\}$, and when $n_2 = N_2$, $n_4 = N_4$, we have $S_{\mathbf{n}} = \{(N_2 - 1, N_4), (N_2, N_4 - 1)\}$. If the process reaches either the region defined by R or the region $\bar{R}$ defined by

$$\bar{R} = \{(n_2, n_4) : n_2 = 0\} \ , \tag{6.86}$$

the process stops.

Probability of extinction

By a first step analysis argument, for which further details can be found in Ref. (Allen, 2003), we write

$$\mathcal{P}_{\mathbf{n}} - \sum_{\mathbf{m} \in S_{\mathbf{n}}} \rho_{\mathbf{m},\mathbf{n}} \mathcal{P}_{\mathbf{m}} = \sigma \ . \tag{6.87}$$

We define σ as follows: when $\mathbf{n} \in R$, $\sigma = 1$, and $\sigma = 0$ if $\mathbf{n} \notin R$. We can express equation (6.87) in the form

$$A\mathcal{Q} = a \ , \tag{6.88}$$

where A is a $(N_2 N_4) \times (N_2 N_4)$ matrix that depends on the variables $\rho_{\mathbf{m},\mathbf{n}}$, $\mathcal{Q}$ is a $(N_2 N_4) \times 1$ (column) vector that depends on the variables $\mathcal{P}_{\mathbf{n}}$, and a is a $(N_2 N_4) \times 1$ (column) vector that depends on the variables σ. In order to construct A, $\mathcal{Q}$ and a, we first define a bijection ψ from the set $K = \{0, \ldots, N_2\} \times \{0, \ldots, N_4\}$ to the set $\mathcal{K} = \{0, \ldots, (N_2 + 1)(N_4 + 1) - 1\}$, such that an ordering for all states in K can be introduced. We note that the ordering of the states in K defined by the bijection is irrelevant to the calculation, therefore any choice of bijection ψ will suffice. Let $A = (A_{i,j})$, $\mathcal{Q} = (\mathcal{Q}_k)$ and $a = (a_k)$, with $i, j, k \in \mathcal{K}$. We then define

$$A_{i,j} = 1 \quad \text{if } i = j \ ,$$

$$A_{i,j} = -\rho_{\psi^{-1}(i),\psi^{-1}(j)} \quad \text{if } \psi^{-1}(i) \in S_{\psi^{-1}(j)} \ ,$$

$$a_k = 1 \quad \text{if } \psi^{-1}(k) \in R \ ,$$

$$a_k = 0 \quad \text{if } \psi^{-1}(k) \notin R \ ,$$

$$\mathcal{Q}_k = \mathcal{P}_{\psi^{-1}(k)} \ .$$

Since the matrix A has been defined so that $A_{i,i} = 1$, A is non-singular and thus, invertible. In this case, the numerical solution is

$$\mathcal{Q} = A^{-1}a \ . \tag{6.89}$$

One immediate drawback of this method is the computational time it takes to invert the matrix A. As one increases the size of the state space, A increases with the square of N_2N_4. It, therefore, follows that the computational time to invert A grows like $(N_2N_4)^2$ as N_2 and N_4 increase.

Expected time to extinction

In a similar manner to the calculation of the probability of extinction, we can also compute the expected time to extinction of the populations of effector and regulatory T cells. Let $\tau_{\mathbf{n}}$ be the expected time to reach the set of states $\Omega = R \cup (0,0)$ from $\mathbf{n} \notin \Omega$. Then, by a first step analysis argument we have (Allen, 2003)

$$\tau_{\mathbf{n}} - \sum_{\mathbf{m} \in S'_{\mathbf{n}}} \rho_{\mathbf{m},\mathbf{n}} \tau_{\mathbf{m}} = i_{\mathbf{n}} \ , \tag{6.90}$$

where $i_{\mathbf{n}}$ is the mean time the process waits in state $\mathbf{n}$. This waiting time is given by $i_{\mathbf{n}} = \frac{1}{q_{\mathbf{n},\mathbf{n}}}$ (Allen, 2003). Note that $S'_{\mathbf{n}}$ is the set of all states that can be reached from state $\mathbf{n}$ in a single transition and that are not in Ω. For $\mathbf{n} \in \Omega$ we impose $\tau_{\mathbf{n}} = 0$.

We solve the above equation by setting it up as a linear algebra problem as we did before. Define a bijection φ from the set $K = \{0, \ldots, N_2\} \times \{0, \ldots, N_4\} \backslash \Omega$ to the set $\mathcal{K} = \{0, \ldots, (N_2+1)(N_4+1) - 1 - |\Omega|\}$. Given $i, j \in \mathcal{K}$, let $B = (B_{i,j})$, $b = (b_0, b_1, \ldots, b_{(N_2+1)(N_4+1)-1-|\Omega|})^{\mathrm{T}}$ and $\mathcal{T} = (\mathcal{T}_0, \mathcal{T}_1, \ldots, \mathcal{T}_{(N_2+1)(N_4+1)-1-|\Omega|})^{\mathrm{T}}$, and define

$$B_{i,j} = 1 \quad \text{if } i = j \ ,$$

$$B_{i,j} = -\rho_{\varphi^{-1}(i),\varphi^{-1}(j)} \quad \text{if } \varphi^{-1}(i) \in S'_{\varphi^{-1}(j)} \ ,$$

$$b_k = i_{\varphi^{-1}(k)} \ ,$$

$$\mathcal{T}_k = \tau_{\varphi^{-1}(k)} \ ,$$

for $i, j, k \in \mathcal{K}$. The solution for the expected time to absorption into the set Ω is

$$\mathcal{T} = B^{-1} b \ . \tag{6.91}$$

6.5.3 Numerical results: extinction of regulatory T cells

Figures 6.7 A) and B) present numerical (Gillespie) simulations of the stochastic process for two different sets of parameters, differing in the value of $\lambda_{2_{\mathrm{H}}}$. Figures 6.7 C) and D) make use of the method described in Section 6.5.2 to compute probabilities of extinction. Finally, Figures 6.7 E) and F) make use of the matrix method described in Section 6.5.2 to compute the expected time to extinction for both sets of parameter values. The regions R and $\bar{R}$, introduced in Section 6.5, are given by

$$R = \{(n_2, n_4) : n_2 \neq 0, n_4 = 0\} \ , \quad \text{and} \quad \bar{R} = \{(n_2, n_4) : n_2 = 0\} \ . \tag{6.92}$$

Probabilities of regulatory T cell extinction conditioned on the non-extinction of the IL-2 producing T cell population, and the expected time to extinction, are given in Table 6.2. We note that the value of $\lambda_{2_{\mathrm{H}}} = 0.022$ corresponds to a parameter set that yields a deterministic stable steady state with no regulatory T cells, and $\lambda_{2_{\mathrm{H}}} = 0.080$ to a parameter set that yields a deterministic stable steady state with both effector and regulatory T cells present.

6.5.4 Numerical results: extinction of IL-2 producing T cells

Figures 6.8 A) and B) make use of the method described in Section 6.5.2 to compute probabilities of extinction of IL-2 producing T cells, conditioned on the non-extinction of regulatory T cells. We have generated numerical realisations of the stochastic process for two different sets of parameters, as described in Table 6.1, differing only in the value of $\lambda_{2_{\mathrm{H}}}$. In Figures 6.8 C) and D), we make use of the matrix method described in Section 6.5.2 to compute the expected time to extinction for both sets of parameter values.

Summary We consider two sets of parameter values. In the first, there are no regulatory cells in the steady state of the deterministic model of Section 6.3.2. However, we may choose an initial condition with numbers of regulatory T cells sufficiently

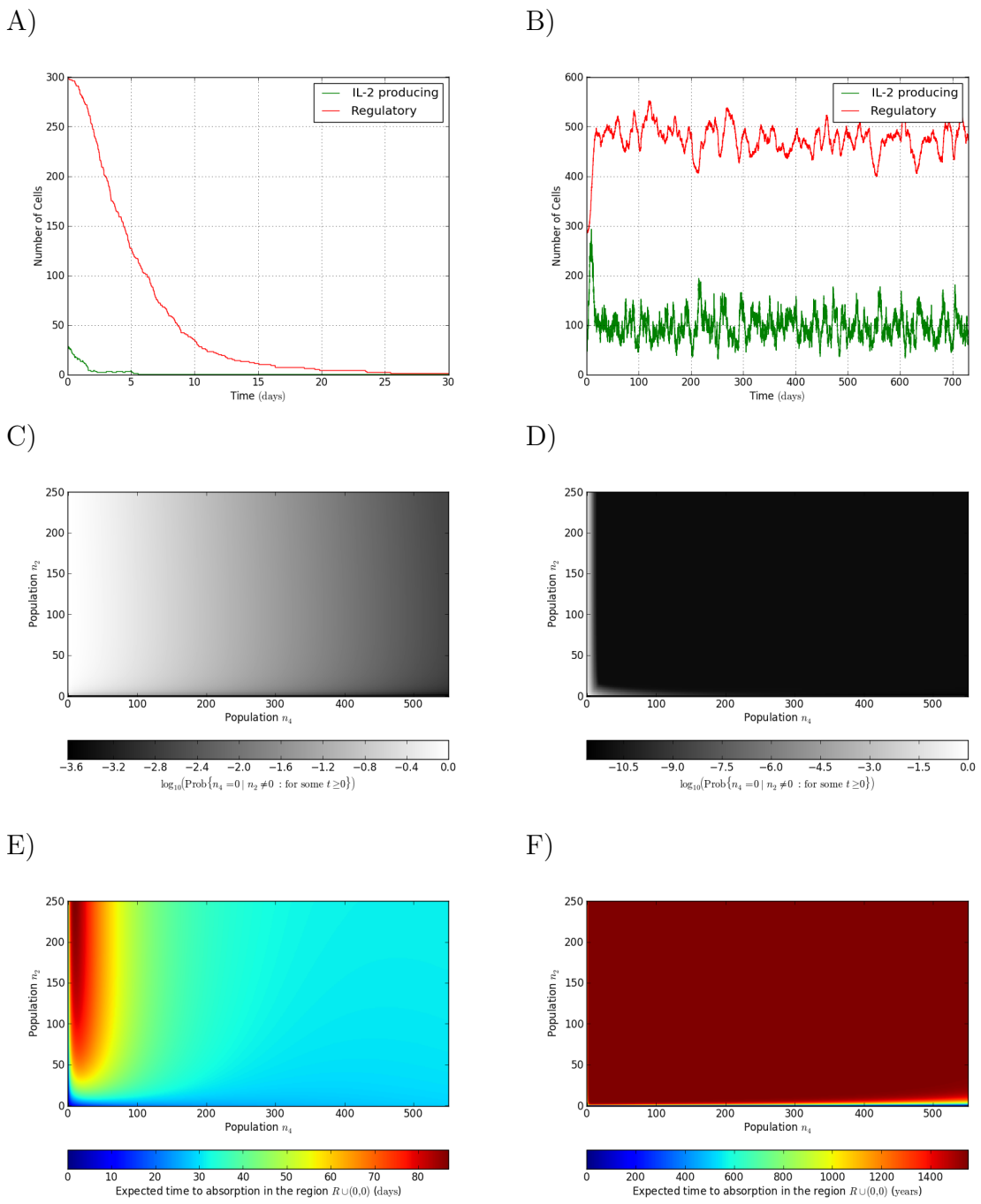

Figure 6.7: (Caption continued on the following page.)

Figure 6.7: A) Gillespie realisation of populations 2 and 4 for the parameter set given in Table 6.1, taking $\lambda_{2_H} = 0.022$ h^{-1}. Using this value ensures the deterministic steady state of the form $(n_2^* > 0, n_4^* = 0)$ is stable. Initial conditions were chosen such that the stochastic realisation begins with 30 IL-2 producing T cells and 300 regulatory T cells and is run for 30 days. B) Gillespie realisation for the same initial conditions as in A), with a time interval of two years, and the same parameter set except $\lambda_{2_H} = 8 \times 10^{-2}$ h^{-1}. This proliferation rate guarantees the stability of a deterministic steady state of the form $(n_2^* > 0, n_4^* > 0)$. As the populations do not exceed 250 effector T cells or 550 regulatory T cells, we impose these values for N_2 and N_4, respectively. C) Probability of reaching the region R from a general state (n_2, n_4), with a maximum state space given by $N_2 = 250$ and $N_4 = 550$. The parameter set is the one used for Figure A). D) Probability of reaching the region R from a general state (n_2, n_4) with a maximum state space $N_2 = 250$ effector cells and $N_4 = 550$ regulatory cells with parameters as chosen in Figure B). For this parameter set the probability of population 4 going extinct before population 2 is $\sim 10^{-12}$ for most initial conditions. E) Expected time to absorption in the region defined by $R \cup (0, 0)$ with a maximum state space of $N_2 = 250$ effector T cells and $N_4 = 550$ regulatory T cells. Parameters have been chosen as in Figures A) and C). F) Expected time to reach $R \cup (0, 0)$ with same parameters as chosen in Figures B) and D).

large to drive the IL2-producing population to extinction. In the second case, the steady state of the deterministic model corresponds to a situation where a non-zero population of regulatory cells moderates the size of the IL2-producing population. Here, by choosing an initial condition with large numbers of IL2-producing cells, we are able to explore the possibility that this population can avoid regulation.

6.6 Conclusions

The quorum-sensing mechanism allows an IL-2 producing population to be maintained at a regulated size that does not depend on the absence or presence of specific antigen. In the latter case, a larger number of regulatory T cells is required to maintain the homeostatic distribution of the CD4$^+$ T cell population. Such scenarios include the late part of an immune response, once it has peaked (Almeida *et al.*, 2012).

The model presented here does not include competition for IL-2 at the receptor/molecular level. However, implicit in choosing the proliferation of regulatory T cells to be antigen independent, is the assumption that regulatory T cells are more sensitive to IL-2 than IL-2 producing cells (Feinerman *et al.*, 2010). We do

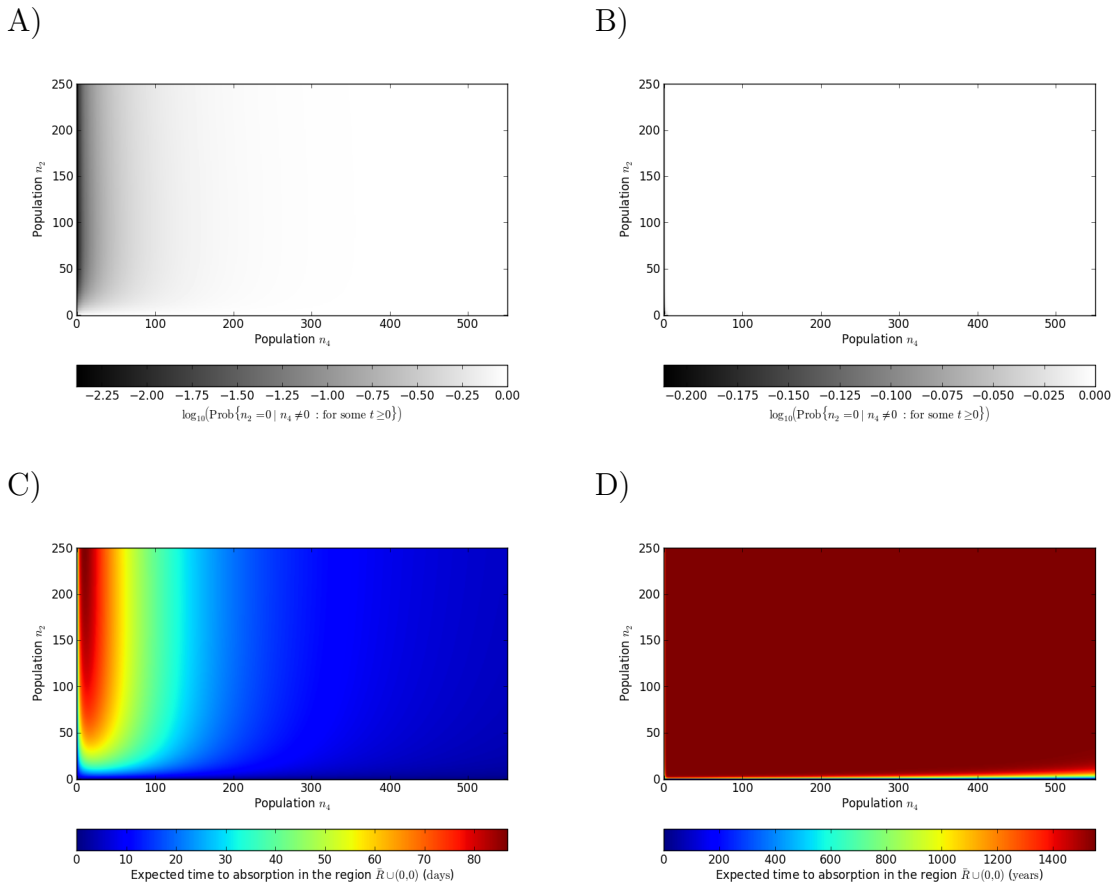

Figure 6.8: Upper plots) Probability of extinction of the IL-2 producing population conditioned on survival of the regulatory population. The parameter set used for the left (right) plot corresponds to the same parameter set used for the left (right) plot in Figure 6.7. Lower plots) Expected time to absorption in the region $\bar{R} \cup (0,0)$ with parameter sets corresponding to the above plots. Plot D) looks qualitatively similar to plot F) in Figure 6.7. This is due to the fact that the most probable path of extinction in Figure 6.7 F) is by absorption in the region $\bar{R}$. Furthermore, the amount of time spent in region R is short relative to the time scales shown in D).

$\lambda_{2_H} = 0.022\ h^{-1}$

IC (n_2, n_4)	Prob n_4 ext	Expected time (days)
(40,100)	0.38732	41.794
(80,200)	0.12850	34.339
(120,300)	0.039915	31.820
(160,400)	0.012389	31.243
(200,500)	0.0038638	31.314

$\lambda_{2_H} = 0.080\ h^{-1}$

IC (n_2, n_4)	Prob n_4 ext	Expected time (years)
(40,100)	9.0657e-12	1552.2
(80,200)	9.0657e-12	1552.2
(120,300)	9.0657e-12	1552.2
(160,400)	9.0657e-12	1552.2
(200,500)	9.0656e-12	1551.9

Table 6.2: Probabilities and expected times to extinction that correspond to Figure 6.7. The Table provides the conditional probability of extinction of the regulatory T cell population and the expected time to this extinction event given initial conditions for $\lambda_{2_H} = 0.022\ h^{-1}$ and $\lambda_{2_H} = 0.080\ h^{-1}$.

not assume this limits the proliferative capacity of IL-2 producing cells, as in our model the limiting factor of proliferation for IL-2 producing cells is the number of cells themselves; regulatory cells play a role through the suppressive term β (Qureshi *et al.*, 2011; Wing *et al.*, 2008).

A possible extension of the model is to include a carrying capacity, for the IL-2 induced proliferation terms, which encodes some concept of space or availability of other trophic factors; availability would become limiting for large enough cell numbers. Another similar approach is that of Yates *et al.* (Callard *et al.*, 2003), where T cells are assumed to induce fratricidal apoptosis due to Fas-FasL interactions. The simplest method of including such a mechanism in the model would be to add non-linear death terms in the ODEs for the populations of antigen-experienced cells (IL-2 non-producing and IL-2 producing T cells).

In vivo, and due to the cross-reactivity of T cell clonotypes, IL-2 producing T cells might be suppressed by regulatory T cells of different TCR specificities. Interclonal suppression would limit the degree of proliferation the effector population could undergo. Additionally, regulatory T cells may make use of IL-2 produced by effector T cells of different TCR specificities, a hypothesis not considered in our model, but that should be included in future mathematical models of $CD4^+$ T cell populations (Müller *et al.*, 2012).

$\lambda_{2_H} = 0.022$ h^{-1}

IC (n_2, n_4)	Prob n_2 ext	Expected time (days)
(40,100)	0.61268	34.561
(80,200)	0.87150	19.493
(120,300)	0.96008	11.774
(160,400)	0.98761	7.9934
(200,500)	0.99613	5.9972

$\lambda_{2_H} = 0.080$ h^{-1}

IC (n_2, n_4)	Prob n_2 ext	Expected time (years)
(40,100)	1.0000	1552.2
(80,200)	1.0000	1552.1
(120,300)	1.0000	1552.1
(160,400)	1.0000	1552.1
(200,500)	1.0000	1551.9

Table 6.3: Conditional probability of IL-2 producing T cell extinction conditioned on the non-extinction of the regulatory T cell population, and the expected time to this extinction.

A regulatory T cell phenotype can be induced in non-regulatory cells (Bettelli *et al.*, 2006; Chen *et al.*, 2003; Kretschmer *et al.*, 2005) via the transforming growth factor TGF-β, perhaps providing additional protection against losses in the regulatory T cell population. It is, however, unclear if regulatory T cells can be induced from all non-regulatory phenotypes or just naive phenotypes. These considerations are out of the scope of this chapter.

Recent experimental studies have provided a molecular basis for the cell-extrinsic function of the co-receptor CTLA-4 (Qureshi *et al.*, 2011). As regulatory T cells constitutively express the co-receptor CTLA-4 on their surface, this mechanism can allow them to capture, via CTLA-4 trans-endocytosis of CD80 and CD86, these ligands from APCs. In this way, regulatory T cells can deplete CD80 and CD86 molecules from the surface of APCs, and in turn suppress the activation of CD4$^+$ T cells. This mechanism will be explored in future work.

If a tolerant steady state exists and is stable, the model predicts that the equilibrium number of IL-2 producing T cells is the same regardless of whether these cells see specific antigen or not. In the former case, we observe a larger number of regulatory T cells to compensate for the increased turnover of effector cells. The model further predicts that an imbalance in the number of regulatory and effector T cells can lead to large populations of effector cells. However, this is only in the event these

cells see specific antigen. Such an imbalance could result from a stochastic fluctuation, or from the immune activity of other T cell clonotypes during an immune response. Exploring potential mechanisms driving this imbalance would require a more comprehensive future model to be developed.

In this chapter, we have restricted ourselves to examining the model under the restriction of constant antigen presentation. This restriction has been appropriate as we have not modelled the precise details of an immune response, which require a general function $f(t)$. We conclude our discussion with numerical results that describe the time evolution, in the case of time-dependent specific antigen presentation, of the n_2, n_3 and n_4 populations. In Figure 6.9, we present example trajectories for non-constant antigen presentation. We first assume $f(t) = 0$ for seven days. Between days seven and fourteen we let $f(t) = 1$, and following day fourteen we set $f(t) = \mathrm{e}^{-0.027(t-14\times 24)}$. That is, from day fourteen $f(t)$ is a decreasing exponential, which decreases from 1 to 1/100 by approximately day twenty one. Trajectories were computed using the parameter set given in Table 6.1; at day zero we let initial conditions be equal to the steady state solution subject to setting $f(t) = 0$. This figure shows that there is only a modest increase in the number of IL-2 producing T cells. It seems the main factor allowing growth of the total $\mathrm{CD4}^+$ pool is not a large increase in the amount of available IL-2 (assumed to be proportional to the number of IL-2 producing T cells). We have assumed recognition of antigen by the non-regulatory populations allows them to up-regulate IL-2Rα. It would appear that it is this extra responsiveness to the available IL-2, which drives growth of the population. A caveat to these observations is that we have made the simplification that IL-2 levels are proportional to the size of the IL-2 producing subset. Such an assumption does not take into account any notion of space or competition for IL-2, which may be the case in vivo.

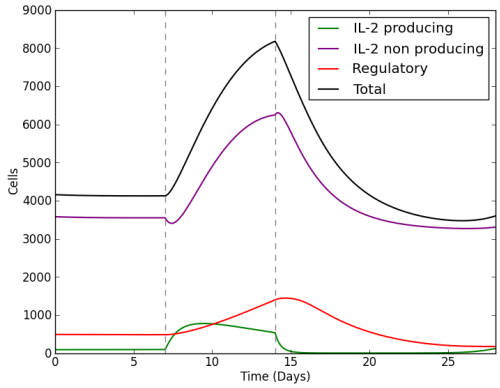

Figure 6.9: For the first seven days we have set $f(t) = 0$. Between days seven and fourteen, we set $f(t) = 1$. After day fourteen we set $f(t) = \mathrm{e}^{-0.027(t-14\times24)}$ (an exponentially decreasing function which reduces from 1 to 1/100 in approximately seven days). The parameter set used for these trajectories is given in Table 6.1, taking $\lambda_{2_\mathrm{H}} = 0.08\ \mathrm{h}^{-1}$. Furthermore, we have increased α_{32} by a factor of 10 ($\alpha_{32} = 0.01\ \mathrm{h}^{-1}$) to give a more distinct peak within the second week period. Initial conditions are given by the steady state solution subject to setting $f(t) = 0$.

Chapter 7

Concluding remarks

Mathematical approaches to modelling expanding populations of cells can be traced back to the Smith-Martin model, for which many generalisations have been developed (Lee & Perelson, 2008). The Smith-Martin approach introduces two variables to, respectively, describe the number of cells in the resting phase of the cell cycle (G_0) and the number of cells undergoing cycling (G_1, S, G_2 and M). Callard *et al.*, Yates *et al.* and Seddon *et al.* have favoured the two compartment approach to modelling lymphocyte populations, from which the models presented in Chapters 3 and 5 are heavily inspired (Bains *et al.*, 2009b; Callard *et al.*, 2003; Hogan *et al.*, 2013; Yates *et al.*, 2007, 2008). In these studies, the two compartment approach has been applied to populations of naive T cells, memory T cells, and when considering these phenotypes as a single population.

In the models presented in Chapters 3 and 5, we have assumed that following division, two daughter cells are produced in the resting compartment. However, there are other possibilities that may be considered, such as both daughter cells immediately proceeding through another round of division. In an earlier paper we used the simple model to explore two further hypotheses: firstly, that both daughter cells remain in the cycling pool following a round of division, and secondly, one daughter cell remains in the cycling pool whilst the other becomes a resting cell (Reynolds *et al.*, 2012). These assumptions required the introduction of a relaxation term allowing cycling T cells to revert back to a resting state. In this paper we explored the differences in the steady state solutions (with thymic output) of the simple model arising from these assumptions. Based on the study we discussed how one may potentially test for these differences in an experimental setting.

Given that one may choose to describe a population of T cells by this two compartment model, the most immediate question is how one should choose to model

the transitions between compartments, also noting that T cells may die. In the deterministic formulation, a first approach is to assume all transitions are linear, as we have done for the simple model presented in Section 3.1. Assuming linear transition rates has of course the immediate drawback that, if there are no source terms for T cells (for example thymic output), then the only steady state corresponds to extinction of the populations. To remedy this, a typical approach taken in the literature is to replace one of the linear terms by one which allows for the existence of a positive steady state. Examples include assuming cell-cell induced fratricide due to interactions between the Fas receptor and the Fas ligand, introduced via the inclusion of a second order death term (Bains *et al.*, 2009b; Callard *et al.*, 2003) and, more recently, assuming density dependent death and cell cycle entry rates (Hogan *et al.*, 2013). We explored examples of these changes in Section 3.2.

The novelty of the approach taken in Chapter 5 is in the introduction of a resource, which for naive T cells, is assumed to be IL-7. The approach taken for this model has its roots in the observations of Palmer *et al.* (Palmer *et al.*, 2011). In this paper, naive $CD8^+$ T cell responses in vitro were reported to be dependent on the concentration of IL-7 these cells were exposed to. The authors suggested naive $CD8^+$ T cells require a threshold in IL-7 signalling to be surpassed to enable survival of the cells, whilst a second, higher, threshold must be surpassed before a T cell can enter the cell cycle. Assuming this behaviour is also true for $CD4^+$ T cells (such that we can model both cell types with a single variable), we took an approach where we assume the death and cell cycle entry rates in the two compartment model were functions of the average amount of IL-7 induced signalling with respect to signalling thresholds for survival and division.

Modelling the resource in the manner discussed above required us to relate the concentration of IL-7 to the amount of IL-7 induced signalling, and developing a relationship for this has been the focus of Chapter 4. Whilst we have attempted to establish the model from biological observations, the two compartment model ultimately is a modified version of the linear model in which two terms are replaced by functions of the resource ($\bar{\mu}_R(S(t))$ and $\bar{\rho}(S(t))$). These functions qualitatively resemble hill functions (Gesztelyi *et al.*, 2012). That is, the rates of resting T cell death and entry into the cell cycle possess a maximum which is reached if IL-7 induced signalling is in excess. The parameter α determines the "steepness" of these functions, with the functions being linear in the limit $\alpha \to 0^+$, whilst tending to step functions in the limit $\alpha \to +\infty$.

The analysis of the model in Chapter 5 highlighted how sensitive the model is to changes in the parameter α. An accurate determination of the true values of α (for humans and mice) would require experiments specifically designed with measuring this parameter in mind. Despite this, our results suggest that α should be smaller for the human parameter set, relative to the mouse parameter set. Biologically, this implies greater variability in IL-7 signalling thresholds for a human population of naive T cells, compared with a murine population. If the diversity in signalling thresholds could be measured experimentally, it would be interesting to see if these differences between human and mice T cells exist.

Let us suppose the suggested diversity in IL-7 signalling thresholds for human T cells occurs mainly between different T cell clonotypes. Then we might expect that there exist clonotypes within the repertoire which survive and enter cell division preferentially when compared with other clonotypes. We might further expect that the number of T cells in clonotypes which are homeostatically "fitter" for IL-7 would increase. Correspondingly, the clonotypes which require the most amount of signalling for survival and division may well be lost from the repertoire. Thus, a consequence of this variability in IL-7 signalling thresholds between clonotypes could result in a loss of diversity of clonotypes. For young individuals, lost clonotypes are presumably replaced by new T cell clonotypes maturing in the thymus. However, in later life, when thymic output has waned considerably, loss of T cell clonotypes may leave holes in the repertoire, resulting in oligoclonality and insufficient immune coverage. Oligoclonality in this respect would result from homeostatic selection of T cell clonotypes which possess lower than average signalling thresholds for survival and division. This is in contrast to oligoclonality resulting from persistent antigenic stimulation of T cell clonotypes, as has been observed for various pathological conditions such as autoimmunity and response to tumours (Balk *et al.*, 1991; Even *et al.*, 1995; Sakkas *et al.*, 2002).

Previous studies have shown that naive T cells acquire a memory-like phenotype following repeated homeostatic division (Cho *et al.*, 2000; Murali-Krishna & Ahmed, 2000). We might therefore expect that the T cell clonotypes with the lowest IL-7 signalling thresholds would become memory-like T cells. This, somewhat paradoxically, may increase the overall average level of signalling thresholds across the naive T cell pool by leaving behind the clonotypes which possess higher thresholds. The remaining naive T cell pool would thus, over time, become less responsive to IL-7. A mathematical confirmation of this suggestion would require a modification of the

model in Chapter 5 to be introduced in which we include a division dependent differentiation term for naive T cells being lost to the memory pool. Given that we have struggled to estimate the parameters for the model presented in this work, estimating the parameters of a more complicated model would require experiments to be designed with these measurements in mind. Developing such a model is therefore beyond the scope of this study.

In the derivation of the signalling relation in Chapter 4, we have assumed receptor/signal dynamics are in equilibrium. This allowed us to assume all T cells in the population receive the same amount of IL-7 induced signalling for a given concentration of IL-7. Furthermore, this signalling occurs continuously. A study by Singer *et al.* suggests, for $CD8^+$ T cells, continuous IL-7 signalling causes these cells to express interferon-γ (IFN-γ), resulting in cell death (Kimura *et al.*, 2013). This was observed in vitro, for IL-7 at a concentration of 1 ng ml^{-1}, which, in the context of our results, is more than sufficient to drive T cells into the cell cycle. Indeed, in the studies of Singer *et al.* extensive proliferation was observed for $CD8^+$ T cells cultured at this concentration. Previous studies have shown that extensive proliferation of naive T cells causes them to acquire a memory like phenotype (Cho *et al.*, 2000; Murali-Krishna & Ahmed, 2000), and thus it is likely that interferon-γ production results from naive T cells acquiring a memory/effector phenotype. Indeed, the authors of (Kimura *et al.*, 2013) reported that proliferating T cells acquired memory markers. What is unclear from this study is if the same observations are true for lower concentrations of IL-7. In the supplementary material of (Kimura *et al.*, 2013), it was reported that the same observations are true for low concentrations of IL-7 at 0.6 ng ml^{-1}. However, in the context of our model, 0.6 ng ml^{-1} is by no means a low concentration of IL-7 since from equation (5.1) this produces approximately 574 signalling units at equilibrium, well above the thresholds for proliferation which were found to be around 483 and 555 for OT-1 and F5 T cells respectively. It would be interesting to see if the same results hold for IL-7 concentrations in the range where we expect T cell quiescence, approximately 5.4×10^{-3}-1.9×10^{-2} ng ml^{-1}.

Continuous signalling was reported to be interrupted by intermittent signalling through the TCR. These findings were established both in vivo and in vitro by comparing the dynamics of two $CD8^+$ T cell types, one of which was specific for a given peptide, whilst the other was not (Kimura *et al.*, 2013). The authors conclude that IL-7 signalling must be intermittent to promote homeostasis of naive T cells. From a modelling perspective this presents a challenge, since under these assumptions, for each individual T cell, its current state in signalling, which under

these assumptions oscillates, must be recorded. Deterministic modelling, as used in Chapters 3 and 5, is unsuitable for this, since, we would require a set of ODEs to be solved for each T cell in the population. A more suitable framework would be agent based modelling, a computational approach in which each T cell is considered an autonomous agent. To date however, due to the computational cost involved, agent based approaches are not capable of effectively simulating population sizes typical of the number T cells found in a lymphoreplete mouse, let alone a human. However, it is likely that in the near future, computational approaches will become the prominent modelling platform.

The model in Chapter 6 was developed in collaboration with Freitas *et al.*, resulting in a publication proposing the quorum-sensing hypothesis for $CD4^+$ T cells (Almeida *et al.*, 2012). Within this paper we introduced an earlier, deterministic version of the stochastic model analysed in Chapter 6. One key difference between these two models is in the implementation of a carry capacity allowing the model to possess positive steady state solutions. In the earlier version, we used logistic growth terms, however such terms were unsuitable for the stochastic model. A logistic growth term has the general form $an(1-n/k)$, where a is the growth rate, k is the carrying capacity and n is the population size. For populations sizes where $n > k$, this term becomes negative. Within a continuous time Markov process, transition probabilities must be non-negative, thus the appearance of this term in the transition probabilities of a Markov process becomes contextual depending on the state of the process. Instead, we replaced logistic growth terms by density dependent growth terms of the form $ae^{n/k}$. These terms are strictly positive and thus suitable for use in the Markov model.

The number of T cells in each sub-population of the $CD4^+$ T cell pool has been described by a single variable. This is in contrast to the earlier chapters, wherein, for a given population, we distinguish between cells which are either resting or cycling. Since the study of the quorum-sensing mechanism deals with four sub-populations, this has been done to reduce the overall number of variables from eight to four. This does however create some problems for the division rates, which we highlight in the following sentences. Consider the IL-2 dependent growth terms, which, for the population of IL-2 producing T cells, take the form λn^2. These terms describe the time scales for a cell to divide and produce two daughter cells, resulting from IL-2 stimulation. Consider that as the population grows, the average time for a cell to complete division, given by $(\lambda n)^{-1}$, tends to zero. That is, in modelling T cell division in this manner, we impose no lower limit for the time it takes a cell to

divide. Indeed, λ must be chosen keeping the size of the cell populations in mind. If we choose to model populations at a significantly different size, a different value of λ should be chosen. Using the two compartment approach, one may allow resting cells to enter the cell cycle at an arbitrary fast rate, however we still maintain a fixed length of time for the cell to complete the cell cycle. We therefore place an upper limit to the rate at which a population can expand. This makes sense from a biological perspective and furthermore aids the stability of numerical schemes when solving ODEs[1].

The quorum-sensing hypothesis was explored using a continuous-time Markov process. In process we have used, waiting times for events such as cellular division or death are assumed to be exponentially distributed. Studies by Hawkins *et al.* have shown that more appropriate distributions to describe waiting times for cellular events are right skewed distributions allowing for a minimum waiting time for events, such as the log-normal distribution (Duffy *et al.*, 2012; Hawkins *et al.*, 2009, 2007; Markham *et al.*, 2010). The stochastic analysis of the times to extinction of the IL-2 producing and regulatory populations in Section 6.5 could be improved by recasting the Markov model into a modified version of the Cyton model, developed by Hawkins *et al.* (Hawkins *et al.*, 2007). This would however introduce more parameters into the model, and the extra mathematical scrutiny would be wasted without coinciding experimental approaches to determine the parameters of the model.

Regulatory T cell suppression of IL-2 producing T cells is likely mediated through contact with an APC (Kubo *et al.*, 2004; Sepúlveda & Carneiro, 2011). Therefore, the number of available APCs as well as their spacial distribution within the tissue, are likely to contribute to the homeostatic balance between effector T cells and regulatory T cells. Such considerations may become important for future modelling of effector/regulatory T cell dynamics. Indeed, spacial considerations will likely become important for much of the future modelling of T cell homeostasis in vivo.

In this study we have explored the homeostasis of the peripheral T cell pool. We used the two compartment approach to study the homeostasis of the peripheral naive T cell population. We presented a model of the naive T cell pool in which we have assumed cell survival is dependent on the concentration of available IL-7. With this model we could describe the expansion of a naive T cell population in a lymphopenic

[1]With the current implementation, if the sub-populations of cells with growth terms of the form λn^2 becomes too large, these growth terms dominate. This quickly results in a typical time-scale for division being smaller than the time-steps used for the numerical scheme. At this point the numerical scheme quickly loses stability.

mouse. However, using the available data we were unable to estimate the parameters of the model uniquely. The model less accurately described the homeostasis of the naive T cell pool in humans. We felt this is most likely because the model does not take into account competition for IL-7 from the memory T cell pool, nor do we describe differentiation of naive T cells into memory T cells. Developing the model further to take the memory T cell pool into account is an obvious direction for further modelling efforts. Given our uncertainties in the parameters of the model thus far, further modelling efforts would benefit greatly from being developed alongside experimental approaches.

In addition to our study of the homeostasis of the naive T cell pool we presented a mathematical treatment of the quorum-sensing hypothesis proposed by Freitas *et al.* (Almeida *et al.*, 2012). The main findings from this study was that the quorum-sensing mechanism implies the number of IL-2 producing T cells at equilibrium is the same in the cases where specific antigen is either not presented or presented at a constant level. In the latter case, a larger number of regulatory T cells are required to maintain the equilibrium. Dynamics representative of autoimmunity are obtained when either the survival or death rates (or both) of the regulatory sub-population are compromised. Lastly, we found that the rate of suppression of IL-2 producing T cells has no effect on the number of IL-2 producing T cells at equilibrium.

Appendix A

The limit $\mathbb{E}[\mathbb{X}_i] \to 0$, $i \in \{1, \ldots, n\}$ for log-normal moment closure polynomials

Definition 1 (Positive-definite matrix)**.** *Let A be an $n \times n$ square matrix with real entries (a_{ij}), $1 \leq i, j \leq n$. The matrix A is defined to be positive-definite if for all non-zero real column vectors $\boldsymbol{b}$,*

$$\boldsymbol{b}^T A \boldsymbol{b} > 0. \tag{A.1}$$

Lemma 1. *Let A be a positive-definite $n \times n$ matrix. Then each diagonal element $a_{ii} > 0$ for all $i \in \{1, \ldots, n\}$.*

Proof. Let $A = (a_{ij})_{i,j=1,\ldots,n}$ be a real-valued positive-definite matrix and $\boldsymbol{b} = (b_1, \ldots, b_n)^T$ be a non-zero real valued vector. Then by the definition of a positive-definite matrix

$$\sum_{i,j=1}^{n} b_i b_j a_{ij} > 0. \tag{A.2}$$

Suppose $a_{kk} < 0$ for some $k \in \{1, \ldots, n\}$, we show that under this assumption we can always find a b_k such that equation (A.2) does not hold. To find such a b_k, notice that

$$\begin{aligned} &\sum_{i,j=1}^{n} b_i b_j a_{ij} = b_k^2 a_{kk} + \sum_{\substack{i=1,\\ i\neq k}}^{n} b_i^2 a_{ii} + \sum_{\substack{i,j=1,\\ i\neq j}}^{n} b_i b_j a_{ij} > 0, \\ \Rightarrow \quad &\sum_{\substack{i=1,\\ i\neq k}}^{n} b_i^2 a_{ii} > -a_{kk} \left(b_k^2 + \frac{1}{a_{kk}} \sum_{\substack{i,j=1,\\ i\neq j}}^{n} b_i b_j a_{ij} \right). \end{aligned}$$

Completing the square we find

$$\sum_{\substack{i,j=1,\\ i,j\neq k}}^{n} b_i b_j a_{ij} - \frac{1}{4a_{kk}} \left(\sum_{\substack{j=1,\\ j\neq k}}^{n} b_j a_{kj} + \sum_{\substack{i=1,\\ i\neq k}}^{n} b_i a_{ik} \right)^2 > -a_{kk} \left(b_k + \frac{1}{2a_{kk}} \left(\sum_{\substack{j=1,\\ j\neq k}}^{n} b_j a_{kj} + \sum_{\substack{i=1,\\ i\neq k}}^{n} b_i a_{ik} \right) \right)^2 .$$

Since we assume $a_{kk} < 0$, we may divide both sides by $-a_{kk}$ without changing the direction of the inequality, this gives

$$\frac{1}{4a_{kk}^2} \left(\sum_{\substack{j=1,\\ j\neq k}}^{n} b_j a_{kj} + \sum_{\substack{i=1,\\ i\neq k}}^{n} b_i a_{ik} \right)^2 - \frac{1}{a_{kk}} \sum_{\substack{i,j=1,\\ i,j\neq k}}^{n} b_i b_j a_{ij} > \left(b_k + \frac{1}{2a_{kk}} \left(\sum_{\substack{j=1,\\ j\neq k}}^{n} b_j a_{kj} + \sum_{\substack{i=1,\\ i\neq k}}^{n} b_i a_{ik} \right) \right)^2 . \tag{A.3}$$

The right hand side of equation (A.3) is strictly positive, it follows that the left hand side must also be positive. We are free to take the positive square root, from which we find b_K must satisfy

$$\sqrt{\frac{1}{4a_{kk}^2} \left(\sum_{\substack{j=1,\\ j\neq k}}^{n} b_j a_{kj} + \sum_{\substack{i=1,\\ i\neq k}}^{n} b_i a_{ik} \right)^2 - \frac{1}{a_{kk}} \sum_{\substack{i,j=1,\\ i,j\neq k}}^{n} b_i b_j a_{ij}} - \frac{1}{2a_{kk}} \left(\sum_{\substack{j=1,\\ j\neq k}}^{n} b_j a_{kj} + \sum_{\substack{i=1,\\ i\neq k}}^{n} b_i a_{ik} \right) > b_k. \tag{A.4}$$

We are free to choose b_k greater than the left hand side of equation (A.4) to negate the inequality (A.2), hence the proof follows. Note that if we relax the assumption $a_{kk} < 0$, existence of real solutions when computing the above square root is not guaranteed and hence we are not guaranteed to find b_k to negate (A.2). □

Lemma 2. *Let $\mathbb{X} = (\mathbb{X}_1, \mathbb{X}_2, \ldots, \mathbb{X}_n)$ be a random vector where the components of $\mathbb{X}$ have a multivariate log-normal distribution. Define $\boldsymbol{s} = (s_1, s_2, \ldots, s_n)$ where $s_i \in \mathbb{N}$, $i = 1, \ldots, n$. Then*

$$\mathbb{E}\left[\prod_{i=1}^{n} \mathbb{X}_i^{s_i} \right] = \mathrm{e}^{\boldsymbol{s}\cdot\boldsymbol{\mu} + \frac{1}{2}\boldsymbol{s}^T \Sigma \boldsymbol{s}}. \tag{A.5}$$

Proof. The joint probability density function of a multivariate log-normal distribu-

tion is given by

$$f(\boldsymbol{x}) = \frac{1}{(2\pi)^{\frac{n}{2}}|\Sigma|^{\frac{1}{2}}\prod_{i=1}^{n} x_i} \exp\left(-\frac{1}{2}\left(\log \boldsymbol{x} - \boldsymbol{\mu}\right)^T \Sigma^{-1}\left(\log \boldsymbol{x} - \boldsymbol{\mu}\right)\right). \tag{A.6}$$

First notice that

$$\mathbb{E}\left[\prod_{i=1}^{n} \mathbb{X}_i^{s_i}\right] = \int_{\mathbb{R}^n} \prod_{i=1}^{n} x_i^{s_i} f(\boldsymbol{x})\, \mathrm{d}\boldsymbol{x}. \tag{A.7}$$

By definition, Σ is a positive-definite, symmetric, $n \times n$ matrix. We use Cholesky decomposition to write

$$\Sigma = \left(D^T D\right)^{-1}, \tag{A.8}$$

where D is a triangular matrix. Make the substitution

$$\boldsymbol{y} = D\left(\log \boldsymbol{x} - \boldsymbol{\mu}\right). \tag{A.9}$$

Take derivatives of this and multiply by product of $x_i^{s_i}$, $i = 1, \ldots, n$, then we find

$$\mathrm{e}^{\boldsymbol{s}\cdot\boldsymbol{\mu} + \boldsymbol{s}^T D^{-1}\boldsymbol{y}} \mathrm{d}\boldsymbol{y} = \frac{\prod_{i=1}^{n} x_i^{s_i - 1}}{|\Sigma|^{\frac{1}{2}}} \mathrm{d}\boldsymbol{x}. \tag{A.10}$$

Under this change of variables we find

$$\int_{\mathbb{R}^n} \prod_{i=1}^{n} x_i^{s_i} f(\boldsymbol{x})\, \mathrm{d}\boldsymbol{x} = \frac{1}{(2\pi)^{\frac{n}{2}}} \int_{\mathbb{R}^n} \mathrm{e}^{\boldsymbol{s}\cdot\boldsymbol{\mu} + \boldsymbol{s}^T D^{-1}\boldsymbol{y}} \mathrm{e}^{-\frac{1}{2}\boldsymbol{y}^T\boldsymbol{y}}\, \mathrm{d}\boldsymbol{y}. \tag{A.11}$$

Completing the square for the exponent, the right hand side in the above equation becomes

$$\frac{1}{(2\pi)^{\frac{n}{2}}} \mathrm{e}^{\boldsymbol{s}\cdot\boldsymbol{\mu} + \frac{1}{2}\boldsymbol{s}^T\Sigma\boldsymbol{s}} \int_{\mathbb{R}^n} \mathrm{e}^{-\frac{1}{2}\left(\boldsymbol{y} - \left(D^{-1}\right)^T\boldsymbol{s}\right)^T\left(\boldsymbol{y} - \left(D^{-1}\right)^T\boldsymbol{s}\right)}\, \mathrm{d}\boldsymbol{y} = \frac{1}{(2\pi)^{\frac{n}{2}}} \mathrm{e}^{\boldsymbol{s}\cdot\boldsymbol{\mu} + \frac{1}{2}\boldsymbol{s}^T\Sigma\boldsymbol{s}} \int_{\mathbb{R}^n} \mathrm{e}^{-\frac{1}{2}\boldsymbol{z}^T\boldsymbol{z}}\, \boldsymbol{z}, \tag{A.12}$$

$$= \mathrm{e}^{\boldsymbol{s}\cdot\boldsymbol{\mu} + \frac{1}{2}\boldsymbol{s}^T\Sigma\boldsymbol{s}}, \tag{A.13}$$

as required. □

Theorem 1. *Let $\mathbb{X} = (\mathbb{X}_1, \mathbb{X}_2, \ldots, \mathbb{X}_n)$ be a random vector where the components of $\mathbb{X}$ have a multivariate log-normal joint probability distribution with finite covariance matrix Σ. Let*

$$\mathbb{E}\left[\mathbb{X}_i\right] < \infty \tag{A.14}$$

for all $i \in \{1,\ldots,n\}$. *Suppose*

$$\mathbb{E}[\mathbb{X}_j] \to 0, \tag{A.15}$$

for some $j \in \{1,\ldots,n\}$. *Then, if* $s_j \geq 1$,

$$\mathbb{E}\left[\prod_{k=1}^{n} \mathbb{X}_k^{s_k}\right] \to 0. \tag{A.16}$$

Proof. Suppose that

$$\mathbb{E}[\mathbb{X}_i] = \mathrm{e}^{\mu_i + \frac{1}{2}\Sigma_{ii}} \to 0 \tag{A.17}$$

for some $i \in \{1,\ldots,n\}$. The covariance matrix Σ is positive-definite by definition, therefore by Lemma 1 it follows $\Sigma_{ii} > 0$ for all $i \in \{1,\ldots,n\}$. Thus, the expectation in (A.17) tends to zero if and only if $\mu_i \to -\infty$. Suppose $\mu_i \to -\infty$, from Lemma 2,

$$\lim_{\mu_i \to -\infty} \mathbb{E}\left[\prod_{k=1}^{n} \mathbb{X}_k^{s_k}\right] = \lim_{\mu_i \to -\infty} \mathrm{e}^{\boldsymbol{s}\cdot\boldsymbol{\mu} + \frac{1}{2}\boldsymbol{s}^T\Sigma\boldsymbol{s}} = 0 \tag{A.18}$$

if $s_i \geq 0$, $i \in \{1,\ldots,n\}$ and $\Sigma, \boldsymbol{\mu} < \infty$. □

Appendix B

Miscellaneous results

Lemma 3. *Let $\mathbb{X}_1, \ldots, \mathbb{X}_k$ be k discrete random variables. Impose the condition*

$$\mathbb{E}\left[\prod_{i=1}^{k}(\mathbb{X}_i - \mu_i)^{n_i}\right] = 0 \tag{B.1}$$

where μ_i is the mean of random variable $\mathbb{X}_i$ and $n_i \in \mathbb{Z}$. Then

$$\mathbb{E}\left[\prod_{i=1}^{k}\mathbb{X}_i^{n_i}\right] = \prod_{i=1}^{k}\mu^{n_i}. \tag{B.2}$$

Proof. First construct a bijection from $\mathbb{Z} \leftrightarrow \mathbb{Z}^k$ such that we define a natural ordering on the set $\mathbb{Z}^k$. Denote the nth element of $\mathbb{Z}^k$ by $n = (n_1, \ldots, n_k)$. By the linearity property of the expectation operator and the multi-binomial theorem we have

$$\begin{aligned}
\mathbb{E}\left[\prod_{i=1}^{k}(\mathbb{X}_i - \mu_i)^{n_i}\right] &= \mathbb{E}\left[\sum_{j=0}^{n}\prod_{i=1}^{k}\binom{n_i}{j_i}\mathbb{X}_i^{j_i}(-\mu_i)^{n_i-j_i}\right], \\
&= \sum_{j=0}^{n}\prod_{i=1}^{k}\binom{n_i}{j_i}(-\mu_i)^{n_i-j_i}\mathbb{E}\left[\prod_{i=1}^{k}\mathbb{X}_i^{j_i}\right], \\
&= \mathbb{E}\left[\prod_{i=1}^{k}\mathbb{X}_i^{n_i}\right] + \prod_{i=1}^{k}\mu_i^{n_i}\sum_{j=0}^{n-1}\prod_{i=1}^{k}\binom{n_i}{j_i}\mu_i^{-j_i}(-1)^{n_i-j_i}\mathbb{E}\left[\prod_{i=1}^{k}\mathbb{X}_i^{j_i}\right], \\
&= \mathbb{E}\left[\prod_{i=1}^{k}\mathbb{X}_i^{n_i}\right] + \prod_{i=1}^{k}\mu_i^{n_i}\sum_{j=0}^{n-1}\prod_{i=1}^{k}\binom{n_i}{j_i}(-1)^{n_i-j_i} = 0.
\end{aligned} \tag{B.3}$$

Now considering that

$$\sum_{j=0}^{n-1}\prod_{i=1}^{k}\binom{n_i}{j_i}(-1)^{n_i-j_i} = -1+\sum_{j=0}^{n}\prod_{i=1}^{k}\binom{n_i}{j_i}(-1)^{n_i-j_i} = -1+\prod_{i=1}^{k}(1+(-1))^{n_i} = -1, \tag{B.4}$$

the result follows from equation (B.3), we have

$$0 = \mathbb{E}\left[\prod_{i=1}^{k}\mathbb{X}_i^{n_i}\right]+\prod_{i=1}^{k}\mu_i^{n_i}(-1) \Rightarrow \mathbb{E}\left[\prod_{i=1}^{k}\mathbb{X}_i^{n_i}\right] = \prod_{i=1}^{k}\mu_i^{m_i}. \tag{B.5}$$

□

Appendix C

Time to degradation of an IL-7 receptor

Consider the location of a single unbound IL-7 receptor in a T cell. Let us assume the receptor can be either expressed on the cell membrane (state 1), internalised in an endosome (state 2), or degraded in a lysosome (state 3). Let us describe the location of the receptor by a 3-state Markov process. The transition probability for going from the cell membrane to the endosome, in a small time Δt, $(1 \to 2)$ is $\mu_U \Delta t + o(\Delta t)$. The transition probability for returning to the cell membrane from the endosome $(2 \to 1)$ is given by $\xi_U \Delta t + o(\Delta t)$. The transition probability for transiting to the lysosome $(2 \to 3)$ is $\delta_U \Delta t + o(\Delta t)$. We assume the lysosome (state 3) is an absorbing state, and for this process the probability of the receptor being degraded (entering state 3) is 1. Define τ_i, $i = 1, 2, 3$, to be the expected time for a receptor to enter state 3 from state i, $i = 1, 2, 3$. The transitions between states are illustrated in Figure C.1.

From a first step analysis argument (for which further details can be found in (Allen,

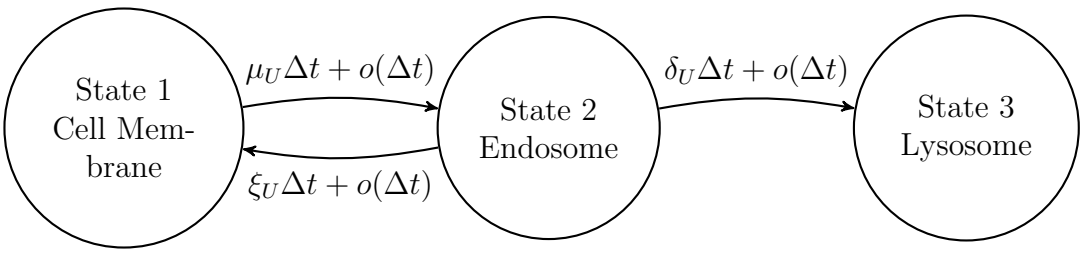

Figure C.1: Illustration of the transition probabilities between states of the three-state Markov process.

2003)), each τ_i satisfies

$$\tau_1 = \tau_2 + \frac{1}{\mu_U}, \tag{C.1}$$

$$\tau_2 = \frac{\xi_U}{\xi_U + \delta_U}\tau_1 + \frac{\delta_U}{\xi_U + \delta_U}\tau_3 + \frac{1}{\xi_U + \delta_U}, \tag{C.2}$$

$$\tau_3 = 0. \tag{C.3}$$

Therefore, the expected time to degradation for an expressed, unbound, receptor is given by

$$\tau_1 = \frac{\mu_U + \xi_U + \delta_U}{\mu_U \delta_U}. \tag{C.4}$$

References

Allen, L. (2003). *An introduction to stochastic processes with applications to biology*. Pearson/Prentice Hall Upper Saddle River (New Jersey).

Almeida, A., Rocha, B., Freitas, A. & Tanchot, C. (2005). Homeostasis of T cell numbers: from thymus production to peripheral compartmentalization and the indexation of regulatory T cells. In *Seminars in Immunology*, vol. 17, 239–249, Elsevier.

Almeida, A., Zaragoza, B. & Freitas, A. (2006a). Competition controls the rate of transition between the peripheral pools of $CD4^+$ $CD25^-$ and $CD4^+$ $CD25^+$ T cells. *International Immunology*, **18**, 1607–1613.

Almeida, A., Zaragoza, B. & Freitas, A. (2006b). Indexation as a novel mechanism of lymphocyte homeostasis: the number of $CD4^+$ $CD25^+$ regulatory T cells is indexed to the number of IL-2-producing cells. *Journal of Immunology*, **177**, 192.

Almeida, A., Amado, I., Reynolds, J., Berges, J., Lythe, G., Molina-París, C. & Freitas, A. (2012). Quorum-sensing in $CD4^+$ T cell homeostasis: A hypothesis and a model. *Frontiers in Immunology*, **3**.

Almeida, A.R., Legrand, N., Papiernik, M. & Freitas, A.A. (2002). Homeostasis of peripheral CD4+ T cells: IL-2Rα and IL-2 shape a population of regulatory cells that controls CD4+ T cell numbers. *The Journal of Immunology*, **169**, 4850–4860.

Antony, P., Piccirillo, C., Akpinarli, A., Finkelstein, S., Speiss, P., Surman, D., Palmer, D., Chan, C., Klebanoff, C., Overwijk, W. *et al.* (2005). $CD8^+$ T cell immunity against a tumor/self-antigen is augmented by $CD4^+$ T helper cells and hindered by naturally occurring T regulatory cells. *The Journal of Immunology*, **174**, 2591.

Aspinall, R. & Andrew, D. (2000). Thymic involution in aging. *Journal of clinical immunology*, **20**, 250–256.

Bains, I., Antia, R., Callard, R. & Yates, A. (2009a). Quantifying the development of the peripheral naive CD4+ T-cell pool in humans. *Blood*, **113**, 5480–5487.

Bains, I., Thiébaut, R., Yates, A. & Callard, R. (2009b). Quantifying thymic export: combining models of naive T cell proliferation and TCR excision circle dynamics gives an explicit measure of thymic output. *Journal of Immunology*, **183**, 4329–4336.

Bains, I., Thiébaut, R., Yates, A. & Callard, R. (2009c). Quantifying thymic export: combining models of naive T cell proliferation and TCR excision circle dynamics gives an explicit measure of thymic output. *The Journal of Immunology*, **183**, 4329–4336.

Balk, S.P., Ebert, E.C., Blumenthal, R.L., McDermott, F.V., Wucherpfennig, K.W., Landau, S.B. & Blumberg, R.S. (1991). Oligoclonal expansion and CD1 recognition by human intestinal intraepithelial lymphocytes. *Science*, **253**, 1411–1415.

Banchereau, J., Pascual, V. & O'Garra, A. (2012). From IL-2 to IL-37: the expanding spectrum of anti-inflammatory cytokines. *Nature Immunology*, **13**, 925–931.

Belkaid, Y. & Rouse, B.T. (2005). Natural regulatory T cells in infectious disease. *Nature immunology*, **6**, 353–360.

Berard, M. & Tough, D. (2002). Qualitative differences between naive and memory T cells. *Immunology*, **106**, 127–138.

Bettelli, E., Carrier, Y., Gao, W., Korn, T., Strom, T., Oukka, M., Weiner, H. & Kuchroo, V. (2006). Reciprocal developmental pathways for the generation of pathogenic effector TH17 and regulatory T cells. *Nature*, **441**, 235–238.

Bluestone, J.A. & Abbas, A.K. (2003). Natural versus adaptive regulatory T cells. *Nature Reviews Immunology*, **3**, 253–257.

Bradley, L.M., Haynes, L. & Swain, S.L. (2005). IL-7: maintaining T-cell memory and achieving homeostasis. *Trends in immunology*, **26**, 172–176.

Bremaud, P. (1999). *Markov chains: Gibbs fields, Monte Carlo simulation, and queues*, vol. 31. springer.

Brocker, T. (1997). Survival of mature CD4 T lymphocytes is dependent on major histocompatibility complex class II–expressing dendritic cells. *Journal of Experimental Medicine*, **186**, 1223–1232.

Bromley, S.K., Thomas, S.Y. & Luster, A.D. (2005). Chemokine receptor CCR7 guides T cell exit from peripheral tissues and entry into afferent lymphatics. *Nature immunology*, **6**, 895–901.

Brualdi, R.A. (1992). *Introductory combinatorics*. New York.

Brunner, T., Mogil, R., LaFace, D., Yoo, N., Mahboubi, A., Echeverri, F., Martin, S., Force, W., Lynch, D., Ware, C. *et al.* (1995). Cell-autonomous Fas (CD95)/Fas-ligand interaction mediates activation-induced apoptosis in T-cell hybridomas. *Nature*, **373**, 441–444.

Burmaster, D.E. & Crouch, E.A. (1997). Lognormal distributions for body weight as a function of age for males and females in the united states, 1976–1980. *Risk Analysis*, **17**, 499–505.

Burroughs, N., Ferreira, M., Oliveira, B. & Pinto, A. (2011). Autoimmunity arising from bystander proliferation of T cells in an immune response model. *Mathematical and Computer Modelling*, **53**, 1389–1393.

Callard, R., Stark, J. & Yates, A. (2003). Fratricide: a mechanism for T memory-cell homeostasis. *Trends in Immunology*, **24**, 370–375.

Carneiro, J., Leon, K., Caramalho, Í., Van Den Dool, C., Gardner, R., Oliveira, V., Bergman, M., Sepúlveda, N., Paixão, T., Faro, J. *et al.* (2007). When three is not a crowd: a crossregulation model of the dynamics and repertoire selection of regulatory $CD4^+$ T cells. *Immunological Reviews*, **216**, 48–68.

Chen, W., Jin, W., Hardegen, N., Lei, K.j., Li, L., Marinos, N., McGrady, G. & Wahl, S.M. (2003). Conversion of peripheral $CD4^+$ $CD25^-$ naive

T cells to CD4$^+$ CD25$^+$ regulatory T cells by TGF-β induction of transcription factor Foxp3. *The Journal of experimental medicine*, **198**, 1875–1886.

Cheng, G., Yu, A. & Malek, T. (2011). T-cell tolerance and the multi-functional role of IL-2R signaling in T-regulatory cells. *Immunological Reviews*, **241**, 63–76.

Cho, B., Rao, V., Ge, Q., Eisen, H. & Chen, J. (2000). Homeostasis-stimulated proliferation drives naive T cells to differentiate directly into memory T cells. *Journal of Experimental Medicine*, **192**, 549.

Coddington, E.A. & Levinson, N. (1955). *Theory of ordinary differential equations*. Tata McGraw-Hill Education.

Cooper, G. (2000). The Cell: A Molecular Approach. *Sunderland (MA): Sinauer Associates*.

Cose, S. (2007). T-cell migration: a naive paradigm? *Immunology*, **120**, 1–7.

Curtsinger, J.M., Schmidt, C.S., Mondino, A., Lins, D.C., Kedl, R.M., Jenkins, M.K. & Mescher, M.F. (1999). Inflammatory cytokines provide a third signal for activation of naive CD4+ and CD8+ T cells. *The Journal of Immunology*, **162**, 3256–3262.

Dadi, H., Ke, S. & Roifman, C. (1994). Activation of phosphatidylinositol-3 kinase by ligation of the interleukin-7 receptor is dependent on protein tyrosine kinase activity. *Blood*, **84**, 1579–1586.

Datta, S., Brunet, A. & Greenberg, M. (1999). Cellular survival: a play in three Akts. *Genes and development*, **13**, 2905–2927.

DeGroot, M.H. & Schervish, M.J. (2002). Probability and Statistics.

den Braber, I., Mugwagwa, T., Vrisekoop, N., Westera, L., Mögling, R., Bregje de Boer, A., Willems, N., Schrijver, E.H., Spierenburg, G., Gaiser, K. *et al.* (2012). Maintenance of peripheral naive T cells is sustained by thymus output in mice but not humans. *Immunity*, **36**, 288–297.

Diggle, S., Griffin, A., Campbell, G. & West, S. (2007). Cooperation and conflict in quorum-sensing bacterial populations. *Nature*, **450**, 411–414.

Dirac, P.A.M. (1947). The principles of quantum mechanics. *The International Series of Monographs on Physics, Oxford: Clarendon Press, 1947*, **1**.

Duffy, K.R., Wellard, C.J., Markham, J.F., Zhou, J.H., Holmberg, R., Hawkins, E.D., Hasbold, J., Dowling, M.R. & Hodgkin, P.D. (2012). Activation-induced B cell fates are selected by intracellular stochastic competition. *Science*, **335**, 338–341.

Edelstein-Keshet, L. (2005). *Mathematical models in biology*. SIAM.

Even, J., Lim, A., Puisieux, I., Ferradini, L., Dietrich, P.Y., Toubert, A., Hercend, T., Triebel, F., Pannetier, C. & Kourilsky, P. (1995). T-cell repertoires in healthy and diseased human tissues analysed by T-cell receptor β-chain CDR3 size determination: evidence for oligoclonal expansions in tumours and inflammatory diseases. *Research in immunology*, **146**, 65–80.

Eynon, E., Livák, F., Kuida, K., Schatz, D. & Flavell, R. (1999). Distinct effects of Jak3 signaling on αß and $\gamma\delta$ thymocyte development. *Journal of Immunology*, **162**, 1448–1459.

Feinerman, O., Jentsch, G., Tkach, K., Coward, J., Hathorn, M., Sneddon, M., Emonet, T., Smith, K. & Altan-Bonnet, G. (2010). Single-cell quantification of IL-2 response by effector and regulatory T cells reveals critical plasticity in immune response. *Molecular Systems Biology*, **6**.

Feuerer, M., Hill, J.A., Kretschmer, K., von Boehmer, H., Mathis, D. & Benoist, C. (2010). Genomic definition of multiple ex vivo regulatory T cell subphenotypes. *PNAS*, **107**, 5919–5924.

Fontenot, J.D., Gavin, M.A. & Rudensky, A.Y. (2003). Foxp3 programs the development and function of CD4+ CD25+ regulatory T cells. *Nature Immunology*, **4**, 330–336.

Fouchet, D. & Regoes, R. (2008). A population dynamics analysis of the interaction between adaptive regulatory T cells and antigen presenting cells. *PLoS ONE*, **3**, e2306.

Freitas, A. & Rocha, B. (2000). Population biology of lymphocytes: the flight for survival. *Annual Review of Immunology*, **18**, 83–111.

Fry, T. & Mackall, C. (2005). The many faces of IL-7: from lymphopoiesis to peripheral T cell maintenance. *Journal of Immunology*, **174**, 6571–6576.

Gantmakher, F.R. (2005). *Applications of the Theory of Matrices*. DoverPublications. com.

Ge, Q., Hu, H., Eisen, H. & Chen, J. (2002). Naive to memory T-cell differentiation during homeostasis-driven proliferation. *Microbes and Infection*, **4**, 555–558.

Germain, R.N. (2002). T-cell development and the CD4–CD8 lineage decision. *Nature Reviews Immunology*, **2**, 309–322.

Gesztelyi, R., Zsuga, J., Kemeny-Beke, A., Varga, B., Juhasz, B. & Tosaki, A. (2012). The Hill equation and the origin of quantitative pharmacology. *Archive for history of exact sciences*, **66**, 427–438.

Gillespie, D.T. (1977). Exact stochastic simulation of coupled chemical reactions. *The journal of physical chemistry*, **81**, 2340–2361.

Goldrath, A.W., Luckey, C.J., Park, R., Benoist, C. & Mathis, D. (2004). The molecular program induced in T cells undergoing homeostatic proliferation. *Proceedings of the National Academy of Sciences of the United States of America*, **101**, 16885–16890.

Grakoui, A., Bromley, S.K., Sumen, C., Davis, M.M., Shaw, A.S., Allen, P.M. & Dustin, M.L. (1999). The immunological synapse: a molecular machine controlling T cell activation. *Science*, **285**, 221–227.

Halnon, N., Jamieson, B., Plunkett, M., Kitchen, C., Pham, T. & Krogstad, P. (2005). Thymic function and impaired maintenance of peripheral T cell populations in children with congenital heart disease and surgical thymectomy. *Pediatric Research*, **57**, 42–48.

Hapuarachchi, T., Lewis, J. & Callard, R.E. (2013). A mechanistic model for naive CD4 T cell homeostasis in healthy adults and children. *Frontiers in immunology*, **4**.

Haugen, F., Norheim, F., Lian, H., Wensaas, A.J., Dueland, S., Berg, O., Funderud, A., Skålhegg, B.S., Raastad, T. & Drevon, C.A. (2010). Il-7 is expressed and secreted by human skeletal muscle cells. *American Journal of Physiology-Cell Physiology*, **298**, C807–C816.

Hawkins, E., Markham, J., McGuinness, L. & Hodgkin, P. (2009). A single-cell pedigree analysis of alternative stochastic lymphocyte fates. *Proceedings of the National Academy of Sciences*, **106**, 13457–13462.

Hawkins, E.D., Turner, M.L., Dowling, M.R., Van Gend, C. & Hodgkin, P.D. (2007). A model of immune regulation as a consequence of randomized lymphocyte division and death times. *Proceedings of the National Academy of Sciences*, **104**, 5032–5037.

Haynes, B. & Hale, L. (1998). The human thymus. *Immunologic Research*, **18**, 175–192.

Henriques, C.M., Rino, J., Nibbs, R.J., Graham, G.J. & Barata, J.T. (2010). IL-7 induces rapid clathrin-mediated internalization and JAK3-dependent degradation of IL-7Rα in T cells. *Blood*, **115**, 3269–3277.

Hogan, T., Shuvaev, A., Commenges, D., Yates, A., Callard, R., Thiebaut, R. & Seddon, B. (2013). Clonally Diverse T Cell Homeostasis Is Maintained by a Common Program of Cell-Cycle Control. *The Journal of Immunology*, **190**, 3985–3993.

Hurwitz, A. (1964). On the conditions under which an equation has only roots with negative real parts. *Selected Papers on Mathematical Trends in Control Theory (R. Bellman and R. Kalaba, eds.)*, **65**.

Iglehart, D. (1964). Multivariate competition processes. *The Annals of Mathematical Statistics*, 350–361.

Jameson, S. (2005). T cell homeostasis: keeping useful T cells alive and live T cells useful. In *Seminars in immunology*, vol. 17, 231–237, Elsevier.

Janeway, C., Travers, P., Walport, M. & Capra, J. (2001). *Immunobiology: the immune system in health and disease*. Current Biology.

Jelley-Gibbs, D., Lepak, N., Yen, M. & Swain, S. (2000). Two distinct stages in the transition from naive CD4 T cells to effectors, early antigen-dependent and late cytokine-driven expansion and differentiation. *Journal of Immunology*, **165**, 5017–5026.

Jenkins, M., Khoruts, A., Ingulli, E., Mueller, D., McSorley, S., Reinhardt, R., Itano, A. & Pape, K. (2001). In vivo activation of antigen-specific CD4 T cells. *Annual Review of Immunology*, **19**, 23–45.

Jiang, Q., Li, W., Aiello, F., Mazzucchelli, R., Asefa, B., Khaled, A. & Durum, S. (2005). Cell biology of IL-7, a key lymphotrophin. *Cytokine and Growth Factor Reviews*, **16**, 513–533.

Johnson, N.L., Kotz, S. & Balakrishnan, N. (1970). *-Distributions in Statistics: Continuous Univariate Distributions: Vol.: 2*. Houghton Mifflin New York.

Josefowicz, S.Z., Lu, L.F. & Rudensky, A.Y. (2012). Regulatory T cells: mechanisms of differentiation and function. *Annual Review of Immunology*, **30**, 531–564.

Ju, S.T., Matsui, K. & Ozdemirli, M. (1999). Molecular and Cellular Mechanisms RegulatingTand B Cell Apoptosis through Fas/FasL Interaction. *International reviews of immunology*, **18**, 485–513.

Kang, J. & Coles, M. (2012). IL-7: The global builder of the innate lymphoid network and beyond, one niche at a time. *Seminars in Immunology*, **24**, 190–197.

Karlin, S. & McGregor, J. (1957). The classification of birth and death processes. *Transactions of the American Mathematical Society*, **86**, 366–400.

Kieper, W., Burghardt, J. & Surh, C. (2004). A role for TCR affinity in regulating naive T cell homeostasis. *Journal of Immunology*, **172**, 40–44.

Kim, P., Lee, P. & Levy, D. (2007). Modeling regulation mechanisms in the immune system. *Journal of Theoretical Biology*, **246**, 33–69.

Kimura, M., Pobezinsky, L., Guinter, T., Thomas, J., Adams, A., Park, J., Tai, X. & Singer, A. (2012). IL-7 signaling must be intermittent, not continuous, during $CD8^+$ T cell homeostasis to promote cell survival instead of cell death. *Nature Immunology*.

Kimura, M.Y., Pobezinsky, L.A., Guinter, T.I., Thomas, J., Adams, A., Park, J.H., Tai, X. & Singer, A. (2013). IL-7 signaling must be intermittent, not continuous, during $CD8^+$ T cell homeostasis to promote cell survival instead of cell death. *Nature immunology*, **14**, 143–151.

Koenen, P., Heinzel, S., Carrington, E.M., Happo, L., Alexander, W.S., Zhang, J.G., Herold, M.J., Scott, C.L., Lew, A.M., Strasser, A. *et al.* (2013). Mutually exclusive regulation of T cell survival by IL-7R and antigen receptor-induced signals. *Nature Communications*, **4**, 1735.

Kondrack, R., Harbertson, J., Tan, J., McBreen, M., Surh, C. & Bradley, L. (2003). Interleukin 7 regulates the survival and generation of memory CD4 cells. *Journal of Experimental Medicine*, **198**, 1797–1806.

Kretschmer, K., Apostolou, I., Hawiger, D., Khazaie, K., Nussenzweig, M. & Von Boehmer, H. (2005). Inducing and expanding regulatory T cell populations by foreign antigen. *Nature Immunology*, **6**, 1219–1227.

Kubo, T., Hatton, R.D., Oliver, J., Liu, X., Elson, C.O. & Weaver, C.T. (2004). Regulatory T cell suppression and anergy are differentially regulated by proinflammatory cytokines produced by TLR-activated dendritic cells. *The Journal of immunology*, **173**, 7249–7258.

Lanzavecchia, A. & Sallusto, F. (2005). Understanding the generation and function of memory T cell subsets. *Current opinion in immunology*, **17**, 326–332.

Lee, H.Y. & Perelson, A.S. (2008). Modeling T cell proliferation and death in vitro based on labeling data: generalizations of the Smith–Martin cell cycle model. *Bulletin of mathematical biology*, **70**, 21–44.

León, K., Perez, R., Lage, A. & Carneiro, J. (2000). Modelling T-cell-mediated suppression dependent on interactions in multicellular conjugates. *Journal of Theoretical Biology*, **207**, 231–254.

León, K., Peréz, R., Lage, A. & Carneiro, J. (2001). Three-cell interactions in T cell-mediated suppression? a mathematical analysis of its quantitative implications. *Journal of Immunology*, **166**, 5356.

León, K., Lage, A. & Carneiro, J. (2003). Tolerance and immunity in a mathematical model of T-cell mediated suppression. *Journal of Theoretical Biology*, **225**, 107–126.

Li, W.Q., Jiang, Q., Khaled, A.R., Keller, J.R. & Durum, S.K. (2004). Interleukin-7 inactivates the pro-apoptotic protein Bad promoting T cell survival. *Journal of Biological Chemistry*, **279**, 29160–29166.

Linsley, P.S. & Ledbetter, J.A. (1993). The role of the CD28 receptor during T cell responses to antigen. *Annual review of immunology*, **11**, 191–212.

Malek, T. & Castro, I. (2010). Interleukin-2 receptor signaling: at the interface between tolerance and immunity. *Immunity*, **33**, 153–165.

Malek, T., Yu, A., Vincek, V., Scibelli, P. & Kong, L. (2002). CD4 regulatory T cells prevent lethal autoimmunity in IL-2Rβ-deficient mice: implications for the nonredundant function of IL-2. *Immunity*, **17**, 167–178.

Markham, J.F., Wellard, C.J., Hawkins, E.D., Duffy, K.R. & Hodgkin, P.D. (2010). A minimum of two distinct heritable factors are required to explain correlation structures in proliferating lymphocytes. *Journal of The Royal Society Interface*, **7**, 1049–1059.

Markiewicz, M.A., Brown, I. & Gajewski, T.F. (2003). Death of peripheral CD8$^+$ T cells in the absence of MHC class I is Fas-dependent and not blocked by Bcl-xL. *European Journal of Immunology*, **33**, 2917–2926.

Martin, B., Bourgeois, C., Dautigny, N. & Lucas, B. (2003). On the role of MHC class II molecules in the survival and lymphopenia-induced proliferation of peripheral CD4$^+$ T cells. *Proceedings of the National Academy of Sciences*, **100**, 6021–6026.

Martin, B., Bécourt, C., Bienvenu, B. & Lucas, B. (2006). Self-recognition is crucial for maintaining the peripheral CD4$^+$ T-cell pool in a nonlymphopenic environment. *Blood*, **108**, 270–277.

Mazzucchelli, R. & Durum, S. (2007). Interleukin-7 receptor expression: intelligent design. *Nature Reviews Immunology*, **7**, 144–154.

McCaughtry, T.M., Wilken, M.S. & Hogquist, K.A. (2007). Thymic emigration revisited. *The Journal of experimental medicine*, **204**, 2513–2520.

Miller, M. & Bassler, B. (2001). Quorum sensing in bacteria. *Annual Reviews in Microbiology*, **55**, 165–199.

Min, B., McHugh, R., Sempowski, G.D., Mackall, C., Foucras, G. & Paul, W.E. (2003). Neonates support lymphopenia-induced proliferation. *Immunity*, **18**, 131–140.

Mitchell, W.A., Meng, I., Nicholson, S.A. & Aspinall, R. (2006). Thymic output, ageing and zinc. *Biogerontology*, **7**, 461–470.

Mombaerts, P., Iacomini, J., Johnson, R.S., Herrup, K., Tonegawa, S. & Papaioannou, V.E. (1992). RAG-1-deficient mice have no mature B and T lymphocytes. *Cell*, **68**, 869–877.

Mueller, S.N. & Germain, R.N. (2009). Stromal cell contributions to the homeostasis and functionality of the immune system. *Nature Reviews Immunology*, **9**, 618–629.

Müller, A.J., Filipe-Santos, O., Eberl, G., Aebischer, T., Späth, G.F. & Bousso, P. (2012). $CD4^+$ T cells rely on a cytokine gradient to control intracellular pathogens beyond sites of antigen presentation. *Immunity*.

Murali-Krishna, K. & Ahmed, R. (2000). Cutting edge: naive T cells masquerading as memory cells. *The Journal of Immunology*, **165**, 1733–1737.

Nikolich-&Zcaron, J. *et al.* (2004). The many important facets of T-cell repertoire diversity. *Nature Reviews Immunology*, **4**, 123–132.

Palmer, M., Mahajan, V., Chen, J., Irvine, D. & Lauffenburger, D. (2011). Signaling thresholds govern heterogeneity in IL-7-receptor-mediated responses of naïve $CD8^+$; T cells. *Immunology and Cell Biology*, **89**, 581–594.

Palmer, M.J., Mahajan, V.S., Trajman, L.C., Irvine, D.J., Lauffenburger, D.A., Chen, J. *et al.* (2008). Interleukin-7 receptor signaling network: an integrated systems perspective. *Cellular and Molecular Immunology*, **5**, 79–89.

Park, J., Yu, Q., Erman, B., Appelbaum, J., Montoya-Durango, D., Grimes, H. & Singer, A. (2004). Suppression of IL7Rα transcription by IL-7 and other prosurvival cytokines: a novel mechanism for maximizing IL-7-dependent T cell survival. *Immunity*, **21**, 289–302.

Pepper, M. & Jenkins, M. (2011). Origins of $CD4^+$ effector and central memory T cells. *Nature Immunology*, **131**, 467–471.

Perko, L. (1991). *Linear Systems*. Springer.

Powrie, F. & Maloy, K. (2003). Regulating the regulators. *Science*, **299**, 1030.

Prelog, M., Keller, M., Geiger, R., Brandstätter, A., Würzner, R., Schweigmann, U., Zlamy, M., Zimmerhackl, L.B. & Grubeck-Loebenstein, B. (2009). Thymectomy in early childhood: Significant alterations of the $CD4^+$ $CD45RA^+$ $CD62L^+$ T cell compartment in later life. *Clinical immunology*, **130**, 123–132.

Qureshi, O.S., Zheng, Y., Nakamura, K., Attridge, K., Manzotti, C., Schmidt, E.M., Baker, J., Jeffery, L.E., Kaur, S., Briggs, Z. *et al.* (2011). Trans-endocytosis of CD80 and CD86: a molecular basis for the cell-extrinsic function of CTLA-4. *Science*, **332**, 600–603.

Rathmell, J., Farkash, E., Gao, W. & Thompson, C. (2001). Il-7 enhances the survival and maintains the size of naive t cells. *Journal of Immunology*, **167**, 6869–6876.

Reynolds, J., Coles, M., Lythe, G. & Molina-París, C. (2012). Deterministic and stochastic naive T cell population dynamics: symmetric and asymmetric cell division. *Dynamical Systems*, **27**, 75–103.

Reynolds, J., Amado, I.F., Freitas, A.A., Lythe, G. & Molina-París, C. (2013a). A mathematical perspective on $CD4^+$ T cell quorum-sensing. *Journal of theoretical biology*.

Reynolds, J., Coles, M., Lythe, G. & Molina-París, C. (2013b). Mathematical model of naive T cell division and survival IL-7 thresholds. *Frontiers in Immunology*, **4**.

Ribeiro, R.M. & de Boer, R.J. (2008). The contribution of the thymus to the recovery of peripheral naïve T cell numbers during antiretroviral treatment for HIV infection. *Journal of acquired immune deficiency syndromes (1999)*, **49**, 1.

Sakaguchi, S. (2000). Regulatory T cells: key controllers of immunologic self-tolerance. *Cell*, **101**, 455.

Sakaguchi, S. (2004). Naturally arising $CD4^+$ regulatory T cells for immunologic self-tolerance and negative control of immune responses. *Annual Review of Immunology*, **22**, 531–562.

Sakaguchi, S., Sakaguchi, N., Asano, M., Itoh, M. & Toda, M. (1995). Immunologic self-tolerance maintained by activated T cells expressing IL-2 receptor alpha-chains (CD25). breakdown of a single mechanism of self-tolerance causes various autoimmune diseases. *The Journal of Immunology*, **155**, 1151–1164.

Sakkas, L.I., Xu, B., Artlett, C.M., Lu, S., Jimenez, S.A. & Platsoucas, C.D. (2002). Oligoclonal T cell expansion in the skin of patients with systemic sclerosis. *The Journal of Immunology*, **168**, 3649–3659.

Saule, P., Trauet, J., Dutriez, V., Lekeux, V., Dessaint, J.P. & Labalette, M. (2006). Accumulation of memory T cells from childhood to old age: Central and effector memory cells in $CD44^+$ versus effector memory and terminally differentiated memory cells in $CD8^+$ compartment. *Mechanisms of ageing and development*, **127**, 274–281.

Schittler, D., Allgöwer, F. & De Boer, R.J. (2013). A new model to simulate and analyze proliferating cell populations in BrdU labeling experiments. *BMC systems biology*, **7**, S4.

Schluns, K., Kieper, W., Jameson, S. & Lefrançois, L. (2000). Interleukin-7 mediates the homeostasis of naive and memory CD8 T cells in vivo. *Nature Immunology*, **1**, 426–432.

Schüler, T., Hämmerling, G.J. & Arnold, B. (2004). Cutting edge: IL-7-dependent homeostatic proliferation of $CD8^+$ T cells in neonatal mice allows the generation of long-lived natural memory T cells. *The Journal of Immunology*, **172**, 15–19.

Scollay, R.G., Butcher, E.C. & Weissman, I.L. (1980). Thymus cell migration: quantitative aspects of cellular traffic from the thymus to the periphery in mice. *European Journal of Immunology*, **10**, 210–218.

Sears, C.L. (2005). A dynamic partnership: celebrating our gut flora. *Anaerobe*, **11**, 247–251.

Seckinger, P. & Fougereau, M. (1994). Activation of src family kinases in human pre-B cells by IL-7. *Journal of Immunology*, **153**, 97–109.

Seddon, B. & Mason, D. (2000). The third function of the thymus. *Immunology Today*, **21**, 95–99.

Seddon, B. & Zamoyska, R. (2002). TCR and IL-7 receptor signals can operate independently or synergize to promote lymphopenia-induced expansion of naive T cells. *Journal of Immunology*, **169**, 3752–3759.

Seddon, B., Tomlinson, P. & Zamoyska, R. (2003). Interleukin 7 and T cell receptor signals regulate homeostasis of CD4 memory cells. *Nature Immunology*, **4**, 680–686.

Sepúlveda, N. & Carneiro, J. (2011). Dynamics of peripheral regulatory and effector T cells competing for antigen presenting cells. In *Mathematical Models and Immune Cell Biology*, 275–303, Springer.

Shen, C.R., Yang, W.C. & Chen, H.W. (2013). The fate of regulatory T cells: survival or apoptosis. *Cellular & molecular immunology*.

Simpson, J., Gray, E. & Beck, J. (1975). Age involution in the normal human adult thymus. *Clinical and Experimental Immunology*, **19**, 261.

Singh, A. & Hespanha, J.P. (2006a). Lognormal moment closures for biochemical reactions. In *Decision and Control, 2006 45th IEEE Conference on*, 2063–2068, IEEE.

Singh, A. & Hespanha, J.P. (2006b). Moment closure for the stochastic logistic model. Tech. rep., DTIC Document.

Sprent, J. & Surh, C. (2011). Normal T cell homeostasis: the conversion of naive cells into memory-phenotype cells. *Nature Immunology*, **12**, 478–484.

Steinmann, G. (1986). Changes in the human thymus during aging. In *The Human Thymus*, 43–88, Springer.

Stirk, E.R., Lythe, G., van den Berg, H.A., Hurst, G.A. & Molina-París, C. (2010a). The limiting conditional probability distribution in a stochastic model of T cell repertoire maintenance. *Mathematical Biosciences*, **224**, 74–86.

Stirk, E.R., Lythe, G., van den Berg, H.A. & Molina-París, C. (2010b). Stochastic competitive exclusion in the maintenance of the naïve T cell repertoire. *Journal of Theoretical Biology*, **265**, 396–410.

Suda, T., Okazaki, T., Naito, Y., Yokota, T., Arai, N., Ozaki, S., Nakao, K. & Nagata, S. (1995). Expression of the Fas ligand in cells of T cell lineage. *Journal of Immunology*, **154**, 3806–3813.

Surh, C.D. & Sprent, J. (2008). Homeostasis of naive and memory T cells. *Immunity*, **29**, 848–862.

Suzuki, K., Nakajima, H., Saito, Y., Saito, T., Leonard, W. & Iwamoto, I. (2000). Janus kinase 3 (Jak3) is essential for common cytokine receptor γ chain (γc)-dependent signaling: comparative analysis of γc, Jak3, and γc and Jak3 double-deficient mice. *International Immunology*, **12**, 123–132.

Taggart, R. & Starr, L. (2009). *Biology: The unity and diversity of life*. CengageBrain. com.

Takada, K. & Jameson, S. (2009). Naive T cell homeostasis: from awareness of space to a sense of place. *Nature Reviews Immunology*, **9**, 823–832.

Tan, J., Dudl, E., LeRoy, E., Murray, R., Sprent, J., Weinberg, K. & Surh, C. (2001). IL-7 is critical for homeostatic proliferation and survival of naive T cells. *Proceedings of the National Academy of Sciences*, **98**, 8732–8737.

Tanchot, C., Le Campion, A., Martin, B., Léaument, S., Dautigny, N. & Lucas, B. (2002). Conversion of naive T cells to a memory-like phenotype in lymphopenic hosts is not related to a homeostatic mechanism that fills the peripheral naive T cell pool. *The Journal of Immunology*, **168**, 5042–5046.

Tang, Q., Adams, J., Tooley, A., Bi, M., Fife, B., Serra, P., Santamaria, P., Locksley, R., Krummel, M. & Bluestone, J. (2005). Visualizing regulatory T cell control of autoimmune responses in nonobese diabetic mice. *Nature Immunology*, **7**, 83–92.

Trepel, F. (1974). Number and distribution of lymphocytes in man. A critical analysis. *Klinische Wochenschrift*, **52**, 511–515.

Troy, A.E. & Shen, H. (2003). Cutting edge: homeostatic proliferation of peripheral T lymphocytes is regulated by clonal competition. *The Journal of Immunology*, **170**, 672–676.

Truss, J.K. (1997). *Foundations of mathematical analysis*. Clarendon Press Oxford.

Vivien, L., Benoist, C. & Mathis, D. (2001). T lymphocytes need IL-7 but not IL-4 or IL-6 to survive in vivo. *International Immunology*, **13**, 763–768.

von Boehmer, H. (2005). Mechanisms of suppression by suppressor T cells. *Nature Immunology*, **6**, 338–344.

Walker, L.S. & Sansom, D.M. (2011). The emerging role of CTLA4 as a cell-extrinsic regulator of T cell responses. *Nature Reviews Immunology*, **11**, 852–863.

Wallace, E.W. (2010). A simplified derivation of the linear noise approximation. *arXiv preprint arXiv:1004.4280*.

Wan, Y. & Flavell, R. (2009). How diverse–CD4 effector T cells and their functions. *Journal of Molecular Cell Biology*, **1**, 20–36.

Wing, K., Onishi, Y., Prieto-Martin, P., Yamaguchi, T., Miyara, M., Fehervari, Z., Nomura, T. & Sakaguchi, S. (2008). CTLA-4 control over Foxp3+ regulatory T cell function. *Science*, **322**, 271–275.

Wofford, J.A., Wieman, H.L., Jacobs, S.R., Zhao, Y. & Rathmell, J.C. (2008). IL-7 promotes Glut1 trafficking and glucose uptake via STAT5-mediated activation of Akt to support T-cell survival. *Blood*, **111**, 2101–2111.

Yates, A., Bergmann, C., Leo Van Hemmen, J., Stark, J. & Callard, R. (2000). Cytokine-modulated regulation of helper T cell populations. *Journal of Theoretical Biology*, **206**, 539–560.

Yates, A., Stark, J., Klein, N., Antia, R. & Callard, R. (2007). Understanding the slow depletion of memory $CD4^+$ T cells in HIV infection. *PLoS medicine*, **4**, e177.

Yates, A., Saini, M., Mathiot, A. & Seddon, B. (2008). Mathematical modeling reveals the biological program regulating lymphopenia-induced proliferation. *The Journal of Immunology*, **180**, 1414–1422.

Ziegel, E.R. (2002). Statistical inference. *Technometrics*, **44**.